



The  
University  
Of  
Sheffield.

# **Life and Death: Cell Wall Antibiotic killing of *Staphylococcus aureus***

By

Milena von und zur Mühlen, BSc (Hons)  
(University of Sheffield)

A thesis submitted for the degree of Doctor of Philosophy

September 2019

Department of Molecular Biology and Biotechnology,  
University of Sheffield, Firth Court, Western Bank, Sheffield S10 2TN



## Summary

The bacterial cell wall is a complex structure essential for life. The primary structural component of the wall for most bacteria, including the major human pathogen *Staphylococcus aureus*, is peptidoglycan. As peptidoglycan is unique to bacteria its synthesis forms the target for some of the most important clinically used antibiotics. The spread of antibiotic resistance is a global healthcare challenge. Addressing this massive problem requires a multifaceted approach ranging from reducing antibiotic use, to the discovery of new antibiotic interventions and alternatives.

The  $\beta$ -lactam and glycopeptide groups of antibiotics that target cell wall synthesis, exemplified by methicillin and vancomycin respectively, are some of the most commonly used antibiotics to treat *S. aureus* infections. The molecular pathway to bacterial cell death after treatment of *S. aureus* with these compounds is not well understood even after decades of clinical efficacy. To elucidate the bactericidal mechanism of methicillin and vancomycin, an integrated range of approaches was taken.

Characteristically, methicillin treatment initially shows a small increase in cell numbers prior to a decrease due to the action of the antibiotic, whereas vancomycin kills more slowly but without the initial increase. Structured illumination microscopy (SIM) demonstrated that both vancomycin and methicillin led to a significant cell volume increase prior to death in the absence of any peptidoglycan synthesis. Electron microscopy revealed that only with methicillin were bulbous septa apparent. Methicillin-treated cells still divided if they had a complete septum upon antibiotic addition whereas vancomycin treated cells did not. This difference was likely due to the action of peptidoglycan hydrolases at the presumptive septum.

A new model of the action of antibiotics was derived from this research. In combination with other data derived during the time of my PhD, this has led to an overarching theory as to how bacteria can grow and the activity of cell wall antibiotics. Utilisation of this data provides novel avenues for the use of existing antibiotics and the development of new ones.



## Acknowledgements

I would like to thank Prof. Simon Foster and the BBSRC White Rose DTP for giving me the opportunity to carry out my PhD. Thank you to Simon for his guidance over the past four years.

Thank you to all past and present members of the Foster Lab for letting me pick their brains and for making it a pleasant workplace. In particular, thank you to Dr. Victoria Lund for answering my countless questions and guiding me through the process. I would like to thank her along with Dr. Rebecca Hodges, Mina Mohaghegh and Dr. Nicola Galley for their friendship, many coffees and much needed gin and tonics.

Thank you to my Sheffield family and the climbing community for all the incredible adventures. A special thanks to Leo and Naomi for taking me into their home for the final months of my PhD. I wish there was enough space here to thank you all individually, but I appreciate every one of you for your support over the years.

Most importantly, thank you to my family for their unwavering support, not only over the past four years, but throughout my entire life. I would not be here without you and am eternally grateful for your love.

I would like to dedicate this thesis to my late grandfather, Raymond Collins.



## Abbreviation

%	Percentage
~	Approximately
°C	Degree Celsius
µg	Microgram
µl	Microliter
µm	Micrometre/Microns
µM	Micromolar
2D	Two Dimensional
3D	Three Dimensional
ADA	3-Azido-D-alanine
AFM	Atomic Force Microscopy
D-ala	D-alanine
dH <sub>2</sub> O	Distilled water
DMSO	Dimethyl sulphoxide
DNA	Deoxyribonucleic acid
DPM	Disintegrations per minute
ECT	Electron Cryo-tomography
EM	Electron Microscopy
Ery	Erythromycin
FDAAs	Fluorescent D-amino acids
g	Grams
GlcNAc	N-acetyl glucosamine
GTP	Guanosine triphosphate
h	Hour
IM	Inner membrane
HADA	Hydroxycoumarin 3-amino-D-alanine
HMW	High molecular weight
HPLC	High performance liquid chromatography
IPTG	Isopropyl beta-D-1-thiogalactopyranoside
Kan	Kanomycin

L	Liter
L-ala	L-alanine
Lin	Lincomycin
LMW	Low molecular weight
LTA	Lipoteichoic acid
M	Molar
mA	Milliamps
ManNAc	N-acetylmannosamine
m-DAP	meso-diaminopimelate
MEA	Mercaptoethylamine
mg	Milligram
MIC	Minimum inhibitory concentration
min	Minutes
mL	Milliliter
mM	Millimolar
MRSA	Methicillin resistant Staphylococcus aureus
MurNAc	N-acetyl muramic acid
n	Number
NADA	Nitrobenzofurazan 3-amino-D-alanine
NCDAAs	Non-canonical D-amino acid
nm	Nanometres
NMR	Nuclear magnetic resonance
OM	Outer membrane
OD <sub>x</sub>	Optical density at wavelength x (nm)
PALM	Photoactivated localisation microscopy
PBP	Penicillin binding protein
PBS	Phosphate buffered saline
polyGroP	Polyglycerol phosphate
polyRboP	Polyribitol phosphate
rpm	Revolutions per min
SDS	Sodium dodecyl sulphate

SEDS	Shape, elongation, division & sporulation
SIM	Structured illumination microscopy
Spec	Spectinomycin
STED	Stimulated Emission Depleted Microscopy
STORM	Stochastic Optical Reconstruction Microscopy
TA	Toxin-Antitoxin
TADA	Tetramethylrhodamine 3-amino-D-alanine
TCA	Trichloroacetic Acid
TEM	Transmission EM
TSB	Tryptone Soy Broth
UDP	Uridine Diphosphate
UV	Ultraviolet
v/v	Volume for volume
VISA	Vancomycin intermediate Staphylococcus aureus
VRSA	Vancomycin resistant Staphylococcus aureus
w/v	Weight for volume
WGA	Wheat Germ Agglutinin
WTA	Wall teichoic acid
x	Times



# Contents

<b>Summary</b> .....	<b>i</b>
<b>Acknowledgements</b> .....	<b>iii</b>
<b>Abbreviation</b> .....	<b>v</b>
<b>List of Figures</b> .....	<b>xv</b>
<b>List of Tables</b> .....	<b>xix</b>
<b>Chapter 1</b> .....	<b>1</b>
<b>Introduction</b> .....	<b>1</b>
1.1. <i>Staphylococcus aureus</i> .....	1
1.2. Cell Wall.....	1
1.2.1. Gram-negative.....	2
1.2.2. Gram-positive.....	2
1.3. Peptidoglycan chemical structure.....	4
1.4. Peptidoglycan architecture.....	6
1.4.1. Models of glycan chain organisation.....	6
1.4.2. Peptidoglycan architecture in gram-negative bacteria.....	8
1.4.3. Peptidoglycan architecture in gram-positive bacteria.....	10
1.4.3.1. Peptidoglycan architecture of gram-positive rods.....	10
1.4.3.2. Peptidoglycan architecture of gram-positive ovococci.....	10
1.4.3.3. Peptidoglycan architecture of <i>S. aureus</i> (gram-positive cocci).....	11
1.5. Cell wall synthesis.....	13
1.5.1. PG synthesis.....	13
1.5.1.1. Precursor synthesis.....	13
1.5.1.2. Lipid II assembly.....	13
1.5.1.3. Flipping of lipid II across the membrane.....	13
1.5.1.4. Monomer polymerisation.....	15
1.5.2. WTA synthesis.....	16
1.5.3. LTA synthesis.....	16
1.6. Peptidoglycan hydrolysis.....	16
1.6.1. <i>S. aureus</i> hydrolases.....	19
1.6.2. Control of <i>S. aureus</i> hydrolases.....	21
1.7. Cell division – overview.....	22
1.7.1. Rod-shaped bacteria.....	22
1.7.2. Coccoid bacteria.....	23
1.8. Cell division – the divisome.....	25

1.8.1.	Penicillin-binding proteins .....	27
1.9.	Cell division – peptidoglycan dynamics .....	28
1.9.1.	Peptidoglycan synthesis.....	28
1.9.2.	Cell splitting .....	28
1.9.3.	Cell expansion.....	30
1.10.	Cell Wall antibiotics .....	32
1.11.	$\beta$ -lactams .....	32
1.11.1.	Original models of penicillin killing.....	34
1.11.2.	Peter Giesbrecht’s model of penicillin killing of <i>S. aureus</i> .....	34
1.11.3.	Reactive oxygen species (ROS) .....	36
1.11.4.	Thomas Bernhardt’s model of mecillinam killing of <i>E. coli</i> .....	38
1.11.5.	Other insight into $\beta$ -lactam mode of action .....	38
1.12.	Glycopeptides .....	38
1.13.	Resistance to cell wall antibiotics .....	39
1.13.1.	Resistance, tolerance and persistence .....	39
1.13.2.	$\beta$ -lactam resistance.....	39
1.13.3.	Vancomycin resistance .....	40
1.14.	Project aims .....	40
	<b>Chapter 2.....</b>	<b>41</b>
	<b>Materials and Methods.....</b>	<b>41</b>
2.1.	Growth Conditions.....	41
2.1.1.	Media .....	41
2.1.2.	Tryptone Soy Broth (TSB).....	41
2.1.3.	Nutrient Broth (NB) .....	41
2.1.4.	NB Agar .....	41
2.2.	Antibiotics.....	41
2.3.	Buffers & Solutions .....	42
2.3.1.	Phosphate Buffered Saline (PBS).....	42
2.3.2.	Fixative Preparation.....	42
2.3.2.1.	Preparation of 16% (w/v) paraformaldehyde.....	42
2.3.2.2.	Fixative.....	42
2.3.3.	Click-iT® reaction buffer mix.....	42
2.4.	Chemicals & enzymes .....	43
2.5.	Equipment .....	43
2.5.1.	Centrifuges.....	43
2.5.2.	Spectrophotometer .....	43

2.6.	Bacterial strains and growth.....	44
2.6.1.	S. aureus strains.....	44
2.6.2.	B. subtilis strains.....	44
2.7.	Killing assays.....	45
2.7.1.	MIC.....	45
2.7.2.	CFU killing curves.....	45
2.8.	Labelling.....	45
2.8.1.	Fluorescent D-amino acid labelling.....	45
2.8.2.	NHS Ester labelling.....	46
2.8.3.	WGA labelling.....	46
2.9.	Fluorescent microscopy.....	46
2.9.1.	Resolution limited microscopy.....	46
	<i>Sample preparation</i> .....	46
2.9.2.	Structured illumination microscopy.....	47
2.10.	Cell measurements.....	48
2.10.1.	Cell volume estimation.....	48
2.11.	Electron Microscopy.....	48
2.12.	Radioactive incorporation.....	48
	<b>Chapter 3.....</b>	<b>51</b>
	<b>The effect of <math>\beta</math>-lactam antibiotics on <i>S. aureus</i>.....</b>	<b>51</b>
3.1.	Introduction.....	51
3.1.1.	<i>S. aureus</i> cell cycle and peptidoglycan dynamics.....	51
3.1.2.	Methods used to study $\beta$ -lactams.....	52
3.1.3.	Structured illumination microscopy.....	53
3.1.4.	Labelling of the bacterial cell surface.....	53
3.1.5.	Labelling peptidoglycan incorporation.....	54
3.1.6.	Aims of this chapter.....	55
3.2.	Results.....	55
3.2.1.	Killing Dynamics.....	55
3.2.2.	Cell morphology.....	57
3.2.2.1.	Methicillin.....	57
3.2.2.2.	Oxacillin.....	65
3.2.3.	Quantification of peptidoglycan synthesis in the presence of antibiotics.....	65
3.2.3.1.	Methicillin.....	65
3.2.3.2.	Oxacillin.....	68
3.2.4.	Fate of newly incorporated peptidoglycan.....	68

3.2.4.1.	Fate of newly incorporated peptidoglycan in the untreated cell population .....	77
3.2.4.2.	Fate of newly incorporated peptidoglycan after methicillin treatment.....	77
3.2.5.	The effect of methicillin treatment on <i>B. subtilis</i> .....	81
3.2.5.1.	Killing dynamics .....	81
3.2.5.2.	Morphological changes.....	81
3.3.	Discussion .....	81
<b>3.3.1.</b>	<b>Morphological changes</b> .....	<b>81</b>
3.3.2.	Peptidoglycan incorporation and fate .....	86
3.3.3.	Action of cell wall antibiotics on <i>B. subtilis</i> .....	88
	<b>Chapter 4.....</b>	<b>89</b>
	<b>Vancomycin killing of <i>S. aureus</i> .....</b>	<b>89</b>
4.1.	Introduction .....	89
4.1.1.	Aims of this chapter .....	90
4.2.	Results.....	90
4.2.1.	Killing Dynamics .....	90
4.2.2.	Cell morphology.....	90
4.2.3.	Quantification of peptidoglycan incorporation post-treatment .....	96
4.2.4.	Fate of newly incorporated peptidoglycan.....	96
4.2.5.	Action of vancomycin on <i>B. subtilis</i> .....	104
4.2.5.1.	Killing dynamics .....	104
4.2.5.2.	Morphological changes.....	104
4.3.	Discussion .....	105
4.3.1.	Morphological changes.....	110
4.3.2.	Fate of newly incorporated peptidoglycan.....	110
4.3.3.	Action of vancomycin on <i>B. subtilis</i> .....	111
	<b>Chapter 5.....</b>	<b>113</b>
	<b>Investigating the role of cell wall metabolism in the bactericidal effect of antibiotics .....</b>	<b>113</b>
5.1.	Introduction .....	113
5.1.1.	Aims of this chapter .....	114
5.2.	Results.....	114
5.2.1.	The role of glucosaminidases in cell wall antibiotic killing of <i>S. aureus</i> .....	114
5.2.1.1.	Killing dynamics .....	114
5.2.1.2.	Cell morphology.....	118
5.2.2.	The role of wall teichoic acid in cell wall antibiotic killing of <i>S. aureus</i> .....	128
5.2.2.1.	Growth dynamics.....	128
5.2.2.2.	Killing dynamics .....	128

5.2.2.3.	Cell morphology.....	131
5.2.2.4.	Fate of newly incorporated peptidoglycan .....	136
5.3.	Discussion .....	141
5.3.1.	The role of glucosaminidases in cell wall killing of <i>S. aureus</i> .....	141
5.3.2.	The role of wall teichoic acid in the cell wall antibiotic killing of <i>S. aureus</i> .....	144
	<b>Chapter 6.....</b>	<b>149</b>
	<b>General Discussion.....</b>	<b>149</b>
6.1.	Associated data .....	149
6.1.1.	The impact of cell wall antibiotics on peptidoglycan architecture.....	149
6.1.2.	Role of WalKR in cell wall antibiotic killing of <i>S. aureus</i> .....	151
6.2.	Beta-lactams vs. vancomycin: similarities and differences .....	151
6.3.	Model of beta-lactam and vancomycin killing of <i>S. aureus</i> .....	157
6.3.1.	Comparison to previous models.....	157
6.4.	Future directions .....	160
	<b>References.....</b>	<b>163</b>



## List of Figures

Figure 1.1. Overview of the gram-positive and gram-negative cell envelopes.....	3
Figure 1.2. <i>S. aureus</i> peptidoglycan chemical structure.....	5
Figure 1.3. Models of glycan chains organisation. ....	7
Figure 1.4. Models of peptidoglycan architecture in <i>B. subtilis</i> , <i>S. aureus</i> and <i>E. coli</i> . ....	9
Figure 1.5. Piecrust location and remodelling in <i>S. aureus</i> . ....	12
Figure 1.6. Schematic of peptidoglycan synthesis in <i>S. aureus</i> . ....	14
Figure 1.7. Diagram of LTA synthesis and turnover in <i>S. aureus</i> . ....	17
Figure 1.8. Peptidoglycan hydrolase activity. ....	18
Figure 1.9. Schematic of different bacterial division planes. ....	24
Figure 1.10. Diagram of the cell division machinery in (A) <i>E. coli</i> (B) <i>B. subtilis</i> . ....	26
Figure 1.11. Model of peptidoglycan insertion in <i>S. aureus</i> . ....	29
Figure 1.12. Representation of the proposed three-for-one peptidoglycan growth model. ....	31
Figure 1.13. Cell wall antibiotic targets along the peptidoglycan synthesis pathway. ....	33
Figure 1.14. Giesbrecht’s model of penicillin induced death. ....	35
Figure 1.15. Model of antibiotic-induced ROS killing. ....	37
Figure 3.1. Effect of 40 µg/mL (10 x MIC) methicillin on <i>S. aureus</i> SH1000 cell viability. ....	56
Figure 3.2. Effect of 40 µg/mL (10 x MIC) oxacillin on <i>S. aureus</i> SH1000 cell viability. ....	58
Figure 3.3. Effect of methicillin treatment on <i>S. aureus</i> SH1000 cell morphology (SIM images). ....	59
Figure 3.4. Effect of methicillin treatment on <i>S. aureus</i> SH1000 cell volume. ....	61
Figure 3.5. Effect of methicillin treatment on <i>S. aureus</i> SH1000 cell morphology (EM images). ....	63
Figure 3.6. Quantification of cell morphologies in EM images after methicillin treatment. ....	64
Figure 3.7. Effect of oxacillin treatment on <i>S. aureus</i> SH1000 cell morphology. ....	66
Figure 3.8. Effect of oxacillin treatment on <i>S. aureus</i> SH1000 cell volume. ....	67
Figure 3.9. Effect of methicillin treatment on di-peptide incorporation in <i>S. aureus</i> SH1000. ....	69
Figure 3.10. Quantification of the effect of methicillin treatment on di-peptide incorporation in <i>S. aureus</i> SH1000. ....	70
Figure 3.11. Effect of methicillin treatment on <i>S. aureus</i> SH1000 incorporation of <sup>14</sup> C- GlcNAc. ....	71
Figure 3.12. Effect of oxacillin treatment on TADA incorporation in <i>S. aureus</i> SH1000. ....	72
Figure 3.13. Quantification of the effect of oxacillin treatment on TADA incorporation in <i>S. aureus</i> SH1000. ..	73
Figure 3.14. Fate of newly synthesised peptidoglycan after methicillin treatment. ....	75
Figure 3.15. Quantification and model of fate of newly synthesised material over 60 minutes. ....	79

Figure 3.16. Quantification of fate of newly synthesised material after methicillin treatment. ....	80
Figure 3.17. Methicillin killing of <i>B. subtilis</i> . ....	82
Figure 3.18. Effect of methicillin on <i>B. subtilis</i> 168 HR morphology. ....	83
Figure 3.19. The effect of methicillin on <i>B. subtilis</i> 168HR cell length and width. ....	85
Figure 4.1. Effect of 40 µg/mL (10 x MIC) vancomycin on <i>S. aureus</i> SH1000 cell viability. ....	91
Figure 4.2. Effect of vancomycin treatment on <i>S. aureus</i> SH1000 cell morphology (SIM images). ....	92
Figure 4.3. Effect of vancomycin treatment on <i>S. aureus</i> SH1000 cell volume. ....	93
Figure 4.4. Effect of vancomycin treatment on SH1000 cell morphology (EM images). ....	95
Figure 4.5. Quantification of cell morphologies in EM images after vancomycin treatment. ....	97
Figure 4.6. Effect of vancomycin treatment on di-peptide incorporation in <i>S. aureus</i> SH1000. ....	98
Figure 4.7. Quantification of the effect of vancomycin treatment on di-peptide incorporation in <i>S. aureus</i> SH1000.....	99
Figure 4.8. Effect of vancomycin treatment on <i>S. aureus</i> SH1000 incorporation of <sup>14</sup> C- GlcNAc. ....	100
Figure 4.9. Fate of newly synthesised peptidoglycan after vancomycin treatment. ....	102
Figure 4.10. Quantification of the effect vancomycin on the fate of newly synthesised peptidoglycan.....	105
Figure 4.11. Vancomycin killing of <i>B. subtilis</i> . ....	106
Figure 4.12. Effect of vancomycin on <i>B. subtilis</i> 168 HR morphology. ....	107
Figure 4.13. The effect of vancomycin on <i>B. subtilis</i> 168 HR cell length and width. ....	109
Figure 5.1. Effect of methicillin on <i>S. aureus</i> glucosaminidase single mutant cell viability. ....	115
Figure 5.2. Effect of methicillin on the viability of triple glucosaminidase mutants. ....	116
Figure 5.3. Effect of vancomycin on the viability of triple glucosaminidase mutants. ....	117
Figure 5.4. Effect of methicillin on single glucosaminidase mutant morphology. ....	119
Figure 5.5. Effect of methicillin on the cell volume of single glucosaminidase mutants. ....	121
Figure 5.6. Effect of methicillin on triple glucosaminidase mutant cell morphology. ....	122
Figure 5.7. Effect of methicillin on the cell volume of triple glucosaminidase mutants. ....	124
Figure 5.8. Effect of vancomycin on triple glucosaminidase mutant cell morphology. ....	125
Figure 5.9. Effect of vancomycin on the cell volume of triple glucosaminidase mutants. ....	127
Figure 5.10. Growth curve of <i>S. aureus</i> SH1000 <i>tarO</i> compared to the wild-type.....	129
Figure 5.11. Effect of methicillin and vancomycin on <i>S. aureus</i> SH1000 <i>tarO</i> cell viability. ....	130
Figure 5.12. Effect of methicillin and vancomycin on <i>S. aureus</i> SH1000 <i>tarO</i> cell morphology (SIM images) ..	132
Figure 5.13. Effect of methicillin and vancomycin on <i>S. aureus</i> SH1000 <i>tarO</i> cell morphology (EM images). ..	134

Figure 5.14. Quantification of cell morphologies in EM images after treatment of <i>S. aureus</i> SH1000 <i>tarO</i> with methicillin or vancomycin. ....	135
Figure 5.15. Fate of newly synthesised peptidoglycan in <i>S. aureus</i> SH1000 <i>tarO</i> after methicillin or vancomycin treatment. ....	138
Figure 5.16. Quantification of fate of newly synthesised material over 60 minutes. ....	140
Figure 5.17. Model of methicillin induced killing of <i>S. aureus</i> SH1000 <i>sagB</i> . ....	142
Figure 5.18. Model of vancomycin and methicillin induced killing of <i>S. aureus</i> SH1000 <i>tarO</i> . ....	147
Figure 6.1. Changes to cell wall thickness after treatment with methicillin (meth) or vancomycin (vanc). ....	150
Figure 6.2. Effect of methicillin and vancomycin on the number of pores present on the inside surface of sacculi. ....	152
Figure 6.3. Effect of methicillin treatment on <i>S. aureus</i> SH1000 <i>walkR</i> viability in the presence and absence of IPTG. ....	153
Figure 6.4. Effect of vancomycin on <i>S. aureus</i> SH1000 <i>walkR</i> viability in the presence of absence of IPTG. ....	154
Figure 6.5. Model of the effect of methicillin and vancomycin treatment on <i>S. aureus</i> SH1000. ....	158



## List of Tables

Table 1.1. Staphylococcal hydrolases and their function. ....	20
Table 2.1. Antibiotic stock solutions and solvents. ....	41
Table 2.2. Stock solution information for the chemicals and enzymes used in this study. ....	43
Table 2.3. <i>S. aureus</i> strains, genotype and source. ....	44
Table 2.4. <i>B. subtilis</i> strain, genotype and source. ....	45
Table 6.1. Synthesis and hydrolysis requirements for <i>S. aureus</i> survival.....	155



# Chapter 1

## Introduction

### 1.1. *Staphylococcus aureus*

*Staphylococcus aureus* is a non-motile, gram-positive, spheroid bacterium approximately 1 µm in size. It is an opportunistic pathogen that can also live as a commensal organism. In humans, *S. aureus* is found in the anterior nares (Stapleton & Taylor, 2002), where approximately 20% of the population are permanent carriers of *S. aureus*, and 60% are intermittent carriers (Kluytmans, 1997). *S. aureus* opportunist infections are classified into two categories: community-acquired (CA) and hospital-acquired (HA), including endocarditis, pneumonia, toxic shock syndrome, mastitis and skin infections (Boucher & Corey, 2008).

Due to its opportunistic nature, patients with HIV, cancer, type I diabetes, surgical patients and intravenous drug users are at higher risk of developing *S. aureus* infections (Lowy, 1998). *S. aureus* bacteraemia has a case fatality rate of between 15 to 50%, with an incidence ranging from 10 to 30/100000 people per year in industrialised countries (Tong et al., 2015). *S. aureus* is the leading cause of skin and soft tissue infections (SSTIs), infective endocarditis (IE) and joint infections. The mortality rate for IE caused by *S. aureus* is between 22 and 66% (Tong et al., 2015). *S. aureus* can also cause pneumonia, particularly in hospitalised patients, accounting for >40% of health care-associated pneumonia cases in the US (Tong et al., 2015). *S. aureus* pneumonia infections often occur in patients with comorbid illnesses leading to poor prognosis. It is also associated with pneumonia infections in patients with influenza. For example, half the patients hospitalised with influenza A H1N1 in France during the 2009 pandemic had a bacterial coinfection. 31% of those coinfections were caused by *S. aureus* (Cuquemelle et al., 2011). These infections are associated with the cytotoxin Pantone-Valentine leucocidin (PVL), which enhances virulence (Gillet et al., 2007).

*S. aureus* is most renowned for its antibiotic resistance, with Methicillin-Resistant *S. aureus* (MRSA) and more recently Vancomycin-Resistant *S. aureus* (VRSA) as major health-care threats. In 2017/2018 Public Health England reported 12,784 *S. aureus* infections in England, which is a 3.7% increase from 2016/17. 6.6% of the reported infections were caused by MRSA.

### 1.2. Cell Wall

The bacterial kingdom is divided into two main categories according to their cell wall structure. These two categories can be differentiated through gram-staining and are classified as gram-positive (cells are stained) or gram-negative (cells are not stained).

### 1.2.1. Gram-negative

Gram-negative cell walls are made up of three distinct layers: the outer-membrane (OM), the peptidoglycan cell wall and the inner membrane (IM) (Figure 1.1). The space between the inner membrane and the outer-membrane, within which the peptidoglycan cell wall is localised, is called the periplasm (Silhavy et al., 2010). Both the OM and the IM are lipid bilayers with differing compositions. The inner leaflet of the OM is composed of phospholipids and the outer leaflet is composed of glycolipids, mainly lipopolysaccharides (LPS). The IM is a phospholipid bilayer (Silhavy et al., 2010). The peptidoglycan layer found in the periplasm serves as an exoskeleton responsible for maintenance of cell shape. In gram-negatives, the peptidoglycan layer is 2-6 nm thick (Vollmer & Seligman, 2010). The periplasm plays a wide range of roles in cell metabolism from protein transport, to turgor pressure maintenance and cell signalling.

### 1.2.2. Gram-positive

Gram-positive bacteria have a cytoplasm containing phospholipid bilayer encapsulated within a thick outer-layer of peptidoglycan (Silhavy et al., 2010) (Figure 1.1). Gram-positive organisms do not have an outer membrane and have a peptidoglycan layer 20-35 nm thick (Schleifer & Kandler, 1972). The gram-positive cell wall contains teichoic acids, which are long anionic polymers. There are two types of teichoic acids: wall teichoic acids (WTA) and lipoteichoic acids (LTA). WTA are anchored in the peptidoglycan and LTA are anchored in the cell membrane (Silhavy et al., 2010). The cell surface in gram-positives is also decorated with a range of proteins.

Since there is only one lipid bilayer in gram-positive organisms, there is no equivalent to the periplasm present in gram-negative organisms. There is however a space between the lipid bilayer and the peptidoglycan layer: the gram-positive periplasm. Due to its location completely exterior to the cytoplasm and cell membrane, it will be referred to as the exoplasm in this thesis. A gram-positive periplasm, or exoplasm, was first proposed in *S. aureus* in the 1980s (Umeda, et al., 1987). Through separation of cell fractions an exoplasm in *B. subtilis* was hypothesised in 1995 (Merchante et al., 1995). *B. subtilis* and *S. aureus* exoplasms were later confirmed using cryo-transmission electron microscopy (Cryo-TEM) (Matias & Beveridge, 2005; Matias & Beveridge, 2006).

Wall teichoic acids are composed of a disaccharide unit and a polyribitol phosphate (RboP) or polyglycerol phosphate (GroP) chain (Silhavy et al., 2010). RboP and GroP chains vary in length and can be up to 60 repeats long. WTA are anchored in the peptidoglycan layer via a phosphodiester linkage to the C6-hydroxyl of N-acetylmuramic acid (MurNAc) residues. WTA are decorated with D-alanyl esters and/or monosaccharides, modifying their properties and function. WTA are involved in cation homeostasis, autolysin regulation and presentation of envelope proteins among other roles (Neuhaus & Baddiley, 2003). WTA can be modified through D-alanine and monosaccharides on the ribitol phosphate repeats. D-alanylation changes the net

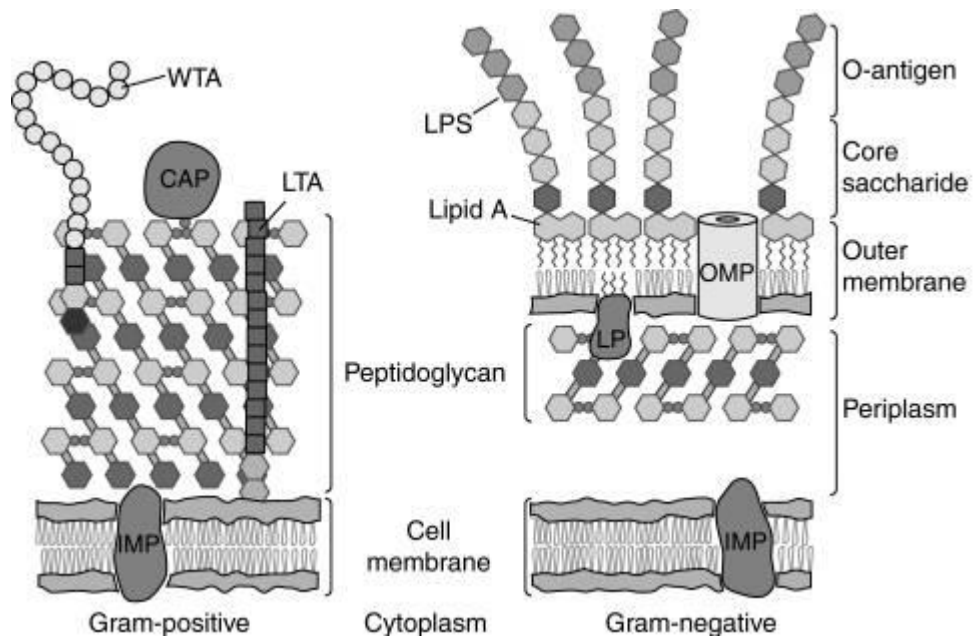


**Figure 1.1. Overview of the gram-positive and gram-negative cell envelopes.** WTA – wall teichoic acid; CAP – covalently attached protein; LTA – lipoteichoic acid; IMP – inner membrane protein; LPS – lipopolysaccharide; LP – lipoprotein; OMP – outer membrane protein. Adapted from (Silhavy et al., 2010).

charge of WTA by introducing positively charged amines. The level of D-alanylation varies according to environmental factors including growth media pH, NaCl concentration and temperature (Neuhaus & Baddiley, 2003).

The role of WTA in the cell is not fully understood but some of its roles in the cell wall metabolism are discussed here. The absence of WTA leads to a decrease in peptidoglycan crosslinking due to interactions with the peptidoglycan metabolism (Atilano et al., 2010). A decrease in crosslinking leads to an increased susceptibility to hydrolysis. The lack of D-alanylation also leads to increased sensitivity to glycopeptides and lytic activity of some host enzymes. WTAs therefore play an important role in protecting peptidoglycan from hydrolysis.

Lipoteichoic acids are anchored in the cell membrane and do not extend beyond the peptidoglycan outer layer. LTA are composed of a glycolipid anchor and a GroP chain (Percy et al., 2014). Like WTA, the GroP chain of LTA is often modified with D-alanyl or glycosyl groups. In *S. aureus* every 9<sup>th</sup> lipid in the outer leaflet of the cell membrane is LTA (Koch et al., 1984). On average, *S. aureus* LTA are 25 GroP units long. LTA and WTA are crucial for the maintenance of a negative charge from the cell membrane through to the outer surface of the peptidoglycan layer. The crucial role teichoic acids play in maintenance of cell viability is demonstrated by the fact that, although neither WTA nor LTA are essential on their own, cells cannot survive without any teichoic acids (Silhavy et al., 2010).

### 1.3. Peptidoglycan chemical structure

Peptidoglycan is composed of a sugar backbone cross-linked by peptide side chains (Figure 1.2). The backbone is a chain of alternating N-acetylglucosamine (GlcNAc) and N-acetylmuramic acid (MurNAc) linked via a  $\beta$ -1-4-glycosidic bond (Vollmer, 2008). The composition of the glycan strand is maintained between species. There are however major variations in the length of glycan strands found in different bacteria. *S. aureus* is known to have particularly short glycan strands due to high glucosaminidase activity. Glucosaminidases are a class of peptidoglycan hydrolases that cleave the peptidoglycan sugar backbone. The average glycan chain in *S. aureus* is 6 disaccharides long (Boneca, et al., 2000). In contrast, *B. subtilis* peptidoglycan contains glycan chains up to 5000 disaccharides long (Hayhurst et al., 2008).

Glycan strands can undergo different secondary modifications such as N-deacetylation, N-glycolylation and O-acetylation (Vollmer, 2008). Both GlcNAc and MurNAc can be deacetylated by peptidoglycan deacetylases giving GlcN and MurN. Deacetylation of peptidoglycan leads to decrease sensitivity to the muramidase lysozyme (Araki et al., 1971). Lysozyme is part of the human immune response, therefore N-deacetylation of the glycan strand will aid in infection of a host. O-acetylation also protects cells from the action of lysozyme. O-acetylation involves the addition of an extra acetyl group to the C6-OH of MurNAc (Bera et al., 2007). N-

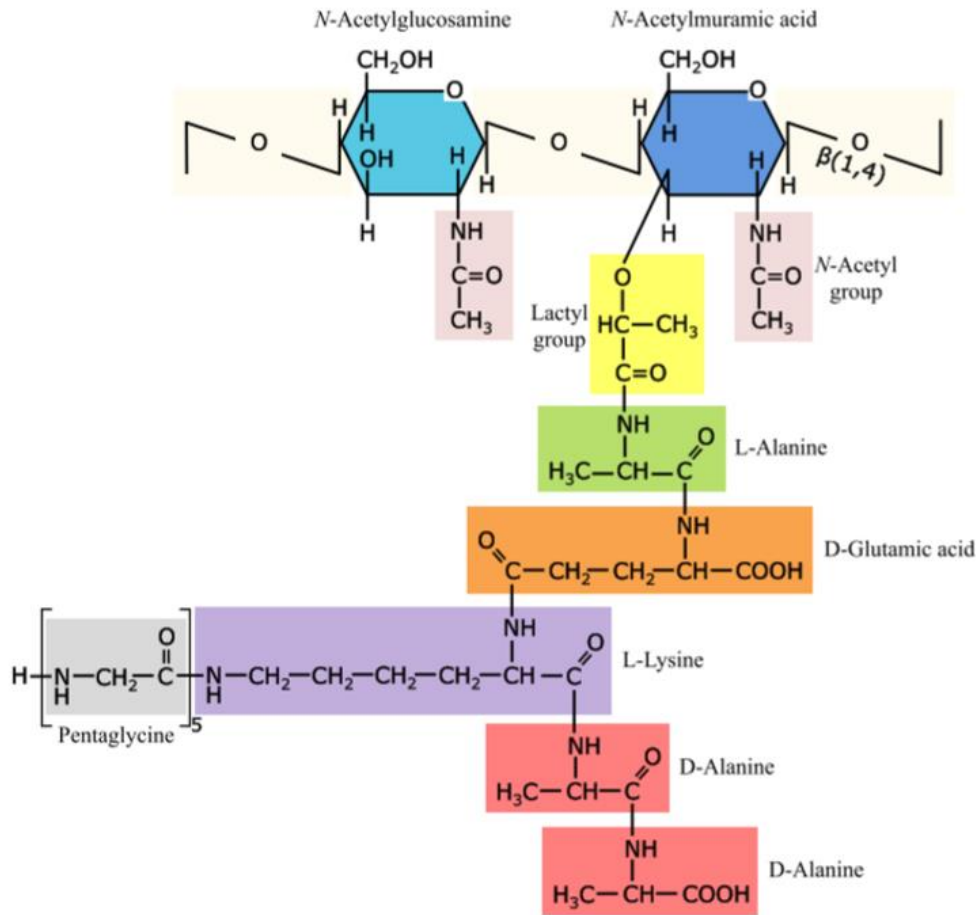


**Figure 1.2. *S. aureus* peptidoglycan chemical structure.** Representation of a disaccharide with an attached peptide side chain. Reproduced from (Panchal, 2018).

glycolylation involves the modification of MurNAc, with a change of its acetate group into a glycolyl group. The biological role of N-glycolylation is not well understood. It has been hypothesised that it plays a role in cell envelope stability (Vollmer, 2008).

Each MurNAc residue in peptidoglycan has its D-lactoyl group substituted by a peptide side chain. Peptide side chains exhibit a great amount of variability between organisms. The most common peptide side chain composition is L-Ala-γ-D-Glu-*meso*-DAP-D-Ala-D-Ala (Bouhss et al., 2008). The third amino acid is the most variable, it is often L-lysine in gram-positive organisms although other di- or mono-amino acids can also be found in this position (Vollmer et al., 2008). The last D-Ala residue is often lost in mature peptidoglycan or altered. Substitution of the terminal D-Ala with D-lactate or D-Ser confers vancomycin resistance (Courvalin, 2006; Vollmer et al., 2008). The peptide side chains are most commonly crosslinked by forming a bond between the third amino acid of one chain and the 4<sup>th</sup> amino acid of another chain. Crosslinks can also be indirect, through amino acid bridges ranging from one to seven residues long (Schleifer & Kandler, 1972; Vollmer et al., 2008). *S. aureus* has particularly high levels of crosslinking in its peptidoglycan (70-80%) mainly due to PBP4 activity (Snowden & Perkins, 1990). Peptide side chains act as anchors for many surface proteins.

#### 1.4. Peptidoglycan architecture

Despite our in depth understanding of peptidoglycan chemical structure, there are still many gaps in our understanding of peptidoglycan architecture and synthesis. Studies of peptidoglycan architecture have overwhelmingly been carried out using purified sacculi. Sacculi were imaged by electron microscopy (EM), electron cryo tomography (ECT) and atomic force microscopy (AFM) allowing for the proposal of several different architectural models.

##### 1.4.1. Models of glycan chain organisation

Two models of glycan chain organisation have been proposed: the planar model and the scaffold model (Figure 1.3, panel C). In the planar model the glycan chains run parallel to the cell membrane and the short axis of the cell (Koch, 1998a). This orientation of glycan chains is supported by the fact that rod-shaped sacculi have greater elasticity in the direction of the long axis of the cell than in the direction of the short axis of the cell (Yao et al., 1999). The difference in elasticity is due to the peptide side chains having greater flexibility than the sugar backbone (Vollmer & Höltje, 2004). It was originally hypothesised that the glycan strands formed elongated straight helices from which the peptide side chains extended perpendicularly to each other (Vollmer & Höltje, 2004) (Figure 1.3, Panel A). In Koch's updated model, glycan strands are arranged in a zigzag pattern (Koch, 1998b). The peptide side chains in the same plane are crosslinked and the smallest, hexagonal holes formed in this structure are named tessera (Figure 1.3, Panel B). When evenly distributed across the cell wall, tessera should not affect the overall stability of the peptidoglycan layer (Koch, 1998b). Due to glycan strands

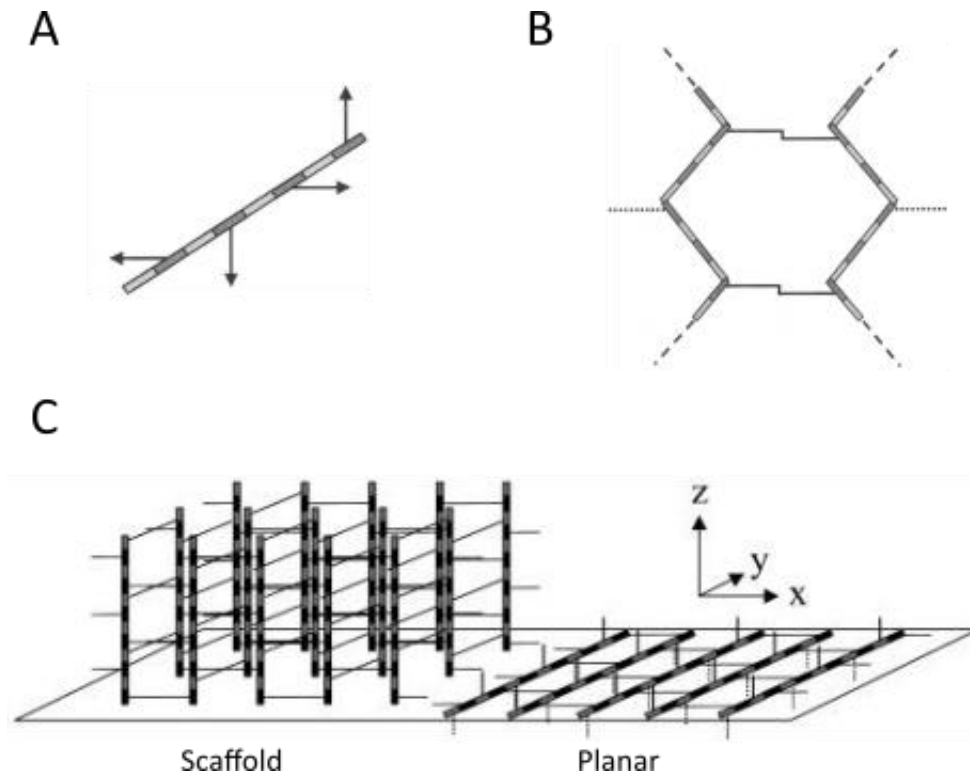


**Figure 1.3. Models of glycan chains organisation.** Dark grey/black bars represent MurNAc residues and light grey bars represent GlcNAc. (A) Representation of a helical glycan strand with peptide side chains (arrows) perpendicular to each other. Every other peptide side chain is in the same plane. (B) Representation of crosslinked zigzag glycan strands forming a tessera. (C) Representation of the scaffold and planar models of glycan strand organisation. Adapted from (Vollmer & Höltje, 2004).

being shorter than the circumference of the cell and crosslinking percentages being lower than 50% in some organisms, larger holes would exist in the peptidoglycan layer based on this model (Koch, 1998). These would be made up of fused tessera (smaller hexagonal holes). In gram-negative organisms, the cell wall is thought to be made up of one stress bearing layer of peptidoglycan with unloaded newly synthesised peptidoglycan on the inside and old, hydrolysed material on the outside. The gram-positive cell wall is proposed to consist of several linked layers of planar peptidoglycan (Vollmer & Höltje, 2004).

The scaffold model of peptidoglycan structure proposes that the glycan strands run perpendicular to the cytoplasmic membrane with the cross-linked peptides side chains parallel to the cell membrane (Dmitriev et al., 2004; Dmitriev et al., 1999; Dmitriev et al., 2003) (Figure 1.3, Panel C). Several different problems arise with this model. Through knowledge of the average glycan chain length and the amount of cell wall material present in a cell, it has been argued that there is not enough peptidoglycan in an *E. coli* cell to cover the entire cell surface if it were arranged in a scaffold structure (Vollmer & Höltje, 2004). Additionally, the peptidoglycan layer in *E. coli* is thought to be between 2.5 and 7 nm thick and to achieve this thickness in the scaffold model, glycan chains would need to be 2.5 to 7 disaccharides long. This is at odds with an average glycan chain length of 25-30 nm (Vollmer & Höltje, 2004).

#### 1.4.2. Peptidoglycan architecture in gram-negative bacteria

Gram-negative bacteria have a thin peptidoglycan layer located in the periplasm. It is easier to study cell wall structure using this thin cell wall than using the thick gram-positive cell wall (Turner et al., 2014). ECT studies of *E. coli* and *C. crescentus* revealed a single layer of peptidoglycan making up the cell wall (Gan et al., 2008). Tubular structures, thought to be glycan strands due to their length, were observed along the plane of the sacculus and approximately parallel to the short axis of the cell (Gan et al., 2008). This data supports the planar model of glycan chain organisation. The pattern observed by ECT appeared uniform across the entire sacculi but the observed tubes were not regularly spaced or running exactly parallel to each other (Gan et al., 2008).

More recent work on gram-negative peptidoglycan architecture was carried out using AFM (Turner et al., 2013; Turner et al., 2018). AFM images confirmed the presence of peptidoglycan features running in the plane of the sacculi. Large bands (too wide to be glycan strands) were observed perpendicular to the long axis of the cell (Figure 1.4) (Turner et al., 2013). These bands appeared to be formed by more loosely or densely packed mesh. More recent, higher resolution AFM shows circumferential orientational order of long glycan chains in rod-shaped *E. coli* (Turner et al., 2018). Pores in this mesh were too big to fit the tessera model (Koch, 1998; Turner et al., 2013). The presence of these different bands also leads to a non-uniform thickness of peptidoglycan across the sacculus. Using this information, a new model of peptidoglycan insertion was proposed, whereby new peptidoglycan is inserted in the most porous regions. In this model, growth by elongation occurs through hydrolysis of the less porous bands (Turner et al., 2013). Spherical *E. coli* cells were

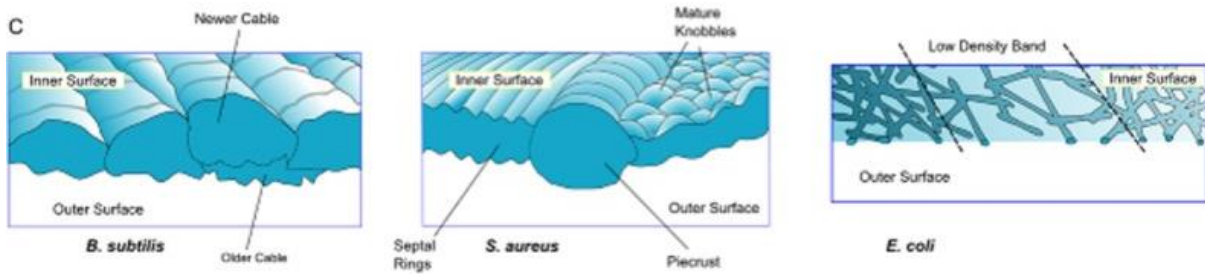


Figure 1.4. Models of peptidoglycan architecture in *B. subtilis*, *S. aureus* and *E. coli*. Adapted from (Turner et al., 2014).

generated, and their peptidoglycan studied. Results showed that cells had shorter glycan chains that showed reduced orientational order, confirming that glycan chain length and organisation impact cell shape (Turner et al., 2018).

#### 1.4.3. Peptidoglycan architecture in gram-positive bacteria

Gram-positive organisms have thicker peptidoglycan layers than gram-negative bacteria. Due its thickness, the gram-positive cell wall is thought to be composed of several layers of peptidoglycan, complicating architectural studies. Proposed peptidoglycan architectures for different gram-positive cell shapes are discussed below.

##### 1.4.3.1. Peptidoglycan architecture of gram-positive rods

*B. subtilis* is the most studied gram-positive rod and has served as the main model for their peptidoglycan architecture. *B. subtilis* has exceptionally long glycan chains, with strands up to 5000 disaccharides long (Hayhurst et al., 2008). Extremely long glycan chains do not fit the scaffold cell wall architecture model where glycans are oriented perpendicular to the cell membrane. AFM was carried out on *B. subtilis* sacculi to help understand glycan strand organisation (Hayhurst et al., 2008). AFM revealed a rough exterior of the cell wall and cable structures on the inside of the cell wall. Previous EM data revealed striations running perpendicular to the short axis of the cell thought to be glycan strands (Verwer & Nanninga, 1976). The wide cable structures were interpreted as coils of several glycan strands, allowing for packaging of the long chains present in *B. subtilis* (Hayhurst et al., 2008). The lack of tubular structures visible on the outside of the cell wall is thought to be due to it consisting of older, more hydrolysed material.

Using ECT to study *B. subtilis* peptidoglycan architecture, Beeby et al. did not identify cable structures in the cell wall (Beeby et al., 2013). Peptidoglycan appeared to be uniformly dense having a smooth inner surface. A gram-negative-like model was proposed with inside-to-outside peptidoglycan synthesis (Beeby et al., 2013). ECT has a high signal to noise ratio, which hinders visualisation of internal structures and is a major limitation of this technique (Turner et al., 2014). The proposed model does not consider previous AFM data. Further structural studies are required to better develop our understanding of *B. subtilis* cell wall architecture.

##### 1.4.3.2. Peptidoglycan architecture of gram-positive ovococci

Ovococci have an elongated cell shape compared to cocci bacteria. *S. pneumoniae*, *Lactococcus lactis* and *Enterococcus faecalis* have been used to investigate cell wall architecture in ovococci (Wheeler et al., 2011). Ovococci have long glycan chains with 44-57% being > 50 disaccharides long (Wheeler et al., 2011). This is close to the 53% of glycan chains over 50 disaccharides long in *B. subtilis* compared to only 14% in *S. aureus*. These results do not fit with a scaffold model of peptidoglycan organisation. Using AFM of sacculi, glycan strands were found to be orientated parallel to the short axis of the cell and the cell membrane (as seen in

rods). The exterior of the cell wall was smooth, unlike the knobby and rough surfaces observed in rods and cocci (1.4.3.1, 1.4.3.3). Annular features thought to be associated with growth and division were revealed. Differences have been observed between the different cocci. *E. faecalis* and *L. lactis* had a single growth annulus, whereas *S. pneumoniae* appeared to have three (Wheeler et al., 2011). These differences were attributed to differences in the cell cycle of all three organisms.

#### 1.4.3.3. Peptidoglycan architecture of *S. aureus* (gram-positive cocci)

Studies of *S. aureus* peptidoglycan architecture were carried out using whole cells and sacculi (Touhami et al., 2004; Turner et al., 2010). Two distinct peptidoglycan organisations are visible in *S. aureus*: knobby material and concentric rings (Figure 1.4). The knobby architecture was thought to display a honeycomb pattern after high resolution AFM whole cell studies (Touhami et al., 2004). Studies of purified sacculi do not display this, suggesting that teichoic acids and cell wall proteins may be responsible for the pattern. The newly synthesised septal plate displays a concentric ring architecture. After cell division, the septum, which is less voluminous than the hemisphere it becomes, needs to be remodelled. Through this remodelling process, the peptidoglycan architecture changes from concentric rings to mature peptidoglycan with a knobby architecture (Turner et al., 2010). The growth of the new cell wall and the ensuing change in peptidoglycan architecture is thought to be due to the combined action of hydrolases and turgor pressure. There is no data suggesting any specific glycan chain orientation in *S. aureus* (Turner et al., 2014).

The two peptidoglycan architectures are separated by a thick ring of peptidoglycan known as the piecrust (Turner et al., 2010). The piecrust feature is posited to play a role in the correct localisation of the next division plane (Figure 1.5). When *S. aureus* divides, the cell splits in the plane of a newly formed piecrust and each daughter cell will inherit half of the piecrust feature. This is then named a rib, as it is less distinct than a piecrust. Upon formation of the following piecrust and cell division, the full rib from the previous cycle will be halved and the cell will get a new rib going all around the cell from the split piecrust from the current cell division cycle (Turner et al., 2010). The next division cycle will give the cells a quarter rib, a half rib and a whole rib (Figure 1.5). The quarter-rib is thought to dictate the location of the next division plane (a new piecrust will be synthesised in this plane). All the ribs intersect at roughly right angles. The presence of the ribs is proposed to allow *S. aureus* to always divide in 3 successive orthogonal planes (Turner et al., 2010).

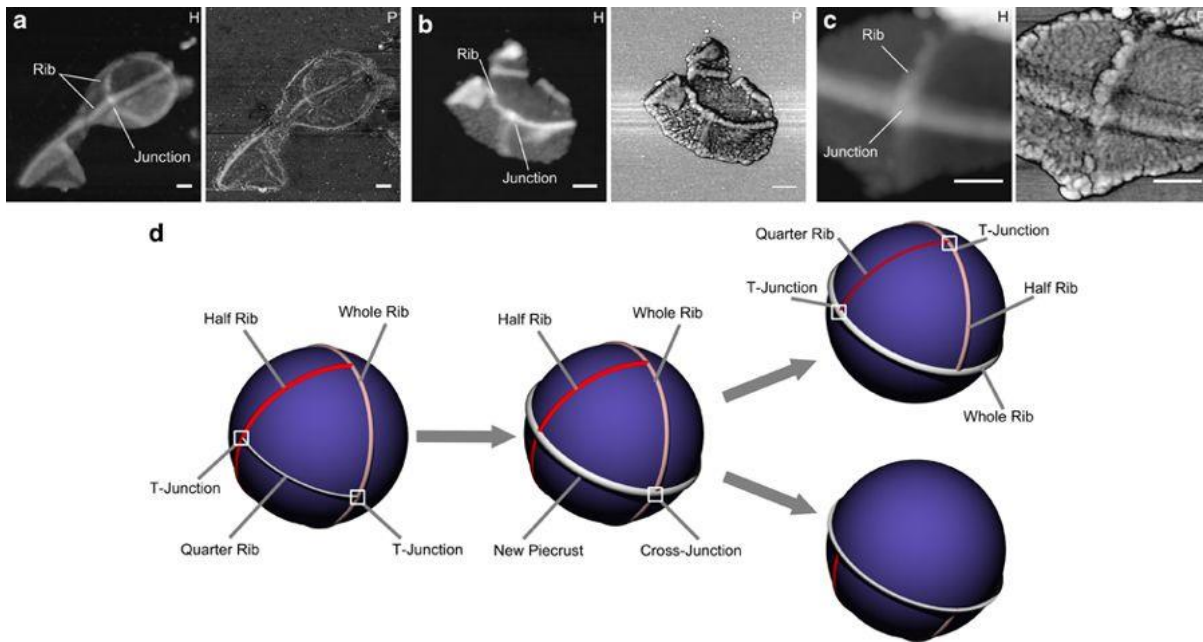


**Figure 1.5. Piecrust location and remodelling in *S. aureus*.** Ribs are the remnants of piecrusts from previous generations. A new piecrust is formed in the plane of the quarter rib, this is the first step of septum formation. Upon cell division, the rib will be split in two and the daughter cells will have a new rib pattern. This pattern specifies the next division plane (same plane as the new quarter rib). (a, b, c) AFM height (H) and phase (P) images showing ribs and rib junctions. (d) Model of piecrust remodelling throughout the cell cycle. Reproduced from (Turner et al., 2010).

## 1.5. Cell wall synthesis

### 1.5.1. PG synthesis

Peptidoglycan synthesis can be split into four stages: precursor synthesis, assembly of the lipid linked muropeptides, flipping of lipid II across the membrane, monomer polymerisation (Typas et al., 2012)(Figure 1.6). The peptidoglycan synthesis pathway is conserved in gram-positive and gram-negative organisms.

#### 1.5.1.1. Precursor synthesis

Peptidoglycan precursor synthesis takes place in the cytoplasm. The first step in precursor synthesis is the transfer of enolpyruvyl from phosphoenolpyruvate (PEP) to uridine diphosphate (UDP)-GlcNAc. This reaction is catalysed by MurA and produces enolpyruvyl UDP-GlcNAc (Lovering et al., 2012). Next, enolpyruvyl UDP-GlcNAc is converted into UDP-MurNAc. This step is catalysed by the reductase MurB and is NADPH-dependent (Lovering et al., 2012). The pentapeptide side chain is then assembled onto UDP-MurNAc in a stepwise manner. The assembly is catalysed by four highly conserved Mur ligases: MurC, MurD, MurE and MurF (Bouhss et al., 1997; Eveland et al., 1997). MurC catalyses the addition of L-Ala to UDP-MurNAc generating UDP-MurNAc-L-Ala. D-Glu is then added onto the MurC product by MurD. MurE catalyses the addition of the third side chain peptide. The third peptide varies in different species, with the addition of meso-DAP in *E. coli* and addition of L-Lys in *S. aureus*. The final two D-Ala units are added to the peptide side chain in one step as a D-Ala-D-Ala dipeptide. This final step is catalysed by MurF (Lovering et al., 2012).

#### 1.5.1.2. Lipid II assembly

The next step of peptidoglycan synthesis involves transfer of the UDP-MurNAc-pentapeptide onto the undecaprenyl phosphate carrier Und-P, which is anchored in the membrane (Lovering et al., 2012). This step is catalysed by MraY, a membrane protein (Bouhss et al., 2004). The membrane-associated product of this reaction is commonly known as lipid I. Finally, MurG catalyses the attachment of UDP-GlcNAc to lipid I giving lipid II. The MraY and MurG reactions are coupled to avoid unnecessary accumulation of precursors. This cooperation allows the cell to have a small pool of lipid I and lipid II: approximately 700 molecules/cell and 2000 molecules/cell respectively in *E. coli* (van Heijenoort et al., 1992).

#### 1.5.1.3. Flipping of lipid II across the membrane

Lipid II is found on the inside of the membrane and needs to be flipped across the membrane before

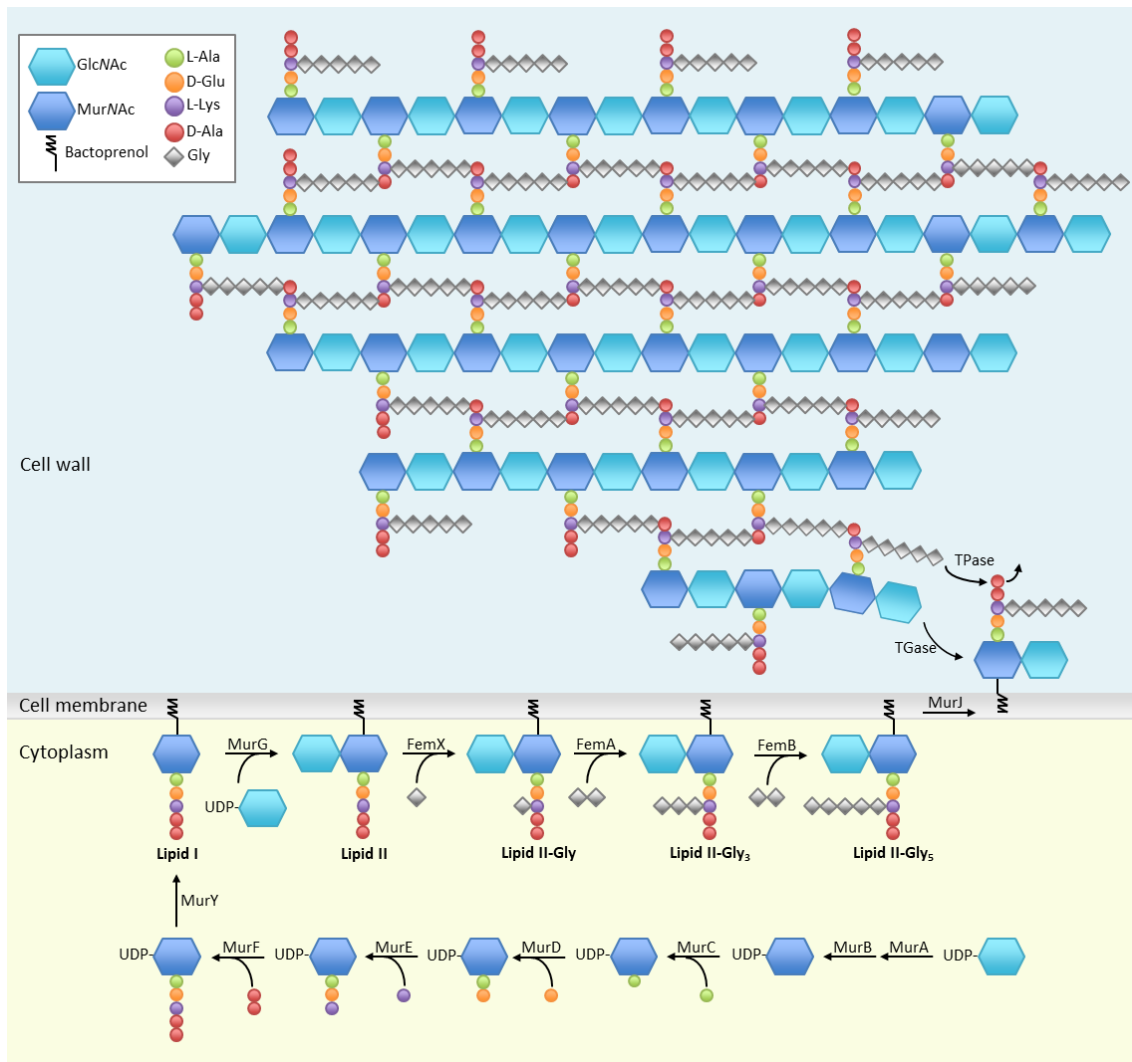


**Figure 1.6. Schematic of peptidoglycan synthesis in *S. aureus*.** Precursor synthesis occurs in the cytoplasm. Precursors are then flipped across the membrane before being added to the cell wall peptidoglycan by transglycosylase (TGase) and transpeptidase (TPase) reactions. Adapted from (Typas et al., 2012; Wacnik, 2016).

it can be polymerised into peptidoglycan in the periplasm or exoplasm. The flippase is required to create a conduit for lipid II (hydrophilic) to cross the hydrophobic centre of the cell membrane lipid bilayer (Ruiz, 2015). The mechanism by which flipping occurs is also poorly understood. There was long a debate around whether FtsW/RodA type proteins or MurJ type proteins carry out this role. Recent research has elucidated other cellular roles of FtsW/RodA proteins in *S. aureus*, suggesting that MurJ is the likely flippase (Taguchi et al., 2019). An overview of the different flippase candidates will be presented here.

FtsW, a member of the shape, elongation, division and sporulation (SEDS) family of proteins, was shown to translocate lipid II across the membrane in *E. coli* membrane vesicles (Mohammadi et al., 2011). MurJ showed no such activity in this model. There is no evidence to date showing FtsW flippase activity *in vivo* and inactivation of FtsW and RodA *in vivo* does not inhibit lipid II translocation (Sham et al., 2014). FtsW has now also been shown to have glycosyltransferase activity *in vitro* (Cho et al., 2016; Taguchi et al., 2019).

MurJ was identified as a candidate lipid II translocase in *E. coli* through a bioinformatics screen (Ruiz, 2008). MurJ is a member of the multidrug/oligo-saccharidyl-lipid/polysaccharide (MOP) exporter family of proteins. MurJ depletion is lethal in *E. coli* and leads to a decrease in peptidoglycan synthesis coupled with an increase in precursors, including lipid intermediates (Inoue et al., 2008). Deletion of MurJ *in vivo* results in lack of lipid II translocation to the outside of the inner-membrane in *E. coli* (Sham et al., 2014).

#### 1.5.1.4. Monomer polymerisation

Once lipid II has been flipped to the outside of the cell membrane, it is polymerised into glycan strands by transglycosylases. There are monofunctional and bifunctional transglycosylases. Bifunctional transglycosylases also have transpeptidase activity and are known as Class A PBPs (Typas et al., 2012). PBP2 is the only bifunctional PBP in *S. aureus*, which also possesses several monofunctional transglycosylases: Mgt, SgtA and FtsW (Reed et al., 2011; Taguchi et al., 2019). In bacteria with the Rod system, RodA also functions as a transglycosylase (Emami et al., 2017). Lipid II polymerisation takes place through the formation of a glycosidic bond between MurNAc on the growing peptidoglycan strand and the GlcNAc residue of lipid II (Fuchs Cleveland & Gilvarg, 1976; Ward & Perkins, 1973). At this stage, the Und-P carrier is recycled back into the cytoplasm for dephosphorylation and use in peptidoglycan precursor synthesis (van Dam et al., 2009).

The next step of peptidoglycan synthesis is crosslinking of the newly formed peptidoglycan strands (Lovering et al., 2012). Peptide side chains are linked via transpeptidase activity. Class B PBPs are monofunctional transpeptidases that carry out this activity along with the bifunctional Class A PBPs. The transpeptidase noncovalently binds the donor strand before forming an acyl-enzyme intermediate, releasing the terminal D-Ala in the process (Lovering et al., 2012). The acyl-enzyme intermediate is then crosslinked with the acceptor

strand (another peptide side chain). Alternatively, the acyl-enzyme intermediate can be hydrolysed by water, releasing a shortened peptide (carboxypeptidation) (Lovering et al., 2012).

### 1.5.2. WTA synthesis

Genes involved in WTA biosynthesis in *S. aureus* are called *tar* (teichoic acid ribitol) genes. WTA synthesis begins with TarO, which transfers GlcNAc onto a membrane linked Und-P carrier lipid (Brown et al., 2008). TarA then transfers ManNAc onto the C4 hydroxyl of GlcNAc forming ManNAc- $\beta$ -(1,4)-GlcNAc-pp-udp. Next, glycerol-3-phosphate is added to the C4 hydroxyl of the ManNAc residue by TarB. TarF adds one GroP to the disaccharide unit. Finally, TarL is responsible for building the polyribitol-phosphate polymer through addition of CDP-ribitol monomers (Brown et al., 2008). Deletion of *tarO* in *S. aureus* is not lethal allowing for the study of a population lacking the wall teichoic acid biosynthetic pathway and therefore lacking WTAs.

### 1.5.3. LTA synthesis

The first step of LTA biosynthesis involves production of the glycolipid anchor in the cytoplasm by Ypfp, a glycosyltransferase (Percy & Gründling, 2014)(Figure 1.7). The glycolipid anchor is then flipped across the cell membrane, possibly by LtaA. LtaS then synthesises the GroP chain using GroP subunits which are derived from the head group of lipid phosphatidylglycerol found in the membrane. The number of LtaS-type enzymes involved in GroP chain synthesis varies from species to species (Percy & Gründling, 2014). LTA synthesis is closely linked to lipid biosynthesis and turnover due to its use of lipid phosphatidylglycerol from the membrane. In fact, the cellular pool of lipid phosphatidylglycerol is thought to be turned around more than twice per generation to allow for sufficient LTA synthesis (Koch et al., 1984).

## 1.6. Peptidoglycan hydrolysis

Peptidoglycan hydrolases play a role in a large number of cellular processes from cell growth, cell division and autolysis to peptidoglycan turnover and sporulation (Vollmer et al., 2008). There is a hydrolase capable of hydrolysing every bond found in peptidoglycan (**Figure 1.8**):

- **Acetylmuramyl-L-alanine amidases** (amidases) hydrolyse the amide bond between MurNAc and L-alanine separating the sugar backbone and the peptide side chain.
- **Carboxy- and endopeptidase** (peptidases) cleave the different bonds between D- and L-amino acids in the peptide side chains.
- **N-acetylglucosaminidases** (glucosaminidases) cleave the bond in the sugar back bone between the GlcNAc and MurNAc residues.

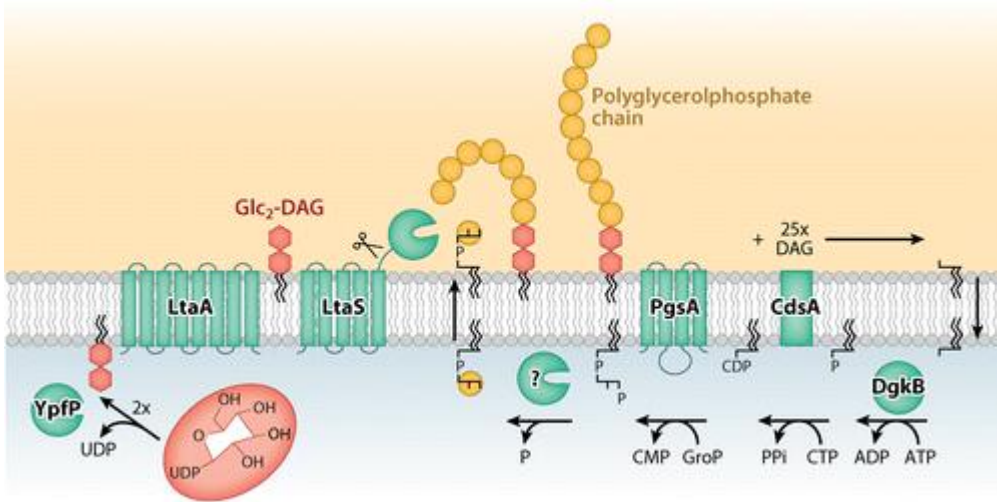
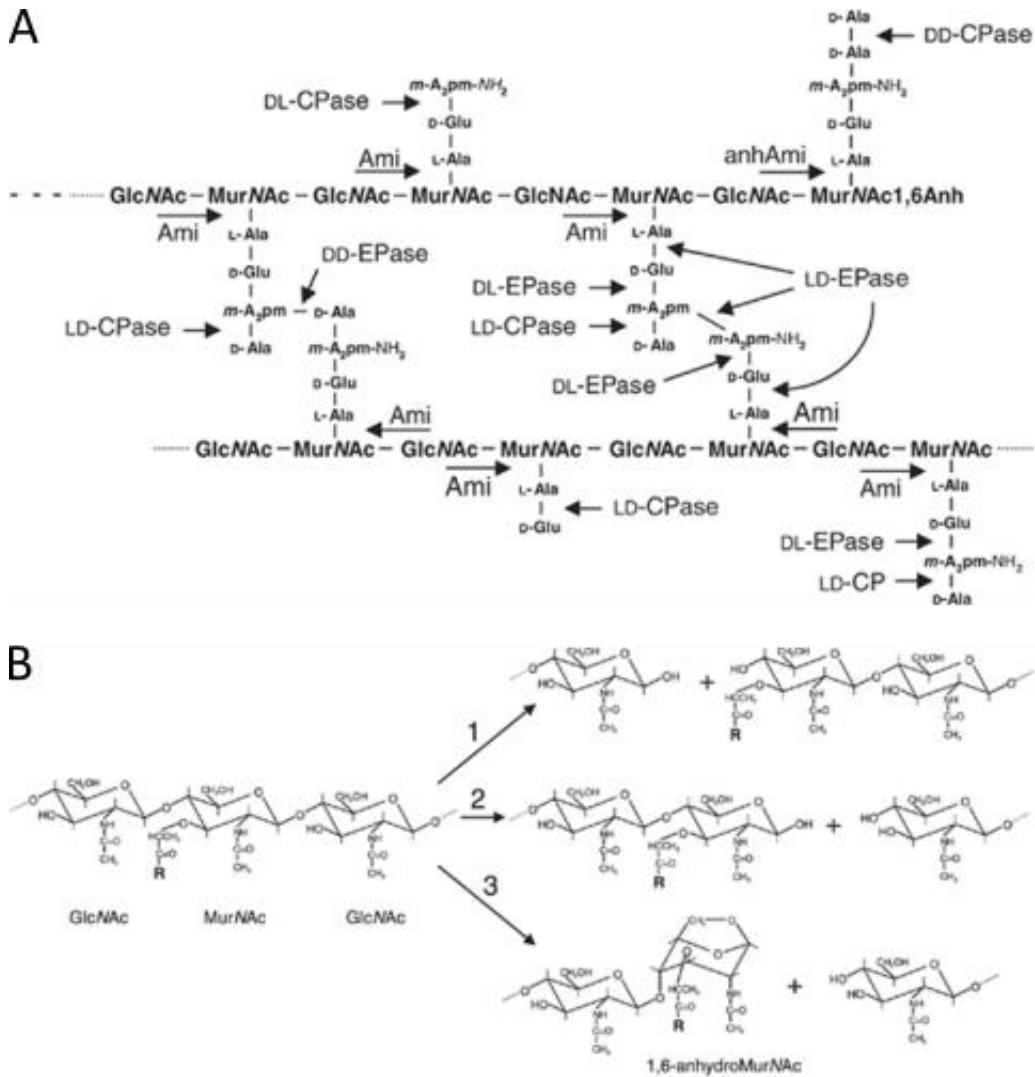


Figure 1.7. Diagram of LTA synthesis and turnover in *S. aureus*. Reproduced from (Percy & Gründling, 2014).



**Figure 1.8. Peptidoglycan hydrolase activity.** (A) Cleavage sites on the peptide side chain. (B) Cleavage side on the glycan backbone. 1 – Glucosaminidases; 2 – lysozyme-like; 3 – lytic transglycosylases. Adapted from (Vollmer et al., 2008).

- **N-acetyl-β-D-muramidases** (muramidases) hydrolyse the β1,4-glycosidic bond between MurNAc and GlcNAc residues. Lysozyme-like enzymes and lytic transglycosylases are the two types of muramidases.

Peptidoglycan hydrolases play important roles throughout the cell cycle, which is reflected in the high amount of redundancy amongst them. Bacteria often have several different enzymes that can cleave each bond, and even the different classes of enzymes have overlapping functions. *E. coli* has at least 13 peptidoglycan hydrolases located in its periplasm (Typas et al., 2012). PscB in *Streptococcus pneumoniae* is the only hydrolase known to be individually essential (Ng et al., 2004). There are however, examples of essential groups of hydrolases. In *S. aureus*, the four putative glucosaminidases, SagA, SagB, ScaH and Atl are essential as a group (Wheeler et al., 2015). In *B. subtilis* YvcE and LytE cannot both be absent, and in *E. coli*, lack of Spr, YdhO and YebA is synthetically lethal (Bisicchia et al., 2007; Singh et al., 2012).

#### 1.6.1. *S. aureus* hydrolases

There is a total of 19 known putative hydrolases in *S. aureus*. All of these have been listed in Table 1.1. Many of the hydrolases are not characterised. Most of the uncharacterised hydrolases have been identified as having a cysteine, histidine-dependent amidohydrolases/peptidases (CHAP) domain. Enzymes with a CHAP domain are proposed to act as peptidoglycan hydrolases (Bateman & Rawlings, 2003). In *S. aureus*, all the Sca proteins have CHAP domains (Pourmand et al., 2006).

Atl is one of the best characterised peptidoglycan hydrolases in *S. aureus*. *atl* encodes a 137 kDa protein, which is exported and processed into two hydrolases, one glucosaminidase (C-terminal domain) and one amidase (N-terminal domain) (Foster, 1995). Atl has been linked to the secretion of proteins, cell division, post-death lysis and peptidoglycan release from the cell surface (Foster, 1995; Pasztor et al., 2010; Wheeler et al., 2015). In a wild-type cell, Concanavalin A (ConA, a lectin that binds WTA) labelling revealed that WTA are not found at the septum. WTA localisation dictates Atl localisation, excluding Atl due to changes in proton-binding sites available in the cell wall (Biswas et al., 2012). Thus Atl is located at the centre of the septal plate through the absence of WTA in the septal plate peptidoglycan (Schlag et al., 2010). In a strain lacking WTA, Atl is observed all across the cell wall (Schlag et al., 2010). Lack of WTA therefore leads to faster lysis using Triton X-100 autolysis assays because Atl can act across the entire cell wall.

Atl is one of four putative glucosaminidases with ScaH, SagB and SagA (Wheeler et al., 2015). As a group glucosaminidases are essential and are involved in reshaping new cell wall after cell division. Their action allows for cell expansion and a decrease in cell wall stiffness through glycan chain shortening (Wheeler et al., 2015). SagB was shown to play the biggest role in shortening of glycan strands (Wheeler et al., 2015).

IsaA and SceD are the two putative lytic transglycosylases identified in *S. aureus*. When IsaA is absent, ScaD (CHAP domain containing) and SceD are both present in greater quantities, likely as a compensation

<b>Protein</b>	<b>Putative identification</b>	<b>References</b>
<b>Atl</b>	Amidase & Glucosaminidase	(Foster, 1995; Oshida, Takano, Sugai, Suginaka, & Matsushita, 1998; Wheeler et al., 2015)
<b>SagA</b>	Glucosaminidase	(Wheeler et al., 2015)
<b>SagB</b>	Glucosaminidase	(Wheeler et al., 2015)
<b>ScaA/Sle1/Aaa</b>	Amidase & CHAP domain	(Heilmann et al., 2005; Pourmand et al., 2006)
<b>ScaB</b>	CHAP domain	(Pourmand et al., 2006)
<b>ScaC</b>	CHAP domain	(Pourmand et al., 2006)
<b>ScaD</b>	CHAP domain	(Pourmand et al., 2006)
<b>ScaE</b>	CHAP domain, LysM domain	(Pourmand et al., 2006)
<b>ScaF</b>	CHAP domain	(Pourmand et al., 2006)
<b>ScaG</b>	CHAP domain	(Pourmand et al., 2006)
<b>ScaH</b>	Glucosaminidase & CHAP domain	(Pourmand et al., 2006; Wheeler et al., 2015)
<b>ScaJ</b>	CHAP domain	(Pourmand et al., 2006)
<b>IsaA</b>	Lytic transglycosylase	(M. R. Stapleton et al., 2007)
<b>LytM</b>	Lysostaphin	(Ramadurai & Jayaswal, 1997)
<b>LytN</b>	Amidase/Endopeptidase	(Frankel et al., 2011; Sugai et al., 1998)
<b>SceD</b>	Lytic transglycosylase	(M. R. Stapleton et al., 2007)
<b>SA0191</b>	Lysostaphin	(Wheeler, 2012)
<b>LytH</b>	Amidase	(Wheeler, 2012)
<b>SA2195</b>	Lysostaphin	(Wheeler, 2012)

**Table 1.1. Staphylococcal hydrolases and their function.**

mechanism (Stapleton et al., 2007). The upregulation of *sceD* after *isaA* inactivation suggests the two hydrolases have overlapping functions. SceD is thought to be involved in peptidoglycan remodelling in high salt environments (Stapleton et al., 2007; Vijaranakul et al., 1995). In the presence of high levels of NaCl, *sceD* expression levels go up. Lack of IsaA and SceD also leads to an increased degree of clumping, suggesting the hydrolases play a role in cell division (Stapleton et al., 2007). IsaA and SceD are also required for virulence (Stapleton et al., 2007).

Mutants lacking Sle1 or LytN showed impaired cell division, with excessive cell clumping, suggesting both hydrolases play a role in cell division (Frankel et al., 2011; Kajimura et al., 2005). LytN and Sle1 both contain a LysM domain. The LysM and CHAP domains are required for binding of LytN to peptidoglycan (Frankel & Schneewind, 2012). The LysM domain is required for LytN and Sle1 association with peptidoglycan void of WTA, and as a consequence, localisation to the septum (Frankel & Schneewind, 2012). The LysM domain is not essential for LytN but is for Sle1 function.

#### 1.6.2. Control of *S. aureus* hydrolases

Due to the large number of hydrolases in *S. aureus*, and the fact that only a subset of them have been studied, there is only limited understanding of how hydrolase activity is controlled. Tight restrictions on hydrolase activity are however important to ensure a perfect balance between peptidoglycan synthesis and hydrolysis throughout the cell cycle. Hydrolases are controlled by a complex web of cellular regulators. IsaA and SceD provide good examples of the complexity of hydrolase regulation in *S. aureus*. IsaA is positively regulated by SarA, YycFG (WalkR) and oxygen levels (Fuchs et al., 2007; Stapleton et al., 2007). SarA, LytSR and SaeR are negative regulators of SceD and sigma factor B ( $\sigma^B$ ), Agr, and YycFG/WalkR are positive regulators (Stapleton et al., 2007).

The WalkR/YycFG two-component system (TCS) plays a major role in regulation of the cell wall metabolism and is essential in *S. aureus* (Dubrac et al., 2007; Dubrac & Msadek, 2004). Walk is a histidine kinase and WalR is a response regulator. A conditional (IPTG-dependant WalkR expression) mutant has been used to study the effect of WalkR depletion on cells. The following putative hydrolases are thought to be positively controlled by WalkR: Atl, ScaB, ScaC, ScaD (SsaA), ScaE, ScaJ, IsaA, LytM, SceD (Dubrac et al., 2007). These hydrolases have different activities, amongst them are glucosaminidases, transglycosylases/muramidases, amidases and endopeptidases. WalkR-depleted cells aggregate more and are more lysis resistant than wild-type cells (Dubrac et al., 2007). Due to the diminished hydrolase activity in a WalkR mutant, cells develop thick cell walls and do not divide correctly (Delaune et al., 2011). The absence of WalkR can be partially complemented by LytM and ScaD/SsaA. This suggests that depletion of WalkR leads to cell death through an imbalance between cell wall synthesis and cell wall hydrolysis.

## 1.7. Cell division – overview

Cell division refers to the fundamental process of bacterial replication. Prokaryotes predominantly replicate by binary fission. Cells replicate and segregate their chromosomes, ensuring each daughter cell gets an identical set before forming a septum, normally placed at the mid-cell, and dividing. The correct execution of these steps is extremely important and spatial and temporal control are crucial.

### 1.7.1. Rod-shaped bacteria

Before cell division can take place, rod-shaped bacterial cells elongate. The increase in cell length allows cells to increase in volume while maintaining a constant diameter. Cell division will only occur once cells have reached a minimum length (Donachie & Begg, 1989; Sharpe & Errington, 1998). Chromosome segregation then takes place and septum formation can begin without risking uneven chromosome distribution in the daughter cells. Once complete, the septum is hydrolysed and the cell splits into two daughter cells. Correct selection of the division plane is extremely important.

Temporally, cells must divide only when they have reached the correct size, which is in large part determined by nutrient availability. In *B. subtilis*, nutrient availability leads to faster growing, longer cells and growth in nutrient poor media leads to shorter cells (Sargent, 1975). The glucosyltransferase UgtP localises at the septum in a nutrient-dependant manner and inhibits FtsZ assembly (Weart et al., 2007). A 1:1 FtsZ:UgtP ratio results in 90% inhibition of FtsZ assembly. In nutrient rich environments, UgtP is highly expressed and localised across the cytoplasm with a high concentration at the midcell in exponential phase (Weart et al., 2007). In the nutrient rich media, UgtP allows for increased elongation.

Spatially, the septum is precisely positioned at the mid-cell with little deviation (~1%) (Trueba, 1982). Septum formation begins with the localisation of FtsZ to the mid-cell and assembly of the Z-ring. The Z-ring recruits other cell division components. In *E. coli* and *B. subtilis*, the Min system and nucleoid occlusion are responsible for Z-ring positioning. In *E. coli*, MinC, MinD and MinE form the Min system (Raskin & De Boer, 1997). MinC and MinD form a complex (MinCD) which negatively regulates the Z-ring due to MinC inhibiting FtsZ polymerisation through direct interaction with it. MinE prevents MinC activity at the mid-cell allowing correct localisation of the Z-ring. MinC and MinD have been shown to oscillate from one pole to the other as a result of which MinC concentrations are highest at the poles, inhibiting FtsZ assembly (Hu & Lutkenhaus, 1999). *B. subtilis* has MinCD homologues but not MinE. Instead, DivIVA acts as a topological factor. DivIVA recognises cell curvature and localises at the poles (Bramkamp et al., 2008; Lenarcic et al., 2009). With the aid of MinJ, DivIVA recruits MinD to the cell poles then recruits MinC, thus inhibiting z-ring assembly at the poles. The relocation of MinC from the old poles to the site of division suggests that it may also inhibit the assembly of more than one Z-ring at the mid-cell (Migocki et al., 2002). Nucleoid occlusion keeps the cell from dividing near

the chromosome and bisecting the nucleoid. Nucleoid occlusion is achieved through binding of Noc in *B. subtilis* and SlmA in *E. coli* to specific DNA sequences (Wu & Errington, 2012). Noc inhibits FtsZ assembly through its physical presence. SlmA prevents the organisations of FtsZ protofilaments into a higher organisation (Bernhardt & De Boer, 2005).

#### 1.7.2. Coccoid bacteria

In coccoid bacteria there are theoretically an infinite number of potential division planes (Figure 1.9). Consequently, division plane selection is more complex. Some coccoid bacteria divide in a single plane (like rod-shaped bacteria), other divide in two or three planes (Zapun et al., 2008). For example, *S. aureus* divides successively in three orthogonal planes (Tzagoloff & Novick, 1977). In this case, the organism requires a way of knowing the division plane from the two previous divisions. This process is unlikely to be encoded in the DNA due to it changing every division cycle. It has been hypothesised that rib/piecrust features in the peptidoglycan, that are remnants from previous division cycles, play a role in the correct choosing of the next division plane in *S. aureus* (Turner et al., 2010). WTA localisation may also play a role in in mid-cell localisation (Atilano et al., 2010; Schlag et al., 2010).

*S. aureus* has not been found to have a Min homologue, it does however have a Noc homologue (Veiga et al., 2011). This process is particularly important in *S. aureus* because its nucleoid occupies a large part of the cytoplasm. Co-localisation of Noc with the nucleoid inhibits Z-ring formation over the bacterial DNA (Veiga et al., 2011).

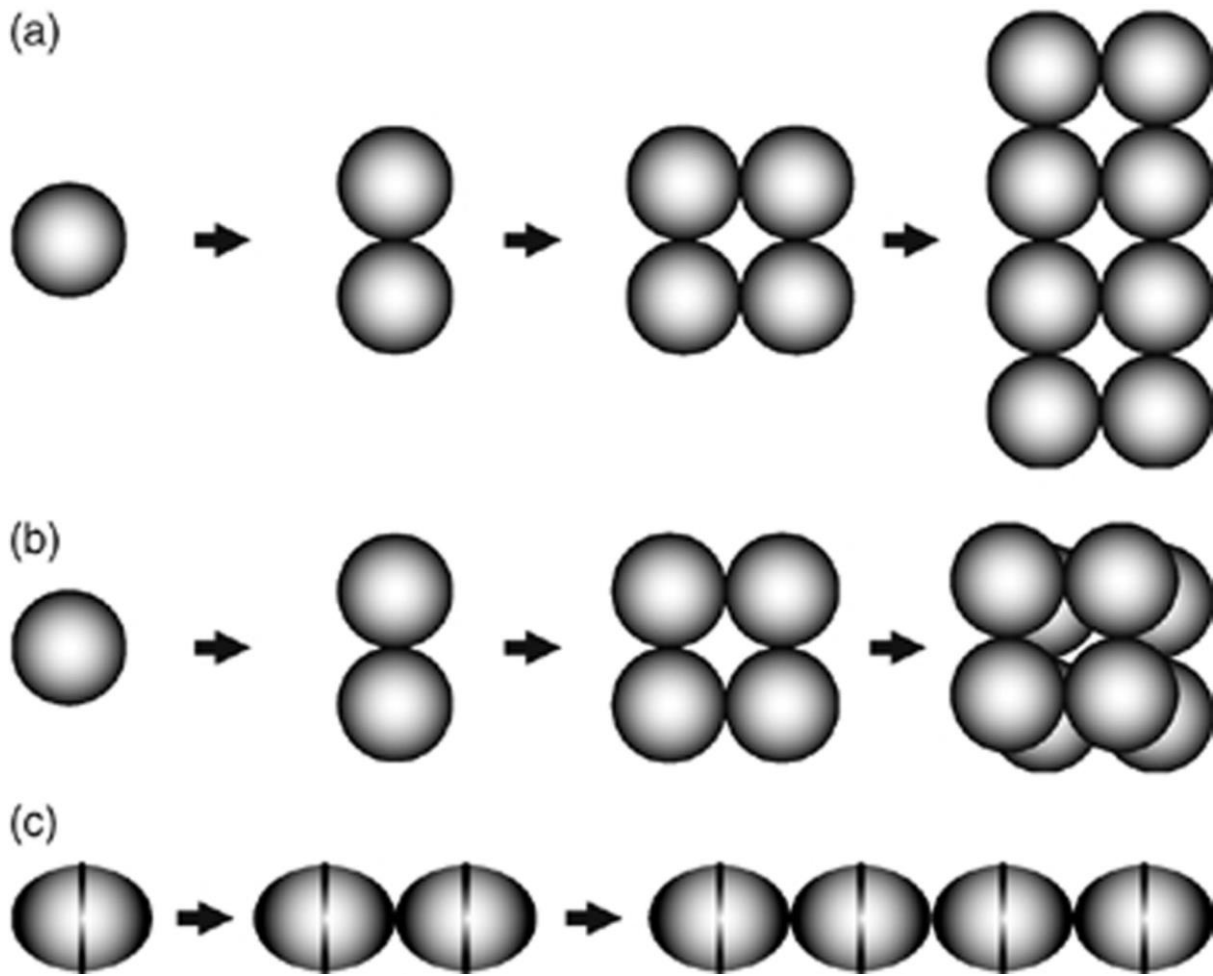


**Figure 1.9. Schematic of different bacterial division planes.** Division in (a) two perpendicular planes, (b) three perpendicular planes, (c) one parallel plane. Reproduced from (Zapun et al., 2008).

## 1.8. Cell division – the divisome

A large network of proteins is required to carry out cell division (Figure 1.10). FtsZ is the most highly conserved of these and is thought to initiate the process of cell division in *E. coli* (Margolin, 2000). FtsZ localises at the site of new septum formation and polymerises into protofilaments (D. J. Scheffers & Driessen, 2001). These protofilaments organise into a dynamic structure with a short protein turnover time, known as the Z-ring. FtsZ can cause constrictions in liposomes suggesting that it drives the cell constriction required for cell division. FtsZ filament sliding in a complete circle has been hypothesised to be responsible for generating constriction force (Szwedziak et al., 2014). In gram-positive bacteria FtsZ appears to have a dynamic bead-like structure (Strauss et al., 2012).

FtsZ requires other proteins to carry out its role in cell division. FtsA, a membrane-associated protein, enables FtsZ polymers to assemble at the membrane. Formation of the FtsA-FtsZ complex allows for strong enough anchoring to the cell membrane (Loose & Mitchison, 2014). In *E. coli* a second protein, ZipA, appears to carry out a similar function. Both FtsA and ZipA are required for FtsZ lead constriction even though the Z-ring can still form in the presence of only one of them (Pichoff & Lutkenhaus, 2002). ZipA and FtsA together are also credited with recruiting FtsK and other division proteins (Pichoff & Lutkenhaus, 2002). A large number of other FtsZ-interacting proteins help maintain the Z-ring. In *E. coli* these include ZapA, ZapC and ZapD (Durand-Heredia et al., 2011; Galli & Gerdes, 2010). In *B. subtilis* and *S. aureus*, SepF is involved (Hamoen et al., 2006).

EzrA plays an important role in gram-positive cell division, playing an essential role in *S. aureus* although not in *B. subtilis* (Levin et al., 1999; Steele et al., 2011). EzrA is essential for correct cell growth, localisation of cell division proteins and peptidoglycan synthesis (Steele et al., 2011). There are two proposed models of EzrA-FtsZ interaction. The first proposes that EzrA, which is arch shaped, traps FtsZ filament anchoring the protofilaments to the membrane and inhibiting any lateral interactions (Cleverley et al., 2014). It would also be possible for FtsZ to interact with the outer surface of the EzrA ring, allowing another molecule to bind the inside of the arch (Cleverley et al., 2014). Once the Z-ring is fully assembled other cell division components are recruited to the mid-cell. In *E. coli* these include FtsK, FtsQ, FtsL, FtsW, FtsI, FtsN, FtsQ, FtsB and FtsL (Pichoff & Lutkenhaus, 2002). In *S. aureus* the late stage division proteins include FtsL, DivIC, DivIB, FtsW and GpsB (Daniel & Errington, 2003; Steele et al., 2011). PBPs are also recruited for peptidoglycan synthesis and remodelling. In order for cell splitting to take place, cell wall hydrolases are also recruited to the septum.

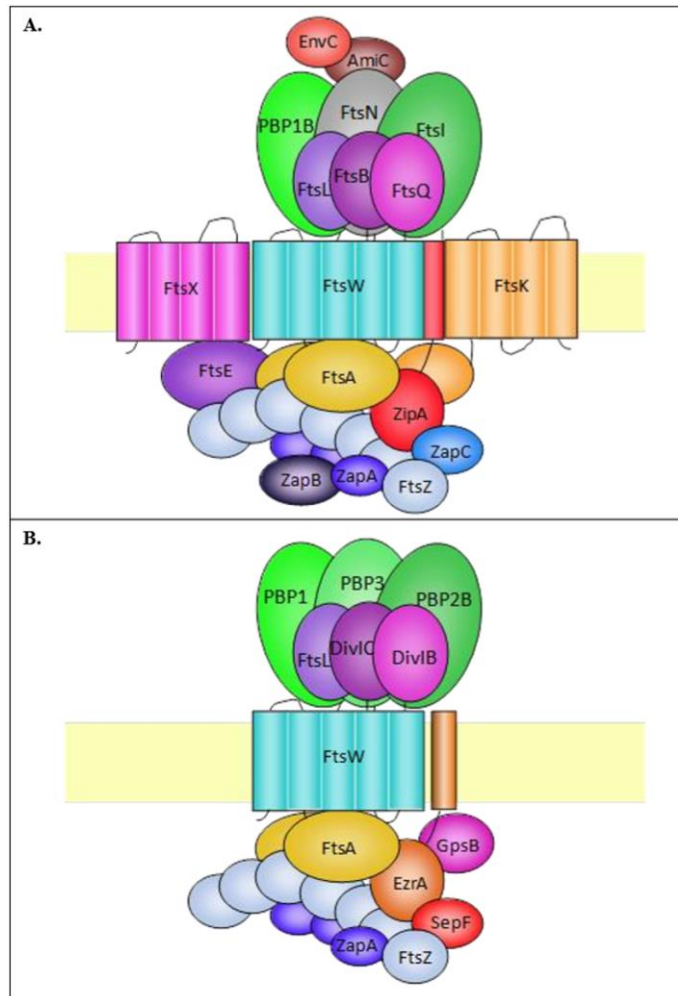


**Figure 1.10. Diagram of the cell division machinery in (A) *E. coli* (B) *B. subtilis*.** Analogues in *E. coli* and *B. subtilis* have been represented in the same colours. This diagram is not exhaustive, some interactions are not represented. Reproduced from (Bottomley, 2011).

### 1.8.1. Penicillin-binding proteins

Penicillin-binding proteins play an integral role in peptidoglycan biosynthesis. PBPs are enzymes with transglycosylation and/or transpeptidation activity (Sauvage et al., 2008). PBPs are of particular interest because they are the targets of the  $\beta$ -lactam class of antibiotics, giving them their name. Modifications to PBPs play a major role in antibiotic resistance (Zapun et al., 2008).

PBPs are split into two classes: high molecular weight (HMW) and low molecular weight (LMW). HMW PBPs are further split into class A and class B. Class A PBPs are bifunctional, they have both transpeptidase and transglycosylase activity (Sauvage et al., 2008). Class B PBPs only have transpeptidase activity. Both classes have C-terminal domains with transpeptidase activity linked by a  $\beta$ -sheet rich linker to N-terminal domains of differing functions (Lovering et al., 2012; Sauvage et al., 2008). The N-terminal domains of A PBPs has transglycosylase activity and that of B PBPs is of unknown function. LMW PBPs possess endopeptidase activity (crosslinking) or carboxypeptidase activity, which prevents further crosslinking through hydrolysis of the peptide side chain (Macheboeuf et al., 2006).

There is a great amount of variation in the number of PBPs present in different bacteria. This partially reflects differences in growth and division modes. *E. coli* has 12 PBPs, *B. subtilis* has 16 PBPs and *S. aureus* only has 4 PBPs (Sauvage et al., 2008). PBP1, PBP2, PBP3 and PBP4 are the four PBPs identified in *S. aureus*. PBP1 and PBP3 are class B HMW PBPs, PBP2 is a class A PBP and PBP4 is a LMW PBP. PBP1 and PBP2 localise at the septum and are both essential although PBP1 essentiality is thought to be independent of its transpeptidase activity (Pereira et al., 2009). Recently, it has been revealed that PBP1 is essential for FtsW transglycosylase activity (Reichmann et al., 2019; Taguchi et al., 2019). PBP1 and FtsW form a SEDS-bPBP pair, which may explain PBP1 essentiality. PBP4, the sole LMW PBP, has transpeptidase activity and is attributed with the high levels of crosslinking present in *S. aureus* peptidoglycan (Wyke et al., 1981). Deletion of PBP4 leads to a reduction in PBP2 transcription and in peptidoglycan crosslinking (Memmi et al., 2008). Lack of PBP3 does not lead to significant changes in muropeptide composition of the cell wall. It does however cause a small decrease in autolysis, suggesting it plays a role in cell division (Pinho et al., 2000). Recent data revealed that PBP3 is required for the correct localisation of RodA (a SEDS protein) at the midcell and that they form a SEDS-bPBP pair (Reichmann et al., 2019). In MRSA, an additional PBP is present, PBP2A, encoded by *mecA* (Hartman & Tomasz, 1984). PBP2A has a lower affinity to  $\beta$ -lactams than PBP2, allowing for continued transpeptidase activity in *S. aureus* after antibiotic treatment (Lim & Strynadka, 2002). The transglycosylase activity of PBP2 is still required to achieve high levels of resistance.

## 1.9. Cell division – peptidoglycan dynamics

### 1.9.1. Peptidoglycan synthesis

The location of peptidoglycan synthesis varies in different organisms. Where peptidoglycan is inserted into the sacculus has an impact on cell shape and growth. Fluorescent vancomycin and fluorescent D-amino acids are effective probes used to look at patterns of peptidoglycan insertion across the cell (Daniel & Errington, 2003). In both *E. coli* and *B. subtilis* a focus of insertion is found at the septum. In *E. coli*, STORM imaging of vancomycin-labelled cells and sacculi revealed that peptidoglycan insertion, for cell elongation, occurs in many discrete foci spread over the cylinder of the cell (Turner et al., 2013). These results disagree with earlier imaging showing a helical pattern of insertion (Varma et al., 2007). The difference can be explained by the use of higher resolution imaging in the more recent study, allowing for more precise localisation. In *B. subtilis* vancomycin labelling revealed a helical pattern of peptidoglycan incorporation (Varma et al., 2007). The Mre proteins have been proposed to be responsible for cell shape in *B. subtilis* (Daniel & Errington, 2003). There are three MreB homologs in *B. subtilis*: MreB, Mbl and MreBH. The three homologs were thought to form a dynamic cable but they have recently been shown to move independently (Domínguez-Escobar et al., 2011). MreC and MreD stabilise the MreB cytoskeleton and MreB is thought to recruit peptidoglycan biosynthesis proteins as well as contribute to their coupling with peptidoglycan precursors (Leaver & Errington, 2005).

In *S. aureus*, peptidoglycan synthesis occurs in a dispersed manner across the whole of the cell wall and the septum, with no discrete foci (Lund et al., 2018). Localisation of peptidoglycan synthesis in *S. aureus* is determined by FtsZ, due to its central role in the localisation of the peptidoglycan biosynthesis machinery. At the septum, peptidoglycan is inserted in a region of insertion around the leading edge of the septum (Lund et al., 2018)(Figure 1.11). The leading edge is thinner than the lagging edge. Once the septum forms a connected septal plate, the centre is still thinner, and further incorporation forms a septum of uniform width before cell division occurs (Lund et al., 2018).

### 1.9.2. Cell splitting

After completion of the septum, cells need to split into two daughter cells. Peptidoglycan hydrolases are thought to be responsible for the splitting of the septal plate into two halves (Giesbrecht et al., 1997). In gram-negative bacteria the mid-cell is also constricted and the outer-membrane needs to be separated. To carry out cell division hydrolases are localised to the cell septum, although no direct interaction has been shown between them and the division machinery.

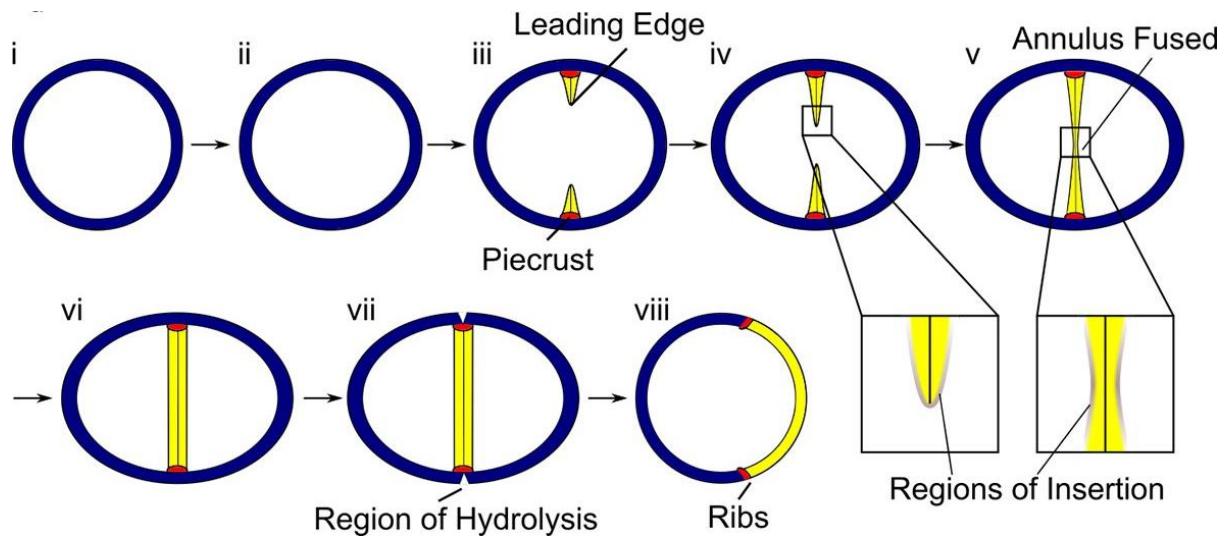


**Figure 1.11. Model of peptidoglycan insertion in *S. aureus*.** (i, ii) Cell size increase before septum formation begins. (iii, iv) Septum formation begins at the piecrust. The septum is thinnest at the leading edge. (v) Annulus fuses. (vi) Synthesis continues to complete a septal plate of homogenous width. (vii, viii) cell division. Reproduced from (Lund et al., 2018).

In *E. coli* the three amidases, AmiA, AmiB and AmiC, play a major role in hydrolysis of the septal plate (Höltje & Heidrich, 2001). Cell splitting can take place with only one of the amidases but at a slower rate. It has been shown that lytic transglycosylases (Slt70, MltA, MltB) and endopeptidases (MepA, PBP4, PBP7) are also involved in the process but play a much smaller role (Höltje & Heidrich, 2001). In *B. subtilis*, LytF and CwlF are thought to be involved in hydrolysis of the septum during cell division (Ohnishi et al., 1999).

In *S. aureus* Atl, Sle1, IsaA and SceD are the major autolysins involved (Biswas et al., 2012; Kajimura et al., 2005; Stapleton et al., 2007; Wheeler et al., 2015). Atl is thought to play the biggest role in hydrolysis of the septum into its two component parts. Atl is a bifunctional enzyme, which is proteolytically cleaved into an amidase and a glucosaminidase (Biswas et al., 2006). It is located at the septum with foci around the pie crust feature (Yamada et al., 1996). Its localisation is thought to be due to the lack of WTA at the septum. Mutants lacking Atl or Sle1 form clusters, suggesting a lack of complete cell division. Deletion of IsaA and SceD, lytic transglycosylases, also leads to impaired cell division. Live-microscopy has revealed that daughter cell separation occurs on a millisecond timescale (Zhou et al., 2015). This rapid separation is thought to be driven by mechanical forces. Cell separation is therefore initiated by hydrolase activity and ends in mechanical separation (Zhou et al., 2015).

### 1.9.3. Cell expansion

After splitting, the daughter cell must grow before it can itself divide. Hydrolases have been proposed as one of the main drivers of sacculus enlargement. A careful balance between hydrolysis and synthesis is required to maintain cell wall integrity during growth. The three-for-one model of peptidoglycan insertion was developed as a possible way cells maintain this balance (Figure 1.12). A peptidoglycan triplet is crosslinked to the inner of the cell wall through free amino groups on the crossbridges between backbone sugars (Höltje & Heidrich, 2001). As a result, the triplet is bound to the peptidoglycan either side of the loading strands. This allows the triplet to remain unstressed, while the rest of the wall is load bearing (Höltje & Heidrich, 2001). The loading strand is hydrolysed out of the peptidoglycan consequently incorporating the triplet into the stress bearing peptidoglycan chain. This model can be used for both gram-negative and gram-positive cell walls (Höltje & Heidrich, 2001).

In *S. aureus*, after cell division the septum must be remodelled to form mature peptidoglycan. The reshaping of the new cell wall is the growth mechanism used by *S. aureus* before the next round of septum formation begins (Bailey et al., 2014; Wheeler et al., 2015). After daughter cell splitting, the newly exposed material is stiffer than the rest of the cell wall (Bailey et al., 2014). The newly exposed peptidoglycan's stiffness decreases as the wall expands to gain a spherical shape. The four putative glucosaminidases, Atl, SagA, SagB and ScaH have been shown to be responsible for this remodelling process (Wheeler et al., 2015). The cell wall of a conditional mutant lacking all four glucosaminidases did not expand correctly after division and remained

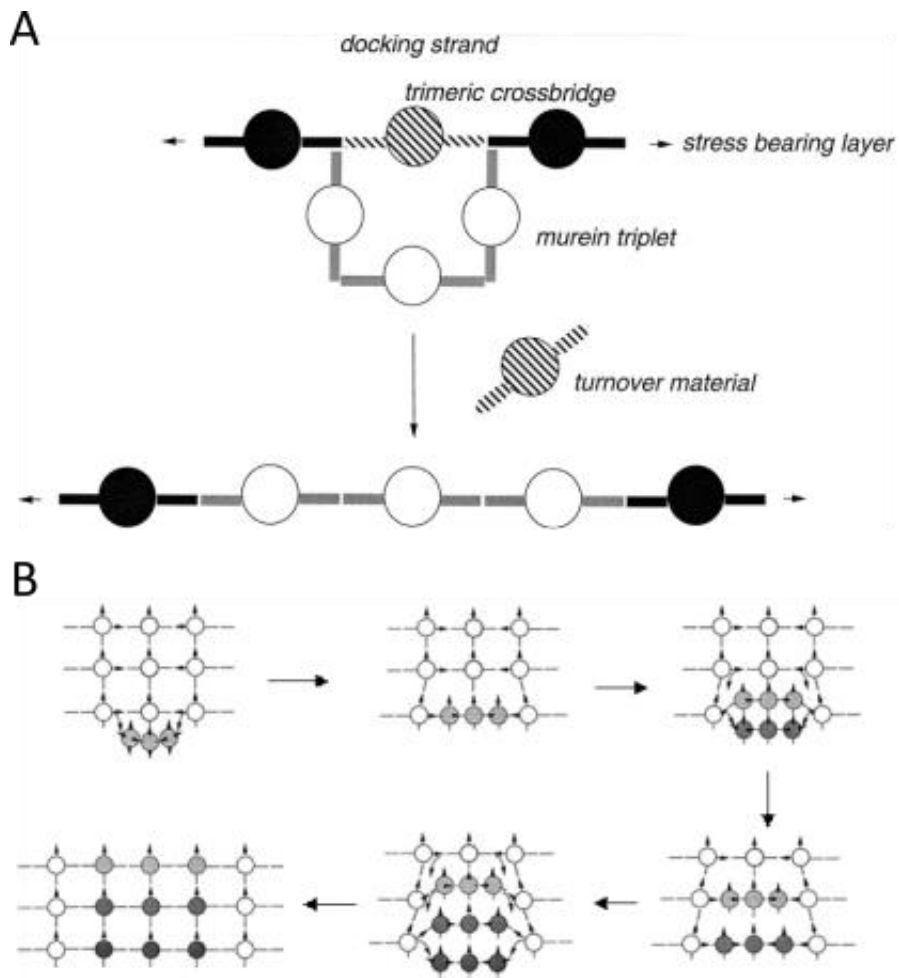


**Figure 1.12. Representation of the proposed three-for-one peptidoglycan growth model.** Circles represent glycan strands crosslinked by peptide side chains represented in bar form. (A) Hypothetical mechanism in a thin, gram-negative-like cell wall. (B) Hypothetical mechanism in a thick, gram-positive-like cell wall. Modified from (Höltje & Heidrich, 2001).

stiffer. SagB plays the biggest role in this process out of the four enzymes (Wheeler et al., 2015). The glucosaminidases' remodelling of the new peptidoglycan is responsible for the short glycan chain length in *S. aureus* (Boneca et al., 2000).

### 1.10. Cell Wall antibiotics

The cell wall and its associated machinery are highly conserved across bacterial species and are not present in mammalian cells, making them excellent targets for antibiotics. Additionally, many of them are essential (Bugg et al., 2011; Lovering et al., 2012). Most cell wall antibiotics are natural products isolated from other organisms that produce them for competition in their native environments (Bugg et al., 2011). The steps targeted by cell wall antibiotics can be split into three categories: cytoplasmic steps, lipid-linked steps and cell surface/assembly steps. Most currently used cell wall antibiotics target the lipid-linked and assembly steps of peptidoglycan synthesis (Figure 1.13). Only D-cycloserine and fosfomycin target peptidoglycan precursor synthesis.

Antibiotic resistance is a rising global issue. A recent study estimated that antibiotic resistant infections caused 33110 deaths in the European Economic Area (EEA) in 2015 (Cassini et al., 2019). The burden (deaths and disability-adjusted life years) increased for all antibiotic-resistant infections between 2007 and 2015 (Cassini et al., 2019). As a consequence, new antibiotic development is required and the cell wall is an excellent target to consider in this context.

The two most widely used classes of cell wall antibiotics are  $\beta$ -lactams and glycopeptides. We have a good understanding of their targets but only limited understanding of how binding to these targets leads to cell death. A better understanding of the cellular pathway to cell death could provide insight into potential new targets for antimicrobials and offer a better understanding of resistance mechanisms. Our current understanding of  $\beta$ -lactams and glycopeptides is presented below.

### 1.11. $\beta$ -lactams

$\beta$ -lactams are cell-wall synthesis inhibiting antibiotics.  $\beta$ -lactams are chemically defined by their  $\beta$ -lactam ring, a four membered lactam (Aoki & Okuhara, 1980).  $\beta$ -lactams are commonly subdivided according to their chemical structure into penams, cepheems, monobactams and carbapenems.  $\beta$ -lactams are PBP substrate analogues and act as inhibitors of PBP function (Tipper & Strominger, 1965).  $\beta$ -lactams mimic the D-ala-D-ala dipeptide, that is found at the end of the peptide side chain of peptidoglycan. They inhibit PBP function by acylating the active site serine hydroxyl group. The deacylation is very slow, forming a covalent acyl-enzyme complex (Pratt, 2008). Different  $\beta$ -lactams preferentially bind different PBPs.

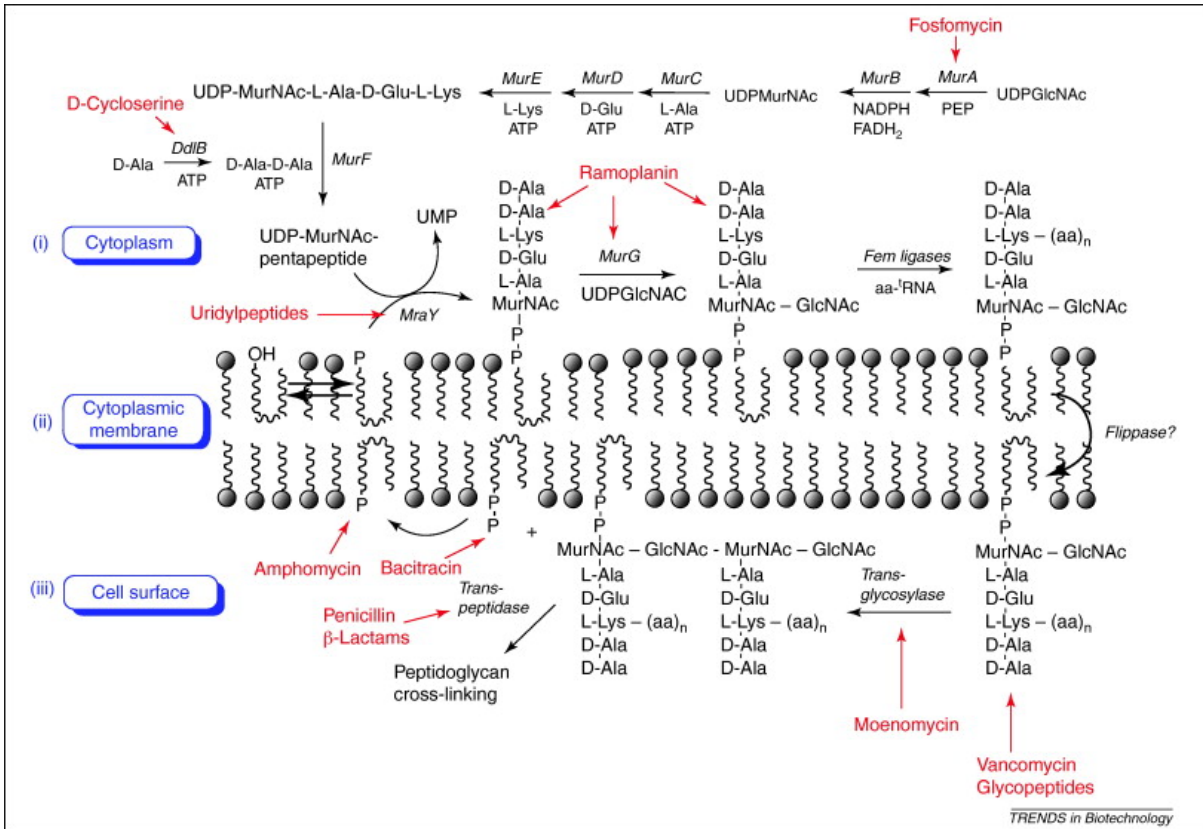


Figure 1.13. Cell wall antibiotic targets along the peptidoglycan synthesis pathway.

$\beta$ -lactams are bactericidal antibiotics that only act on cells that are actively growing and dividing, not on stationary phase cells. It has long been accepted that  $\beta$ -lactam killing occurs through an imbalance between peptidoglycan synthesis and hydrolysis (A Tomasz, 1979). However, this has been more of an accepted idea rather than a proven model. Peter Giesbrecht created the most comprehensive model of  $\beta$ -lactam killing, specifically penicillin killing, of *S. aureus* (Giesbrecht et al., 1998). More recent research has focused on  $\beta$ -lactam resistance, rather than mechanism of action, in *S. aureus*, or used other model organisms, often *E. coli*, to study the killing mechanism of  $\beta$ -lactams (Banzhaf et al., 2012; Cho, Uehara et al., 2014; Chung et al., 2009).

#### 1.11.1. Original models of penicillin killing

Early in the study of the action of  $\beta$ -lactams, researchers came to the conclusion that  $\beta$ -lactams inhibit peptidoglycan crosslinking (Tipper & Strominger, 1965; Wise & Park, 1965). It was postulated that long uncrosslinked glycan chains were being incorporated into the cell wall. The uncrosslinked material forms a weaker cell wall. Continued production of cytoplasmic material was suggested to lead to swelling of the cytoplasm, eventually bursting the weakened cell wall (Tipper & Strominger, 1965; Tomasz, 1979). Later evidence showed that post-treatment lysis did not take place in autolysin deficient pneumococci and *B. subtilis* (Tomasz et al., 1970). This suggests that the observed lysis is enzymatically driven, not mechanically.  $\beta$ -lactams appeared to act in a more bacteriostatic than bactericidal manner in the autolysin-deficient strains. These results ushered in the idea that inhibition of PBPs was the cause for cell growth arrest but that killing was due to other cellular processes, one of which may be peptidoglycan hydrolysis (Tomasz, 1979). Other results from the same lab showed that penicillin-induced generalised cell lysis did not occur and penicillin tolerance was observed when experiments were done at a low pH 5 instead of pH7/7.5 (Goodell et al., 1976). It was hypothesised that the low pH either inhibited hydrolase activity and/or stabilised the plasma membrane (Goodell et al., 1976).

#### 1.11.2. Peter Giesbrecht's model of penicillin killing of *S. aureus*

When treated with 0.1  $\mu\text{g}/\text{mL}$  penicillin, *S. aureus* dies when initiating the second cell cycle after addition of the antibiotic (Giesbrecht et al., 1998)(**Figure 1.14**). During the first cell cycle after addition of penicillin, the bacteria can no longer crosslink their newly incorporated glycan chains, but they continue synthesising at the septum. This leads to loose, mesh-like material forming large, deformed septa and the cells do not divide. In the next cell cycle, instead of forming a new septum, *S. aureus* continues to add material to the existing, malformed septum (Giesbrecht et al., 1998). However, instead of initiating cell splitting at the location of the existing septum, the murosomes perforate the cell wall at the location where the cell should have laid a new septum but didn't (Giesbrecht et al., 1998). The perforation of the cell wall at 90° from the septum leads to cytoplasm leakage and cell death. Generalised lysis of the cells takes place in the third cell cycle after penicillin

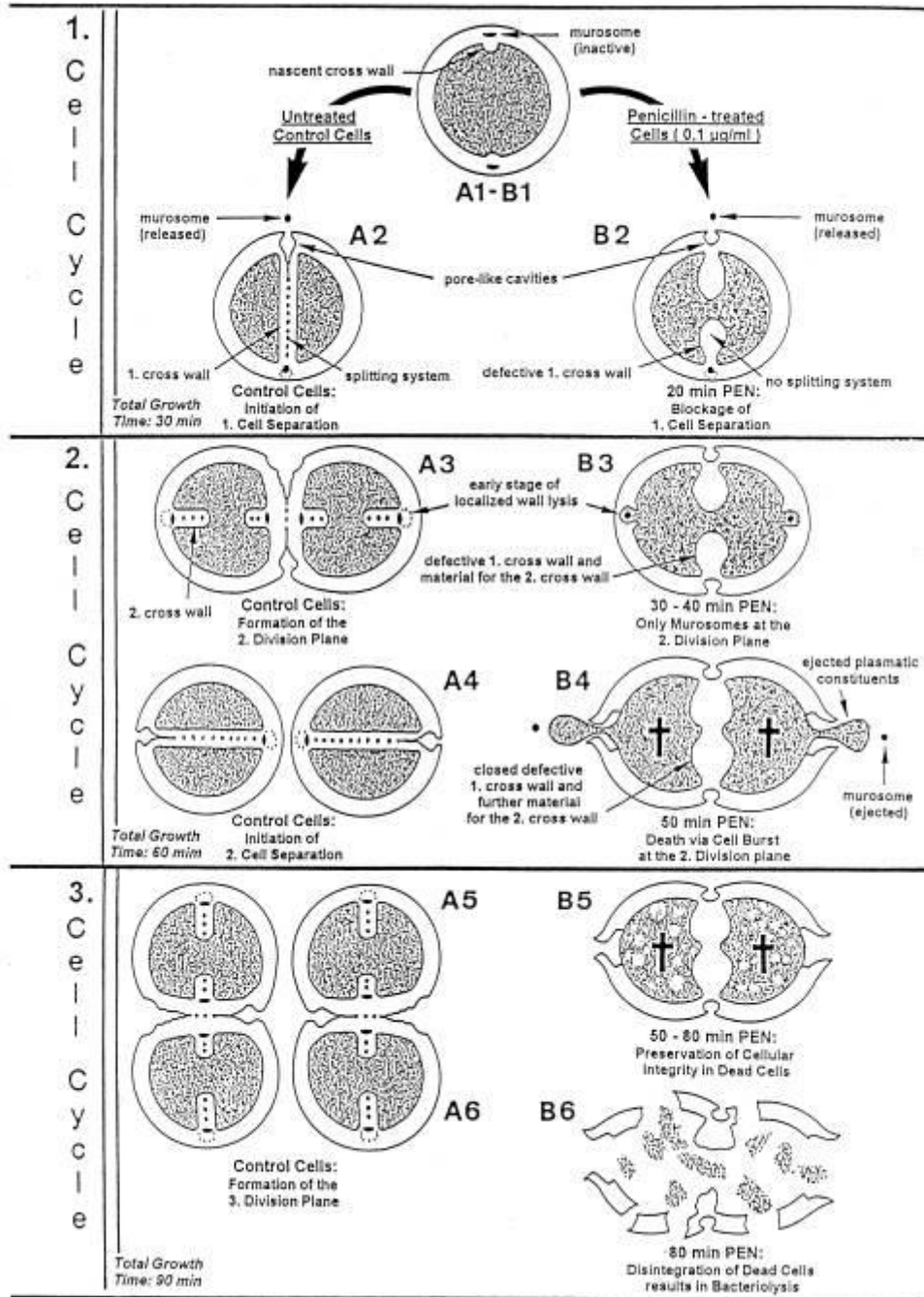


**Figure 1.14. Giesbrecht's model of penicillin induced death.** After penicillin treatment cells finish their current division cycle before dying upon initiation of the second cell division and lysing within 80 minutes of treatment. Reproduced from (Peter Giesbrecht et al., 1998).

addition (Giesbrecht et al., 1998). Generalised lysis is thought to be due to the action of remaining hydrolases after death of the cell.

At higher concentrations of penicillin, 10 µg/mL, a second type of cell death is observed (Giesbrecht et al., 1994). A subset of the population dies within 15 to 20 minutes of penicillin being added to the growth media. Cells that had incomplete septa upon addition of the antibiotic attempt to divide along their incomplete septa and puncture a hole in their cell wall, leading to loss of cytoplasm (Giesbrecht et al., 1994). At higher concentrations, this subset is therefore dying from attempting to split along an incomplete septum rather than a non-existent septum.

### 1.11.3. Reactive oxygen species (ROS)

The production of reactive oxygen species was proposed as a common killing mechanism for the three main bactericidal antibiotic classes: aminoglycosides, quinolones and β-lactams (Kohanski et al., 2007)(Figure 1.15). This killing model was proposed to apply to both gram-positive and gram-negative organisms and be due to oxidative DNA lesions. Hydroxyphenyl fluorescein (HPF) was used to measure hydroxyl radical formation after antibiotic treatment. Within 3 hours of treatment with quinolone, aminoglycoside and ampicillin significant increases in hydroxyl radical formation were observed (Kohanski et al., 2007). Decrease in lethality in the presence of an iron chelator or a hydroxyl radical scavenger support this model (Wang & Zhao, 2009).

This model of killing was contradicted by subsequent studies. *E. coli* was still killed by β-lactams in the absence of oxygen and an increase in hydrogen peroxide production was not observed after treatment (Liu & Imlay, 2013). ROS quenchers were shown to protect cells from antibiotic treatment not only in aerobic conditions but also in anaerobic conditions (Keren et al., 2013). These results suggest that ROS is not responsible for the bactericidal effect of antibiotics, although it may play a small contributing role (Zhao et al., 2015).

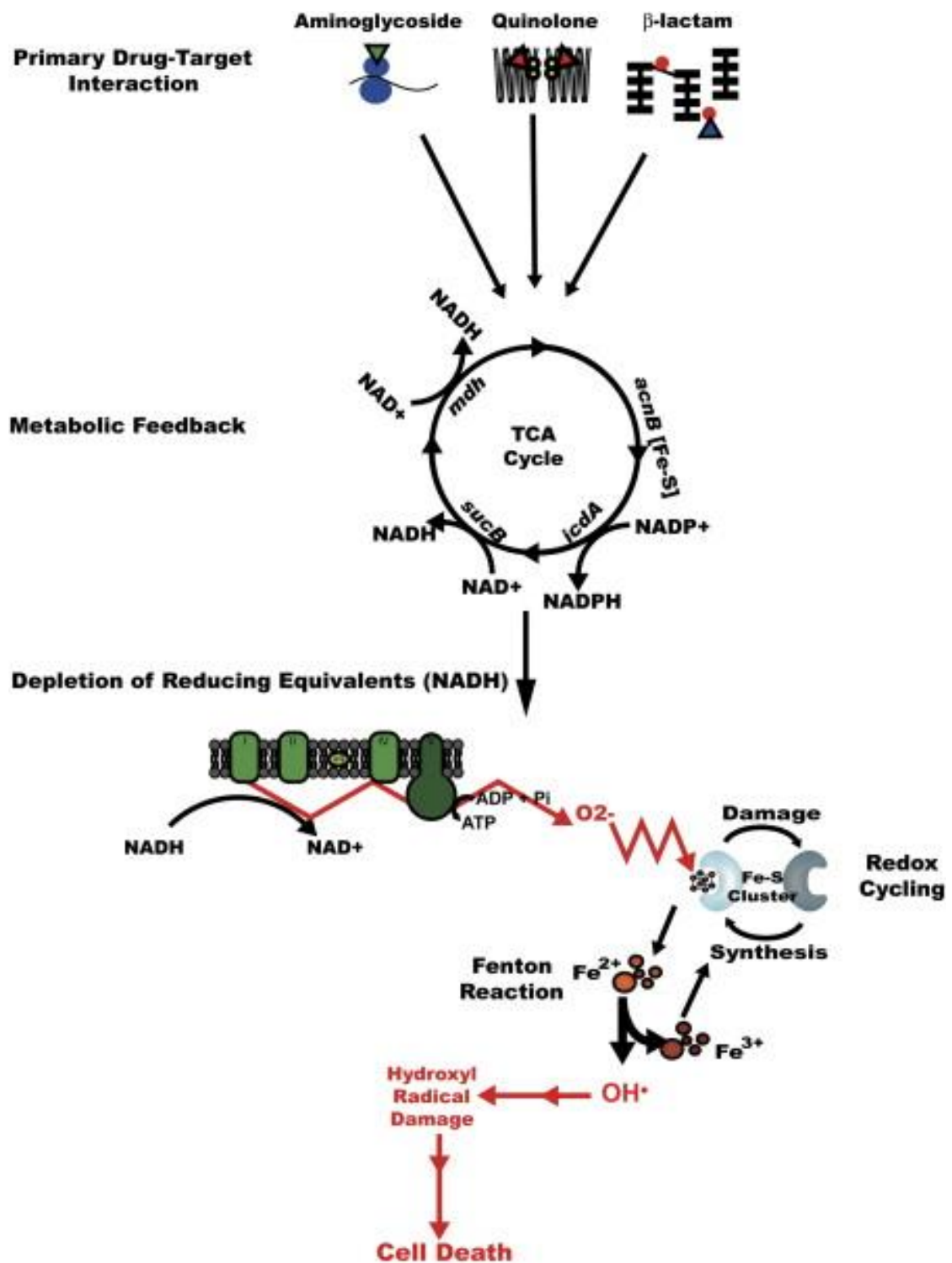


**Figure 1.15. Model of antibiotic-induced ROS killing.** Drug-target interactions are proposed to trigger NADH oxidation through the electron transport chain and TCA cycle. This would lead to hyperactivation of the electron transport chain, which would in turn stimulate superoxide formation. Iron-sulfur clusters would be damaged by superoxide and ferrous iron would be made available triggering the Fenton reactions. This cascade of events would finally lead to hydroxyl radical formation and DNA damage. Reproduced from (Kohanski et al., 2007).

#### 1.11.4. Thomas Bernhardt's model of mecillinam killing of *E. coli*

More recently the Thomas Bernhardt group has shown the presence of a futile cycle after  $\beta$ -lactam treatment in *E. coli* (Cho et al., 2014). *E. coli* cells were treated with mecillinam, which inhibits the TP activity of PBP2. PBP2 is essential to the Rod system, which is responsible for cell elongation in rod-shaped bacteria. PBP2 can be rendered non-essential by overproduction of FtsZ, allowing the study of the impact of treatment on cell wall metabolism in a strain with FtsZ upregulated. After treatment, a futile cycle of peptidoglycan synthesis and breakdown begins, where newly synthesised material is broken down and peptidoglycan precursor pools are depleted (Cho et al., 2014). Cho et al. argue that this futile cycle eventually leads to cell death by depleted cellular resources.

*S. aureus* only has one peptidoglycan synthesis machinery, therefore conclusions based on the Rod system in a rod-shaped bacterium, cannot be applied to *S. aureus*. The effect might also differ in gram-positive vs. gram-negative organisms. Mecillinam is also mainly used to treat gram-negative infections and is not effective against most gram-positive infections. This leaves us with very little understanding of the killing mechanisms in action when *S. aureus* is treated with  $\beta$ -lactams.

#### 1.11.5. Other insight into $\beta$ -lactam mode of action

The Kenneth Bayles group found that the homologous *cidAB* and *lrgAB* operons play a role in penicillin sensitivity (Groicher et al., 2000; Rice et al., 2003). LrgA acts as an antiholin inhibiting the holin-like *cidA* gene product. The presence of the *cidA* gene product leads to more extracellular hydrolase activity, which increases penicillin sensitivity (Groicher et al., 2000; Rice et al., 2003). Mutation of *cidA* leads to a decrease in sensitivity to penicillin. The difference in extracellular hydrolase activity is thought to be due to changes in hydrolase secretion (Rice et al., 2003).

### 1.12. Glycopeptides

In 1956 Eli Lilly discovered vancomycin, the first identified glycopeptide antibiotic (Levine, 2006). Glycopeptides are glycosylated tricyclic or tetracyclic heptapeptides (Reynolds, 1989; Sarkar et al., 2017). The residue in positions 1 and 3 of the heptapeptide determine which subclass a glycopeptide belongs to. The five representative glycopeptides are avoparcin, vancomycin, ristocetin, complestatin and teicoplanin (Sarkar et al., 2017). Glycopeptides target lipid II. First generation glycopeptides such as vancomycin and teicoplanin bind the D-Ala-D-Ala terminus (Perkins, 1969). The following generations of glycopeptides have additional interaction features. For example, some anchor themselves in the membrane, others can bind D-Ala-D-Lac (found in vancomycin-resistant bacteria) (Sarkar et al., 2017). Van der Waals bonds and five hydrogen bonds hold the D-Ala-D-Ala-glycopeptide complex together. The binding of glycopeptides to lipid II inhibits

peptidoglycan synthesis (Watanakunakorn, 1984). Vancomycin readily forms dimers in solution, which is thought to enhance ligand binding (Jia et al., 2013). Unlike for  $\beta$ -lactams, there is a lack of developed models of vancomycin killing. Due to vancomycin's ability to dimerise in a variety of manners and its structural complexity, much of the research around it has been biochemically focused (Kahne et al., 2005). Another extensive body of research around vancomycin focuses on vancomycin resistance. Before the peptidoglycan biosynthetic pathway was even well understood, researches showed that incorporation of radiolabelled MurNAc and GlcNAc was inhibited after vancomycin treatment (Anderson et al., 1965; Reynolds, 1961).

Secondary interactions of glycopeptides within the cell have also been reported, with studies showing interactions with cell wall metabolism members PBP2 and Atl (Leimkuhler et al., 2005; Eirich et al., 2011). The glycopeptides vancomycin and oritavancin have been shown to inhibit WTA biosynthesis (Singh et al., 2017). WTA synthesis is inhibited due to antibiotic binding of lipid II preventing lipid carrier recycling. The lipid carrier is required for the first steps of both peptidoglycan and WTA synthesis (Singh et al., 2017). In *E. faecalis*, vancomycin inhibits an ABC transporter potentially disrupting the uptake of nutrients (Eirich et al., 2011).

### 1.13. Resistance to cell wall antibiotics

#### 1.13.1. Resistance, tolerance and persistence

Resistance, tolerance and persistence are terms used to describe different bacterial population responses to antibiotic treatment. Resistance is described by a change in MIC and is commonly caused by an inherited mutation (Brauner et al., 2016). A population resistant to a certain concentration of antibiotic is capable of replicating in the presence of that drug concentration. A tolerant bacterial population is able to survive transient antibiotic concentration and can be treated using longer exposure rather than a higher concentration of antibiotic (Tuomanen, Durack, & Tomasz, 1986). The difference between sensitive and tolerant strains is related to death kinetics rather than lack of effect, which is the case for resistance. Persistence involves only a sub-population of a bacterial culture. The persistent population is not killed after treatment with an antibiotic that effectively eliminated the rest of the population (Brauner et al., 2016). Some researchers consider persistence to be due to phenotypic, non-inherited changes (Balaban et al., 2004). Persistence is often associated with slow growth and is a form of antibiotic tolerance.

#### 1.13.2. $\beta$ -lactam resistance

There are three main mechanisms of  $\beta$ -lactam resistance: reduced access to the target PBPs, production of  $\beta$ -lactamases and reduced binding affinity through a modified target PBP. *S. aureus* uses two different resistance mechanisms, the production of penicillinase or the production of PBP2a. Penicillinase hydrolyses  $\beta$ -lactams rendering them inactive (Sabath, 1982). Methicillin resistance in *S. aureus* is mediated by the staphylococcal chromosomal cassette *mec* (SCC*mec*). The *mecA* gene on SCC*mec* expresses PBP2a which is an additional PBP

with a lower affinity for  $\beta$ -lactams. The reduced accessibility to the active site of PBP2a leads to a decrease of 3 to 4 orders of magnitude in the rate constant for acylation and an elevated dissociation constant for the pre-acylation complex (Fuda et al., 2004). The presence of PBP2a allows for continued cell wall biosynthesis in the presence of  $\beta$ -lactams. PBP2a on its own is not however able to confer high levels of resistance. PBP2a is a class B PBP and therefore does not have transglycosylase activity and cooperated with PBP2 to synthesise peptidoglycan (Pinho et al., 2001). Other factors such as *fem* (factors essential for methicillin resistance) and *aux* (auxiliary) loci are also involved in conferring high levels of resistance in the presence of PBP2a (Chambers, 1997).

### 1.13.3. Vancomycin resistance

Vancomycin resistant *S. aureus* strains can be split into two categories: vancomycin intermediate-resistant and vancomycin-resistant *S. aureus* (VISA and VRSA respectively). VISA strains do not have genetic elements carrying vancomycin resistance. These strains develop resistance through selective pressure and mutation during vancomycin treatment (Gardete & Tomasz, 2014). Most VISA strains develop in patients on long courses of vancomycin for MRSA infections. VISA strains are characterised by a thicker cell wall, decreased autolysis and defective daughter cell separation (Howden et al., 2010). Despite only a small increase in MIC, treatment failure is common in VISA infections (Gardete & Tomasz, 2014).

VRSA strains modify the vancomycin target to achieve high levels of resistance. This modification is transposon mediated and was first detected in *Enterococcus* species, before it was transferred to *S. aureus* (Faron et al., 2016). In *Enterococcus*, several different Van elements have been found, but so far, only VanA-type resistance has been found in *S. aureus* (Courvalin, 2006). The D-Ala-D-Ala dipeptide that vancomycin binds to is replaced by D-Ala-D-Lac, which decreases target affinity for vancomycin and in some cases teicoplanin making treatment with these drugs ineffective. The dehydrogenase VanH reduces pyruvate to D-Lac and the VanA ligase catalyses the bond formation between D-Ala and D-Lac (Courvalin, 2006).

### 1.14. Project aims

The aim of this project was to build on our existing knowledge of cell wall antibiotic mode of action to try and further elucidate the mechanism by which these antibiotics kill bacteria. New labels and imaging techniques were used to attempt to gain novel insight into the effect of  $\beta$ -lactams and vancomycin on *S. aureus*.

## Chapter 2

### Materials and Methods

#### 2.1. Growth Conditions

##### 2.1.1. Media

All growth media was dissolved in distilled water and autoclaved at 121 °C for 15 minutes. Tryptone Soy Broth was used for all *S. aureus* experiments. Nutrient broth was used for all *B. subtilis* experiments.

##### 2.1.2. Tryptone Soy Broth (TSB)

Tryptone Soy Broth (Oxoid) 30 g l<sup>-1</sup>  
1% (w/v) Bacteriological Agar (VWR) was added to make TSB Agar.

##### 2.1.3. Nutrient Broth (NB)

Nutrient Broth (Oxoid) 13 g l<sup>-1</sup>

##### 2.1.4. NB Agar

Nutrient Broth Agar (Sigma-Aldrich) 28 g l<sup>-1</sup>

#### 2.2. Antibiotics

Stock solutions of antibiotics were filter sterilised, using a 0.22 µm pore size filter, before being stored at -20°C. To make antibiotic-containing agar plates, the antibiotic was added to molten agar cooled to below 55°C. All antibiotics used in this study are listed in **Table 2.1**.

Antibiotic	Stock solution (mg ml <sup>-1</sup> )	Solvent
Tetracycline (Tet)	5	50% (v/v) ethanol
Minocycline (Min)	2	dH <sub>2</sub> O
Kanamycin (Kan)	50	dH <sub>2</sub> O
Erythromycin (Ery)	5	95% (v/v) ethanol
Spectinomycin (Spec)	100	dH <sub>2</sub> O
Vancomycin	10	dH <sub>2</sub> O
Methicillin	10	dH <sub>2</sub> O
Oxacillin	1	dH <sub>2</sub> O

**Table 2.1.** Antibiotic stock solutions and solvents.

## 2.3. Buffers & Solutions

All solutions were prepared with dH<sub>2</sub>O except when stated otherwise and autoclaved where necessary.

### 2.3.1. Phosphate Buffered Saline (PBS)

Phosphate Buffered Saline Tablets (Sigma)	5 tablets l <sup>-1</sup>
---	---------------------------

### 2.3.2. Fixative Preparation

#### 2.3.2.1. Preparation of 16% (w/v) paraformaldehyde

*100 mM sodium phosphate buffer pH 7.0:*

1 M Na <sub>2</sub> HPO <sub>4</sub>	57.7 mL
--------------------------------------	---------

1 M NaH <sub>2</sub> PO <sub>4</sub>	42.3 mL
--------------------------------------	---------

The final volume was adjusted to 1 L.

*16% (w/v) paraformaldehyde:*

100 mM sodium phosphate buffer pH 7.0	50 mL
---------------------------------------	-------

Paraformaldehyde	8.0 g
------------------	-------

The paraformaldehyde was added to 100 mM sodium phosphate buffer (pH 7.0), heated to 60°C and mixed. While heat and stirring were maintained, NaOH (≥ 5 M) solution was added dropwise until the solution cleared. The solution was stored at 4°C for up to 3 months.

#### 2.3.2.2. Fixative

16% (w/v) paraformaldehyde	0.5 mL
----------------------------	--------

PBS	2 mL
-----	------

### 2.3.3. Click-iT<sup>®</sup> reaction buffer mix

The reaction buffer components were purchased from Molecular Probes and made up as per their instructions.

Click-iT <sup>®</sup> cell reaction buffer	440 µL
--	--------

100 mM Copper (II) sulphate	10 µL
-----------------------------	-------

Click-iT <sup>®</sup> cell additive	50 µL
-------------------------------------	-------

## 2.4. Chemicals & enzymes

Stock Solution	Concentration	Solvent	Storage
Di-peptide (3-azido-D-alanine- D-alanine)	100 mM	DMSO	-20°C
TADA (Tetramethylrhodamine-3-amino-D-alanine)	100 mM	DMSO	-20°C dark
ADA (3-azido-D-alanine) (Iris Biotechnology)	100 mM	DMSO	-20°C
NHS ester Alexa Fluor™ 555 (Molecular Probes)	0.5 mg ml <sup>-1</sup>	DMSO	-20°C dark
NHS ester Alexa Fluor™ 405 (Molecular Probes)	0.5 mg ml <sup>-1</sup>	DMSO	-20°C dark
WGA Alexa Fluor™ 594 (Molecular Probes)	1 mg ml <sup>-1</sup>	dH <sub>2</sub> O	-20°C dark
Alkyl Atto 488	1 mg ml <sup>-1</sup>	DMSO	-20°C dark
Alkyl Alexa Fluor™ 594 (ThermoFisher)	0.5 mg ml <sup>-1</sup>	DMSO	-20°C dark
<sup>14</sup> C-GlcNAc (Hartmann analytic)	250 µCi in 2.5 ml	N/A	4°C

**Table 2.2. Stock solution information for the chemicals and enzymes used in this study.**

## 2.5. Equipment

### 2.5.1. Centrifuges

For small volumes, Eppendorf Centrifuge 5418 was used. It has a max speed of 21,130 g and max volume of 2 mL. For larger volumes, the Sigma 4K15 centrifuge was used, which takes tubes up to 50 mL and has a max speed of 21,040 g.

### 2.5.2. Spectrophotometer

Optical density (OD) measurements were acquired using the WPA Biowave Spectrophotometer at 600 nm (OD<sub>600</sub>).

## 2.6. Bacterial strains and growth

### 2.6.1. *S. aureus* strains

The *S. aureus* strains used in this study are listed in **Table 2.3**. Strains were stored in Microbank beads at - 80°C for long term storage. For use, strains were grown on TSB agar plates containing relevant antibiotics when they were required to maintain resistance marker selection. Plates were stored for up to two weeks at 4°C. To carry out experiments in liquid culture, 10 mL of TSB medium in a 25 mL universal tube was inoculated with a single colony and grown overnight at 37°C on a rotary shaker (250 rpm). Except specified otherwise, 50 mL of TSB medium in a 250 mL conical flask was inoculated with the overnight culture to an OD<sub>600</sub> of 0.05 and grown to early exponential phase (OD<sub>600</sub> 0.2-0.3) at 37°C on a rotary shaker (250 rpm).

Strain	Genotype	Source
<i>S. aureus</i> SH1000	Functional <i>rsbU</i> <sup>+</sup> derivative of 8325-4	(Horsburgh et al., 2002)
<i>S. aureus</i> SH1000 <i>sagA</i>	<i>sagA::tetL</i> ; Tet <sup>R</sup>	
<i>S. aureus</i> SH1000 <i>scaH</i>	<i>scaH::tetM</i> ; Tet <sup>R</sup>	
<i>S. aureus</i> SH1000 <i>sagB</i>	<i>sagB::kan</i> ; Kan <sup>R</sup>	
<i>S. aureus</i> SH1000 <i>atl</i>	<i>atl::pAZ106</i> ; Ery <sup>R</sup>	
<i>S. aureus</i> SH1000 <i>atl sagA sagB</i>	<i>atl::pAZ106 sagA::tetK sagB::kan</i> ; Ery <sup>R</sup> , Tet <sup>R</sup> , Kan <sup>R</sup>	(Wheeler et al., 2015)
<i>S. aureus</i> SH1000 <i>atl sagA scaH</i>	<i>Atl::spc sagA::tetK scaH::tetM</i> ; Spec <sup>R</sup> , Tet <sup>R</sup> , Min <sup>R</sup>	(Wheeler et al., 2015)
<i>S. aureus</i> SH1000 <i>sagA sagB scaH</i>	<i>sagA::tetL sagB::kan scaH::tetM</i> ; Tet <sup>R</sup> , Kan <sup>R</sup> , Min <sup>R</sup>	(Wheeler et al., 2015)
<i>S. aureus</i> SH1000 <i>atl sagB scaH</i>	<i>atl::pAZ106 sagB::kan scaH::tetM</i> ; Ery <sup>R</sup> , Kan <sup>R</sup> , Tet <sup>R</sup>	(Wheeler et al., 2015)
<i>S. aureus</i> SH1000 <i>tarO</i>	<i>tarO::ery/lyn</i> , Ery <sup>R</sup>	

**Table 2.3.** *S. aureus* strains, genotype and source.

### 2.6.2. *B. subtilis* strains

*B. subtilis* strains used in this study are listed in **Table 2.4**. For long-term storage, strains were kept in Microbank beads stored at - 80°C. Strains were grown on NB agar plates for short-term storage and stored for up to 5 days at room temperature. Overnight cultures consisted of 50 mL NB medium in a 250 mL conical flask inoculated with a single colony. Overnight cultures were grown at 37°C on a rotating shaker (250 rpm).

A preculture was carried out before all *B. subtilis* experiments. For the preculture, 50 mL NB media in a 250 mL conical flask was inoculated with the overnight to an OD<sub>600</sub> of 0.01 and grown up to an OD<sub>600</sub> of 0.6 at 37°C on a rotary shaker (250 rpm). The preculture was then used to inoculate 50 mL NB in a 250 mL conical flask to an OD<sub>600</sub> of 0.05. The culture was then grown at 37°C on a rotary shaker (250 rpm) to early exponential phase.

Strain	Genotype	Source
<i>B. subtilis</i> 168 HR	HR trpC2	

Table 2.4. *B. subtilis* strain, genotype and source.

## 2.7. Killing assays

### 2.7.1. MIC

To determine the minimum inhibitory concentration (MIC) of a compound, it was serially diluted in 10 mL of growth media (TSB for *S. aureus* strains, NB for *B. subtilis* strains) in 50 mL universal tubes. The universal tubes containing 10 mL growth media and different concentrations of the compound were inoculated with overnight culture to an OD<sub>600</sub> of 0.05 and were grown at 37°C on a rotary shaker (250 rpm) for 24 hours. The OD<sub>600</sub> of each tube was measured after 24 hours and the MIC was set as the lowest concentrations at which no growth was observed.

### 2.7.2. CFU killing curves

50 mL of media (TSB for *S. aureus*, NB for *B. subtilis*) in a 250 mL conical flask was inoculated from an overnight culture for *S. aureus* or a preculture for *B. subtilis* to an OD<sub>600</sub> of 0.05 and incubated shaking (250 rpm) at 37 °C until early exponential phase was reached (OD<sub>600</sub> 0.2-0.3). The antibiotic was then added for a final concentration of 10 x MIC. 100 µL samples were taken at different time-points, washed and resuspended in PBS to eliminate any antibiotic. Samples were then serially diluted and were either spotted (5 µL spots) in three repeats onto agar plates or spread (50 µL of sample) onto TSB or NB Agar plates using glass beads. Plates were incubated overnight at 37°C. The number of colonies were then counted, and the CFU/mL of the original sample was calculated.

## 2.8. Labelling

### 2.8.1. Fluorescent D-amino acid labelling

Three different types of fluorescent D-amino acids were used: di-peptide with an azide linker, ADA with a fluorescent probe already attached and ADA with an azide linker. The two first in this list are not commercially available and were synthesised by members of Dr. Simon Jones' research group in the Chemistry Department at the University of Sheffield. ADA was purchased from Iris Biotech.

Cells were grown to early exponential phase. A 1 mL sample was removed and added to 10  $\mu$ L of 100 mM FDAA in a 1.5 mL eppendorf and placed at 37°C shaking for 5 minutes. Samples were centrifuged and the pellets were washed once with PBS ready for further experimental use.

For samples where di-peptide and ADA with an azido group were used, an alkaline-containing fluorescent dye was attached using the Click-iT<sup>®</sup> reaction. The Click reaction is carried out on samples after fixation (2.3.2.2). Cells were incubated with 0.5 mL Click-iT reaction buffer mix and 10  $\mu$ L alkyne fluorescent dye for 30 minutes on a rotator at room temperature.

#### 2.8.2. NHS Ester labelling

1 mL of sample was taken from the desired culture and fixed according to the protocol described in 2.3.2.2. For SIM imaging, pellets of fixed samples were resuspended in 300  $\mu$ L of PBS and 20  $\mu$ L of 0.5 mg/mL NHS ester stock. Samples were incubated on a rotator at room temperature for 30 minutes before being washed and prepared for imaging.

#### 2.8.3. WGA labelling

1 mL of sample was taken from the desired culture and fixed. Samples were resuspended in dH<sub>2</sub>O and 25  $\mu$ L 1 mg/mL WGA stock and 25  $\mu$ L 1M calcium chloride solution were added. Samples were incubated at 37°C for 5 minutes before being washed and prepared for imaging.

### 2.9. Fluorescent microscopy

#### 2.9.1. Resolution limited microscopy

##### *Sample preparation*

After fixation and required labelling, samples were washed and diluted in dH<sub>2</sub>O. The appropriate dilution was estimated by eye. 5  $\mu$ L of the sample was applied to a poly-l-lysine slide (Sigma) and left to air-dry. The slide was then washed with dH<sub>2</sub>O and dried using nitrogen gas. 5  $\mu$ L PBS was used to mount a coverslip, which was then sealed with nail polish.

##### *Microscopy*

Samples were imaged using the Nikon dual-cam microscope in the Wolfson Light Microscopy Facility at the University of Sheffield. This microscope consists of a Nikon Ti inverted microscope fitted with a Lumencor SpectraX light engine (395, 440, 470, 508, 561 & 640 nm) and several emission filters (DAPI, GDP, RFP, Cy5 and Quad of each of the previous filters). Images are acquired using a 100x PlanApo (1.4 NA) oil objective, 1.518 RI oil and the Dual Andor Zyla sCMOS camera along with the NIS elements software.

### *Image rendering*

Images were processed using Fiji, a software based on ImageJ 1.52i. Maximum intensity projections were made of images for presentation in this thesis.

#### 2.9.2. Structured illumination microscopy

### *Coverslip preparation*

For SIM imaging, samples were mounted onto high precision coverslips (No. 1.5H, 22 x 22 mm, 170±5 µm, Marienfeld). Before mounting of the bacterial sample, the coverslips were washed by sonication in 1 M KOH for 15 minutes. The coverslips were then rinsed and incubated for 30 minutes at room temperature in 2 mL poly-L-lysine (Sigma). After poly-L-lysine coating, the coverslips were washed and dried using nitrogen.

### *Sample preparation*

The bacterial sample was appropriately diluted in dH<sub>2</sub>O and 5 µL of the sample was applied to a poly-L-lysine coated high precision coverslip. The sample was dried on using nitrogen gas. 5 µL SlowFade® Diamond Antifade (Molecular Probes) was used to mount the coverslip (sample side down) onto a poly-L-lysine coated slide. Nail polish was used as a sealant.

### *Microscope*

Samples were imaged using the Deltavision/GE OMX SIM (v. 4) in the Wolfson Light Microscopy Facility at the University of Sheffield. This SIM is fitted with 4 laser lines (405 nm, 488 nm, 568 nm, 642 nm) and four filter sets (436/31, 528/48, 609/37, 683/40). Images were acquired using 1.518 RI oil and a 60x 1.42 oil planapochromat lens. Z steps between slices were 0.125 nm. Images were reconstructed using SoftWoRx (v. 6.1.3).

### *Image rendering*

After reconstruction, a macro (Dr. Christa Walther, unpublished) was used to threshold images in an automated manner (same thresholding process as can be found and done manually in the SIM check plugin). This macro is run using Fiji. The use of Fourier transformation in image reconstruction generated negative intensity values. The thresholding process puts all grey level bins below 0 into the 0 bin. The macro also converts 36-bit grey level images into 16-bit grey level images for easier handling. When several fluorescent channels were present, false colours were applied and composite images were made. Maximum intensity projections of images are presented in this thesis.

## 2.10. Cell measurements

### 2.10.1. Cell volume estimation

Methodology adapted from (Zhou et al., 2015).

Cell volume estimations were carried out on SIM images of NHS Ester labelled cells. In ImageJ, an average intensity Z project stack was made of the sample images. This projection was used for the following analysis. To ensure accuracy, measurements were done on cells in clusters of 4 or less. A line was drawn through the long axis of the cell and a fluorescence profile was generated. The distance between peaks was measured to generate a diameter measurement. The process was repeated at a 90-degree angle to the previous line. From the diameters, the radiuses (R1 and R2) were calculated. These measurements were inserted into the following equation:  $\frac{4}{3} \times \pi \times R1 \times R2^2$ , generating an estimated cell volume. This was carried out on 100 cells for each sample.

## 2.11. Electron Microscopy

After PFA fixation, samples were chemically fixed by resuspension in 2.5% glutaraldehyde overnight at 4°C. A secondary fixation was carried out with 2% aqueous osmium tetroxide for 2 hours at room temperature. The cells were then washed before being resuspended in progressively higher concentrations of ethanol to dehydrate them. Cells were first resuspended in 75% ethanol for 15 minutes, then 95% ethanol for 15 minutes, then 100% ethanol for 15 minutes, and finally 100% dried ethanol for 15 minutes. Cells were then resuspended in propylene oxide for 15 minutes after which the cells were transferred to a glass vial. Cells were incubated shaking at 2 rpm overnight in a 50/50 mix of propylene oxide/epon resin. Cells were then further infiltrated and embedded in epon resin and the label was added. The resin was polymerised for 2-3 days at 60°C. The blocks were sectioned with an ultramicrotome at room temperature and post stained with aqueous 3% uranyl acetate and Reynolds lead citrate. The sections were imaged by transmission electron microscopy (TEM).

## 2.12. Radioactive incorporation

Cells were grown to the desired growth phase and 1 mL of cell culture was added to 2.5 µL of <sup>14</sup>C-GlcNAc in a 1.5 mL eppendorf, for a final concentration of 5 µM <sup>14</sup>C-GlcNAc. The sample was incubated shaking at 37 °C for 5 minutes. The cells were then incubated with 1 mL ice-cold 10% (w/v) trichloroacetic acid (TCA) on ice for 1 hour. Samples were filtered through glass microfibre filters (Whatman) with 25 mL of 5% (w/v) TCA. The sample can then be found on the filters and any non-incorporated radioactive material will have been washed off. Filters were immersed in 10 mL Perkin Elmer Ultima Gold® scintillation fluid. Disintegrations per minutes

(DPM) were measured using the Packard Liquid Scintillation Analyzer Model Tri-Carb 31007R with a count time of 10 minutes per sample.



## Chapter 3

### The effect of $\beta$ -lactam antibiotics on *S. aureus*

#### 3.1. Introduction

$\beta$ -lactams target the cell wall synthesis machinery by binding to PBPs and inhibiting the transpeptidation step of peptidoglycan synthesis. A large body of research has tried to understand the molecular pathway to cell death after antibiotic treatment. Peter Giesbrecht developed a model where *S. aureus* dies upon attempting to initiate its second cell division cycle after addition of the antibiotic (Giesbrecht et al., 1998). More recent research suggested that induction of oxidative stress leads to  $\beta$ -lactam killing (Wang & Zhao, 2009). The Bernhardt group has developed a model whereby cells die due to resource depletion after a futile cycle of peptidoglycan synthesis and hydrolysis (Cho et al., 2014). This has created a confusing picture with several different competing models. A more in-depth presentation of previous work on the action of  $\beta$ -lactams can be found in the general introduction to this thesis (1.11).

##### 3.1.1. *S. aureus* cell cycle and peptidoglycan dynamics

*S. aureus* divides sequentially in three orthogonal planes, possibly using peptidoglycan architecture to guide its next division plane (Turner et al., 2010; Tzagoloff & Novick, 1977). Peptidoglycan synthesis occurs in a non-uniform manner, mainly at the septal annulus but also all across the cell (Lund et al., 2018; Pinho & Errington, 2003). During division, peptidoglycan is inserted in a region across the septum (Lund et al., 2018). The leading edge of the septum is thinner than the lagging edge, giving a large surface area for synthesis. Once the septal annulus is closed, further incorporation forms a septum of uniform width before cell scission occurs. Once the septum is completed, peptidoglycan hydrolases, including Atl, hydrolyse the cell wall at the septal plane (Komatsuzawa et al., 1997). Daughter cells then pop apart on a millisecond time-scale (Zhou et al., 2015). After cell division, the peptidoglycan is remodelled by hydrolases to form the prolate spheroid morphology of *S. aureus* (Zhou et al., 2015). This suggests that both peptidoglycan synthesis and peptidoglycan hydrolysis are required for normal cell growth (Wheeler et al., 2015).

Peptidoglycan synthesis can be split into three main stages. First, the precursors (UDP-MurNAc and UDP-GlcNAc) are synthesised in the cytoplasm (Typas et al., 2012). Next, the muropeptides are assembled, forming lipid II, and are flipped across the membrane. Finally lipid II is polymerised into glycan chains that are then inserted into the existing peptidoglycan (Typas et al., 2012). Penicillin-binding proteins (PBPs) catalyse the polymerisation of the glycan strands and crosslinking of the glycan strands (transglycosylation and transpeptidation respectively) during synthesis (Sauvage et al., 2008). Transglycosylation can also be catalysed by several other components: Mgt, SgtA, FtsW & RodA (Emami et al., 2017; Reed et al., 2011; Taguchi et al., 2019). *S. aureus* has four native PBPs: PBP1, PBP2, PBP3 and PBP4 (Canepari et al., 1985). PBP1 and PBP2 are

essential and comprise the minimum peptidoglycan synthesis machinery required for *S. aureus* to grow (Reed et al., 2015). PBP2 is a class A HMW PBP with both transpeptidase and transglycosylase activity. PBP1, PBP3 and PBP4 only have transpeptidase activity (Scheffers & Pinho, 2005).

After cell division, the newly synthesised septum is remodelled by glucosaminidases. *S. aureus* has four glucosaminidases, SagA, SagB, ScaH and Atl, that are collectively essential (Wheeler et al., 2015).

Glucosaminidases cleave the bond between the *N*-acetylglucosamine and *N*-acetylmuramic acid residue of the glycan backbone, creating the shorter glycan strands characteristic of *S. aureus* peptidoglycan (Boneca et al., 2000). All four glucosaminidases play a role in cell enlargement and normal cell morphology although lack of SagB has the biggest impact on cell morphology, with cells remaining smaller and more hemispherical (Wheeler et al., 2015).

### 3.1.2. Methods used to study $\beta$ -lactams

To study the effect of antibiotics, measuring killing is an important step. Optical density (OD) measurements give us a measure of culture turbidity, which is correlated to growth. However, OD is not a very accurate measure for cell death as the rate of cell lysis can affect measurements. A more accurate way of measuring cell viability after antibiotic treatment is to use colony forming units (CFUs). CFUs are a commonly used method to determine the number of live cells present in a culture at any given time. The measure tells us how many units (i.e. bacteria) able to form a colony on an agar plate were present in the culture. The change in the number of CFU in a culture over time is used to measure growth and death.

Imaging has played a role in furthering our understanding of the action of  $\beta$ -lactams. Electron microscopy has been used extensively to study the effect of  $\beta$ -lactams. The most extensive model of  $\beta$ -lactam killing developed by Peter Giesbrecht was based on EM images of *S. aureus* after penicillin treatment (Peter Giesbrecht et al., 1998). EM offers higher resolution images than fluorescence microscopy.

Mutants with altered responses are one of the most common tools used to study antibiotics. Interest is taken in strains that exhibit increased resistance, persistence or tolerance to an antibiotic (Dengler et al., 2013; Germain et al., 2013; Kaspy et al., 2013). These studies can give us insight into the mode of action of antibiotics but mainly help elucidate changes that lead to resistance. The effect of antibiotics on gene expression has also been studied (Mwangi et al., 2013). In the case of  $\beta$ -lactams, most studies looking at gene expression focus on changes in expression of factors relaying resistance (eg. expression of genes encoding  $\beta$ -lactamases).

Since  $\beta$ -lactams target the cell wall metabolism, studies have used methods to measure peptidoglycan synthesis. The existing methods to quantify peptidoglycan synthesis are described in detail later in the introduction to this chapter.

### 3.1.3. Structured illumination microscopy

The resolution of conventional light microscopy is limited by the diffraction of light through the objective of the microscope (Huang et al., 2010). Light converges into a focal point, and this focal point is of finite size due to diffraction. With conventional microscopy, it is not possible to differentiate between two fluorescent molecules located within the focal point. The resolution limit of conventional light microscopy is ~250 nm in the lateral dimension and ~550 nm in the axial dimension (Huang et al., 2010).

A new range of super-resolution microscopy techniques has been developed allowing imaging at resolutions well beyond those of diffraction limited microscopy (Huang et al., 2010). The new techniques can distinguish two molecules within a diffraction-limited region by using the physical properties of fluorescent probes. The main super-resolution microscopy techniques are stimulated emission depletion microscopy (STED), structured illumination microscopy (SIM), stochastic optical reconstruction microscopy (STORM) and fluorescence photoactivation localization microscopy (FPALM).

A more detailed explanation of SIM will be presented here as it was the chosen super-resolution microscopy technique for this project. In SIM, a known regular illumination pattern is juxtaposed over the sample. The unknown sample structure and the known illumination pattern generate a pattern called moiré fringes. The unknown sample structure can be computationally extracted from the moiré fringes (Gustafsson, 2005; Heintzmann et al., 2002). The pattern is rotated at several different angles over the sample, to give a complete rendering of the sample. A resolution of < 50 nm can be obtained with SIM using bright and stable fluorophores (Gustafsson, 2005). One of the main advantages of SIM is that it does not require fluorophores with particular photo-properties – the fluorophores commonly used for conventional fluorescence microscopy can be used with SIM. However, due to the large number of pictures taken of the sample to render one image, bright and photostable fluorophores are required for high quality images.

### 3.1.4. Labelling of the bacterial cell surface

Several labels are available that can be used to visualise the bacterial cell surface. These include fluorescent NHS ester and wheat germ agglutinin (WGA).

N-hydroxysuccinimide (NHS) ester (aka. succinimidyl ester) binds to primary amines of proteins and other amine-containing molecules. On the cell surface it can bind to peptide side chains of peptidoglycan as well as surface proteins. A large range of fluorophores conjugated to NHS Ester can be found commercially, making it a versatile tool for cell surface labelling.

WGA is a lectin extracted from wheat that serves as a barrier to insects, yeast and bacteria. WGA binds GlcNAc making it an effective label of gram-positive bacteria cell wall when conjugated with a fluorophore. WGA and fluorophore conjugates are commercially available.

### 3.1.5. Labelling peptidoglycan incorporation

Over the last 30 years different techniques have been developed to help further our understanding of peptidoglycan synthesis. The first studies that sought to investigate peptidoglycan synthesis used uranyl acetate staining of thin cell sections imaged by EM or autoradiography of radiolabelled sacculi (Merad et al., 1989). Both of these methods use sacculi rather than live cells, limiting their usefulness.

The first method developed using the incorporation of alternate D-amino acids into the peptide side chain was developed in *E. coli* (de Pedro et al., 1997). The growth media was supplemented with D-cysteine which is incorporated as the terminal D-amino acid of the peptide side chain by exchange reaction in the periplasm. D-cysteine contains thiol groups that are then detected by immune-detection and labelled for fluorescence or electron microscopy. Again, this method is limited to use in sacculi.

More recently, fluorescent vancomycin was developed as a tool to label new peptidoglycan (Daniel & Errington, 2003). Vancomycin binds the D-ala-D-ala motif at the end of the peptide side chain. In most species, the terminal D-ala-D-ala is rapidly processed by crosslinking of the peptide side chain or by hydrolysis. Vancomycin can therefore only bind nascent peptidoglycan and can be used as a probe to locate newly synthesised peptidoglycan. *S. aureus* has low carboxypeptidase activity, leaving terminal D-ala-D-ala motifs in mature peptidoglycan (Scheffers & Pinho, 2005). To allow for the use of fluorescent vancomycin in *S. aureus*, the cells must first be grown in the presence of D-serine, which is incorporated into the terminus of the peptide side chain instead of D-ala. The cells are then briefly incubated in the presence of D-ala, allowing for labelling of the new peptidoglycan with vancomycin. This method, although an advancement, does not label live cells.

Fluorescent D-amino acids (FDAAs) developed by the Van Nieuwenhze group allow us to carry out live cell labelling of peptidoglycan synthesis (Kuru et al., 2012). FDAAs are incorporated into position 4 or 5 of the peptide side chain. Around the same time, a second group developed D-amino acid probes with azide and alkyl groups, allowing researchers to use click chemistry to attach a fluorescent dye of their choice (Siegrist et al., 2013).

There are thought to be two possible incorporation pathways for FDAAs: precursor synthesis in the cytosol and periplasmic modification of mature peptidoglycan (Cava et al., 2011). To be incorporated into nascent peptidoglycan, the single D-alanine is joined into a D-alanyl-D-alanine dipeptide by the D-alanine-D-alanine ligase (Ddl). The dipeptide is then added to the growing peptide side chain via MurF. To bypass the question of

whether observed incorporation represents new peptidoglycan or post-synthesis modification, a D-alanyl-D-alanine (or “dipeptide”) label was developed (Liechti et al., 2014). The dipeptide is incorporated into peptidoglycan precursors via MurF. In *S. aureus* all three probes mark regions of new peptidoglycan incorporation (Lund et al., 2018).

Methods are also available to incorporate modified backbone sugars. Peptidoglycan incorporation can be measured by incorporation of  $^{14}\text{C}$ -GlcNAc (Maki et al., 2001). This method allows quantification of incorporation but not for localisation. Most recently, Catherine Grimes’ group developed a method by which NAM derivatives can be incorporated during peptidoglycan synthesis (Liang et al., 2017). However, this novel technique requires genetic manipulation of the organism.

#### 3.1.6. Aims of this chapter

- Investigate the effect of  $\beta$ -lactams on *S. aureus* and *B. subtilis*
- Establish death kinetics
- Study the effects of antibiotics on cell morphology
- Establish the effect of  $\beta$ -lactams on macromolecular synthesis

### 3.2. Results

#### 3.2.1. Killing Dynamics

Methicillin was used as the representative  $\beta$ -lactam as it was developed specifically for treating *S. aureus* infections. Oxacillin was used to confirm findings.

MICs were measured using a serial dilution method. Cultures were grown overnight in the presence of different concentrations of antibiotics. After 24 hours, culture  $\text{OD}_{600}$  was measured and the MIC determined. The MIC of methicillin against *S. aureus* SH1000 was found to be 4  $\mu\text{g}/\text{mL}$ , and the MIC of oxacillin against *S. aureus* SH1000 was 1  $\mu\text{g}/\text{mL}$ . All the experiments described here were carried out using 10 x MIC (i.e. 40  $\mu\text{g}/\text{mL}$  methicillin, 10  $\mu\text{g}/\text{mL}$  oxacillin).

Kill curves were used to assess the killing dynamics of methicillin and oxacillin. Survival was quantified by measuring the number of colony forming units (CFUs) at given time points after treatment. Overnight cultures of *S. aureus* SH1000 were freshly inoculated at a starting  $\text{OD}_{600}$  of 0.05. Cultures were grown, shaking, at 37°C, until they reached an  $\text{OD}_{600}$  of 0.2-0.3 (early exponential phase). The antibiotic was then added to the culture and the CFUs were measured at regular intervals for 6 hours.

When *S. aureus* SH1000 is treated with methicillin, an initial increase in cell numbers was observed for the first 30 minutes to an hour after which killing began (Figure 3.1). 90% killing was reached 5 hours after addition of 10 x MIC methicillin to the growth media.

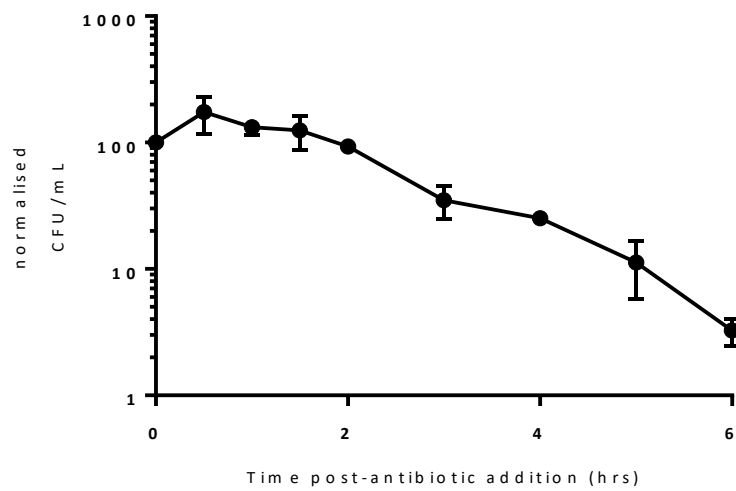


**Figure 3.1. Effect of 40 µg/mL (10 x MIC) methicillin on *S. aureus* SH1000 cell viability.** The CFU/mL was determined at each time-point and the data was normalised by setting the first time point as 100%. The mean and standard deviation are plotted. The experiment was done in triplicate.

Within 30 minutes killing was observed when *S. aureus* SH1000 was treated with 10 µg/mL oxacillin (Figure 3.2). 90% killing was reached between 1.5 and 2 hours after addition of 10 x MIC oxacillin to the growth media.

### 3.2.2. Cell morphology

β-lactams are cell wall antibiotics inhibiting peptidoglycan synthesis. As the cell wall determines cell shape, the effect of β-lactams on cell morphology was investigated.

To investigate changes in cell morphology after treatment with 10 x MIC methicillin, cells were fixed at different time points post-antibiotic treatment. Fixed cells were then labelled with NHS Ester 555 and imaged using SIM. NHS Ester is a fluorescent dye containing probe that binds amines on the cell surface, allowing visualisation of the cell shape. High-resolution SIM images allow insight into cell morphology dynamic after antibiotic treatment. Fixed cells were also imaged using EM.

#### 3.2.2.1. *Methicillin*

Morphological changes could be observed within 60 minutes of treatment with 40 µg/mL methicillin (Figure 3.3). At 60 minutes post-addition of methicillin cells with deformed, wider septa and cells with no septa were observed (Figure 3.3, Panel B). By 120 minutes after the addition of antibiotic some cells were grossly deformed. There were also many sacculi, some of which appear to have ripped at the septum (Figure 3.3, Panel C).

To quantify changes to the cells, cell volume was measured. Cell volume was estimated using ImageJ measurements as described by Zhou et al., 2015. In a non-treated population, the mean cell volume did not change significantly over time. After 60 minutes of treatment with 40 µg/mL methicillin, a highly significant increase in the mean cell volume was observed between the untreated and treated populations (Figure 3.4).

Fixed cells were also imaged using EM (Figure 3.5). 60 minutes after addition of 40 µg/mL methicillin to the growth media gross changes to the cell morphology particularly the appearance of bulging septa and wide cell walls were seen (Figure 3.5, Panel C). What appear to be large septa have an apparent septal plate with its characteristic V-shape but there is also a lesion separating it from the cytoplasmic membrane (Figure 3.5, Panel C). 17.4% of the cells exhibit a morphology where the cell membrane has been separated from the cell wall. The septal plate appears to have been hydrolysed apart into its two component parts (Figure 3.5, panel C).

Four main morphologies were identified in the EM images and quantified: cells with no visible septum, cells with a complete septum, cells with an incomplete septum, cells with an incomplete septum that has been hydrolysed down the middle (split incomplete septum) (Figure 3.6). This quantification does not take into account whether a gap has developed between the cell membrane and the cell wall. In the untreated control,

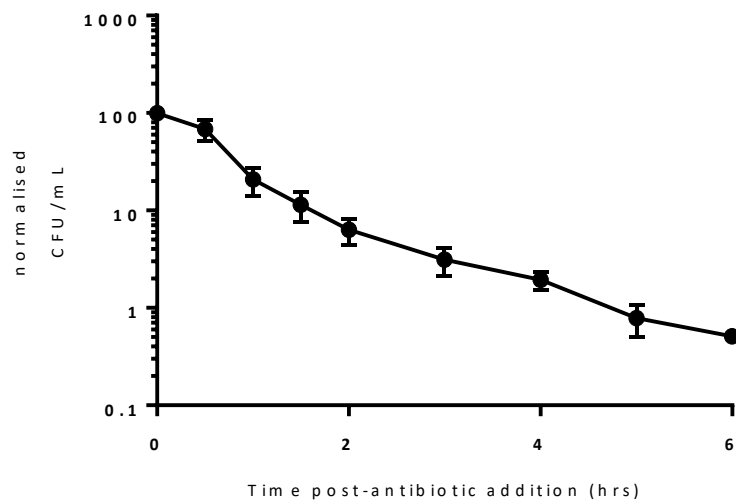


**Figure 3.2. Effect of 10 µg/mL (10 x MIC) oxacillin on *S. aureus* SH1000 cell viability.** *S. aureus* SH1000 was treated with 10 µg/mL methicillin (10 x MIC). The CFU/mL was determined at each time-point and the data was normalised by setting the first time point as 100%. The mean and standard deviation are plotted and the experiment was done in triplicate.

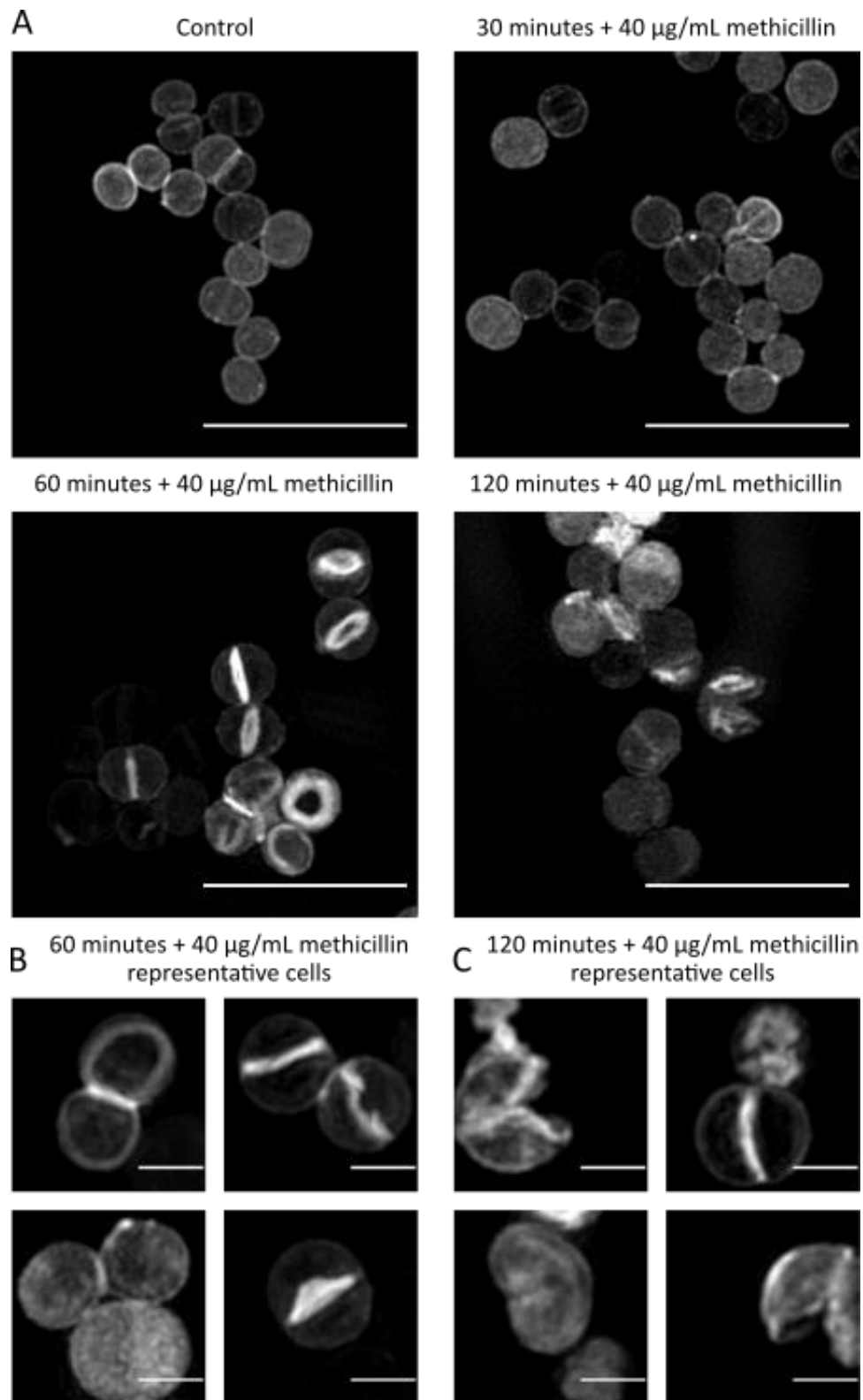


**Figure 3.3. Effect of methicillin treatment on *S. aureus* SH1000 cell morphology (SIM images).** Cells were treated with 40 µg/mL methicillin (10 x MIC), fixed after 0, 30, 60 and 120 minutes of treatment and subsequently labelled with NHS Ester 555. Cells were imaged using the OMX SIM and maximum intensity projections are shown. (A) Fields of cells from each time point, as indicated. All scale bars 5 µm. (B)

Representative cells after 60 minutes of treatment. All scale bars 1  $\mu\text{m}$ . (C) Representative cells after 120 minutes of treatment. All scale bars 1  $\mu\text{m}$ .

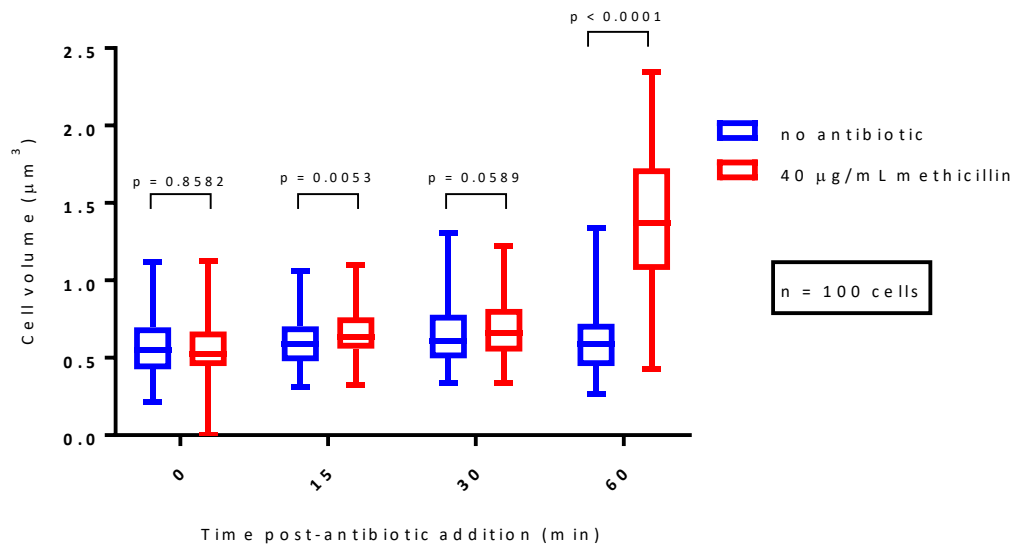
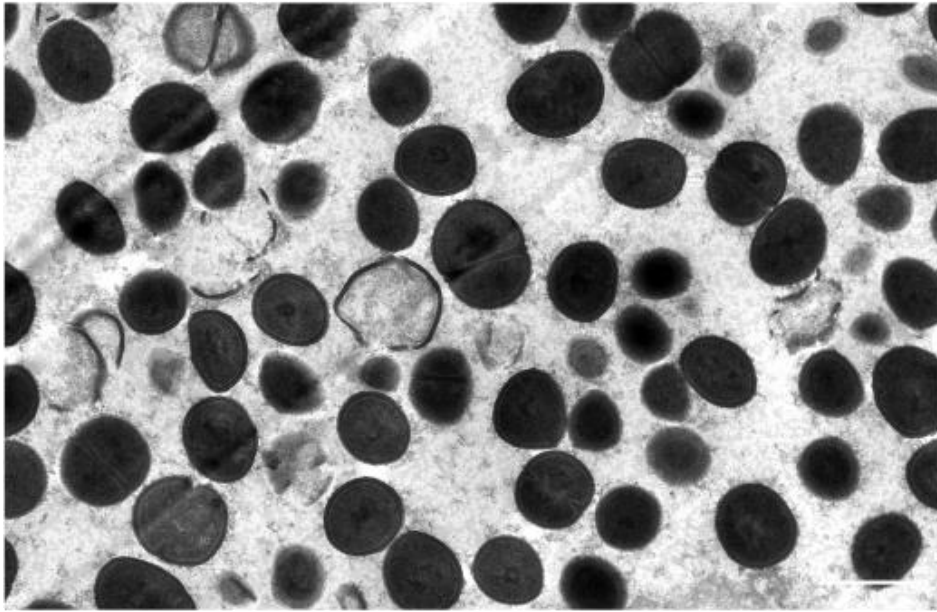


**Figure 3.4. Effect of methicillin treatment on *S. aureus* SH1000 cell volume.** Cell volume was calculated from measurements carried out in ImageJ, on OMX SIM images of NHS Ester 555 labelled cells at different time points after the addition of 40 µg/mL methicillin (10 x MIC). P-values were calculated by Mann-Whitney tests. Whiskers extend from the minimum to the maximum values and boxes from the 25<sup>th</sup> to the 75<sup>th</sup> percentile. The middle of the box is plotted at the median.

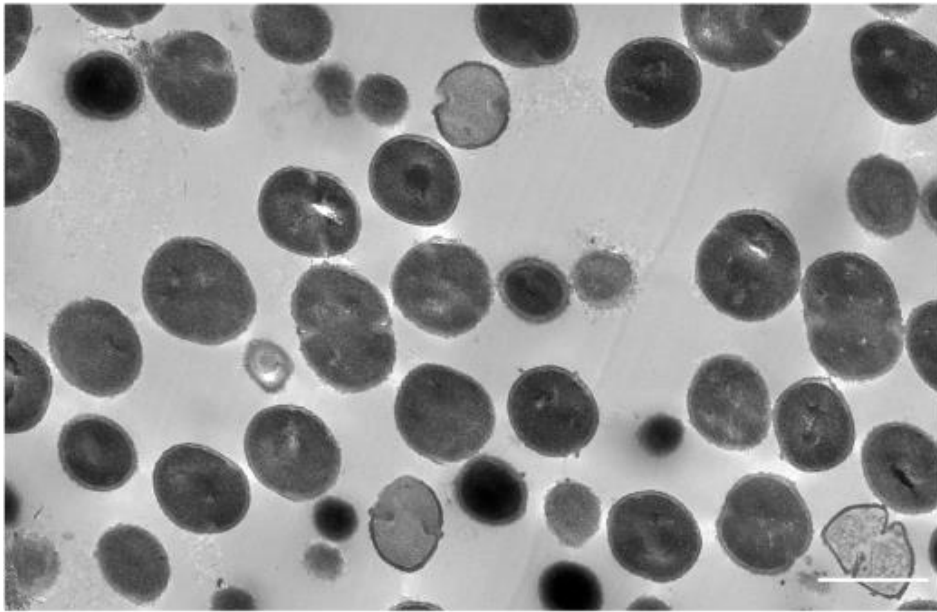
A

Fields of Cells - Control



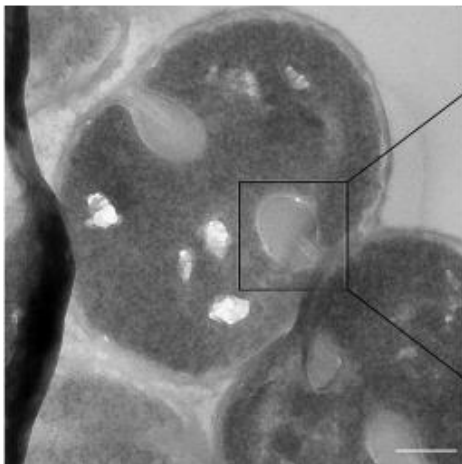
B

Fields of Cells - 60 minutes methicillin



C

Representative Cell  
60 minutes



D

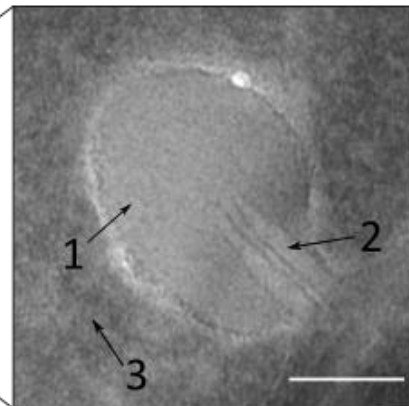


**Figure 3.5. Effect of methicillin treatment on *S. aureus* SH1000 cell morphology (EM images).** Cells were treated with 40 µg/mL methicillin (10 x MIC), fixed after 60 minutes of treatment and imaged by electron microscopy. All EM images were acquired by Lucia Lafage. (A) Field of cells from the control. Scale bar 2 µm. (B) Field of cells after 60 minutes methicillin treatment. Scale bar 2 µm. (C) Representative cell after 60 minutes of treatment. Scale bar 200 nm. (D) Magnification of a cell section from a representative cell after 60 minutes of treatment. 1 – amorphous exoplasmic material, 2 – septum, 3 – cytoplasm. Scale bar 100 nm.

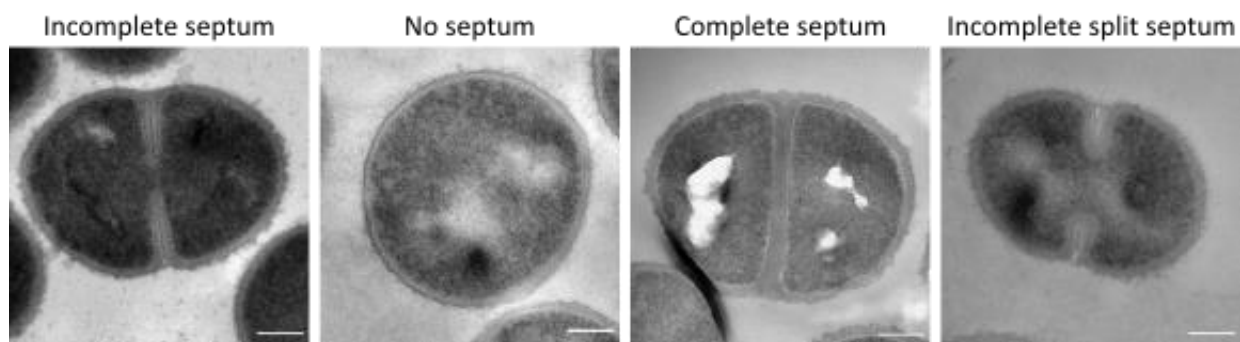
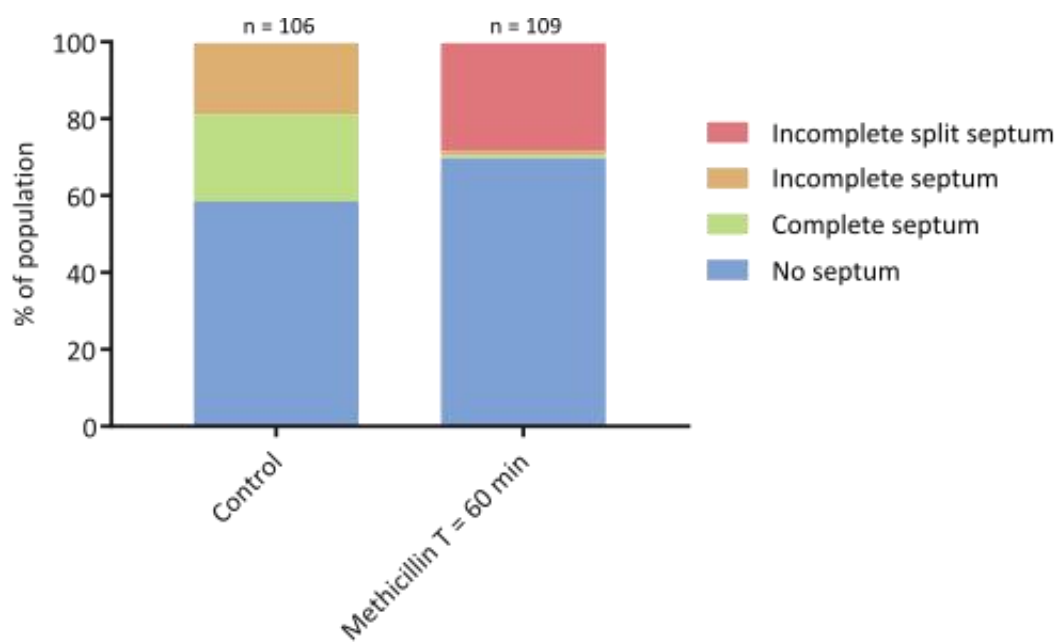


**Figure 3.6. Quantification of cell morphologies in EM images after methicillin treatment.** Four morphologies were identified and quantified in the untreated control and after 60 minutes of treatment with 40  $\mu\text{g}/\text{mL}$  methicillin. Quantification was carried out on a population of approx. 100 cells (n as indicated) for each sample.

58% of the cells do not have a septum, 23% show a complete septum and 19% of the cells have an incomplete septum with a normal septal plate. After an hour of treatment with 10 x MIC methicillin, 69% of the cells didn't have a septum, 1% had a complete septum, 1% of the cells had a normal incomplete septum and 29% of the cells have an incomplete septum that had been split (Figure 3.6).

#### 3.2.2.2. *Oxacillin*

After treatment with 10 µg/mL oxacillin, cells developed unusual morphologies. In Figure 3.7, a variety of morphologies were observed at different time points after treatment with oxacillin. At 60 minutes post-antibiotic addition, cells with deformed septa and cells that had undergone unfinished divisions were seen (Figure 3.7, Panel B). After 120 minutes of treatment, more deformed morphologies were observed and there were many sacculi in the sample (Figure 3.7, Panel C). These morphologies resembled those observed after treatment with 10 x MIC methicillin.

The same increase in cell volume that was observed after methicillin treatment, was found after treatment with 10 x MIC oxacillin (Figure 3.8). A significant increase in cell volume occurred as little as 15 minutes after the addition of oxacillin to the growth media.

#### 3.2.3. Quantification of peptidoglycan synthesis in the presence of antibiotics

Two methods were used to measure peptidoglycan synthesis post-antibiotic treatment:

- Fluorescent D-amino-acid (FDAA) incorporation to determine transpeptidase activity
- <sup>14</sup>C-GlcNAc incorporation to determine transglycosylase activity

The FDAA incorporation experiments carried out with methicillin, were done using dipeptide. Dipeptide is a D-ala-D-ala molecule containing an azide group, to which compatible fluorophores can be attached by click chemistry (Liechti et al., 2014) (2.8.1). The FDAA incorporation experiment carried out with oxacillin, was done using TADA, a D-alanine with a fluorophore already attached to it (Kuru et al., 2015). When grown in the presence of dipeptide or TADA, cells incorporate the labels into the peptide side-chains of their nascent peptidoglycan (Lund et al., 2018).

The dipeptide and TADA were synthesised by Prof. Simon Jones' group in the Department of Chemistry at the University of Sheffield.

#### 3.2.3.1. *Methicillin*

40 µg/mL methicillin (10 x MIC) was added to the growth media of an *S. aureus* SH1000 culture at an OD<sub>600</sub> of 0.2-0.3. 1 mL samples were taken at 0, 15 and 30 minutes post-antibiotic addition. Samples were incubated,

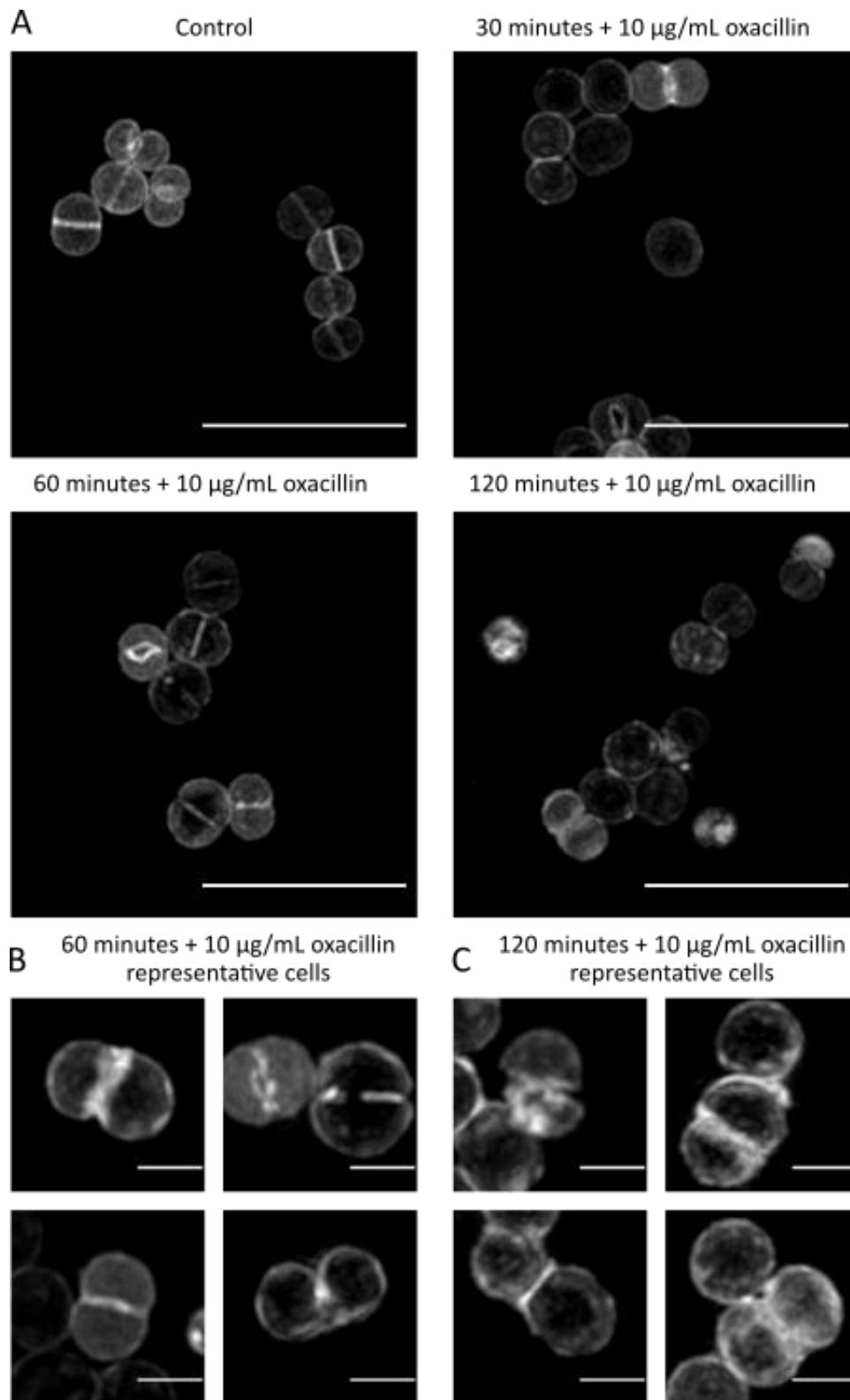


**Figure 3.7. Effect of oxacillin treatment on *S. aureus* SH1000 cell morphology.** Cells were treated with 10 µg/mL oxacillin (10 x MIC), fixed after 0, 30, 60 and 120 minutes of treatment and subsequently labelled with NHS Ester 555. Cells were imaged using the OMX SIM and maximum intensity projections are shown. (A) Fields of cells from each time point, as indicated. All scale bars 5 µm. (B) Representative cells after 60 minutes of treatment. All scale bars 1 µm. (C) Representative cells after 120 minutes of treatment. All scale bars 1 µm.

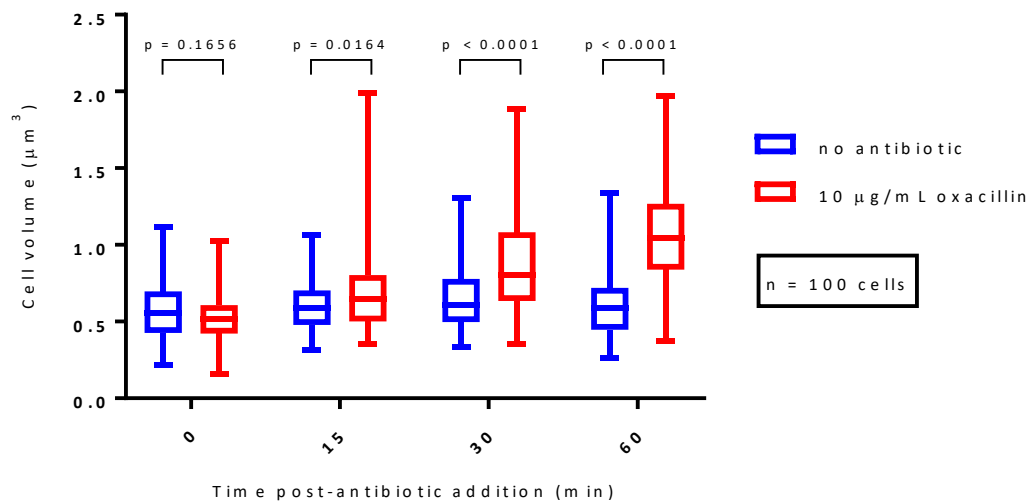


**Figure 3.8. Effect of oxacillin treatment on *S. aureus* SH1000 cell volume.** Cell volume was calculated from measurements carried out in ImageJ, on OMX SIM images of NHS Ester 555 labelled cells at different time points after the addition of 10 µg/mL oxacillin (10 x MIC). P-values were calculated by Mann-Whitney tests. Whiskers extend from the minimum to the maximum values and boxes from the 25<sup>th</sup> to the 75<sup>th</sup> percentile. The middle of the box is plotted at the median.

shaking at 37°C, for 5 minutes in the presence of 10 µL of 100 mM dipeptide. Samples were then fixed and labelled by click chemistry with alkyne Atto 488, which binds to the azide group of the incorporated dipeptides. The samples were imaged using the Nikon Dual Cam.

In Figure 3.9 a decrease in fluorescence after antibiotic treatment was observed. The fluorescence per cell was quantified using image J. The fluorescence/cell was measured for 100 cells per time point (Figure 3.9 & Figure 3.10). A statistically significant reduction in dipeptide incorporation is observed within the first 5 minutes of treatment. This suggests that treatment with 10 x MIC methicillin leads to an immediate reduction in peptidoglycan synthesis. Only residual dipeptide incorporation is observed after 15 minutes.

Incorporation of <sup>14</sup>C-GlcNAc can be used to measure peptidoglycan synthesis. <sup>14</sup>C-GlcNAc is a radioactive derivative of GlcNAc, which the cells incorporate into their nascent glycan chains. Cells were incubated for 5 minutes in the presence of the compound at different points after treatment with 10 x MIC methicillin. Cells were then fixed. The radioactivity of each sample was then measured in disintegrations per minute (DPM) per CFU. A significant drop in incorporation is observed after 15 minutes of methicillin treatment ( $p < 0.0001$ ) (Figure 3.11). However, high residual levels of incorporation are observed. After 60 minutes of methicillin treatment mean DPM/CFU is 30% of the control sample mean DPM/CFU.

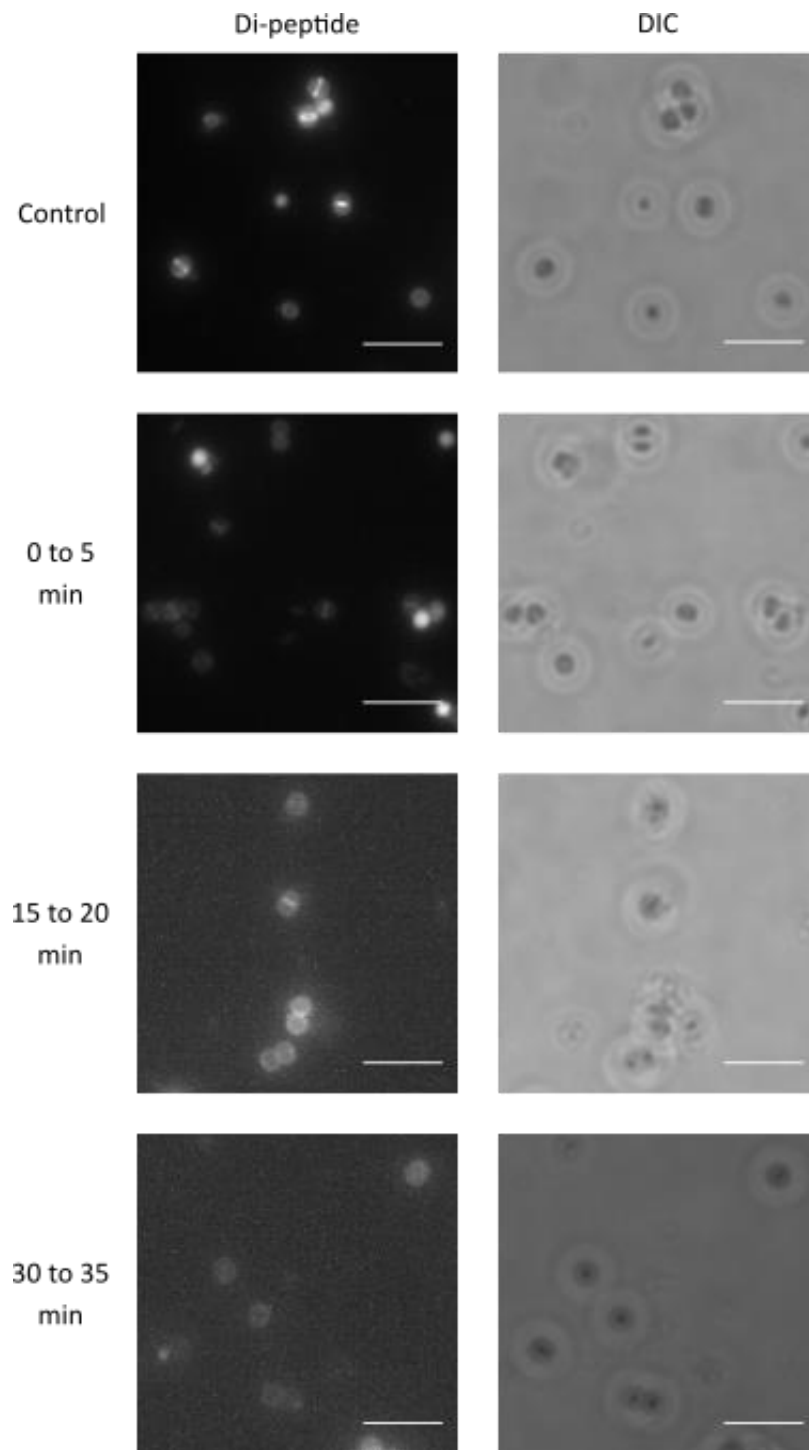
#### 3.2.3.2. *Oxacillin*

Cells were treated with 10 µg/mL oxacillin (10 x MIC) and processed in the same manner as those treated with methicillin, as described in section 3.2.3.1. However, TADA was used as the FDAA. TADA measures both Mur-associated synthesis and exchange reaction, however our previous data shows that dipeptide and TADA are equable. The samples were imaged using the Nikon Dual Cam.

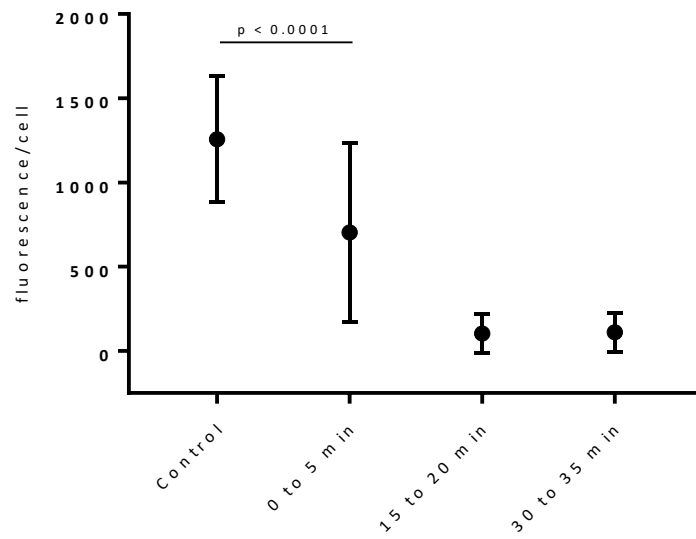
A decrease in fluorescence after treatment with 10 x MIC oxacillin was observed (Figure 3.12). This decrease per cell was quantified and a statistically significant reduction in TADA incorporation was observed within the first 5 minutes after addition of methicillin (Figure 3.13). After 15 minutes only residual levels of TADA incorporation were observed.

#### 3.2.4. Fate of newly incorporated peptidoglycan

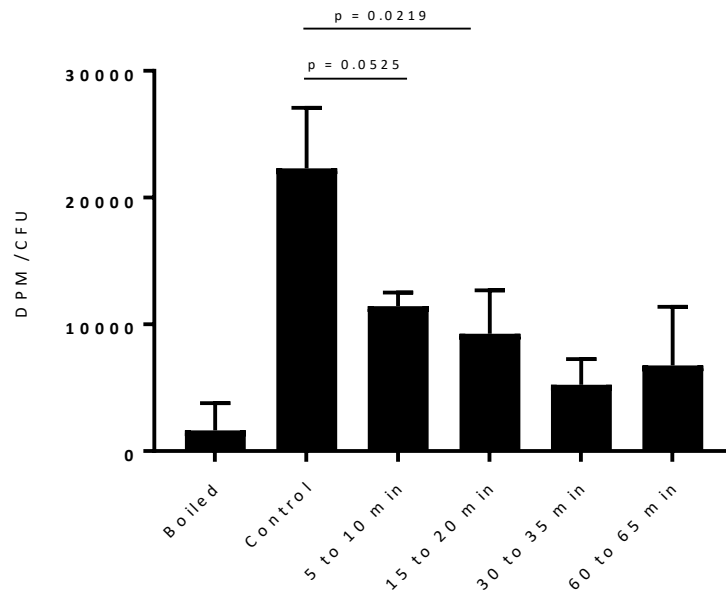
Cells were incubated in the presence of ADA for 5 minutes prior to the addition of 40 µg/mL methicillin to the growth media (treated samples) or incubation in fresh growth media without ADA (untreated sample). The aim of this experiment was to investigate the fate of the peptidoglycan newly synthesised immediately prior to treatment with 10 x MIC methicillin. The cells were also labelled with NHS Ester 405 to allow localisation of the incorporated material in the context of the whole cell (Figure 3.14).



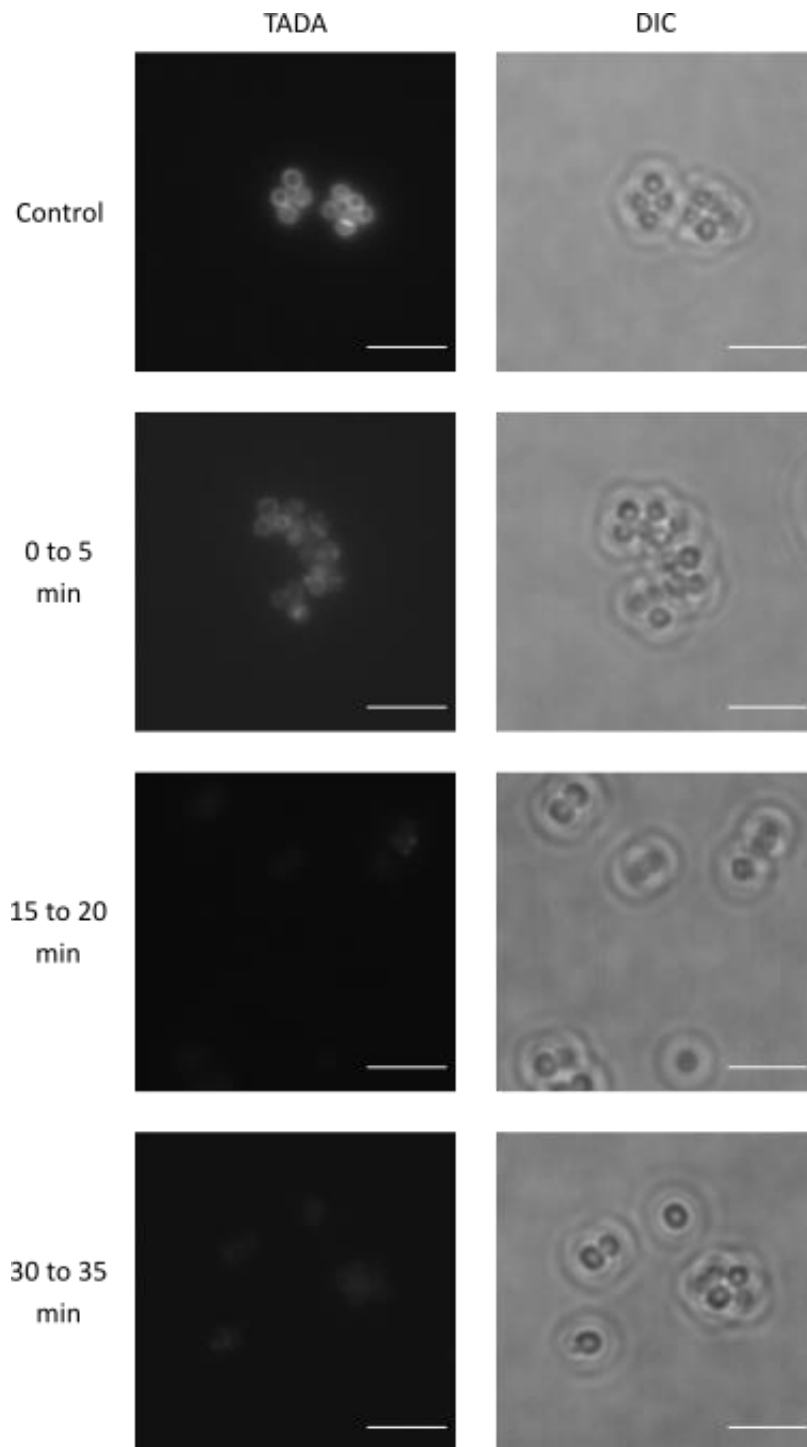
**Figure 3.9. Effect of methicillin treatment on di-peptide incorporation in *S. aureus* SH1000.** Cells were grown in the presence of di-peptide for 5-minute periods after the addition of 40  $\mu\text{g}/\text{mL}$  methicillin (10 x MIC). The newly incorporated material was subsequently labelled by click reaction with atto 488 and imaged on the Nikon widefield microscope. All scale bars 5  $\mu\text{m}$ .



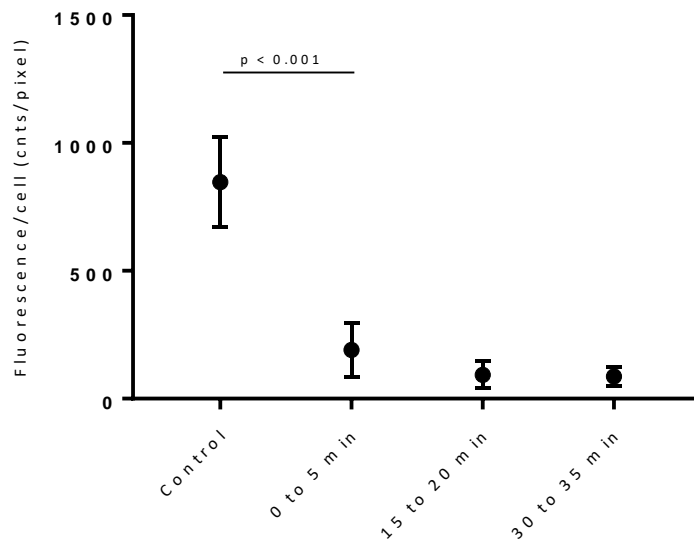
**Figure 3.10. Quantification of the effect of methicillin treatment on di-peptide incorporation in *S. aureus* SH1000.** Cells were treated with 40  $\mu\text{g}/\text{mL}$  methicillin (10 x MIC) and samples were incubated with di-peptide for 5 minutes at different intervals after antibiotic addition. Samples were then fixed and imaged using identical settings. The fluorescence/cell was measured using ImageJ. P-values calculated by Mann-Whitney. Mean and standard deviation are plotted. N = 100 cells.



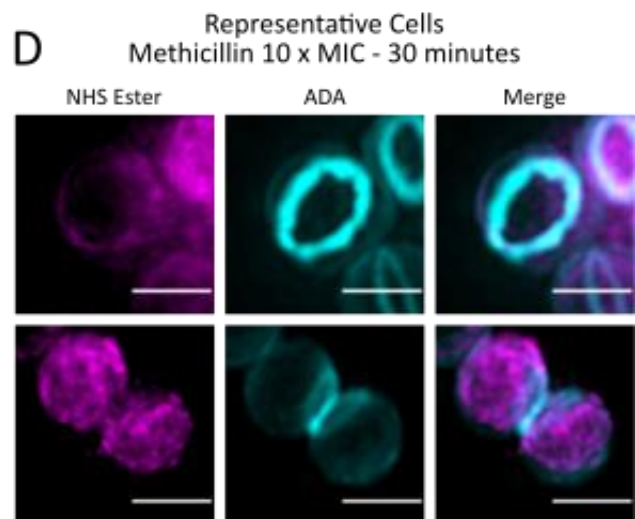
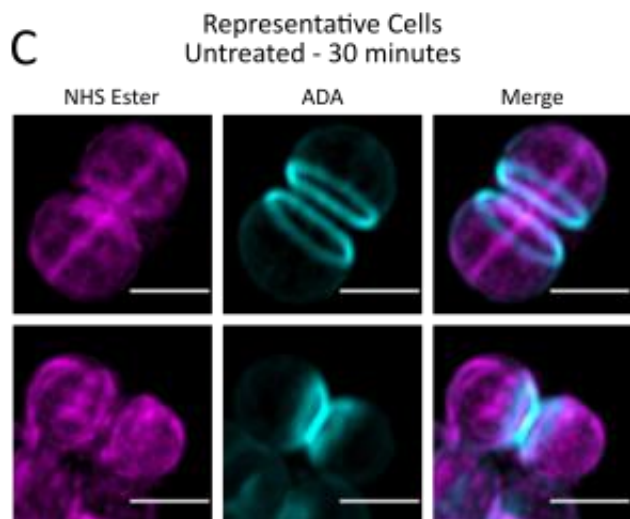
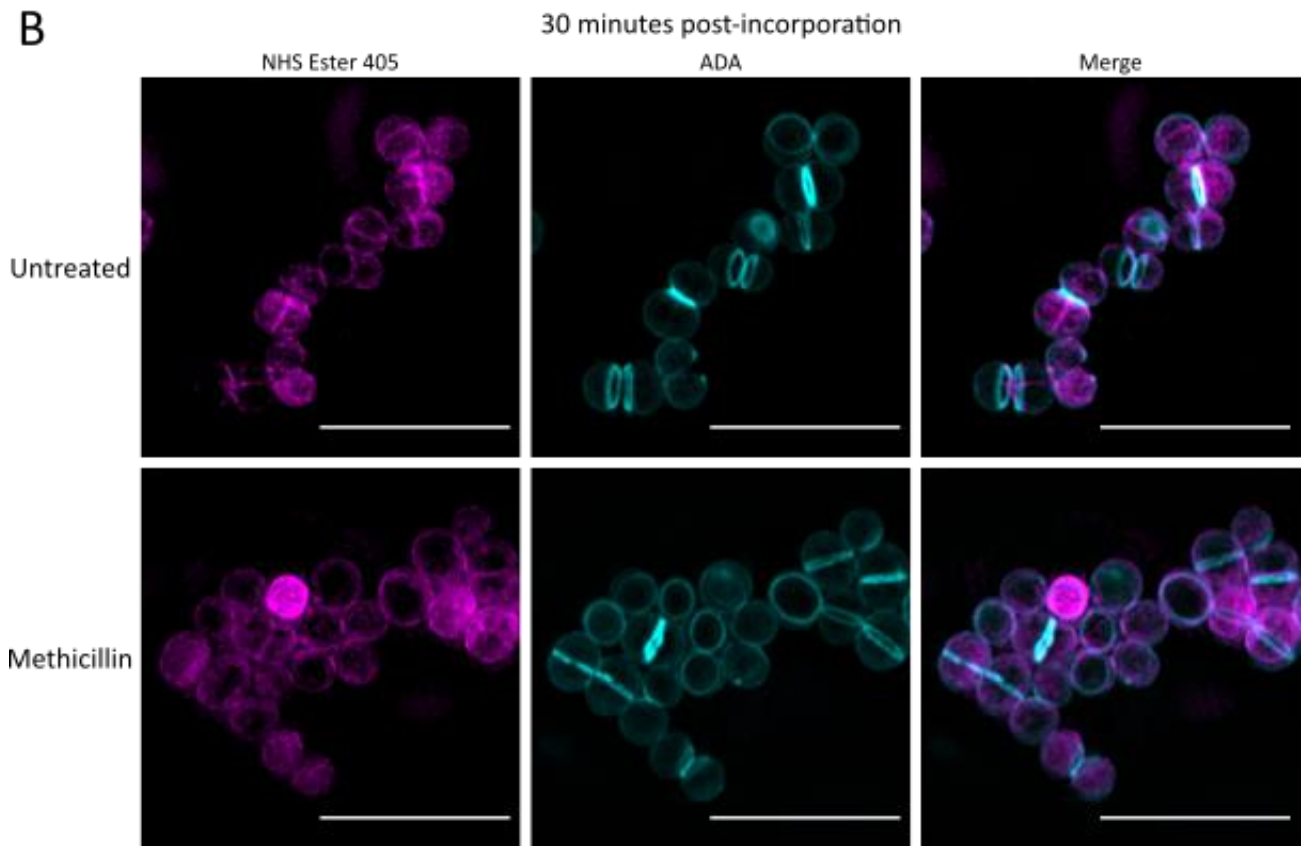
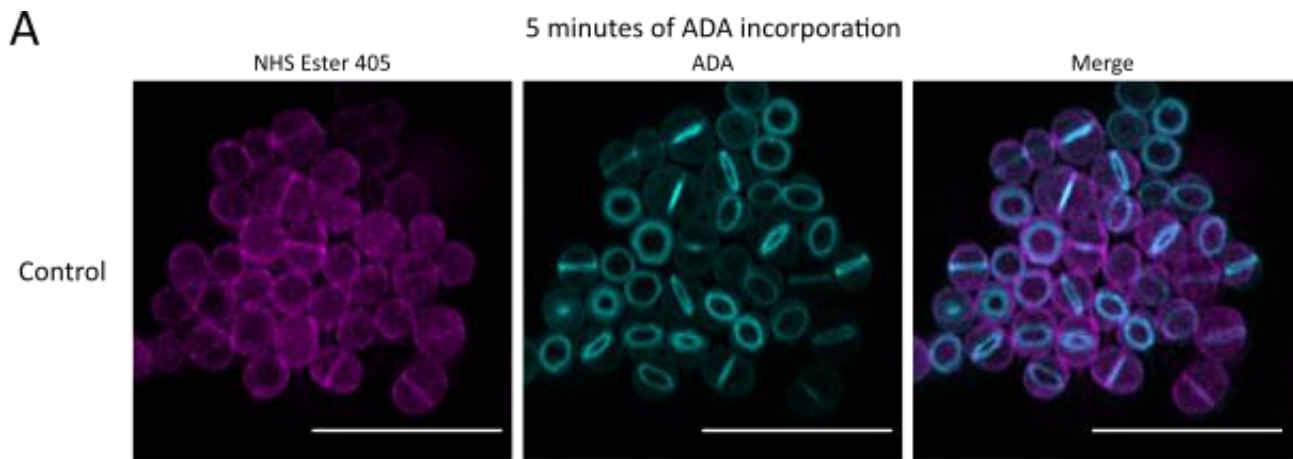
**Figure 3.11. Effect of methicillin treatment on *S. aureus* SH1000 incorporation of <sup>14</sup>C- GlcNAc.** Cells were treated with 40 µg/mL methicillin (10 x MIC) and samples were incubated with <sup>14</sup>C- GlcNAc for 5 minutes at different intervals after antibiotic addition. P-values calculated from unpaired t-tests with Welch's correction. Error bars represent standard deviation of the mean. The experiment was done in triplicate.



**Figure 3.12. Effect of oxacillin treatment on TADA incorporation in *S. aureus* SH1000.** Cells were grown in the presence of TADA for 5-minute periods after the addition of 10  $\mu\text{g}/\text{mL}$  oxacillin (10 x MIC). Cells were imaged and average intensity projections are presented. All scale bars 5  $\mu\text{m}$ .



**Figure 3.13. Quantification of the effect of oxacillin treatment on TADA incorporation in *S. aureus* SH1000.** Cells were treated with 10  $\mu\text{g}/\text{mL}$  oxacillin (10 x MIC) and samples were incubated with TADA for 5 minutes at different intervals after antibiotic addition. Samples were then fixed and imaged using identical settings. The fluorescence/cell was measured using ImageJ. P-values calculated by Mann-Whitney. N = 100 cells.



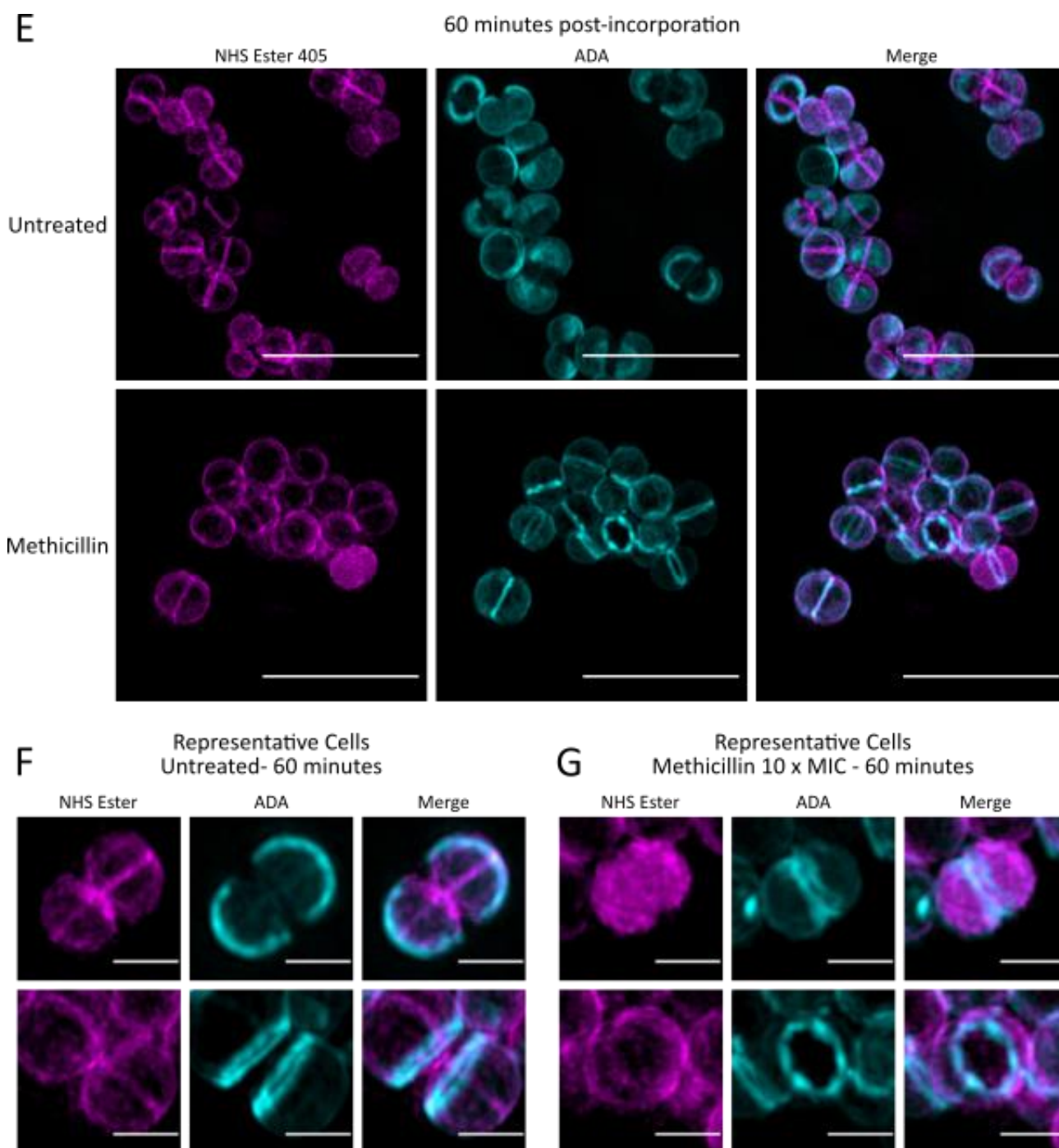


**Figure 3.14. Fate of newly synthesised peptidoglycan after methicillin treatment.** Cells were grown in the presence of ADA for 5 minutes before being washed and treated with 40  $\mu\text{g}/\text{mL}$  methicillin (10 x MIC) or not. Cells were fixed at 0, 30 & 60 minutes after addition of methicillin or resuspension in fresh media. The incorporated ADA was clicked with Alexa Fluor 594 and the cells were labelled with NHS Ester 405. Maximum intensity projections are presented. (A) Fields of cells after 5 minutes of ADA incorporation. All scale bars 5  $\mu\text{m}$ . (B) Fields of cells from the untreated and methicillin samples 30 minutes after ADA incorporation. All scale bars 5  $\mu\text{m}$ . (C) Representative cells 30 minutes after ADA incorporation. All scale bars 1  $\mu\text{m}$ . (D) Representative cells

30 minutes after ADA incorporation and methicillin addition. All scale bars 1  $\mu\text{m}$ . (E) Fields of cells from the untreated and methicillin samples 60 minutes after ADA incorporation. All scale bars 5  $\mu\text{m}$ . (F) Representative cells 60 minutes after ADA incorporation. All scale bars 1  $\mu\text{m}$ . (G) Representative cells 60 minutes after ADA incorporation and methicillin addition. All scale bars 1  $\mu\text{m}$ .

Over 5 minutes, *S. aureus* SH1000 incorporated ADA mainly at the septum with some incorporation over the whole cell wall (Figure 3.14, Panel A). The septum is made as a diffuse ring as the annulus closes. During the cell cycle 5 min ADA incorporation manifests in different incorporation patterns. Septum formation is characterised by an initial bright ring of ADA incorporation, which coincides with the formation of the pie crust. Subsequently, the septal plate is synthesised, thus ADA incorporation will be seen as a ring of diminishing radius. All cells show incorporation around the periphery of the cells.

#### 3.2.4.1. *Fate of newly incorporated peptidoglycan in the untreated cell population*

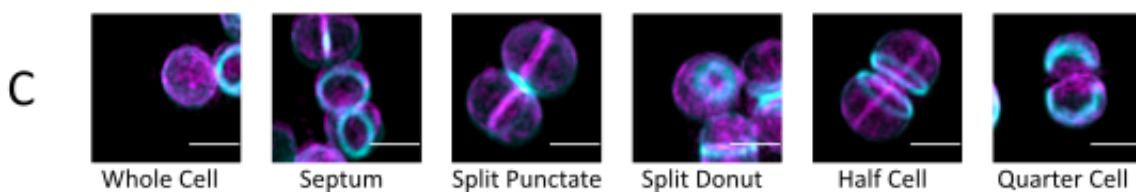
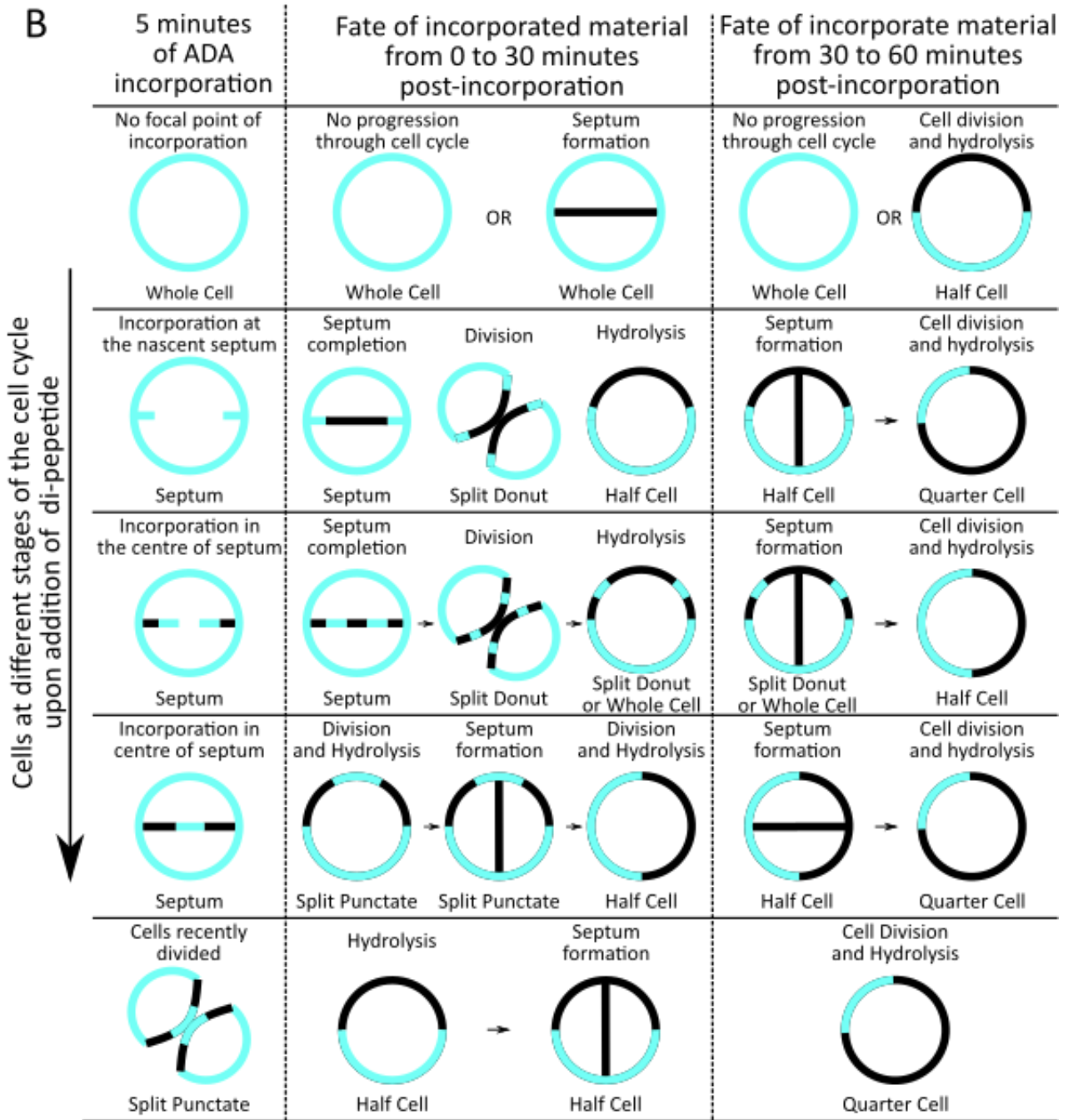
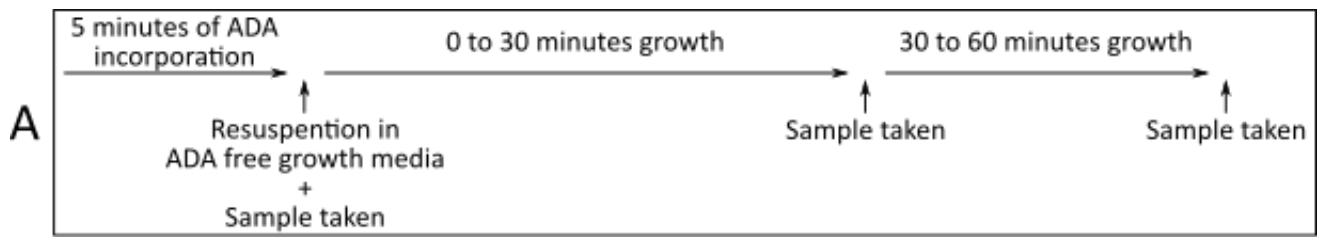
Six different cell morphologies were identified in the images 0, 30 and 60 minutes after the sample was washed and resuspended in ADA-free media (Figure 3.15, Panel C). The prevalence of each morphology was quantified at each time-point (Figure 3.15, Panel D). The model table in panel B of Figure 3.15 shows how each morphology can come about. Above the model cells, the cell cycle stages that lead to the morphology are specified. In the model, one can see how the fate of the incorporated material is different depending on which stage of the cell cycle it was incorporated at. The model explains the different steps leading to each observed pattern of ADA seen in the fluorescent images (Figure 3.14).

After the 5 minutes of incorporation, 80% of the cells incorporated ADA primarily into their septa (Figure 3.15, Panel D). 10% of the cells displayed a split punctate morphology, suggesting they were at the end of septum formation and finished their septa with ADA before splitting. The last 10% of the cells were barely incorporating, suggesting they had just divided when ADA was added, and had not yet begun making a new septum.

After 30 minutes, 45% of the cells had the incorporated ADA covering half of the cell and 45% of the cells had just divided (split punctate + split donut). This shows the cells are progressing through the cell cycle as can be seen in the model figure in panel B. After 60 minutes, 60% of the cells had the incorporated ADA in only a quarter of their cell wall (Figure 3.15, Panel D).

#### 3.2.4.2. *Fate of newly incorporated peptidoglycan after methicillin treatment*

After 30 minutes of treatment with 40 µg/mL (10 x MIC) methicillin the ADA was still mainly localised at the septum in over 50% of the cells, as opposed to less than 10% of the cells after 30 minutes in the untreated sample (Figure 3.16). 25% of the cells show the split punctate ADA pattern, which was the same as the untreated sample after 30 minutes. These cells completed their septa with ADA and split within the first 30 minutes of treatment (Figure 3.15, Panel B). Approx. 23% of the cells had a whole cell ADA pattern after 30 minutes, compared to 6% in the untreated cell population (Figure 3.16).



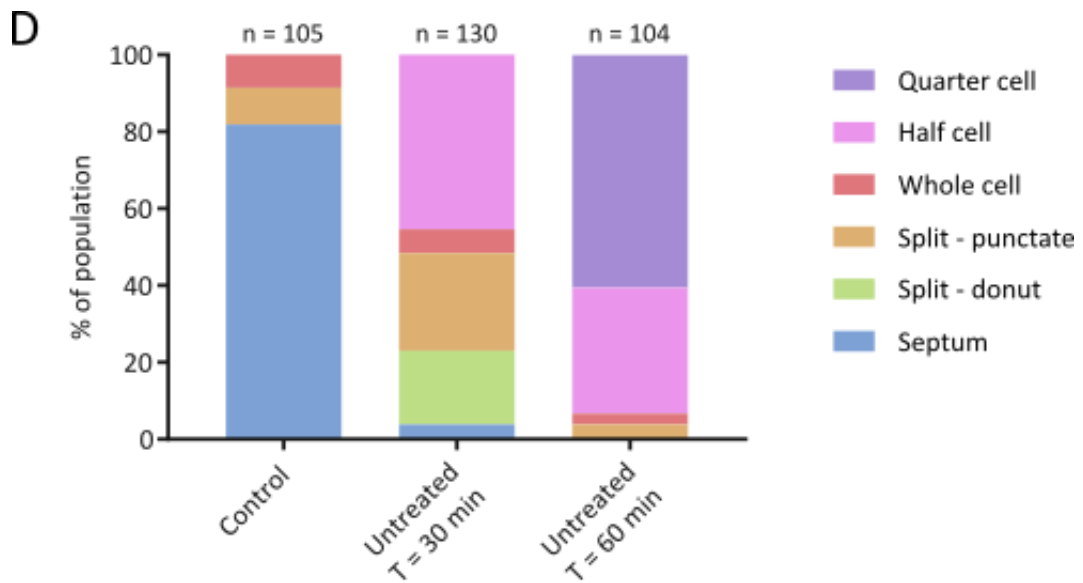


**Figure 3.15. Quantification and model of the fate of newly synthesised material over 60 minutes.** (A) Cells were grown in the presence of ADA for 5 minutes before being washed and resuspended in media without ADA. Cells were fixed 0, 30 and 60 minutes after resuspension. The incorporated ADA was clicked with Alexa Fluor 594 and the cells were labelled with NHS Ester 405. Samples were imaged on the SIM and observed ADA patterns were quantified. (B) Model of the fate of incorporated ADA. Cyan represents incorporated ADA, black represents unlabelled peptidoglycan. Above each model cell is the stage of the cell cycle and below each model cell is the pattern of the cell as shown in panel C. (C) Representative cells of each observed pattern. Composite images where cyan is ADA Clicked with Alexa Fluor 594 and magenta is NHS Ester 405 labelling. Scale bars 1  $\mu\text{m}$ . (D) The prevalence of each morphology was quantified in a population of approx. 100 (n as indicated in the graph) for each sample.

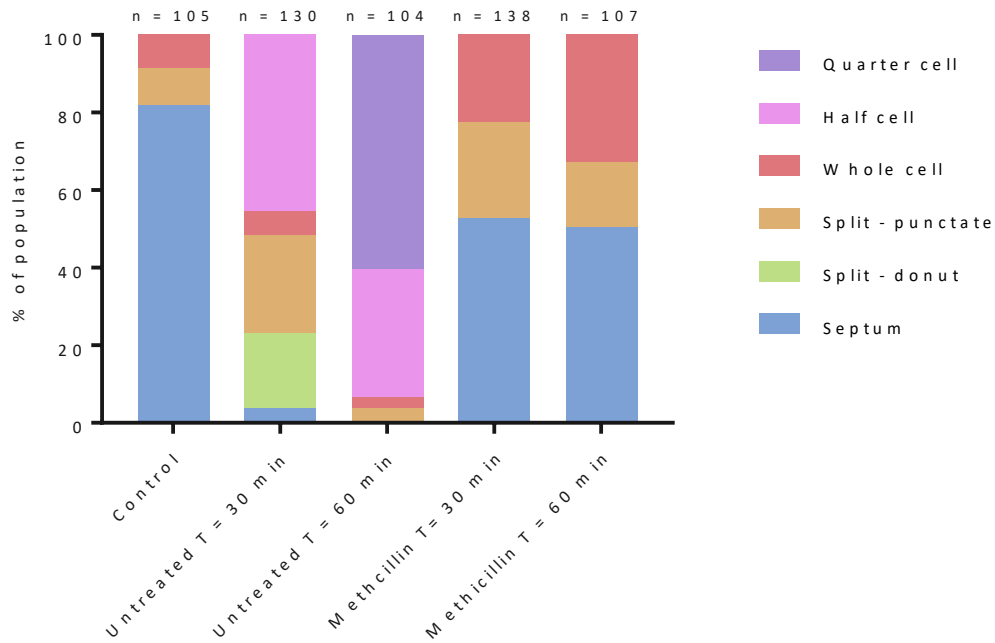


**Figure 3.16. Quantification of the fate of newly synthesised material after methicillin treatment.** The prevalence of each cell morphology (Figure 3.15) was quantified in a population of approx. 100 (n indicated in the graph) for each sample.

After 60 minutes of methicillin treatment the observed ADA patterns are the same as those observed after 30 minutes of treatment: septum, split punctate and whole cell. However, the prevalence of each morphology changed (Figure 3.16). In 50% of the cells, the newly incorporated peptidoglycan was still located at the septum. 17% of the cells still displayed a split punctate ADA pattern and 33% displayed a whole cell ADA pattern.

In the treated samples, at 30 and 60 minutes, no split donut, half or quarter cell morphologies were observed (Figure 3.16).

### 3.2.5. The effect of methicillin treatment on *B. subtilis*

#### 3.2.5.1. Killing dynamics

The MIC of methicillin against *B. subtilis* 168 HR was established using a standard serial dilution method. The MIC of methicillin against *B. subtilis* was found to be 0.25 µg/mL. *B. subtilis* 168 HR died rapidly after the addition of 2.5 µg/mL methicillin to the growth media (Figure 3.17). 90% killing was reached between 30 minutes and 1 hour after treatment with 10 x MIC methicillin.

#### 3.2.5.2. Morphological changes

*B. subtilis* was labelled with WGA at different time points post antibiotic treatment and imaged using the SIM. WGA was used rather than NHS ester, because a large portion of the cells showed intracellular labelling when labelled with NHS ester. Several different fixing and labelling protocols were tested showing no improvement (results not shown). Good quality labelling was obtained with WGA, so this label was used for all *B. subtilis* cell surface labelling.

30 and 60 minutes after the addition of 2.5 µg/mL methicillin (10 x MIC) to the growth media, there were visible changes to the morphology of some cells (Figure 3.18). More sacculi were present in the samples, many of which appear to have ripped at the septum. Many cells had deformed, wider septal regions. Cell length and width were measured using ImageJ. Cells were only described as individuals if complete septa were observed by z stack analysis of the fluorescent images. After 60 minutes of treatment with 10 x MIC methicillin, no significant change in cell length was observed and a small significant increase in cell width was observed (Figure 3.19).

## 3.3. Discussion

### 3.3.1. Morphological changes

Oxacillin and methicillin were both bactericidal for *S. aureus* although oxacillin killed faster and at lower concentrations. After treatment with methicillin and oxacillin, significant increases in cell volume were

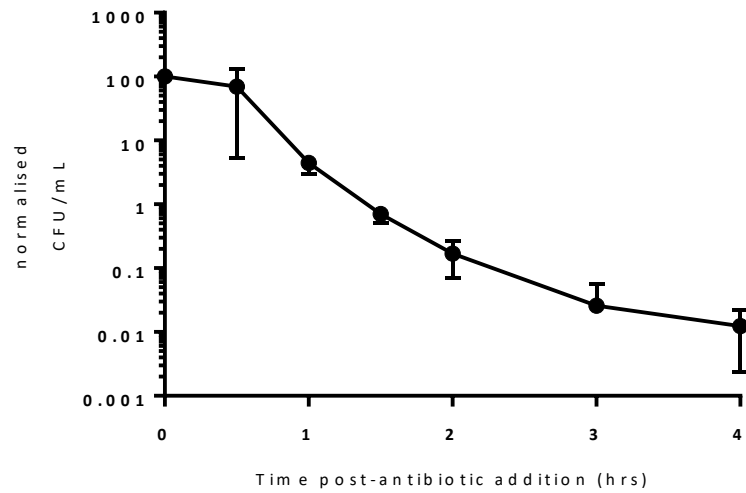


**Figure 3.17. Methicillin killing of *B. subtilis*.** *B. subtilis* 168 HR was treated with 2.5 µg/mL methicillin (10 x MIC). The CFU/mL was determined at each time-point and the data was normalised by setting the first time point as 100%. The mean and standard deviation are plotted. This experiment was done in triplicate.

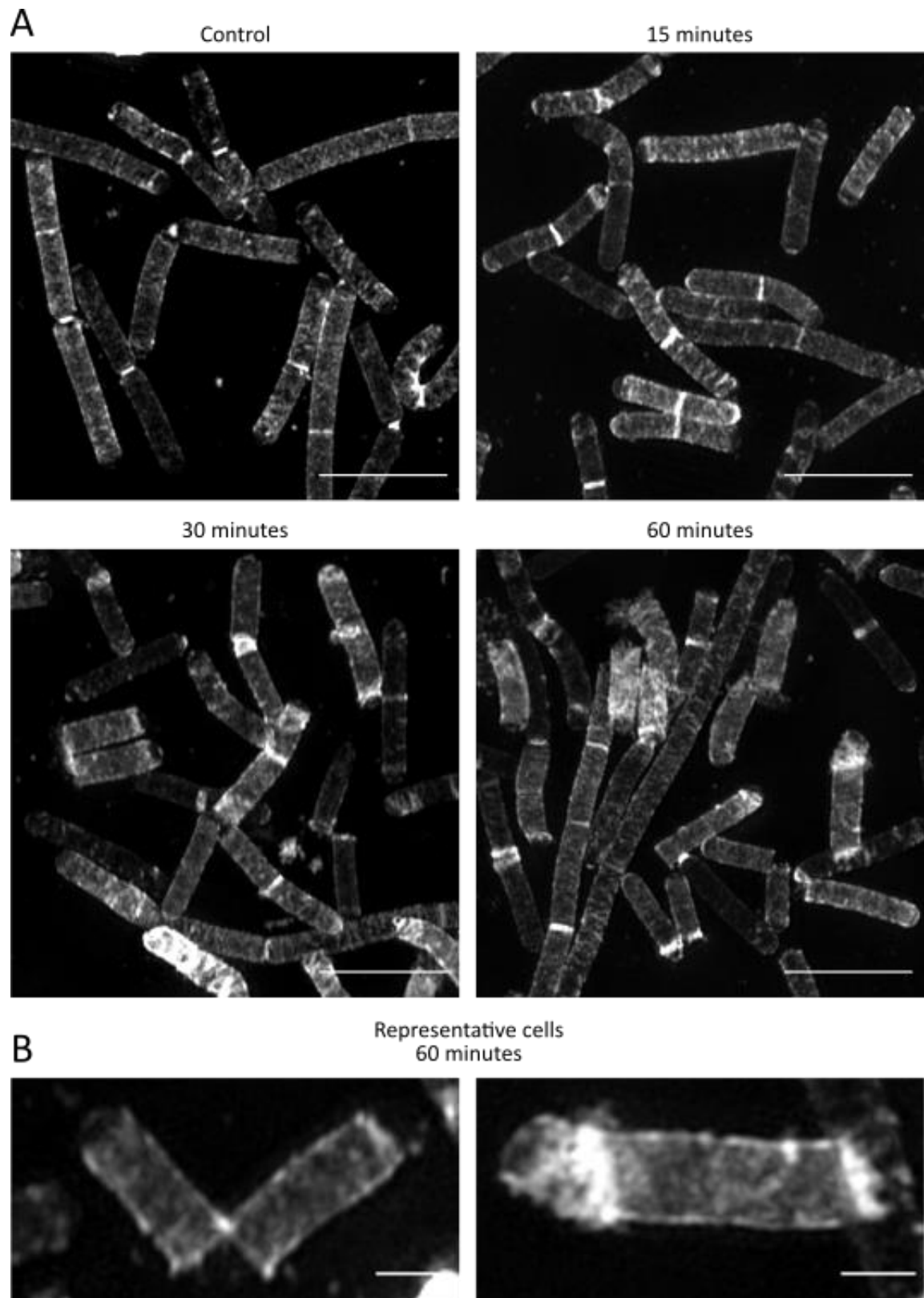


**Figure 3.18. Effect of methicillin on *B. subtilis* 168 HR morphology.** Cells were treated with 2.5  $\mu\text{g}/\text{mL}$  methicillin (10 x MIC), fixed after 0, 15, 30 and 60 minutes and subsequently labelled with WGA 594. Cells were imaged using the OMX SIM and maximum intensity projections are shown. (A) Fields of cells from each

time point, as indicated. All scale bars 5  $\mu\text{m}$ . (B) Representative cells after 60 minutes of treatment. All scale bars 1  $\mu\text{m}$ .

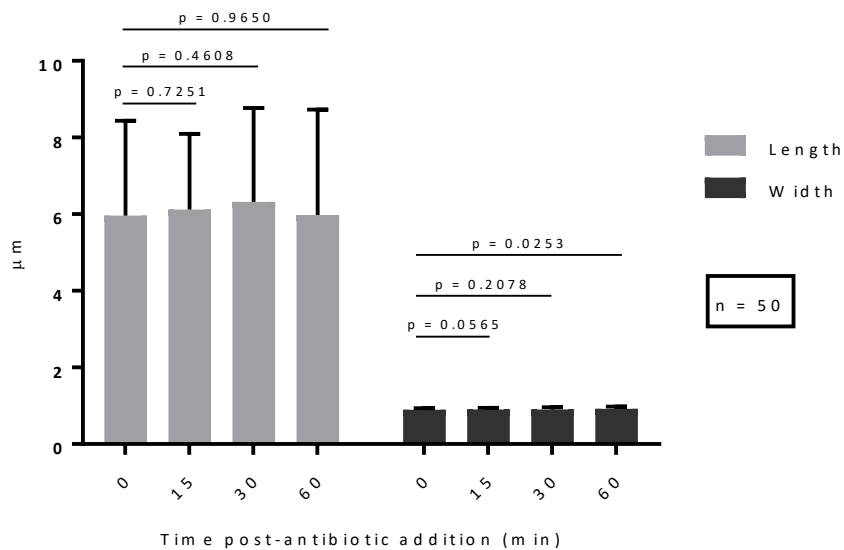


**Figure 3.19. The effect of methicillin on *B. subtilis* 168 HR cell length and width.** Cell length and width were measured in image J using images acquired on the OMX SIM of WGA labelled *B. subtilis* fixed at different time points after the addition of 2.5 µg/mL methicillin (10 x MIC). The error bars represent standard deviation. P-values were calculated by two-tailed t-test with Welch's correction.

observed (Figure 3.4 & Figure 3.8). This could be due to peptidoglycan synthesis and peptidoglycan hydrolysis, which are both required for normal cell growth (Wheeler et al., 2015). However, FDAA and <sup>14</sup>C-GINAc incorporation data showed that methicillin and oxacillin treatment halted peptidoglycan synthesis almost immediately after addition of the antibiotics to the culture (Figure 3.10, Figure 3.11 & Figure 3.13). These results would suggest that the increase in cell volume observed after  $\beta$ -lactam treatment is due to continued hydrolysis of the cell wall after incorporation has been halted.

Unusual morphologies were observed in images of NHS Ester-labelled cells after antibiotic treatment. Some cells had deformed septa, others appeared to have a “dumbbell” shape (Figure 3.3, Panels B & C). The dumbbell shapes observed could be due to attempts to split with incomplete septa. The wider and deformed septa observed in the NHS Ester labelled cells treated with 10 x MIC methicillin could be explained by hydrolysis of the existing septa, creating loose material at the septum. This is supported by observations made in the EM images of methicillin-treated cells (Figure 3.5). After 60 minutes of treatment with 10 x MIC methicillin, the septal plates have been hydrolysed into two halves along their length. This suggests that the hydrolases located at the septum, that are involved in cell division, are still active after treatment with methicillin. Only 1% of the cells have a complete septum after treatment with methicillin, compared to 23% in the untreated control, this can also be explained by the continued action of cell division hydrolases, combined with the halt in peptidoglycan synthesis which inhibits the completion of partially formed septa after methicillin treatment (Figure 3.6). In all the samples, a high proportion of the cells presented with no septum. This can be explained by the fact that in EM, a single slice of the cell has been imaged, and many cells with septa, can easily appear to have no septum if the imaged slice happens to not be in the right plane.

A separate quantification was carried out to measure the number of cells where the cell membrane appeared to have separated from the cell wall. After 60 minutes of methicillin treatment, 17.4% of the cells had a gap between the cell wall and the cell membrane somewhere along the periphery of the cell. In gram-positive organisms there is a periplasm-like space between the cell membrane and the cell wall, which can be called the exoplasm (Matias & Beveridge, 2006). The observed gap between the cell wall and the membrane may be due to excessive material in the exoplasm or it could be explained by a loss of osmotic pressure and pulling away of the membrane from the cell wall.

### 3.3.2. Peptidoglycan incorporation and fate

A significant decrease in FDAA incorporation was observed within the first 5 minutes of treatment with 10 x MIC methicillin and oxacillin and only baseline levels of incorporation remained within 15 minutes. This is not an unexpected result as  $\beta$ -lactams bind penicillin-binding proteins, which are responsible for crosslinking of peptidoglycan. This questions the hypothesis that the cells continue making peptidoglycan for at least a complete cell cycle after treatment (Giesbrecht et al., 1998). Septal expansion is observed, but this is not due

to further incorporation of peptidoglycan. Our images show that the septum itself still maintains its thin V-shape but is surrounded by a bulbous layer of amorphous material or the membrane has pulled away from the cell wall.

The fate of newly incorporated peptidoglycan in the untreated sample concurs with our current understanding of *S. aureus* cell division (Lund et al., 2018; Monteiro et al., 2015). *S. aureus* cells split into two daughter cells at the septum, hydrolysis remodels the new cell wall (previously the septum of the mother cell), remodelling it to give the cell its typical spheroid shape. They divide sequentially in three orthogonal planes, which means that after each division cycle, one half of the cell is composed of new peptidoglycan. The other half of the cell will have 1 quarter from the previous cycle, one eighth from the division cycle before that, etc... In the images presented, we see the labelled peptidoglycan occupy a half and then a quarter of the cell wall as the cells progress through one, then two cell cycles (Figure 3.15).

Investigation of the fate of newly incorporated peptidoglycan after antibiotic treatment, showed that cells are not progressing through the cell cycle after treatment with methicillin. No half, quarter or split donut cells were seen in the treated sample. The change in proportion of the observed morphologies in the treated samples over time, could be explained by hydrolysis of the cell wall. Some of the cells will have finished their septum during the 5 minutes of ADA incorporation and then split over the following 30 minutes, leading to the higher number of cells exhibiting a “Split – punctate” pattern. Cells that had just split prior to antibiotic treatment have hydrolysed the new cell wall making the incorporated ADA more disperse and leading to the increase in “whole cell” morphology. Hydrolases may also have hydrolysed septa that had just begun forming during the 5 minutes of ADA incorporation, with the material then occupying a larger area, the cells would show a “whole cell” morphology by 30 or 60 minutes after treatment. A punctate pattern has also appeared at the septum of many cells. This pattern may be due to the hydrolysis of the septal plate into two halves, as seen in the EM images (Figure 3.5 & Figure 3.16).

After methicillin treatment, some residual incorporation of  $^{14}\text{C}$ -GlcNAc was observed (Figure 3.11). Several explanations are possible for this. Cells could be accumulating precursors to peptidoglycan or using the material in other ways in the cell, such as teichoic acid biosynthesis (Xia et al., 2010). There are several transglycosylases present in *S. aureus* that could still be active: PBP2, Sgt, MgtA, FtsW & RodA. However, if the transglycosylases were still assembling glycan chains that weren't being crosslinked, residual incorporation of di-peptide would also be observed and is not. GlcNAc is also used for WTA synthesis, so residual incorporation may be explained by continued WTA biosynthesis after methicillin treatment.

The combination of lack of incorporation and apparent continued cell wall hydrolysis suggests that weakening of the cell wall might play a role in cell death, possibly through the cell leakage described in Giesbrecht's model. It has been shown that generalised lysis is not the cause of death in *S. aureus* after  $\beta$ -lactam treatment

(Foster, 1995). However, there are 19 putative hydrolases in *S. aureus* this redundancy means the cell wall could still be hydrolysed leading to breaches that allow cytoplasm to leak out, without generalised cell lysis. This also agrees with the fact that  $\beta$ -lactam killing is dependent on cells actively growing and studies have shown that hydrolysis is inhibited during stationary phase (Lioliou et al., 2016). Therefore, stationary phase cells could not be killed by  $\beta$ -lactams because they are not hydrolysing their cell wall.

### 3.3.3. Action of cell wall antibiotics on *B. subtilis*

*B. subtilis* was used as a comparator to *S. aureus* to begin to identify commonalities in the underlying mechanism of  $\beta$ -lactam killing. *B. subtilis* has a much lower MIC and dies much faster than *S. aureus* in the presence of methicillin. Some morphologies observed in NHS Ester labelled *S. aureus* were also visible in *B. subtilis*. There are some deformations at the septa of cells and many sacculi seem to have ripped open at a specific point, often the septum (Figure 3.18). Ripping at the septa and generally across the short axis of the cell corresponds to the weaker axis of the cell wall in *B. subtilis* (Beeby et al., 2013).

An increase in cell length was not observed in *B. subtilis*, but a small increase in cell width was observed, whereas a significant increase in cell volume is observed in *S. aureus* under the same conditions (Figure 3.19). Some differences between *B. subtilis* and *S. aureus* peptidoglycan synthesis and structure could explain this. *B. subtilis* is a rod-shaped organism that grows through elongation followed by septation (Turner et al., 2014). Both organisms have very different glycan strand lengths, *S. aureus* glycan strands are on average 6 disaccharides long, where *B. subtilis* glycan strands are several hundred or thousand disaccharides long (Hayhurst et al., 2008). With such long glycan chains, it may take much longer for hydrolysis of the chains to lead to a significant increase in cell length or width. This difference in glycan chain length combined with the rapid death of *B. subtilis* after treatment lead us to believe that a large increase in cell volume would not be observed in conditions that would show such an increase in *S. aureus*.

These results indicate that *B. subtilis* may also be dying due to hydrolysis of the cell wall, leading to physical failure to maintain the turgor pressure. A more complete set of experiments would need to be completed in *B. subtilis* to give us further insight into the similarities and differences in the effect of methicillin on the two organisms.

## Chapter 4

### Vancomycin killing of *S. aureus*

#### 4.1. Introduction

There are several different classes of antibiotics that target the cell wall. Fosfomycin and D-cycloserine both target the cytoplasmic steps of peptidoglycan production. Fosfomycin irreversibly inhibits MurA, leading to a reduction in peptidoglycan precursors (Bensen et al., 2012). Fosfomycin is the only antibiotic on the market to target a Mur-family protein. D-cycloserine is a structural analogue of D-alanine inhibiting the formation of D-Ala-D-Ala, the terminus of the peptidoglycan side chain, leading to the accumulation of peptidoglycan precursors (Lambert & Neuhaus, 1972; Neuhaus & Lynch, 1964). Its neurological side effects mean it is used only as a second line drug against multidrug resistant infections (Nikolaidis et al., 2014). Beta-lactams and glycopeptides inhibit later steps of peptidoglycan assembly. Beta-lactams bind PBPs inhibiting their transpeptidase activity (Zapun et al., 2008). Glycopeptides non-covalently bind the D-Ala-D-Ala motif of the peptide side chains, inhibiting both transpeptidation and transglycosylation (Barna & Williams, 1984; Perkins, 1969). Vancomycin was the first identified glycopeptide. In 2017, MRSA made up 16.9% of all *S. aureus* infections across the EU/EEA, with levels as high as 44.4% in some countries (“Surveillance of antimicrobial resistance in Europe 2017”). Glycopeptides are often the drug of choice to treat MRSA infections. However, in 2002, the first vancomycin-resistant *S. aureus* (VRSA) isolate was reported in the USA. Due to the rise of VRSA, it is important that we better understand how glycopeptides kill *S. aureus*. A better understanding of the molecular pathways involved in cell death upon treatment with vancomycin can help identify targets for new drug development as well as better dosing regimens.

Glycopeptides have been shown to bind secondary targets in the cell. It has been shown that certain glycopeptides (not vancomycin) bind directly to *S. aureus* PBP2 and cause some inhibition of peptidoglycan assembly through these secondary interactions (Leimkuhler et al., 2005). In *S. aureus* vancomycin binds the amidase unit of Atl, leading to an inhibition of hydrolase activity due to direct binding to the enzyme rather than only through steric hindrance due to binding of their substrate, peptidoglycan (Eirich et al., 2011).

Many of the original studies on the mode of action of glycopeptides were done using the same techniques as were used to study beta-lactams: death kinetics, incorporation of radioactive compounds, culture turbidity (Kahne et al., 2005). Incorporation of <sup>14</sup>C-labelled glutamic acid and glycine was used to study synthesis of new cell wall material after treatment with glycopeptides (Reynolds, 1961). This study showed an 80% decrease in incorporation of the radioactively labelled material within 20 minutes of treatment with 25 µg/mL vancomycin (10 x MIC for the strain used). The uptake of radioactively labelled amino acids into the protein fraction did not change in the first 40 minutes after treatment (Reynolds, 1961). The effect of vancomycin on <sup>14</sup>C-GlcNAc and

<sup>14</sup>C-MurNAc-pentapeptide incorporation was also investigated in the 60s, yielding similar results and indicating that vancomycin inhibits cell wall synthesis (Anderson et al., 1965).

There have been less in-depth studies into the molecular pathway to cell death after treatment with glycopeptides than with beta-lactams. Most of the more recent research surrounding glycopeptides has focused on resistance and tolerance.

In this study, established and novel techniques were used to further investigate the mechanism of action of vancomycin. This enabled comparison to the bactericidal effect of methicillin as determined in Chapter 3.

#### 4.1.1. Aims of this chapter

- Investigate the effect of vancomycin on *S. aureus* and *B. subtilis*
- Establish death kinetics
- Study the effect of vancomycin on cell morphology
- Investigate the effects of vancomycin on macromolecular synthesis

## 4.2. Results

#### 4.2.1. Killing Dynamics

The MIC was determined by standard serial dilution method. The MIC of vancomycin against SH1000 was 4 µg/mL. All experiments carried out with *S. aureus* SH1000 in this chapter were done using 10 x MIC, i.e. 40 µg/mL vancomycin.

A death curve of vancomycin against *S. aureus* SH1000 was done to determine death kinetics. The CFU/mL were determined at different time-points after addition of 10 x MIC vancomycin and the data was normalised by setting the first time point as 100%. A gradual killing of *S. aureus* SH1000 was observed over the 6 hours of treatment with vancomycin, with 90% killing reached after 6 hours (Figure 4.1).

#### 4.2.2. Cell morphology

To investigate cell morphology, cells were treated with 10 x MIC vancomycin, fixed, labelled with NHS Ester 555 and imaged using SIM. In the NHS Ester images of *S. aureus* SH1000 the only morphological change observed is an apparent increase in cell size (Figure 4.2). To quantify changes, the cell volume was measured using the ImageJ software and a method described by Zhou et al., 2015. A highly significant increase in cell volume was observed 15 minutes after addition of 10 x MIC vancomycin to the culture (Figure 4.3). After 30 minutes of vancomycin treatment, the mean cell volume of the population increased by a factor of 1.5.

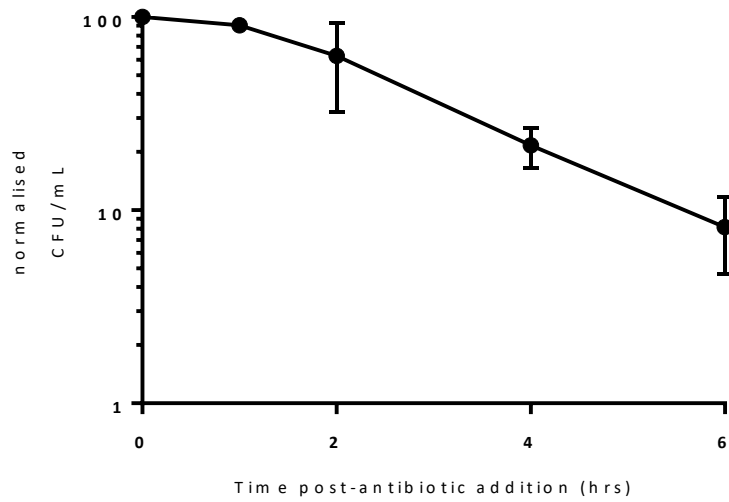


**Figure 4.1. Effect of 40 µg/mL (10 x MIC) vancomycin on *S. aureus* SH1000 cell viability.** The CFU/mL was determined at each time-point and the data was normalised by setting the first time point as 100%. The mean and standard deviation are plotted. The experiment was done in triplicate.

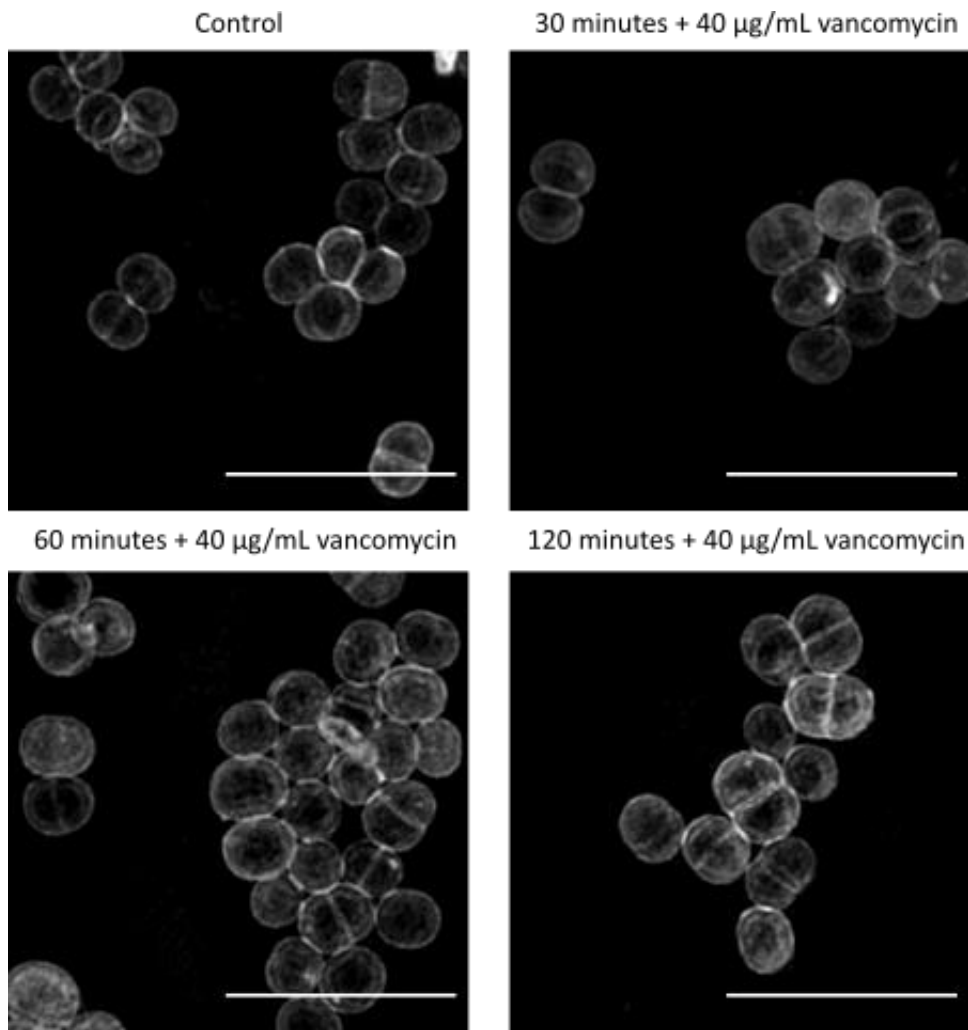


**Figure 4.2.** Effect of vancomycin treatment on *S. aureus* SH1000 cell morphology (SIM images). Cells were treated with 40 µg/mL vancomycin (10 x MIC), fixed after 0, 30, 60 and 120 minutes treatment and subsequently labelled with NHS Ester 555. Cells were imaged using the OMX SIM and maximum intensity projections of fields of cells are shown. All scale bars 5 µm.

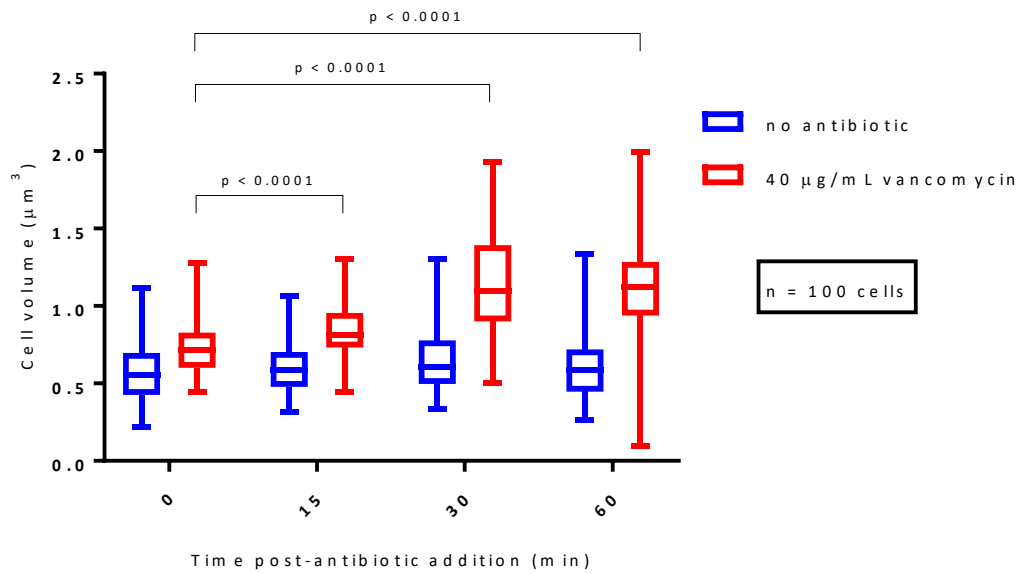


**Figure 4.3. Effect of vancomycin treatment on *S. aureus* SH1000 cell volume.** Cell volume was calculated from measurements carried out in ImageJ, on OMX SIM images of NHS Ester 555 labelled cells at different time points after the addition of 40  $\mu\text{g/mL}$  vancomycin (10 x MIC). P-values were calculated by Mann-Whitney tests. Whiskers extend from the minimum to the maximum values and boxes from the 25<sup>th</sup> to the 75<sup>th</sup> percentile. The middle of the box is plotted at the median.

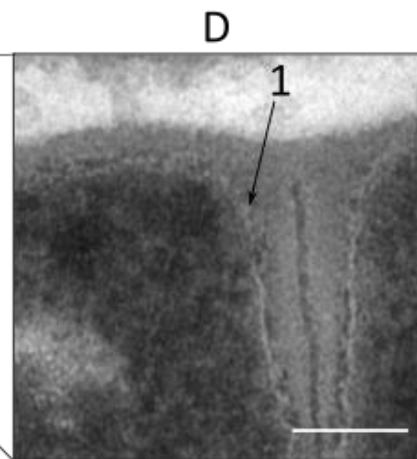
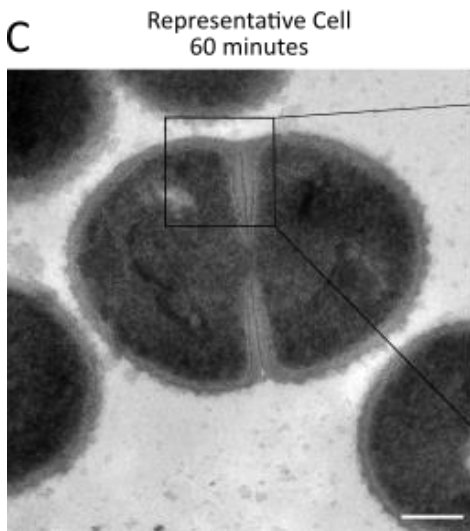
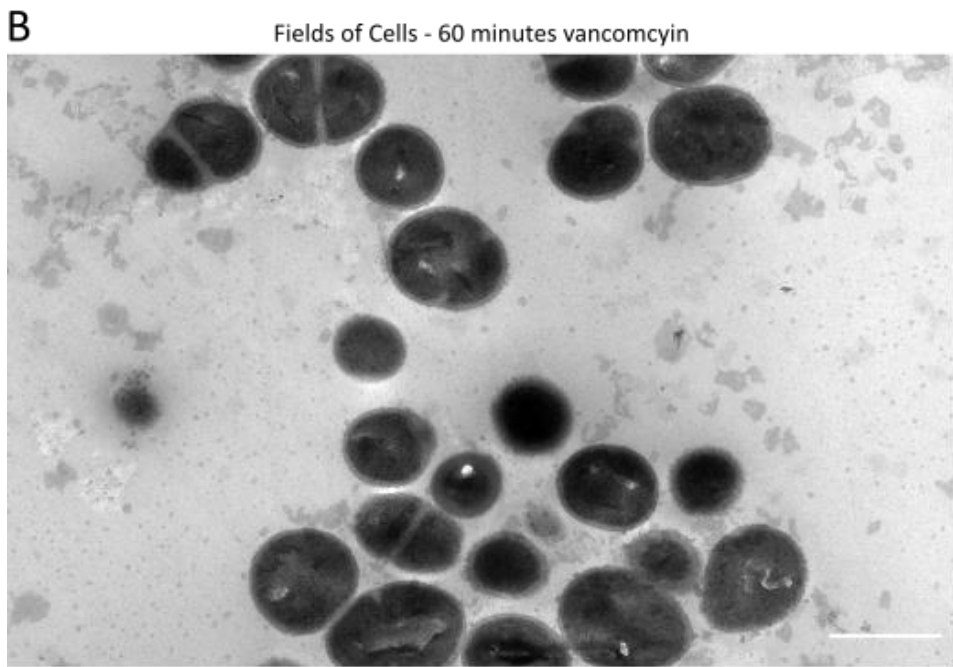
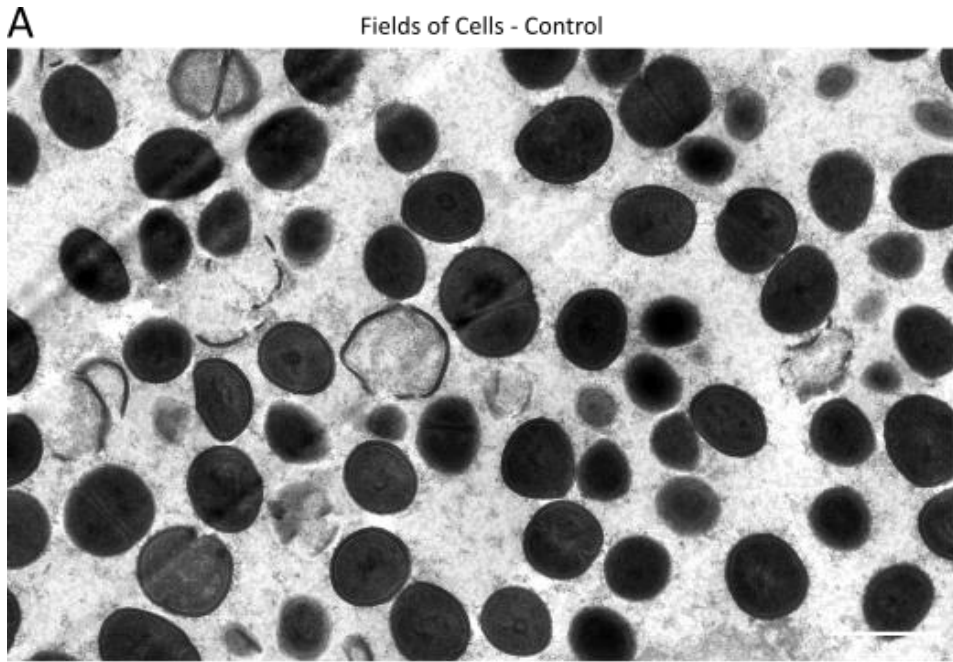


**Figure 4.4. Effect of vancomycin treatment on SH1000 cell morphology (EM images).** Cells were treated with 40 µg/mL vancomycin (10 x MIC), fixed after 60 minutes of treatment and imaged by electron microscopy. All EM images were acquired by Lucia Lafage. (A) Fields of cells before antibiotic treatment. Scale bar 1 µm. (B) Fields of cells after 60 minutes of vancomycin treatment. Scale bar 1 µm. (C) Representative cell after 60 minutes of treatment. Scale bar 200 nm. (D) Magnification of a cell section from a representative cell after 60 minutes of treatment with vancomycin. 1 – intersection of the cell wall and cell membrane. Scale bar 100 nm.

To gain further insight, EM images of fixed *S. aureus* SH1000 cells were taken before and 60 minutes after treatment with 40 µg/mL vancomycin (Figure 4.4). In images of both samples, three morphologies were identified and their prevalence was quantified: cells with a complete septum, cells with an incomplete septum and cells with no visible septum (Figure 4.5). In the untreated sample, 58% of the cells don't have a visible septum, 19% have an incomplete septum and 23% have a complete septum. After 60 minutes of treatment with 10 x MIC vancomycin 63% of the cells don't have a visible septum, 17% have a complete septum and 20% have an incomplete septum. Unlike after methicillin treatment, no cells were observed with their cell membrane separated from the cell wall (Figure 4.4, Panel D).

#### 4.2.3. Quantification of peptidoglycan incorporation post-treatment

Peptidoglycan incorporation was quantified using FDAA di-peptide and <sup>14</sup>C-GlcNAc. Di-peptide incorporation is used as a measure of transpeptidase activity and <sup>14</sup>C-GlcNAc incorporation is used as a measure of transglycosylase activity.

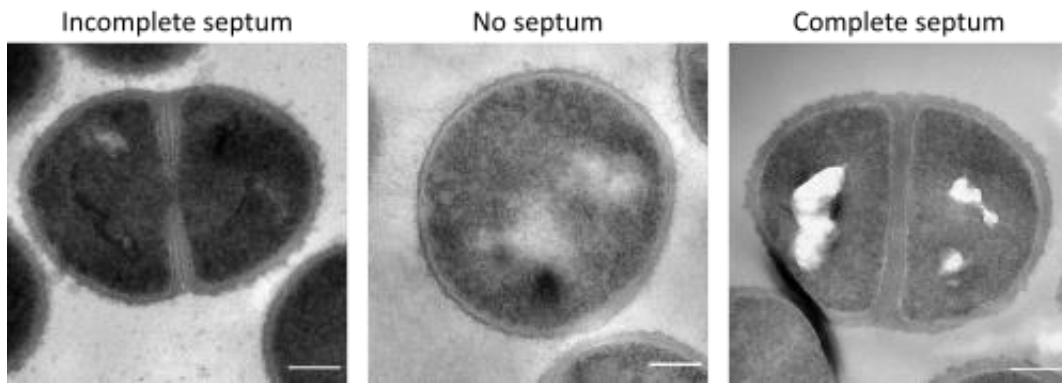
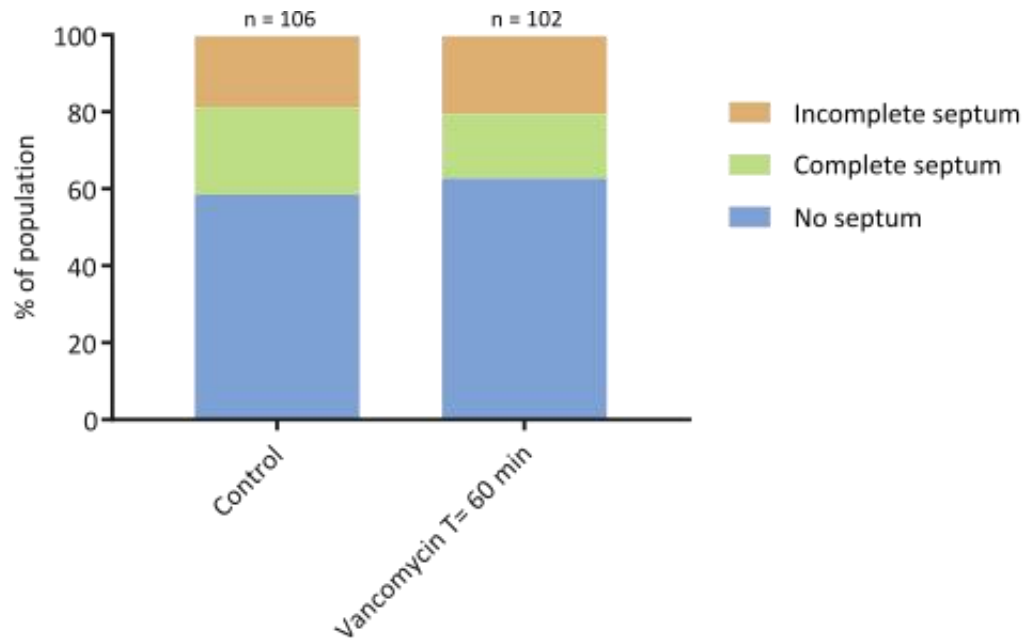
In Figure 4.6, a decrease in di-peptide labelling of cells can be observed. The change in fluorescence/cell was quantified using Image J. The fluorescence per cell was measured for each cell and the background fluorescence was subtracted from this value. In the initial 5 minutes after addition of the antibiotic, a significant decrease ( $p < 0.0001$ ) in labelling was observed (Figure 4.7). Within 15 minutes of vancomycin addition, only baseline levels of fluorescence were observed.

Cells were incubated in the presence of <sup>14</sup>C-GlcNAc for 5 minutes at different time-points after addition of 10 x MIC vancomycin. The cells were then fixed and the radioactivity of each sample was measured in disintegrations per minutes (DPM) per CFU. The data was corrected for CFU count because the number of cells 60 minutes post-antibiotic treatment was smaller than in the control. A significant decrease ( $p = 0.0016$ ) in incorporation was observed within 5 minutes of antibiotic addition (Figure 4.8). <sup>14</sup>C-GlcNAc incorporation reached baseline levels within 5 minutes of antibiotic treatment.

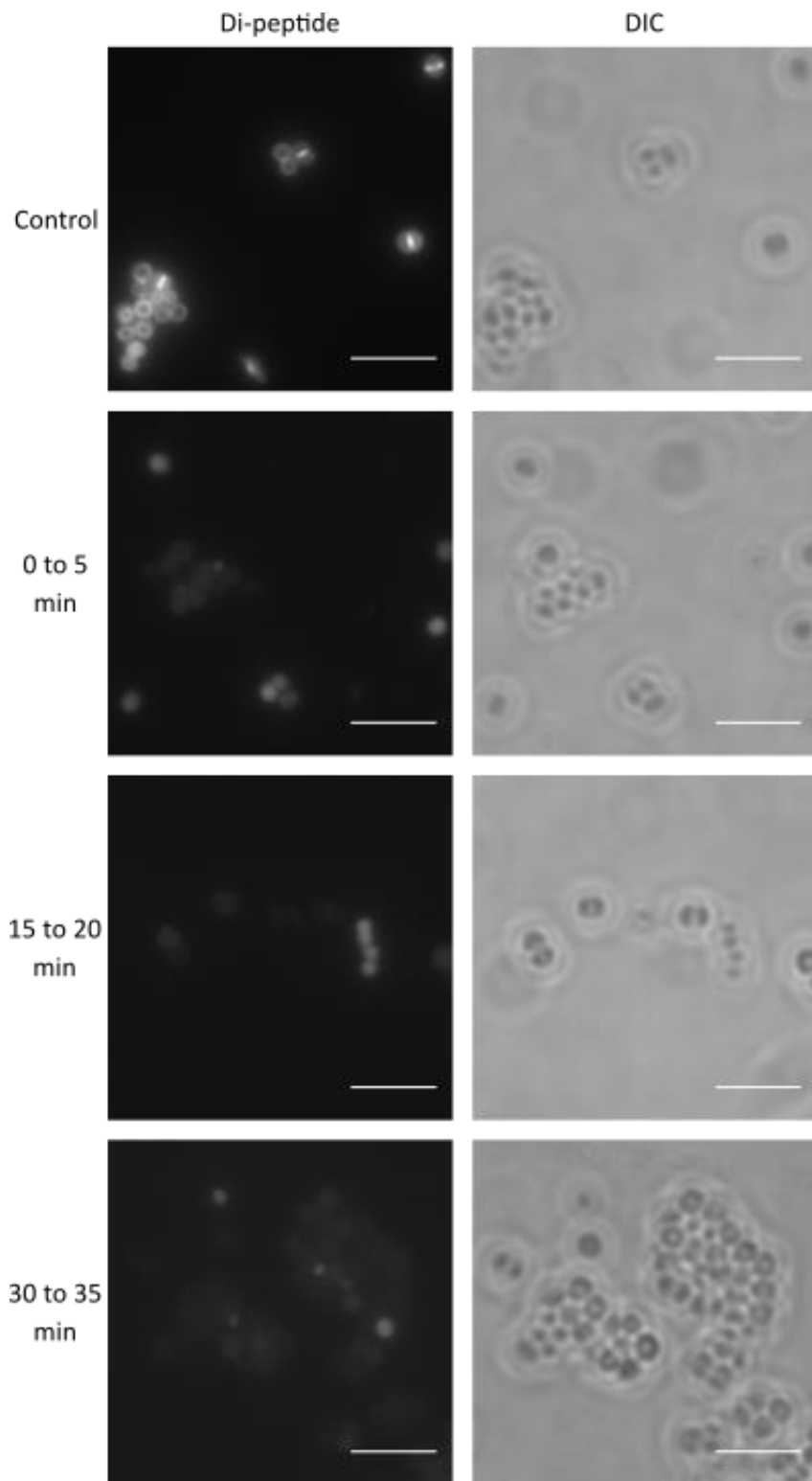
#### 4.2.4. Fate of newly incorporated peptidoglycan

*S. aureus* SH1000 was grown in the presence of ADA for 5 minutes before being washed and resuspended in ADA-free media and treated with 40 µg/mL (10 x MIC) vancomycin or not. The newly incorporated ADA was labelled with Alexa Fluor 594 by click chemistry. The cells were then labelled with NHS Ester 405 to contextualise the newly incorporated peptidoglycan (Figure 4.9). The aim of this experiment was to study the fate of newly incorporated material in an untreated vs. antibiotic treated population.

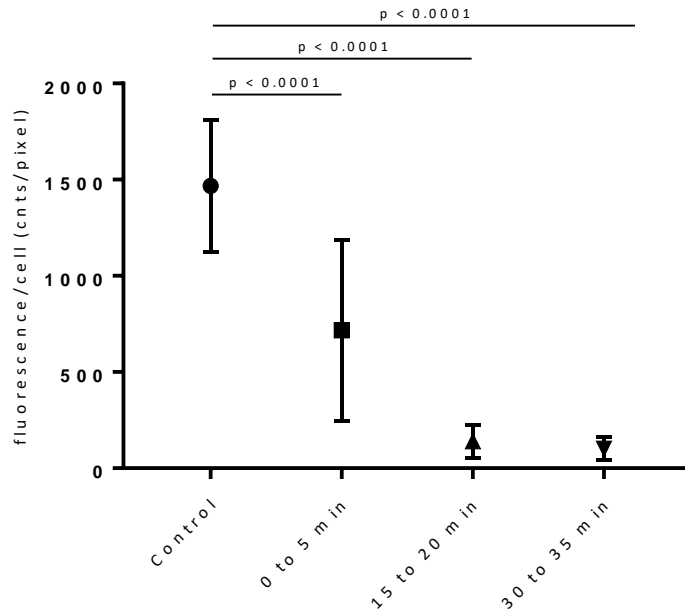
The pattern of newly incorporated peptidoglycan observed depends on the stage of the cell cycle during which it was incorporated prior to antibiotic addition (Figure 3.15). The fate of newly incorporated peptidoglycan in



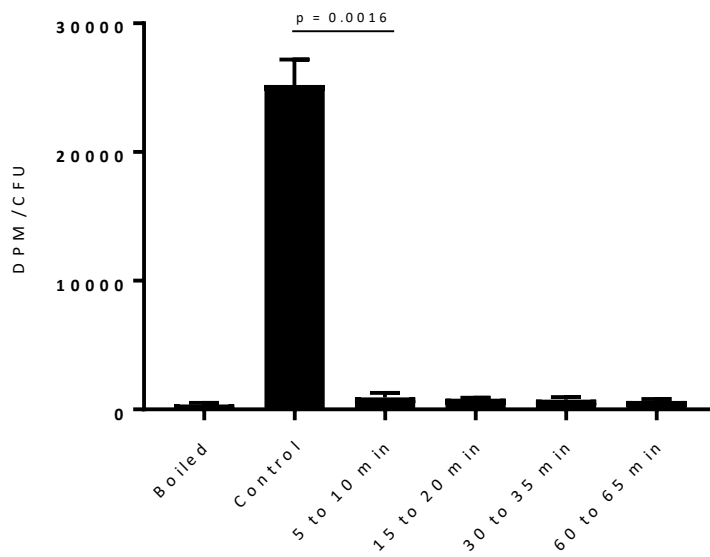
**Figure 4.5. Quantification of cell morphologies in EM images after vancomycin treatment.** In the EM images of the untreated sample and the sample treated with 40  $\mu\text{g}/\text{mL}$  vancomycin (10 x MIC) for 60 minutes, three morphologies were identified and their prevalence was quantified. Quantification was carried out on a population of approx. 100 cells (n as indicated) for each sample.



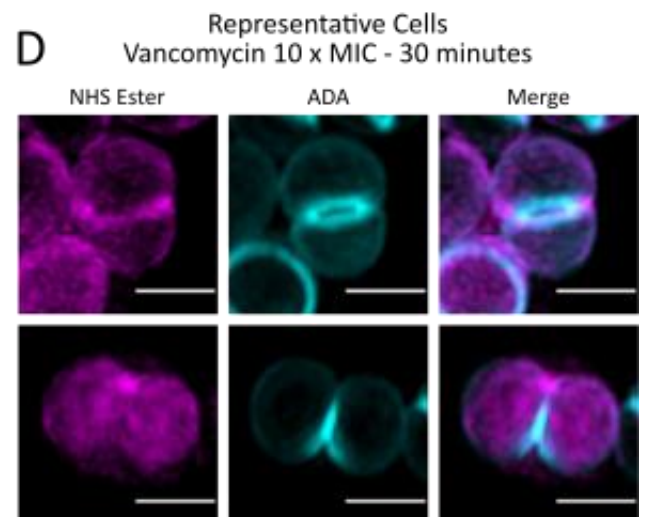
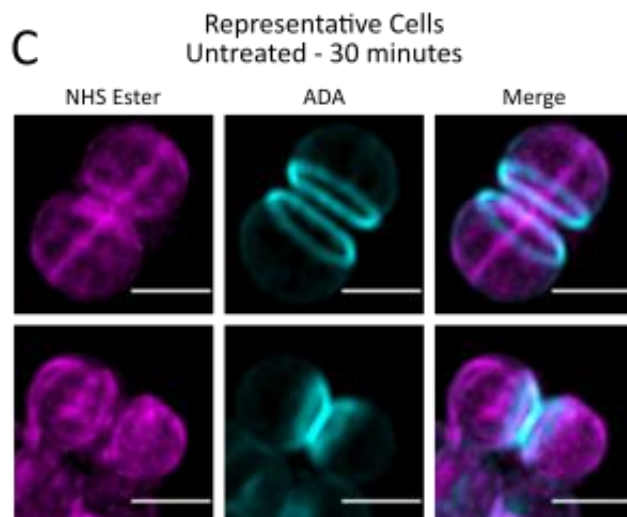
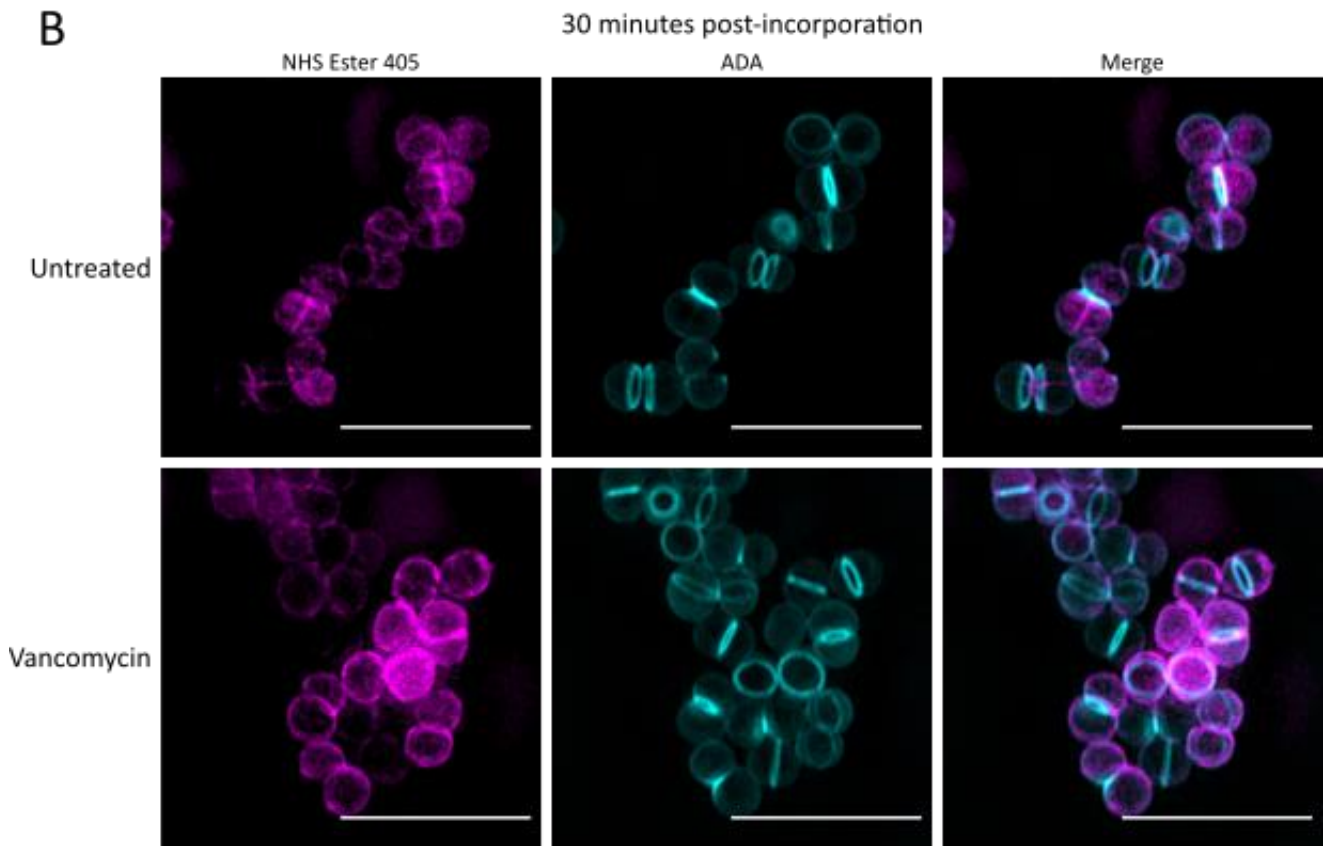
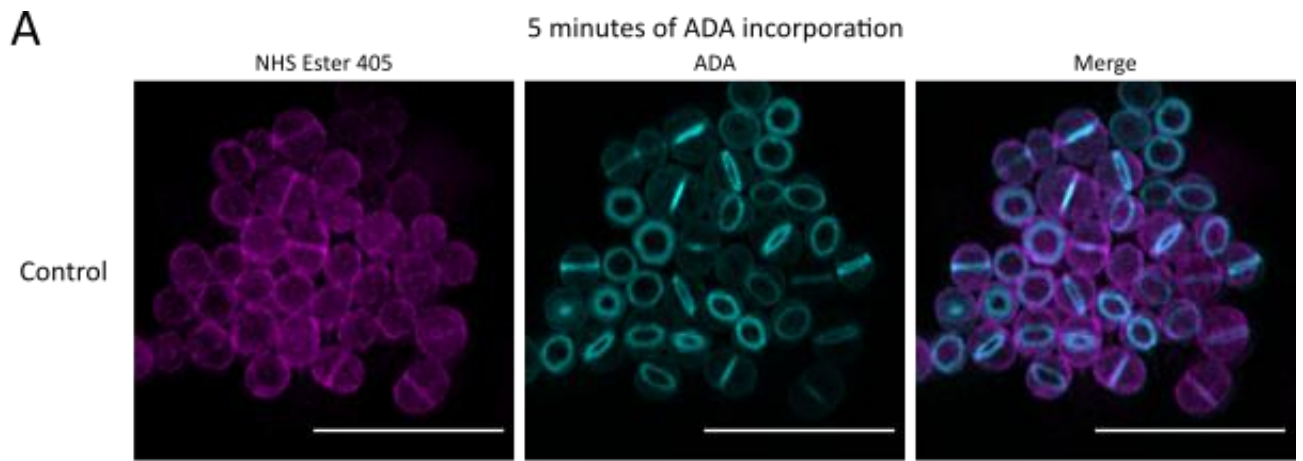
**Figure 4.6. Effect of vancomycin treatment on di-peptide incorporation in *S. aureus* SH1000.** Cells were grown in the presence of di-peptide for 5-minute periods after the addition of 40  $\mu\text{g}/\text{mL}$  vancomycin (10 x MIC). The newly incorporated material was subsequently labelled by click reaction with atto 488 and imaged on the Nikon widefield microscope. All scale bars 5  $\mu\text{m}$ .



**Figure 4.7. Quantification of the effect of vancomycin treatment on di-peptide incorporation in *S. aureus* SH1000.** Cells were treated with 40  $\mu\text{g}/\text{mL}$  vancomycin (10 x MIC) and samples were incubated with di-peptide for 5 minutes at different intervals after antibiotic addition. Samples were then fixed and imaged using identical settings. The fluorescence/cell was measured using ImageJ. P-values calculated by Mann-Whitney. N = 100 cells.



**Figure 4.8. Effect of vancomycin treatment on *S. aureus* SH1000 incorporation of <sup>14</sup>C- GlcNAc.** Cells were treated with 40 µg/mL vancomycin (10 x MIC) and samples were incubated with <sup>14</sup>C- GlcNAc for 5 minutes at different intervals after antibiotic addition. P-values calculated from unpaired t-tests with Welch's correction. Error bars represent standard deviation of the mean.



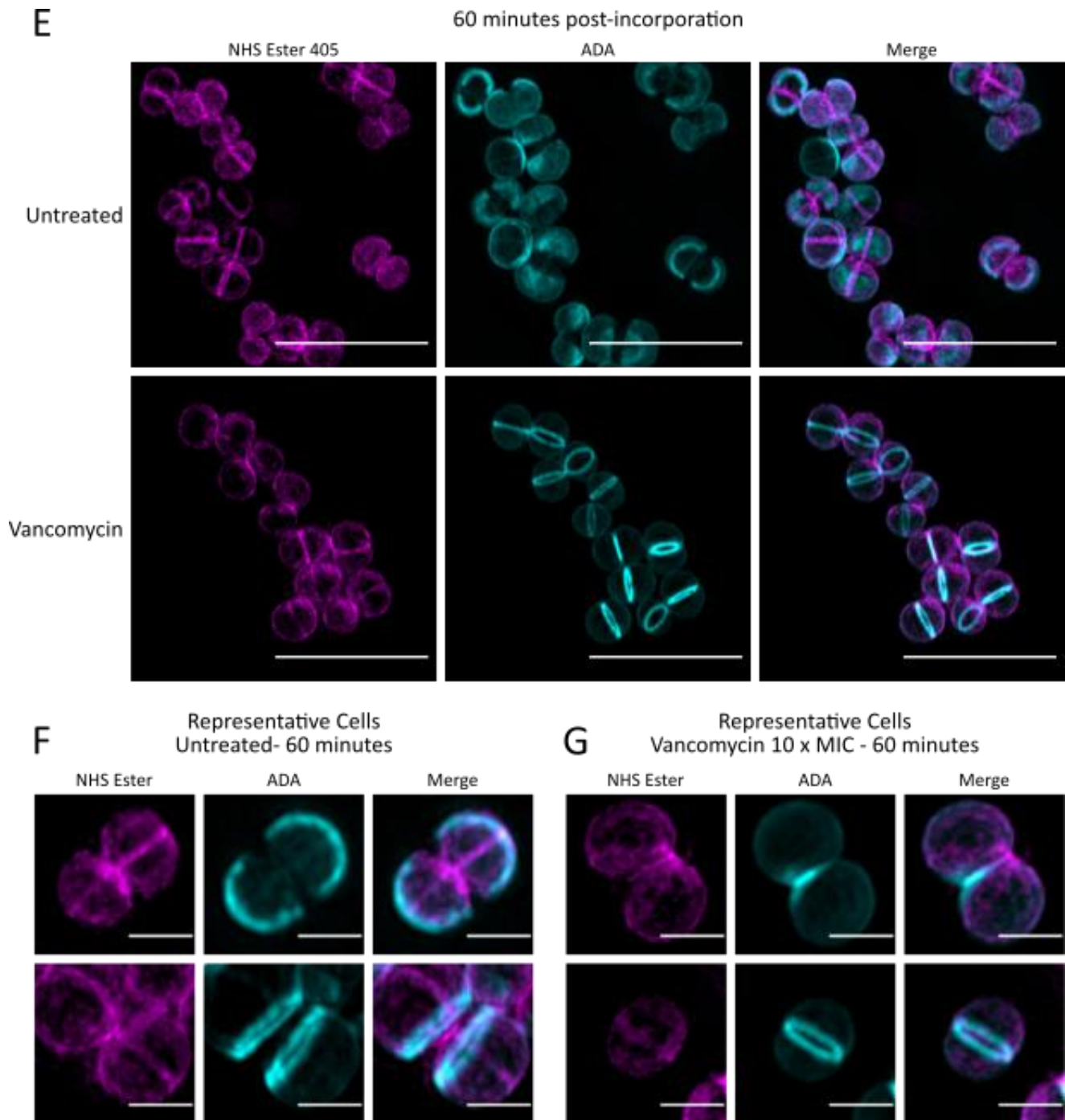


**Figure 4.9. Fate of newly synthesised peptidoglycan after vancomycin treatment.** Cells were grown in the presence of ADA for 5 minutes before being washed and treated with 40  $\mu\text{g}/\text{mL}$  vancomycin (10 x MIC) or, for the untreated sample, being washed and resuspended in media without ADA. Cells were fixed at 0, 30 & 60 minutes after addition of vancomycin or resuspension in fresh media. The incorporated ADA was clicked with Alexa Fluor 594 and the cells were labelled with NHS Ester 405. The data presented here was acquired simultaneously to the data presented in (Figure 3.14), the images for the untreated sample are therefore identical in both figures. (A) Fields of cells after 5 minutes of ADA incorporation. All scale bars 5  $\mu\text{m}$ . (B) Fields of cells from the untreated and vancomycin samples 30 minutes after ADA incorporation. All scale bars 5  $\mu\text{m}$ .

(C) Representative cells 30 minutes after ADA incorporation. All scale bars 1  $\mu\text{m}$ . (D) Representative cells 30 minutes after ADA incorporation and vancomycin addition. All scale bars 1  $\mu\text{m}$ . (E) Fields of cells from the untreated and vancomycin samples 60 minutes after ADA incorporation. All scale bars 5  $\mu\text{m}$ . (F) Representative cells 60 minutes after ADA incorporation. All scale bars 1  $\mu\text{m}$ . (G) Representative cells 60 minutes after ADA incorporation and vancomycin addition. All scale bars 1  $\mu\text{m}$ .

an untreated cell population was discussed in 3.2.4.1. The cells progressed through the cell cycle in a normal manner and the localisation of the newly incorporated peptidoglycan changed accordingly.

Six different morphologies were identified and the prevalence of each morphology was quantified at 0, 30 and 60 minutes after washing and antibiotic addition (Figure 4.10).

After 30 minutes of vancomycin treatment the newly incorporated peptidoglycan was located at the septum in 56% of cells compared to < 10% of cells in the untreated sample. 33% of the treated cells had a split punctate pattern and 11% showed a whole cell pattern. After 60 minutes of treatment, there were only very small changes to the observed patterns and their rate of occurrence compared to 30 minutes after treatment (Figure 4.10).

#### 4.2.5. Action of vancomycin on *B. subtilis*

##### 4.2.5.1. Killing dynamics

The MIC was determined by standard serial dilution method. The MIC of vancomycin against *B. subtilis* 168 HR is 0.25 µg/mL. All the experiments described in this chapter were done with 10 x MIC, i.e. 2.5 µg/mL vancomycin.

A kill curve was carried out with vancomycin, measuring the CFU/mL present in the culture at regular intervals. *B. subtilis* 168 HR dies rapidly after vancomycin treatment. 90% killing was reached in the first 60 minutes after addition of 2.5 µg/mL vancomycin to the growth media (Figure 4.11).

##### 4.2.5.2. Morphological changes

*B. subtilis* 168 HR was fixed at different time points after treatment with 2.5 µg/mL vancomycin and labelled with WGA 594 to visualise cell morphology (Figure 4.12). WGA was used for this experiment rather than NHS ester because NHS ester cytoplasmically labelled a large part of the population (data not shown). This problem did not occur with WGA. After treatment with vancomycin, cell deformations are observed in the septal area. After 15 minutes some wider deformed septa are visible. After 30 and 60 minutes of treatment, sacculi are visible in the sample. These appear to have always ripped across the width of the cell (Figure 4.12, Panel B).

Cell length and width were measured on the WGA SIM images using ImageJ. There was no significant change in cell length after treatment with 2.5 µg/mL vancomycin for 60 minutes (Figure 4.13). There was a significant increase in cell width within 15 minutes of treatment with 10 x MIC vancomycin. The mean cell width of the population increased from 0.892 µm to 0.945 µm.

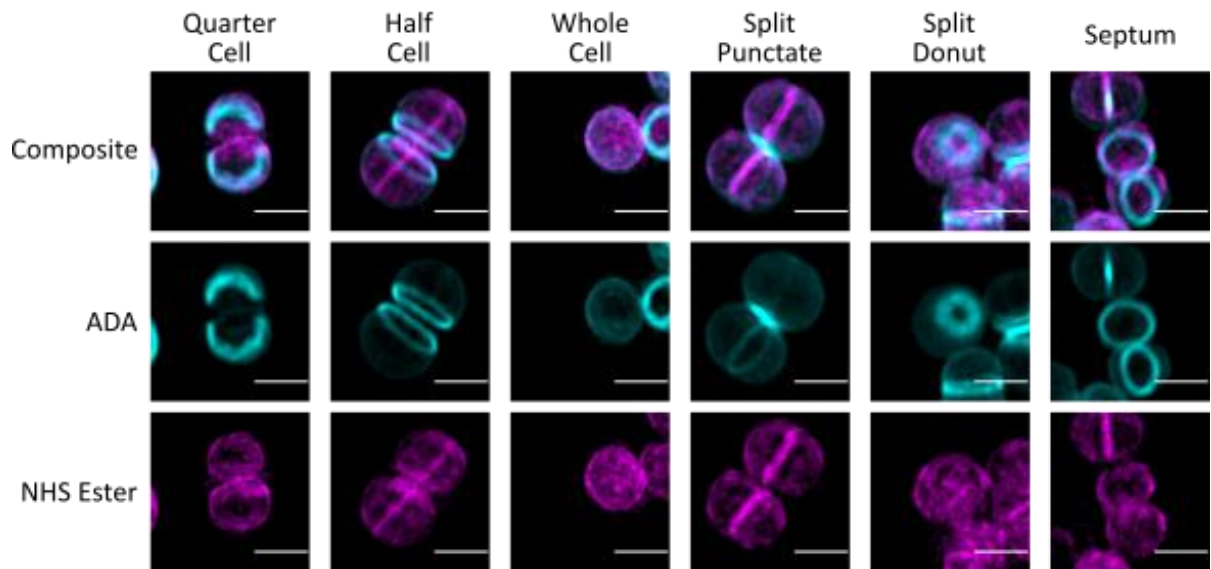
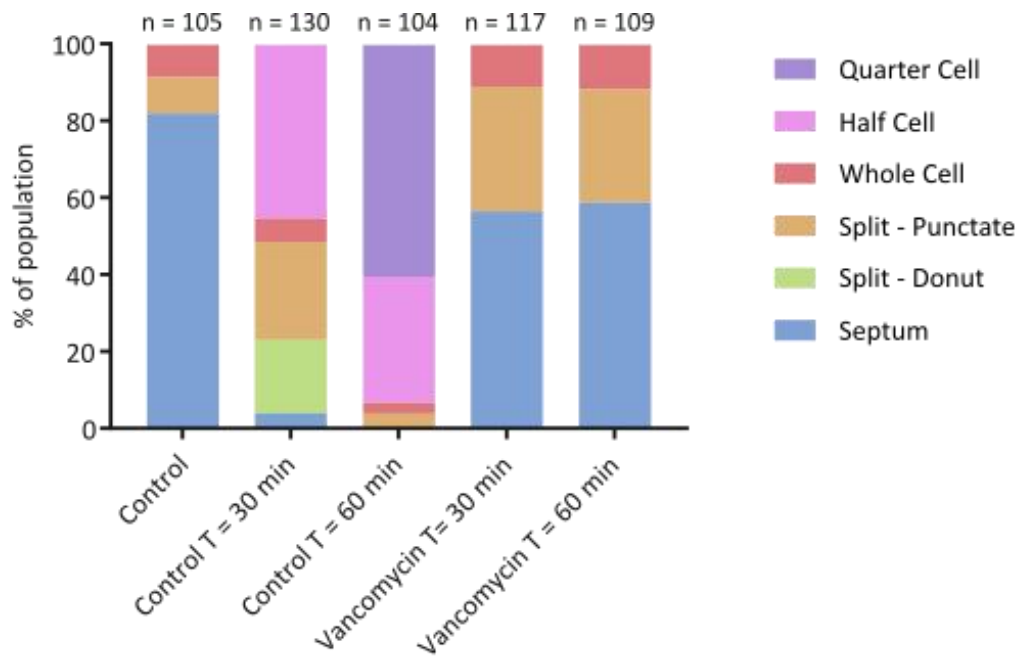


**Figure 4.10. Quantification of the effect vancomycin on the fate of newly synthesised peptidoglycan.** Six different cell morphologies were identified, and representative cells are pictured. The prevalence of each morphology was quantified in a population of approx. 100 (n as indicated in graph) cells for every sample.

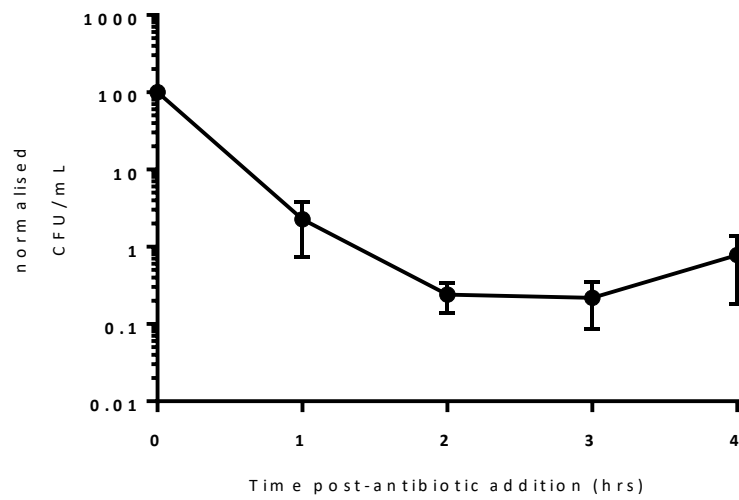


**Figure 4.11. Vancomycin killing of *B. subtilis*.** *B. subtilis* 168 HR was treated with 2.5 µg/mL vancomycin (10 x MIC). The CFU/mL was determined at each time-point and the data was normalised by setting the first time point as 100%. The mean and standard deviation are plotted. This experiment was done in triplicate.

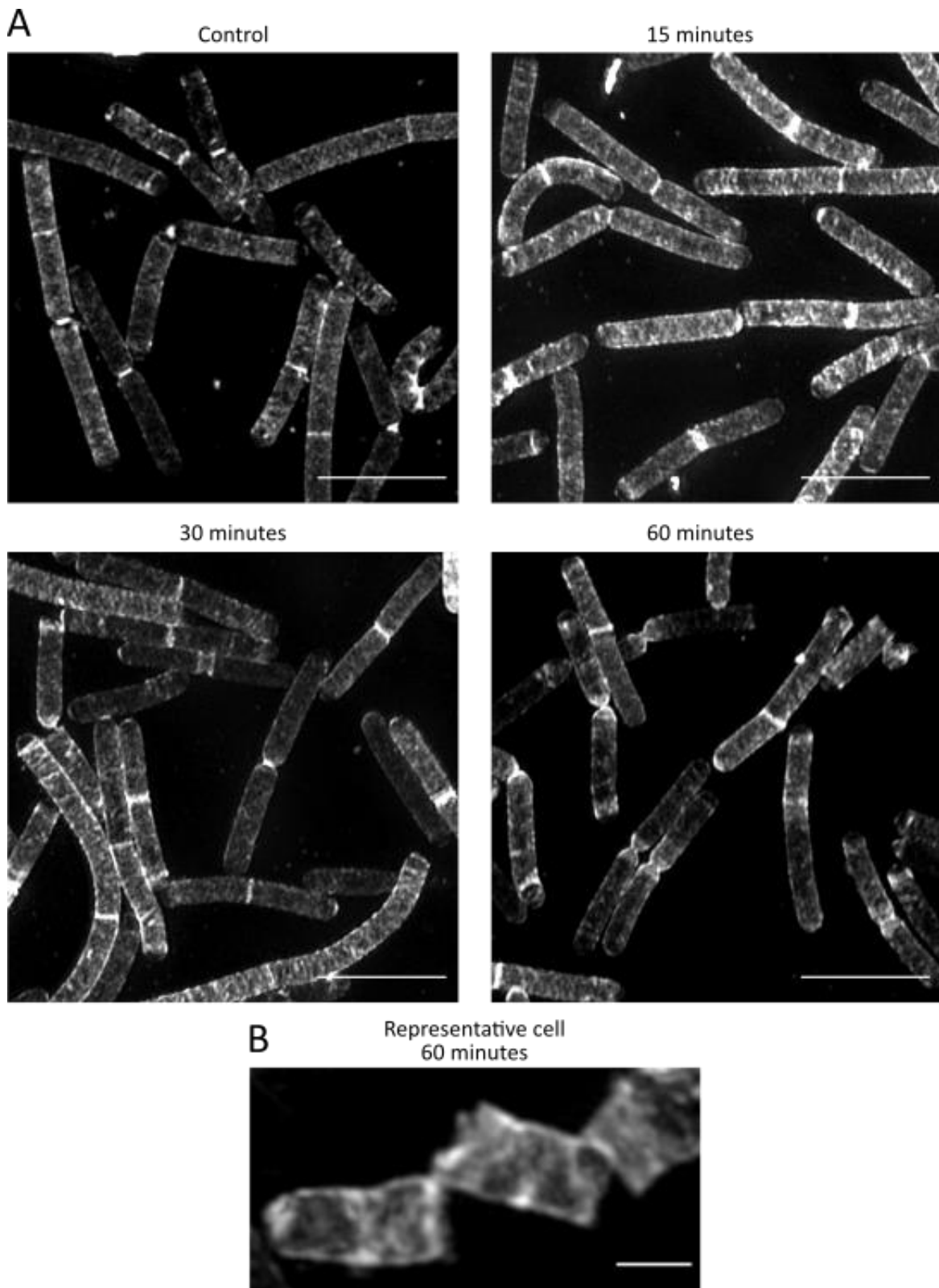


**Figure 4.12. Effect of vancomycin on *B. subtilis* 168 HR morphology.** Cells were treated with 2.5  $\mu\text{g}/\text{mL}$  vancomycin (10 x MIC), fixed after 0, 15, 30 and 60 minutes of treatment and subsequently labelled with WGA 594. Cells were imaged using the OMX SIM and maximum intensity projections are shown. (A) Fields of cells

from each time point, as indicated. All scale bars 5  $\mu\text{m}$ . (B) Representative cell after 60 minutes of treatment. Scale bar 1  $\mu\text{m}$ .

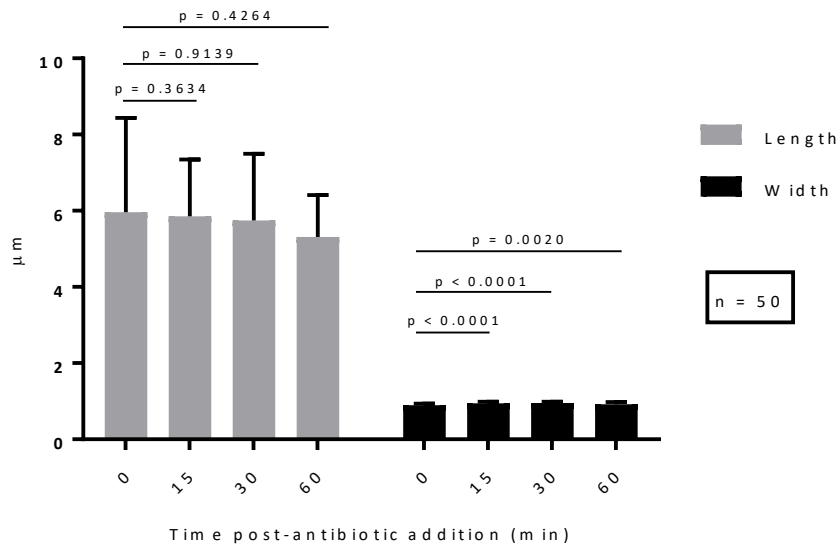


**Figure 4.13. The effect of vancomycin on *B. subtilis* 168 HR cell length and width.** Cell length and width were measured in image J using images acquired on the OMX SIM of WGA labelled *B. subtilis* fixed at different time points after the addition of 2.5  $\mu\text{g}/\text{mL}$  vancomycin (10 x MIC). The error bars represent standard deviation. P-values were calculated by Mann-Whitney.

### 4.3. Discussion

#### 4.3.1. Morphological changes

Vancomycin is bactericidal for *S. aureus*. In the images of *S. aureus* SH1000 labelled with NHS ester after treatment with 10 x MIC vancomycin, no gross morphological changes were observed. The cells appear to maintain their shape. A significant increase in cell size ( $p < 0.0001$ ) was observed after 15 minutes of treatment with 40  $\mu\text{g}/\text{mL}$  vancomycin (Figure 4.3). An increase in cell size could be due to cell wall synthesis and hydrolysis, which are both required for cell growth (Wheeler et al., 2015).

*S. aureus* SH1000 cells imaged by EM after treatment with 10 x MIC vancomycin showed few morphological changes (Figure 4.4). Quantification of observed morphologies showed very little change between the control sample and the sample after 60 minutes of vancomycin treatment (Figure 4.5). Due to the lack of peptidoglycan synthesis, the cells are not progressing through the cell cycle, suggesting their morphology is fixed after treatment with vancomycin.

Cell wall synthesis was studied by measuring  $^{14}\text{C}$ -GlcNAc incorporation and FDAA incorporation after vancomycin treatment (Figure 4.7 & Figure 4.8). The rapid decrease in transglycosylation and transpeptidation observed here agrees with some original studies into the mode of action of vancomycin. These studies looked at the incorporation of  $^{14}\text{C}$ -glutamic acid, noting an ~80% decrease in incorporation into the cell wall fraction after 20 minutes of incubation with 25  $\mu\text{g}/\text{mL}$  vancomycin (Reynolds, 1961). This halt of incorporation suggests that the observed increase in cell size is not due to cell wall synthesis and is therefore likely due to cell wall hydrolysis. The glucosaminidase family of hydrolases is thought to play a crucial role in cell wall growth (Wheeler et al., 2015). Investigating mutants lacking members of the glucosaminidase family would give more insight into the cell size increase observed after vancomycin treatment.

#### 4.3.2. Fate of newly incorporated peptidoglycan

After 5 minutes of ADA incorporation, the newly incorporated ADA is located at the septum in just over 80% of the cells, with 10% of the cells displaying a split punctate pattern and the last 10% showing no focus of incorporation (i.e. "whole cell" pattern) (Figure 4.9 & Figure 4.10). After 30 minutes of treatment with 40  $\mu\text{g}/\text{mL}$  vancomycin, an increase in the number of split punctate cells was seen, which is due to cells that had completed their septa during the 5 minutes of incorporation then dividing. This suggests hydrolases involved in cell division are still active after antibiotic treatment. However, cells are not progressing through the cell cycle due to the lack of peptidoglycan incorporation. There is very little change between 30 and 60 minutes, suggesting the cells have simply halted at whatever stage of the cell cycle they found themselves in when vancomycin was added to the growth culture.

#### 4.3.3. Action of vancomycin on *B. subtilis*

After treatment of *B. subtilis* 168 HR with vancomycin, we see very similar effects as after treatment with methicillin. The same ripping at the septa and across the short axis of the cell wall is observed (Figure 4.12 & Figure 3.18). This corresponds to the weaker axis of the *B. subtilis* cell wall (Beeby et al., 2013). The cells have not significantly increased in cell length but have increased significantly in width after treatment with vancomycin. In *B. subtilis* peptidoglycan is organised in long polysaccharide chains that run circumferentially around the short axis of the cells (Turner et al. , 2014). The glycan chains of *B. subtilis* are 50 - 5000 disaccharides long compared to 6 - 12 disaccharides long in *S. aureus*. The long chains, their spatial organisation and the fact that killing happens rapidly, help explain why no significant increase in cell length is observed. An increase in cell length might require more hydrolysis than the amount required to observe an increase in cell width.



## Chapter 5

### Investigating the role of cell wall metabolism in the bactericidal effect of antibiotics

#### 5.1. Introduction

The *S. aureus* cell wall is composed of a lipid bilayer and a thick outer peptidoglycan layer (20-35 nm thick)(Schleifer & Kandler, 1972). Teichoic acids decorate the cell wall, with wall teichoic acids (WTA) anchored to the peptidoglycan layer and lipoteichoic acids (LTA) tethered to the cell membrane (Silhavy et al., 2010). Cell wall metabolism encompasses both peptidoglycan synthesis and hydrolysis, which together control the function of this essential polymer.

Peptidoglycan synthesis begins in the cytoplasm with the assembly of lipid I and lipid II (Typas et al., 2012). Lipid II is flipped across the membrane before being polymerised into long glycan chains, which are then crosslinked. The action of hydrolases leads to further modification of the peptidoglycan, resulting in the final architecture of the cell wall (Wheeler et al., 2015). The *S. aureus* cell wall is smooth on the inside with very few small holes and has a looser mesh appearance with larger holes on the outside (Pasquina-Lemonche et al., unpublished).

Previous data presented in Chapters 3 and 4 of this thesis showed that treatment of *S. aureus* SH1000 with methicillin or vancomycin lead to inhibition of peptidoglycan synthesis and changes in cell wall structure, leading to the investigation of other components of cell wall metabolism. After treatment with methicillin or vancomycin, an increase in cell size was observed despite a lack of peptidoglycan synthesis. In this chapter, the possibility of this cell size increase being due to the action of cell wall hydrolases is investigated.

There are 20 putative hydrolases in *S. aureus*. Within this, glucosaminidase activity is essential for normal growth of bacteria as discussed in 1.6.1. The four putative glucosaminidases in *S. aureus* are essential as a group of enzymes and are mutually redundant (Wheeler et al., 2015). Peptidoglycan synthesised at the septum has long glycan strands which are cleaved by glucosaminidases, primarily SagB, leading to alterations in the biophysical properties of the cell wall. The action of the glucosaminidases results in *S. aureus* having short glycan strands with an average of 6 disaccharides (Boneca et al., 2000). The involvement of peptidoglycan hydrolases and cell structure and modification in the action of antibiotics is not well understood. Previous research has shown that generalised cell lysis is not the cause of cell death. The generalised cell lysis observed after  $\beta$ -lactam treatment is due to Atl (Foster, 1995). However, degradation of the cell wall by other hydrolases has not been investigated as a cause of cell death.

After methicillin treatment changes to the septal region were observed and presented in chapter 3 of this thesis. The cell membrane and cell wall appear to separate. Additionally, residual GlcNAc incorporation was measured after methicillin treatment. As previously discussed in Chapter 3, the bulbous septa and residual

incorporation could be explained by the presence of excess WTA. The role of WTAs in killing by cell wall antibiotics was therefore investigated and results are presented in this chapter.

#### 5.1.1. Aims of this chapter

- Establish the role of glucosaminidases in cell wall antibiotic killing of *S. aureus*
- Investigate the role of wall teichoic acids in cell wall antibiotic killing of *S. aureus*

## 5.2. Results

### 5.2.1. The role of glucosaminidases in cell wall antibiotic killing of *S. aureus*

To study the role that glucosaminidases play in the killing of *S. aureus* by vancomycin and methicillin, single mutants and multiple mutants were used. Strains each lacking one of the four putative glucosaminidases were used to study the role of individual glucosaminidases (*S. aureus* SH1000 *sagB*, *S. aureus* SH1000 *sagA*, *S. aureus* SH1000 *scaH*, *S. aureus* SH1000 *atl*). To study them as a group of enzymes, triple mutants were used (*S. aureus* SH1000 *atl sagA sagB*, *S. aureus* SH1000 *atl sagA scaH*, *S. aureus* SH1000 *sagA sagB scaH* and *S. aureus* SH1000 *atl sagB scaH*). The glucosaminidases are essential as a group, a quadruple mutant is therefore not viable.

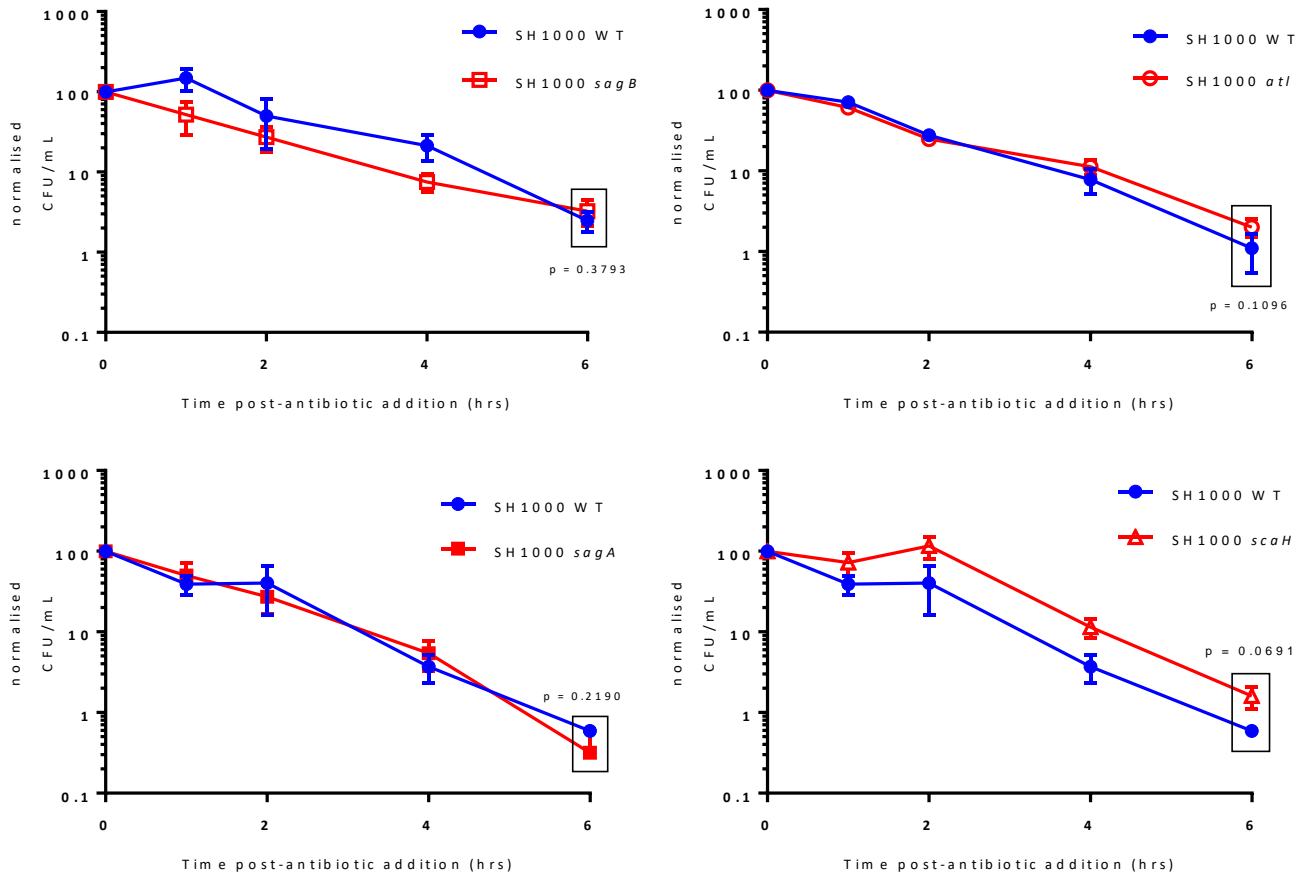
#### 5.2.1.1. Killing dynamics

*S. aureus* SH1000 *sagB*, SH1000 *atl*, SH1000 *sagA* and SH1000 *scaH* were grown to early exponential phase (OD<sub>600</sub> 0.2-0.3) before addition of 40 µg/mL methicillin (10 x MIC) to the growth media. The CFU/mL was measured at regular intervals. No significant difference in killing was observed between the wild-type and any of the glucosaminidase single mutants 6 hours after addition of 10 x MIC methicillin (Figure 5.1).

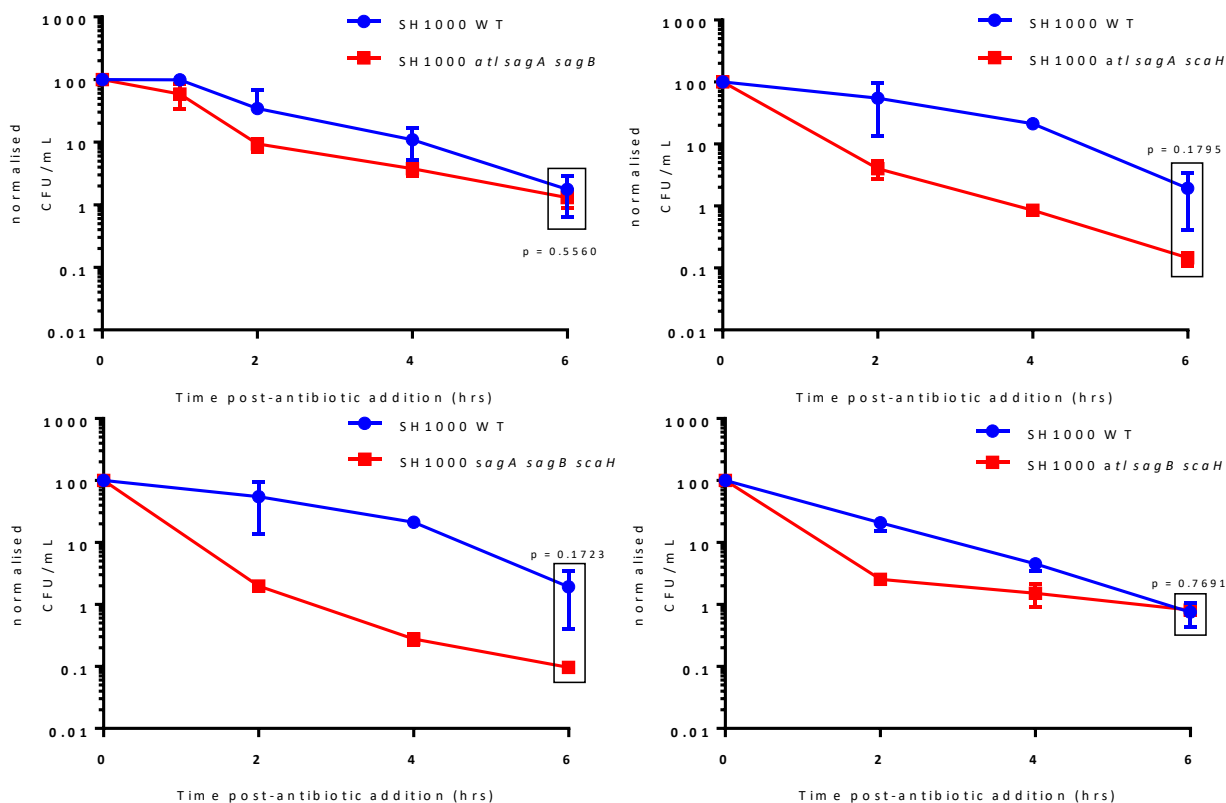
The same experiment was carried out with the four triple glucosaminidase mutants: *S. aureus* SH1000 *atl sagA sagB*, *S. aureus* SH1000 *atl sagA scaH*, *S. aureus* SH1000 *sagA sagB scaH* and *S. aureus* SH1000 *atl sagB scaH*. No significant difference in killing was observed between the wild-type and any of the triple mutants 6 hours after addition of 40 µg/mL methicillin (

Figure 5.2. Effect of methicillin on the viability of triple glucosaminidase mutants. ***S. aureus* SH1000 *atl sagA sagB*, *S. aureus* SH1000 *atl sagA scaH*, *S. aureus* SH1000 *sagA sagB scaH* and *S. aureus* SH1000 *atl sagB scaH* were each treated with 40 µg/mL methicillin (10 x MIC). Each strain is plotted individually with the *S. aureus* SH1000 WT control done on the same day. The CFU/mL was determined at each time-point and the data was normalised by setting the first time point as 100%. The mean and standard deviation are plotted. Each experiment was done in triplicate. P-values were calculated by two-tailed t-test with Welch's correction.**)  
For two of the triple mutants, there appears to be increased killing, although the results are not significant due to variability in the data.

The triple glucosaminidase mutants were treated with 40 µg/mL vancomycin (Figure 5.3). After 6 hours of treatment no significant change in killing compared to *S. aureus* SH1000 was observed for mutants *S. aureus* SH1000 *atl sagA sagB*, *S. aureus* SH1000 *atl sagA scaH*, and *S. aureus* SH1000 *atl sagB scaH*. A slightly significant ( $p = 0.0194$ ) decrease in killing was observed for *S. aureus* SH1000 *sagA sagB scaH*.



**Figure 5.1. Effect of methicillin on *S. aureus* glucosaminidase single mutant cell viability.** *S. aureus* SH1000 *sagB*, SH1000 *atl*, SH1000 *sagA* and SH1000 *scaH* were treated with 40 µg/mL methicillin. Each strain is plotted individually with the *S. aureus* SH1000 WT control done on the same day. The CFU/mL was determined at each time-point and the data was normalised by setting the first time point as 100%. The mean and standard deviation are plotted. Each experiment was done in triplicate. P-values were calculated by two-tailed t-test with Welch's correction.



**Figure 5.2. Effect of methicillin on the viability of triple glucosaminidase mutants.** *S. aureus* SH1000 *atl sagA sagB*, *S. aureus* SH1000 *atl sagA scaH*, *S. aureus* SH1000 *sagA sagB scaH* and *S. aureus* SH1000 *atl sagB scaH* were each treated with 40 µg/mL methicillin (10 x MIC). Each strain is plotted individually with the *S. aureus* SH1000 WT control done on the same day. The CFU/mL was determined at each time-point and the data was normalised by setting the first time point as 100%. The mean and standard deviation are plotted. Each experiment was done in triplicate. P-values were calculated by two-tailed t-test with Welch's correction.

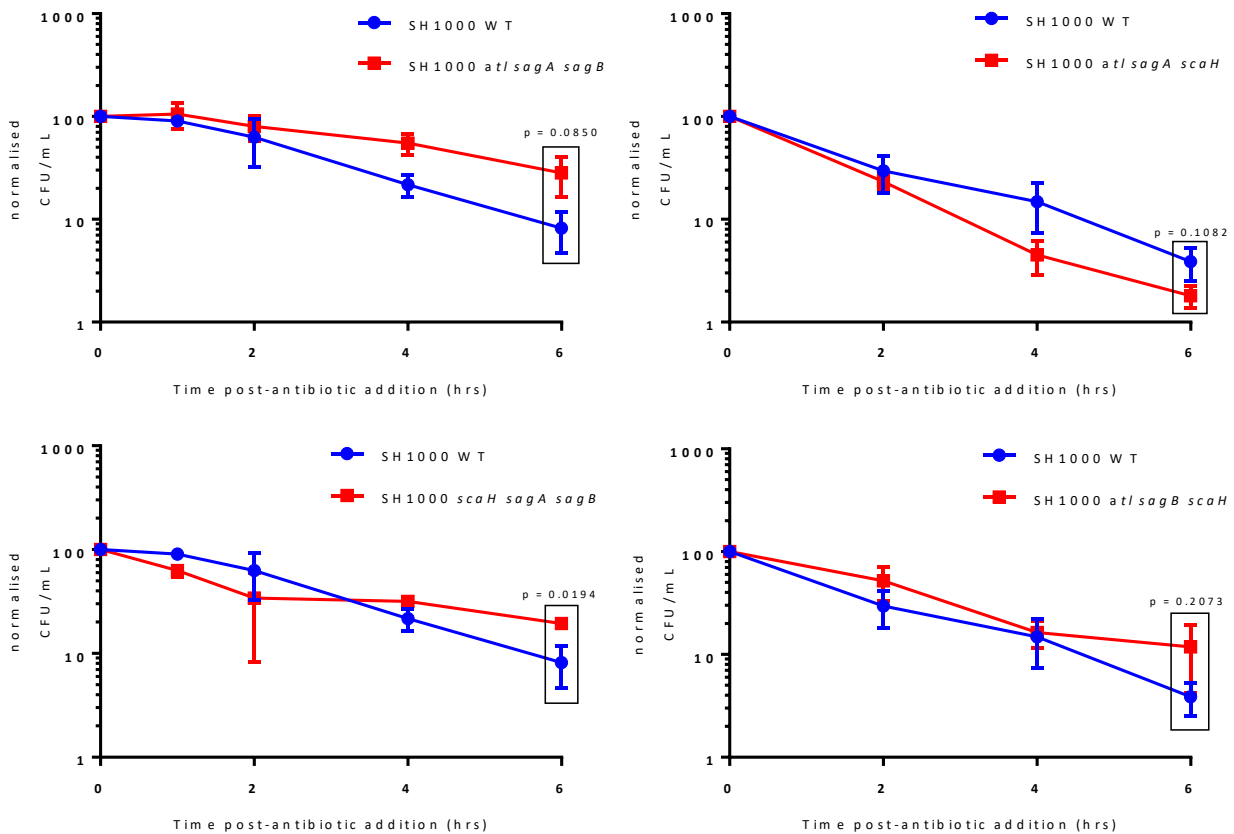


**Figure 5.3. Effect of vancomycin on the viability of triple glucosaminidase mutants.** *S. aureus* SH1000 *atl sagA sagB*, *S. aureus* SH1000 *atl sagA scaH*, *S. aureus* SH1000 *sagA sagB scaH* and *S. aureus* SH1000 *atl sagB scaH* were each treated with 40  $\mu\text{g}/\text{mL}$  vancomycin (10 x MIC). Each strain is plotted individually with the *S. aureus* SH1000 WT control done on the same day. The CFU/mL was determined at each time-point and the data was normalised by setting the first time point as 100%. The mean and standard deviation are plotted. Each experiment was done in triplicate. P-values were calculated by two-tailed t-test with Welch's correction.

### 5.2.1.2. Cell morphology

Cell morphology was investigated by fixing cells 0 & 60 minutes after addition of the antibiotic to the growth media, labelling them with NHS ester 555 and imaging them using SIM, as described in previous chapters.

*S. aureus* SH1000 *sagB*, SH1000 *atl*, SH1000 *sagA* and SH1000 *scaH* were treated with 40 µg/mL methicillin. An hour after treatment, no major changes to cell morphology, other than cell size, were observed (Figure 5.4). To quantify changes in cell size, the cell volume of 100 cells was measured using ImageJ as described by Zhou et al., 2015. The population cell volume increased significantly after 60 minutes of treatment with 40 µg/mL methicillin in all the single glucosaminidase mutants (Figure 5.5), compared to before antibiotic treatment. However, the amount by which each mutant increased in size after antibiotic treatment is different. In *S. aureus* SH1000 WT the mean cell volume of the population increased by a factor of 2.5. This is decreased to an increase of a factor of 2.1 for *S. aureus* SH1000 *atl*, 1.8 for *S. aureus* SH1000 *sagA*, 1.7 for *S. aureus* SH1000 *scaH* and 1.4 for *S. aureus* SH1000 *sagB*.

To investigate changes in cell morphology after antibiotic treatment in the glucosaminidase triple mutants, the same experiment was carried out as with the single mutants. Cells were fixed 0 & 60 minutes post addition of 40 µg/mL methicillin to the growth media, then labelled with NHS ester 555 and imaged using SIM (Figure 5.6).

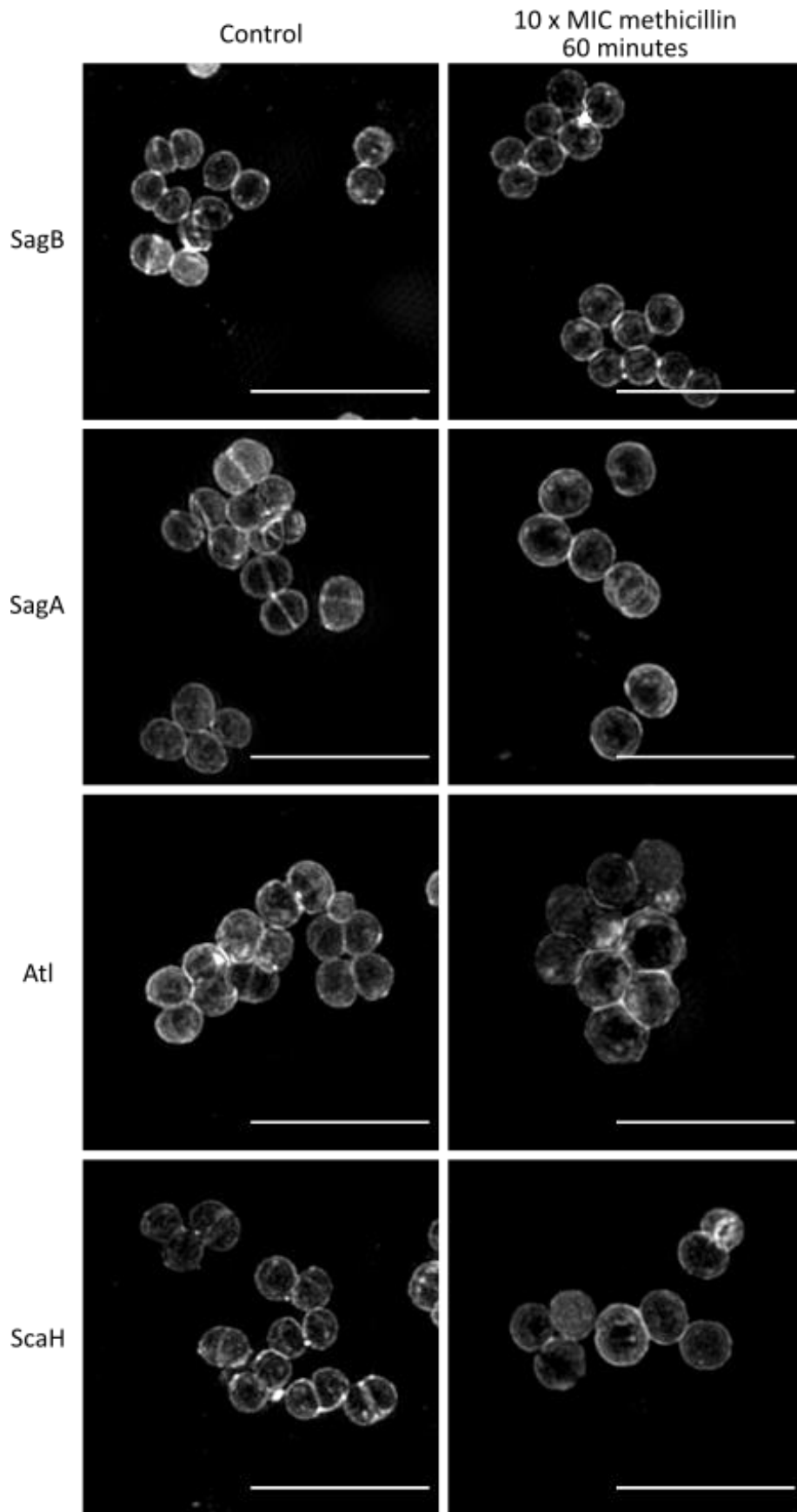
After 60 minutes of treatment with 40 µg/mL methicillin, cell morphologies appeared similar to before treatment apart from changes to cell size (Figure 5.6). Changes in cell volume were quantified in Image J using a method described by Zhou et al., 2015. There was no significant increase in the population cell volume of *S. aureus* SH1000 *atl sagA sagB* ( $p = 0.3035$ ). There was a significant increase in cell volume of *S. aureus* SH1000 *sagA sagB scaH* ( $p = 0.0311$ ), *S. aureus* SH1000 *atl sagA scaH* ( $p < 0.0001$ ) and *S. aureus* SH1000 *atl sagB scaH* ( $p < 0.0001$ ) (

Figure 5.7). Although they still show a significant increase in cell volume, *S. aureus* SH1000 *atl sagB scaH* mean cell volume increased by a factor of 1.3 after 60 minutes of methicillin treatment and *S. aureus* SH1000 *sagA sagB scaH* mean cell volume increased by a factor of 1.1 after 60 minutes of methicillin treatment, compared to an increase in mean cell volume by a factor of 2.5 in the wild-type. In *S. aureus* SH1000 *atl sagA scaH* the cell volume increased by a factor of 1.8 after 60 minutes of methicillin treatment.

The triple glucosaminidase mutants were treated with 40 µg/mL vancomycin and the same experiment and analysis was carried out. All the data in this paragraph was acquired by Elizabeth Tatham. After 60 minutes of vancomycin treatment, no major changes to cell shape were observed apart from changes to cell size (Figure 5.8). All four triple mutants significantly ( $p < 0.0001$ ) increased in cell volume after 60 minutes of treatment with 40 µg/mL vancomycin (

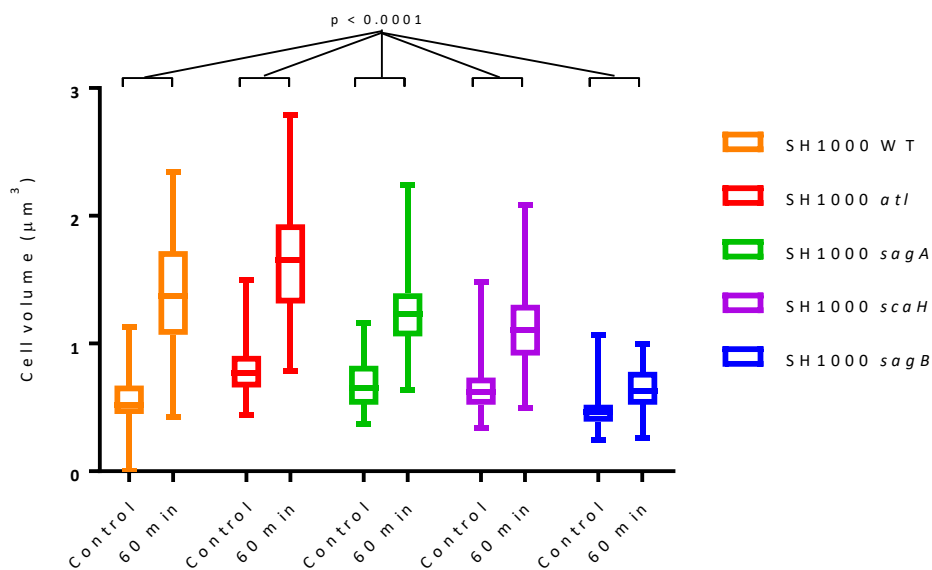
Figure 5.9). The mean cell volume of all four triple glucosaminidase mutants increased by a factor of 1.2 after

vancomycin treatment, compared to an increase by a factor of 1.5 in the mean cell volume of *S. aureus* SH1000 after 60 minutes in the presence of vancomycin.



**Figure 5.4. Effect of methicillin on single glucosaminidase mutant morphology.** *S. aureus* SH1000 *sagB*, *S. aureus* SH1000 *sagA*, *S. aureus* SH1000 *atl* and *S. aureus* SH1000 *scaH* were treated with 40  $\mu\text{g}/\text{mL}$  methicillin

(10 x MIC), fixed after 0 & 60 minutes of treatment and subsequently labelled with NHS ester 555. Cells were imaged using the OMX SIM and maximum intensity projections are shown. All scale bars 5  $\mu\text{m}$ .



Strain	SH1000 WT	SH1000 <i>atl</i>	SH1000 <i>sagA</i>	SH1000 <i>scaH</i>	SH1000 <i>sagB</i>
Size increase	x 2.5	x 2.1	x 1.8	x 1.7	x 1.4

**Figure 5.5. Effect of methicillin on the cell volume of single glucosaminidase mutants.** *S. aureus* SH1000 *atl*, *S. aureus* SH1000 *sagA*, *S. aureus* SH1000 *scaH* and *S. aureus* SH1000 *sagB* were each treated with 40  $\mu\text{g}/\text{mL}$  methicillin, fixed at different time-points after antibiotic addition, labelled with NHS Ester 555 and imaged using the OMX SIM. Cell volume was calculated from measurements carried out in ImageJ on these images. P-values were calculated by Mann-Whitney tests. Whiskers extend from the minimum to the maximum values and boxes from the 25<sup>th</sup> to the 75<sup>th</sup> percentile. The middle of the box is plotted at the median. The factor by which each strain increases in cell volume after 60 minutes of treatment with methicillin is presented in the table.

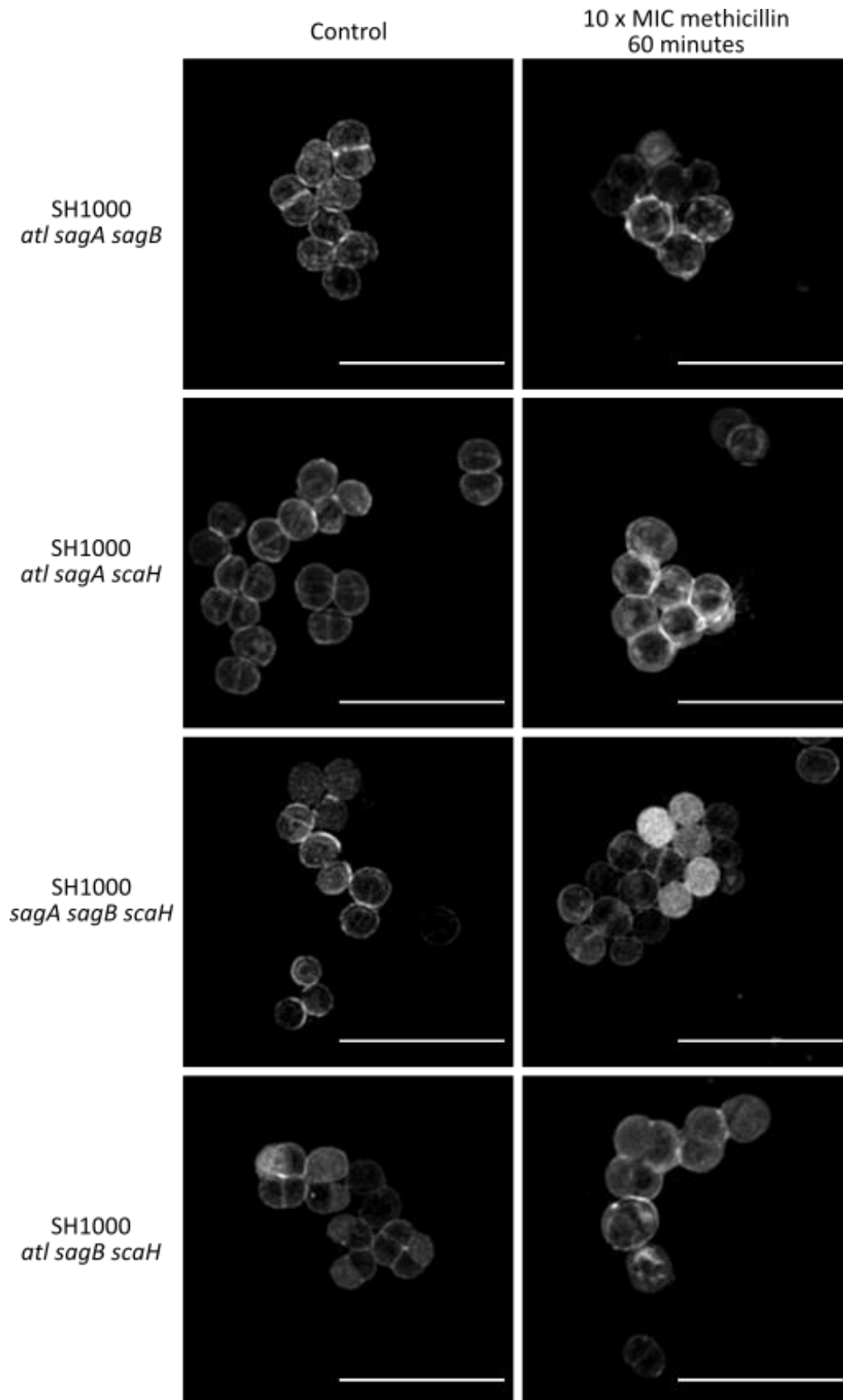
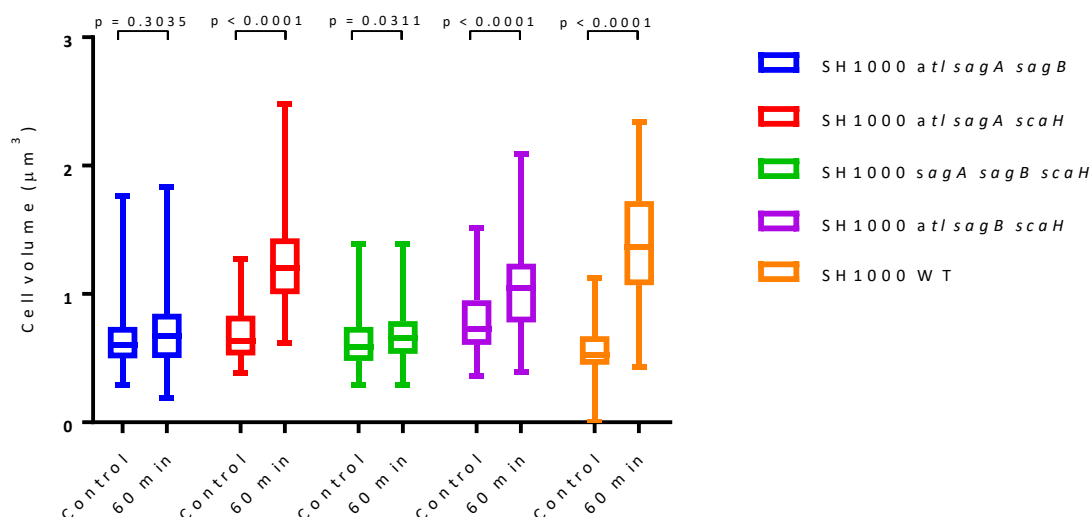


**Figure 5.6. Effect of methicillin on triple glucosaminidase mutant cell morphology.** *S. aureus* SH1000 *atl sagA sagB*, *S. aureus* SH1000 *atl sagA scaH*, *S. aureus* SH1000 *sagA sagB scaH* and *S. aureus* SH1000 *atl sagB scaH*

were treated with 40 µg/mL methicillin (10 x MIC), fixed after 0 & 60 minutes of treatment and subsequently labelled with NHS ester 555. Cells were imaged using the OMX SIM and maximum intensity projections are shown. All scale bars 5 µm.



Strain	SH1000 <i>atl sagA sagB</i>	SH1000 <i>atl sagA scaH</i>	SH1000 <i>sagA sagB scaH</i>	SH1000 <i>atl sagB scaH</i>	SH1000 WT
Size increase	x 1.06	x 1.8	x 1.1	x 1.3	x 2.5

**Figure 5.7. Effect of methicillin on the cell volume of triple glucosaminidase mutants.** *S. aureus* SH1000 *atl sagA sagB*, *S. aureus* SH1000 *atl sagA scaH*, *S. aureus* SH1000 *sagA sagB scaH* and *S. aureus* SH1000 *atl sagB scaH* were each treated with 40 µg/mL methicillin, fixed at different time-points after antibiotic addition, labelled with NHS Ester 555 and imaged using SIM. Cell volume was calculated from measurements carried out in ImageJ on these images. P-values were calculated by two-tailed t-test with welsh's correction. Whiskers extend from the minimum to the maximum values and boxes from the 25<sup>th</sup> to the 75<sup>th</sup> percentile. The middle of the box is plotted at the median. The factor by which each strain increases in cell volume after 60 minutes of treatment with methicillin is presented in the table.

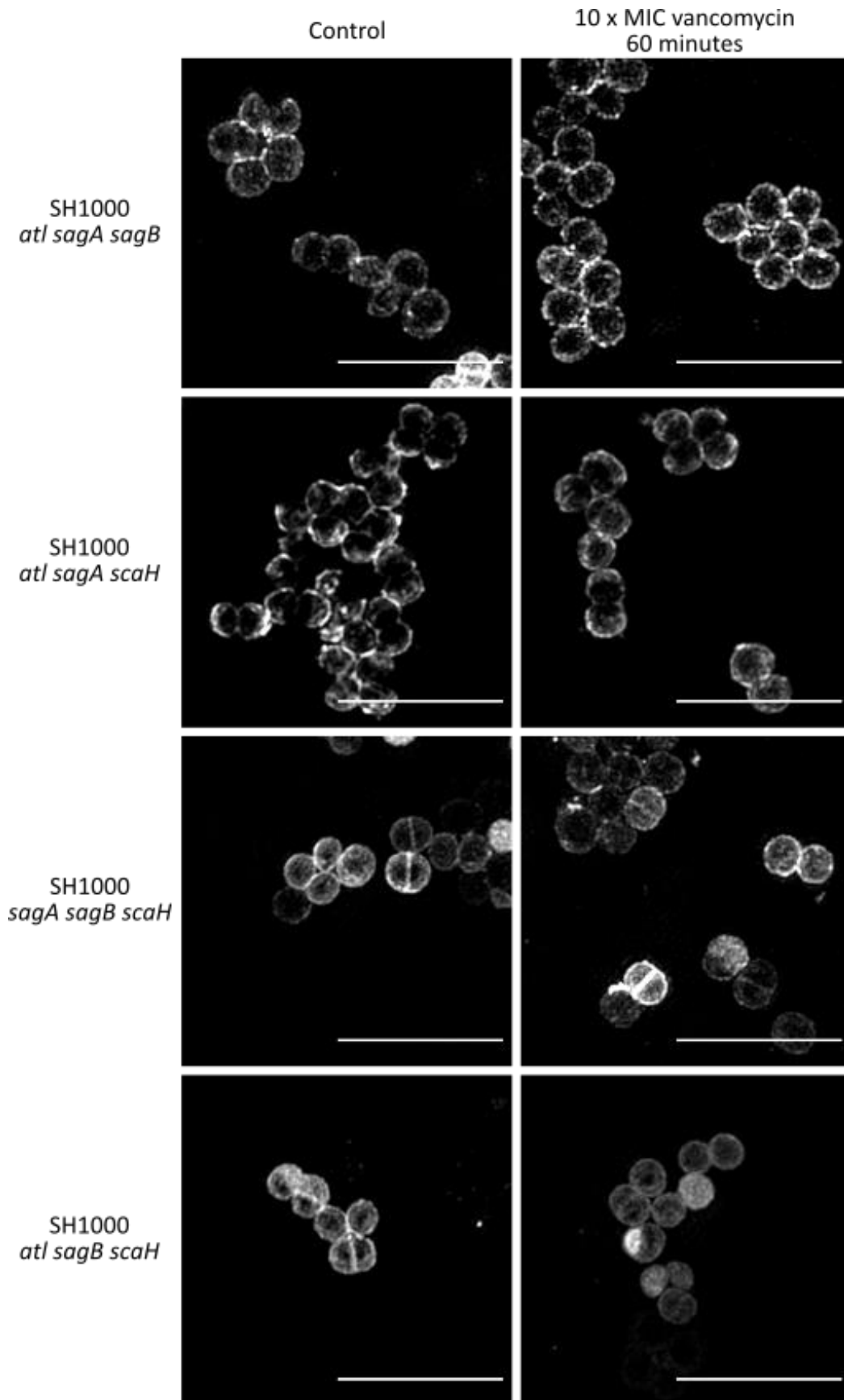
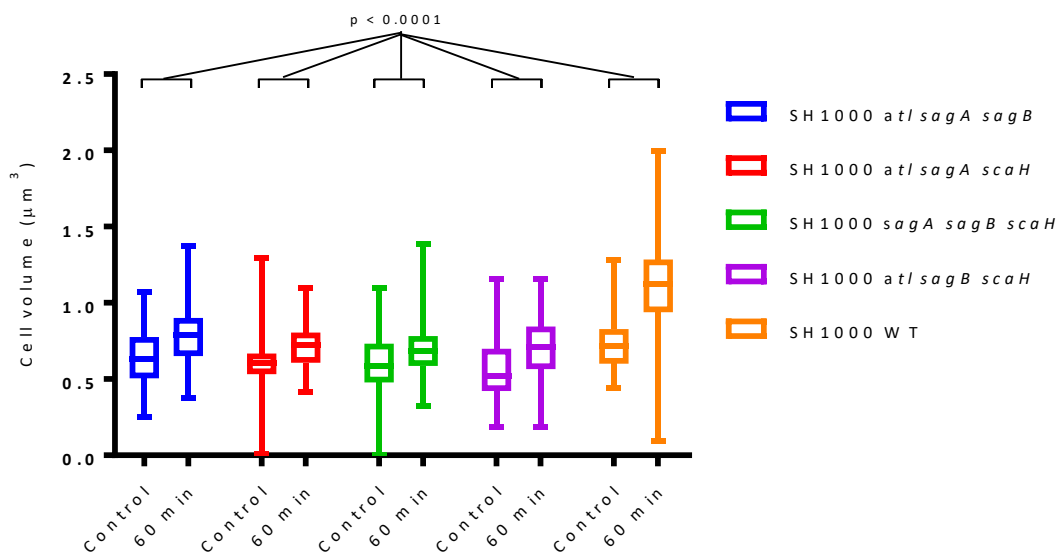


**Figure 5.8. Effect of vancomycin on triple glucosaminidase mutant cell morphology.** *S. aureus* SH1000 *atl sagA sagB*, *S. aureus* SH1000 *atl sagA scaH*, *S. aureus* SH1000 *sagA sagB scaH* and *S. aureus* SH1000 *atl sagB*

*scaH* were treated with 40 µg/mL vancomycin (10 x MIC), fixed after 0 & 60 minutes of treatment and subsequently labelled with NHS ester 555. Cells were imaged using the OMX SIM and maximum intensity projections are shown. All scale bars 5 µm. These images were acquired by Elizabeth Tatham.



Strain	SH1000 <i>atl sagA sagB</i>	SH1000 <i>atl sagA scaH</i>	SH1000 <i>sagA sagB scaH</i>	SH1000 <i>atl sagB scaH</i>	SH1000 WT
Size increase	x 1.2	x 1.2	x 1.2	x 1.2	x 1.5

**Figure 5.9. Effect of vancomycin on the cell volume of triple glucosaminidase mutants.** *S. aureus* SH1000 *atl sagA sagB*, *S. aureus* SH1000 *atl sagA scaH*, *S. aureus* SH1000 *sagA sagB scaH* and *S. aureus* SH1000 *atl sagB scaH* were each treated with 40 µg/mL vancomycin, fixed at different time-points after antibiotic addition, labelled with NHS Ester 555 and imaged using the OMX SIM. Cell volume was calculated from measurements carried out in ImageJ on these images. P-values were calculated by Mann-Whitney tests. Whiskers extend from the minimum to the maximum values and boxes from the 25<sup>th</sup> to the 75<sup>th</sup> percentile. The middle of the box is plotted at the median. Cell volume measurements were carried out by Elizabeth Tatham.

### 5.2.2. The role of wall teichoic acid in cell wall antibiotic killing of *S. aureus*

After 60 minutes of treatment with 40 µg/mL methicillin, amorphous exoplasmic material was observed in EM images of *S. aureus* SH1000 (Figure 3.5). This morphology could be due to wall teichoic acids being made but not being correctly incorporated into the cell wall. To investigate this possibility experiments were done using *S. aureus* SH1000 *tarO*, which lacks WTAs.

#### 5.2.2.1. Growth dynamics

The growth of *S. aureus* SH1000 *tarO* was compared to that of *S. aureus* SH1000. The culture was inoculated to an OD<sub>600</sub> of 0.05 from overnight cultures. OD<sub>600</sub> measurements were taken every hour for 6 hours. To measure the difference in growth, a growth rate was calculated for each strain using the following formula (Neidhardt et al., n.d.):

$$k = \frac{\ln(N1) - \ln(N0)}{t1 - t0}$$

N0 is the OD<sub>600</sub> value at the start of exponential growth (t0) and N1 is the OD<sub>600</sub> value at the end of exponential growth (t1).  $\frac{1}{k}$  gives the generation time, i.e. amount of time required for one doubling of the population.

Growth rate was calculated between 0.5 and 2 hours after inoculation of the culture. *S. aureus* SH1000 generation was 29.1 minutes and *S. aureus* SH1000 *tarO* had a generation time of 38.7 minutes. *S. aureus* SH1000 *tarO* grows slower than the wild-type (Figure 5.10).

#### 5.2.2.2. Killing dynamics

MICs were measured using a serial dilution method. Cultures were grown overnight in the presence of different concentrations of antibiotics. After 24 hours, the OD<sub>600</sub> of the cultures was measured and the MIC determined. The MIC of methicillin against *S. aureus* SH1000 *tarO* was 4 µg/mL, and the MIC of vancomycin against *S. aureus* SH1000 *tarO* was 4 µg/mL. These MICs were identical to the wild-type MICs.

The effect of methicillin and vancomycin on *S. aureus* SH1000 *tarO* viability was investigated by CFU/mL death curve. Cultures were inoculated to an OD<sub>600</sub> of 0.05 and grown to an OD<sub>600</sub> of 0.2-0.3 (early exponential), when the antibiotics were added. CFU/mL measurements were done every hour for 4 hours.

90% killing of *S. aureus* SH1000 *tarO* was achieved within one hour of addition of 40 µg/mL methicillin to the growth media, compared to after 3 hours in the wild-type (Figure 5.11). By 4 hours, 99.9% killing of *S. aureus* SH1000 *tarO* was achieved, compared to just over 90% killing of the wild-type. *S. aureus* SH1000 *tarO* dies significantly (unpaired t-test: p = 0.0222) faster than the wild-type by 4 hours when treated with 10 x MIC methicillin.

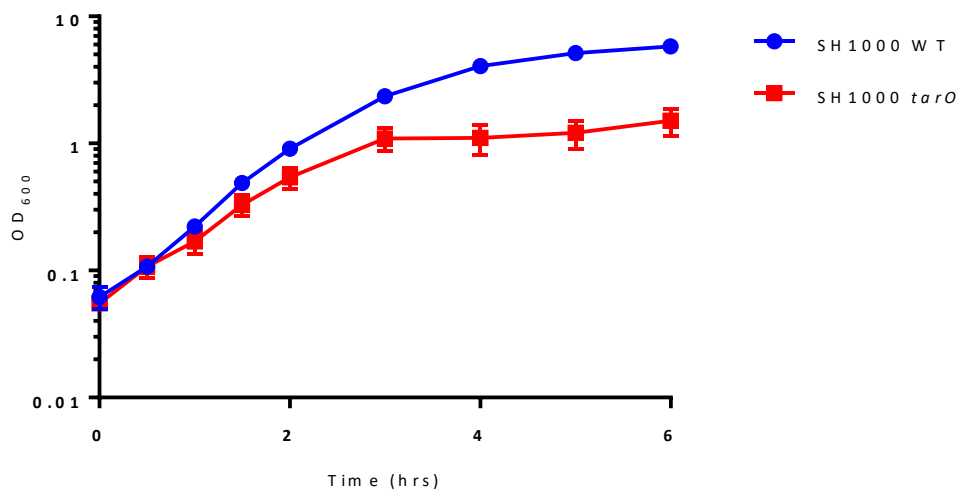


**Figure 5.10. Growth curve of *S. aureus* SH1000 *tarO* compared to the wild-type.** OD<sub>600</sub> measurements were carried out at different time-points. The mean and standard deviation are plotted. This experiment was done in triplicate.

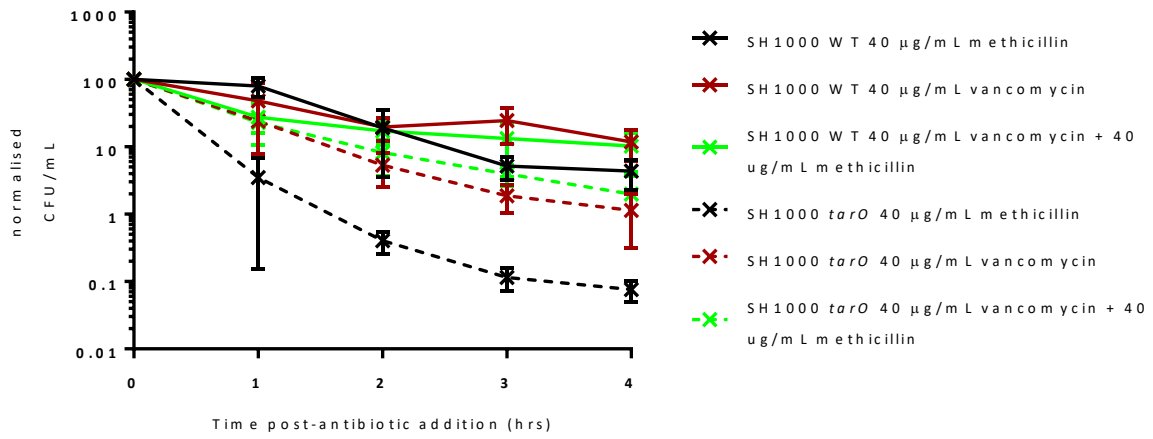


**Figure 5.11. Effect of methicillin and vancomycin on *S. aureus* SH1000 *tarO* cell viability.** *S. aureus* SH1000 *tarO* and *S. aureus* SH1000 WT were treated with 40 µg/mL methicillin (10 x MIC) or 40 µg/mL vancomycin (10 x MIC) or with both antibiotics. The CFU/mL was determined at each time-point and the data was normalised by setting the first time point as 100%. The mean and standard deviation are plotted. This experiment was done in triplicate.

When treated with 40 µg/mL vancomycin, 10% killing of *S. aureus* SH1000 *tarO* is achieved after 2 hours, compared to 4 hours for the wild-type. After 4 hours of treatment with vancomycin, *S. aureus* SH1000 *tarO* has died significantly faster (unpaired t-test:  $p = 0.0323$ ) than *S. aureus* SH1000.

*S. aureus* SH1000 *tarO* was then treated with 40 µg/mL methicillin and 40 µg/mL vancomycin. Both antibiotics were added at the same time. When treated with both antibiotics, killing of *S. aureus* SH1000 *tarO* is not significantly different (unpaired t-test:  $p = 0.4769$ ) to when the strain is treated with vancomycin on its own.

Killing of *S. aureus* SH1000 is similar when it is treated with methicillin alone, vancomycin alone and when it is treated with both antibiotics (Figure 5.11). Unpaired t-test were carried out on the different samples at 4 hours: methicillin vs. vancomycin ( $p = 0.0984$ ), vancomycin vs. vancomycin + methicillin ( $p = 0.7492$ ), methicillin vs. vancomycin + methicillin ( $p = 0.1800$ ).

#### 5.2.2.3. Cell morphology

*S. aureus* SH1000 *tarO* was treated with 10 x MIC vancomycin or 10 x MIC methicillin and fixed at 0 or 60 minutes post-treatment. The samples were labelled with NHS ester 555 and imaged using the OMX SIM. No large cell deformations were observed in the images after treatment with methicillin or vancomycin (Figure 5.12). However, NHS ester provides poor quality labelling of *S. aureus* SH1000 *tarO*. This is likely due to WTA making up a large proportion of the amines of the cell surface, which are the binding sites for NHS ester.

*S. aureus* SH1000 *tarO* cultures were treated with 40 µg/mL methicillin or 40 µg/mL vancomycin (10 x MIC) and fixed at 0 & 60 minutes post-treatment, before being imaged by EM. After 60 minutes of treatment with 10 x MIC methicillin, the sample contained a large amount of cell sacculi (Figure 5.13, panel A). Some cells exhibited similar morphologies to the wild-type treated with 10 x MIC methicillin. The cell membrane and the cell wall were separated by amorphous exoplasmic material (Figure 5.13, panel B). When this occurred around a newly forming septa, the septa maintained its pointed V-shaped morphology. After treatment with 10 x MIC vancomycin no such morphological changes were observed (Figure 5.13, panel C).

Four morphologies were identified in the EM images of the *S. aureus* SH1000 *tarO* samples: cells with no visible septum (no septum), cells with incomplete septa (incomplete septum), cells with a complete septum (complete septum), cells with an aberrant septum (aberrant septum) (Figure 5.14). In the control sample, 48.5% of the cells have no visible septum, 21% have a complete septum and 30.5% have an incomplete septum. After 60 minutes of treatment with 10 x MIC methicillin, 48% of the cells have no visible septum, 16% have complete septa, 22% have incomplete septum and 14% have aberrant septa. Aberrant septa are not found in the control or vancomycin treated sampled, only after 60 minutes of methicillin treatment. After 60 minutes of treatment with 10 x MIC vancomycin 57% of the cells have no visible septum, 20% have complete

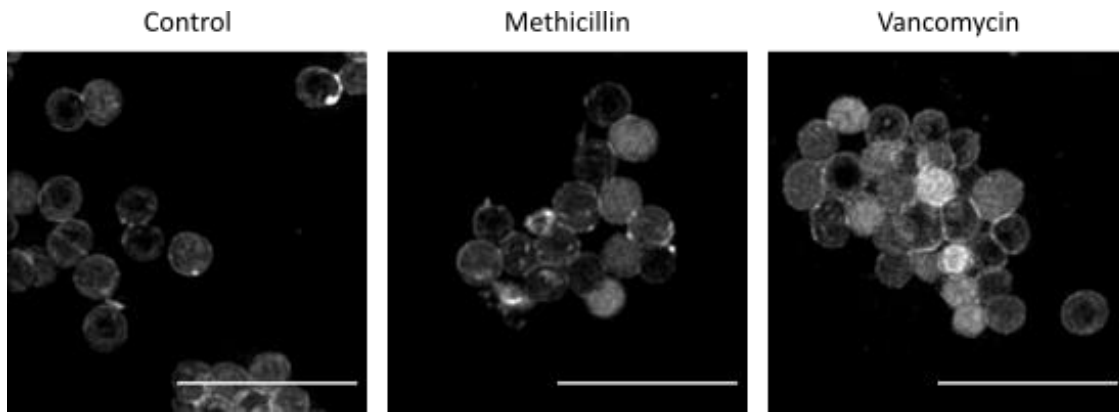
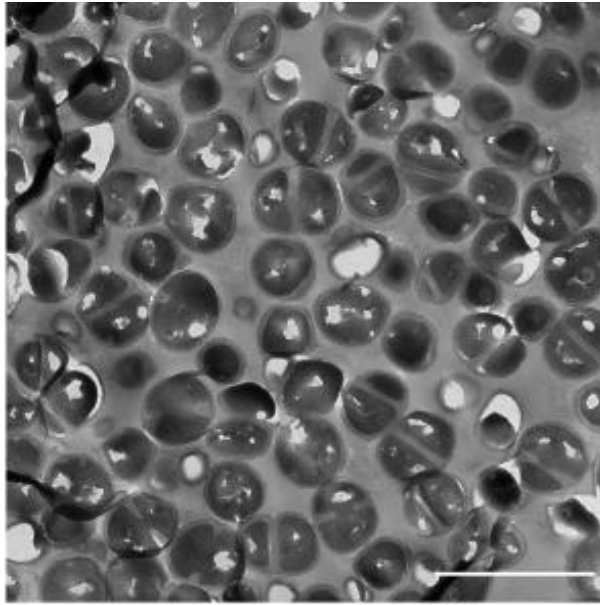


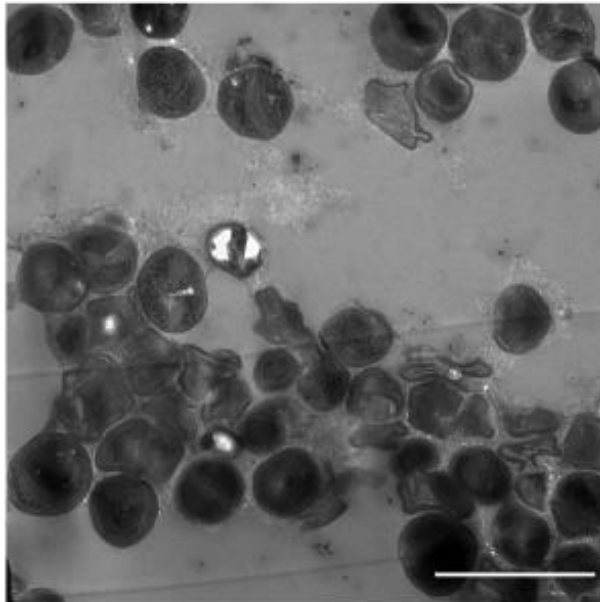
**Figure 5.12. Effect of methicillin and vancomycin on *S. aureus* SH1000 *tarO* cell morphology (SIM images).** *S. aureus* SH1000 *tarO* was treated with 40  $\mu\text{g}/\text{mL}$  methicillin or 40  $\mu\text{g}/\text{mL}$  vancomycin, fixed after 60 minutes of treatment, labelled with NHS ester 555 and imaged with the OMX SIM. Samples as indicated. Maximum intensity projections are shown. All scale bars 5  $\mu\text{m}$ .

A

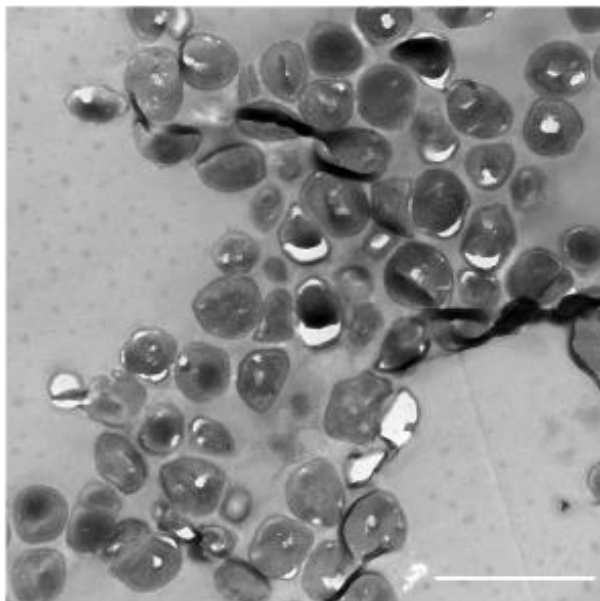
Control



Methicillin



Vancomycin



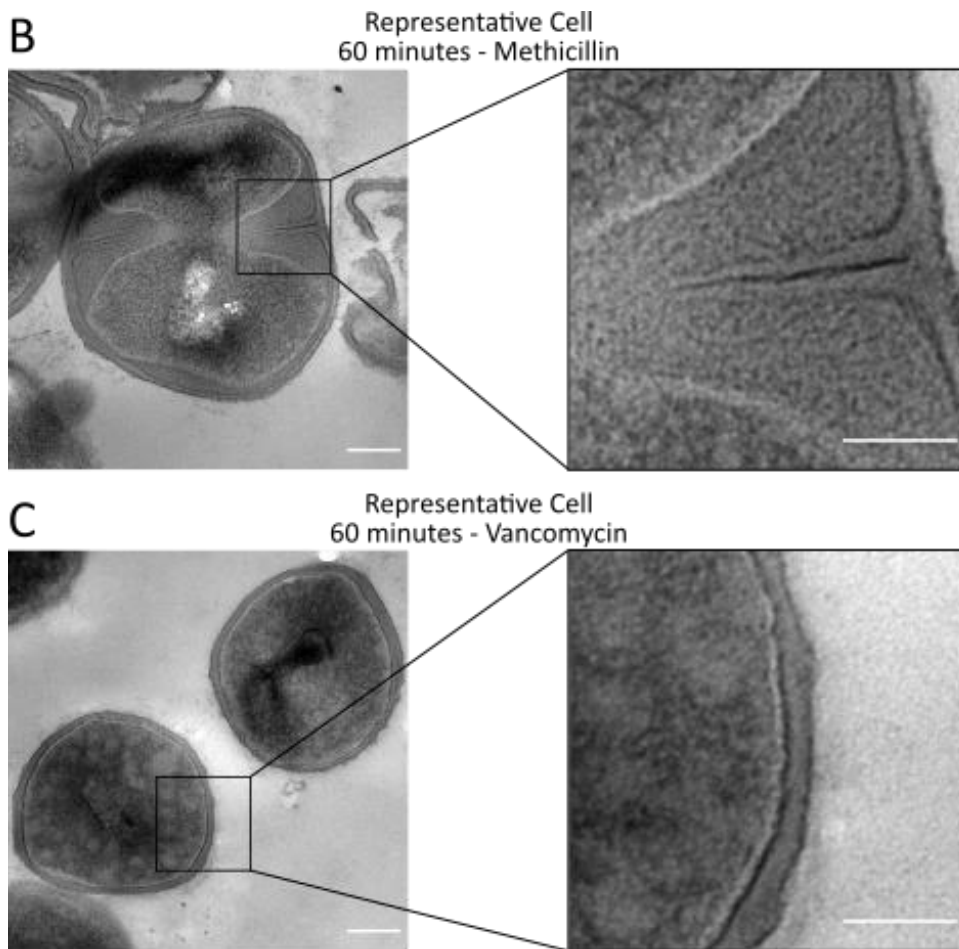


**Figure 5.13. Effect of methicillin and vancomycin on *S. aureus* SH1000 *tarO* cell morphology (EM images).** *S. aureus* SH1000 *tarO* was treated with 40  $\mu\text{g}/\text{mL}$  methicillin or 40  $\mu\text{g}/\text{mL}$  vancomycin, fixed at 0 and 60 minutes after antibiotic addition and imaged by EM. (A) Fields of cells from each sample. Samples as indicated. The methicillin and vancomycin samples were fixed after 60 minutes of treatment. Scale bars 2  $\mu\text{m}$ . (B) Representative cell after 60 minutes of methicillin treatment with 200 nm scale bar. Magnification of a cell section from a representative cell with 100 nm scale bar. (C) Representative cell after 60 minutes of vancomycin treatment with 200 nm scale bar. Magnification of a cell section from a representative cell with 100 nm scale bar.

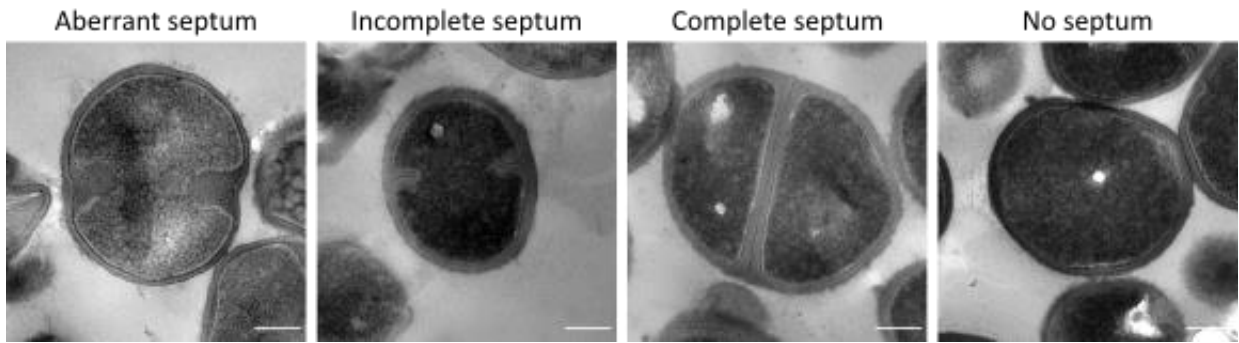
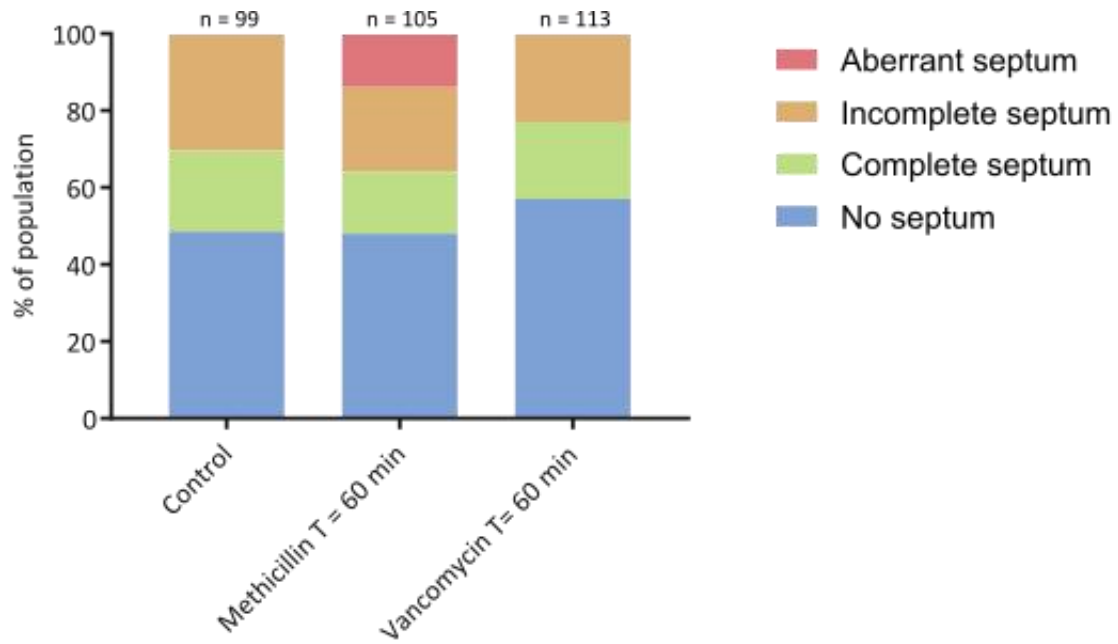


**Figure 5.14. Quantification of cell morphologies in EM images after treatment of *S. aureus* SH1000 *tarO* with methicillin or vancomycin.** *S. aureus* SH1000 *tarO* was treated with 40  $\mu\text{g}/\text{mL}$  methicillin or 40  $\mu\text{g}/\text{mL}$  vancomycin. Samples were fixed and imaged before treatment and 60 minutes after addition of the antibiotic. Four morphologies were identified in the EM images and the prevalence of each morphology was quantified in each sample. Quantification was carried out on a population of approx. 100 cells (n as indicated) for each sample.

septa and 23% have incomplete septa. 65% of methicillin-treated cells exhibited separation of the cell membrane from the cell wall compared to 1% of the cells in the control and vancomycin-treated samples.

#### 5.2.2.4. Fate of newly incorporated peptidoglycan

*S. aureus* SH1000 *tarO* cultures in early exponential phase ( $OD_{600}$  0.2-0.3) were incubated in the presence of ADA for 5 minutes before being washed and treated with 40  $\mu\text{g}/\text{mL}$  methicillin, treated with 40  $\mu\text{g}/\text{mL}$  vancomycin or not treated with any antibiotic. The cells were fixed 0, 30 & 60 minutes after they were resuspended in the presence or absence of antibiotic. After fixation, ADA was clicked with Atto 488 and the cells were labelled with WGA 594. Cells were labelled with WGA rather than NHS ester (used for the wild-type samples in previous chapters) because of the poor labelling of NHS ester in the absence of WTA on the cell surface (Figure 5.12). The samples were imaged using the OMX SIM (Figure 5.15). Six patterns of ADA incorporation were identified throughout the samples (Figure 5.16, panel A). The prevalence of each pattern was quantified for each time point. *S. aureus* SH1000 wild-type data was also included for comparison.

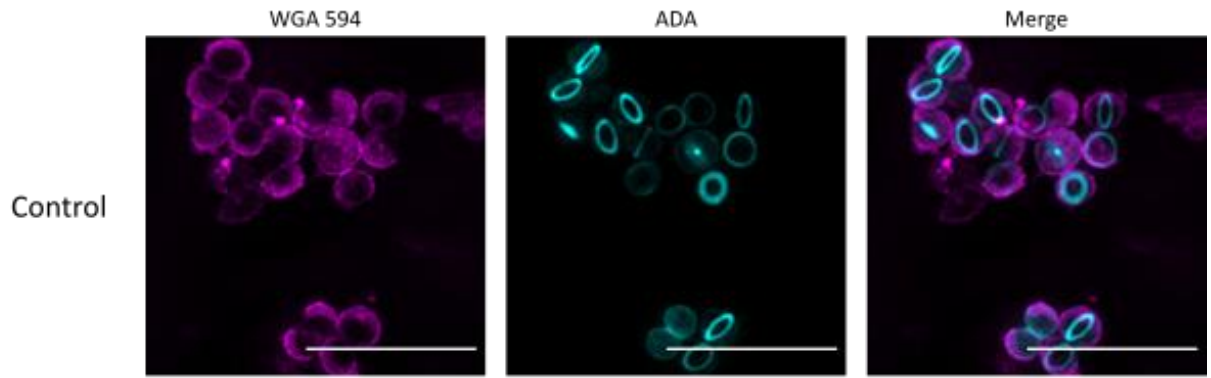
After 5 minutes of ADA incorporation, the newly incorporated material was located at the septum in 80% of the cells (Figure 5.15 & Figure 5.16). The remaining 20% of the cells displayed a split-punctate (4%) or whole cell morphology (16%).

In the untreated population, 30 minutes after ADA incorporation 43% of the population displayed a half-cell morphology, with the rest of the population displaying a range of morphologies (Figure 5.15 & Figure 5.16, panel B). No cells displayed a quarter cell morphology 30 minutes after incorporation. 60 minutes after ADA incorporation, 67% of the cell population displayed a quarter cell ADA pattern and the rest of the population was spread between half cell (13%), whole cell (10%), split punctate (8%) and split donut (1%) morphologies.

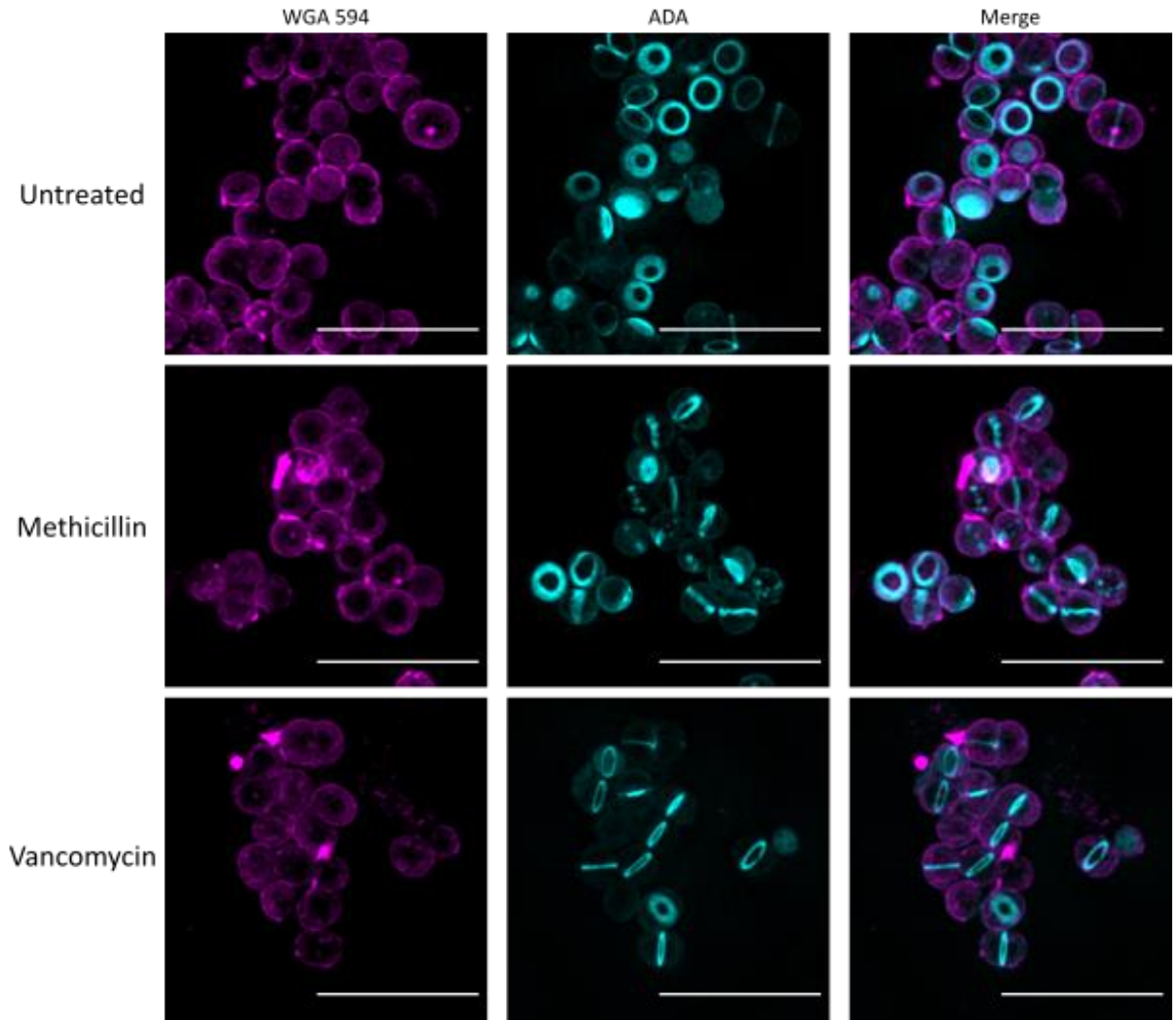
After 30 minutes of treatment with 40  $\mu\text{g}/\text{mL}$  methicillin, 66% of the *S. aureus* SH1000 *tarO* cell population displayed a "septum" ADA pattern (Figure 5.15 & Figure 5.16, panel C). The rest of the cell population displayed either split-punctate or whole cell patterns of ADA. This is a slight increase in the prevalence of split-punctate pattern and a decrease in the septum pattern compared to the control. After 60 minutes of methicillin treatment, the observed morphologies and their prevalence within the cell population were almost identical to the control. No cells display a split-donut, quarter or half-cell ADA pattern after 30 or 60 minutes of treatment with 10 x MIC methicillin (Figure 5.16, panel C).

30 minutes after *S. aureus* SH1000 *tarO* was treated with 40  $\mu\text{g}/\text{mL}$  vancomycin, half the population still displayed a septum ADA pattern. 30% of the cells displayed a whole cell ADA pattern and the remaining 20% showed a split-punctate morphology (Figure 5.16, panel D). No changes in ADA patterns were observed between 30- and 60-minutes post-treatment with 10 x MIC vancomycin.

5 minutes of ADA incorporation



30 minutes post-incorporation



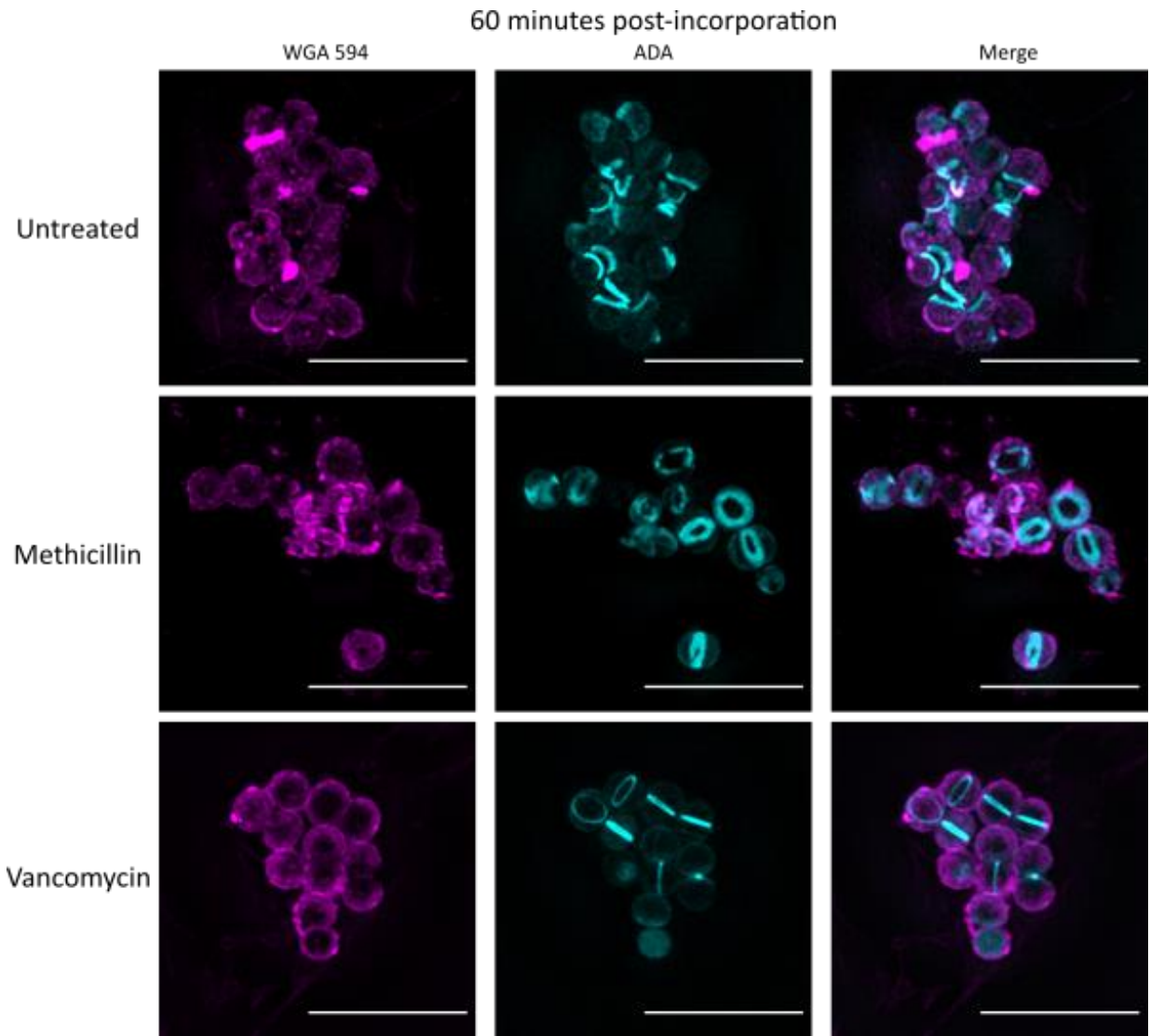


**Figure 5.15. Fate of newly synthesised peptidoglycan in *S. aureus* SH1000 *tarO* after methicillin or vancomycin treatment.** Cells were grown in the presence of ADA for 5 minutes before being washed and treated with 40  $\mu\text{g}/\text{mL}$  vancomycin or 40  $\mu\text{g}/\text{mL}$  methicillin or not. Cells were fixed at 0, 30 & 60 minutes after addition of the antibiotic or resuspension in fresh media. The incorporated ADA was clicked with Atto 488 and the cells were labelled with WGA 594. Fields of cells are presented for each time point and antibiotic as indicated. Maximum intensity projections are presented. All scale bars 5  $\mu\text{m}$ .

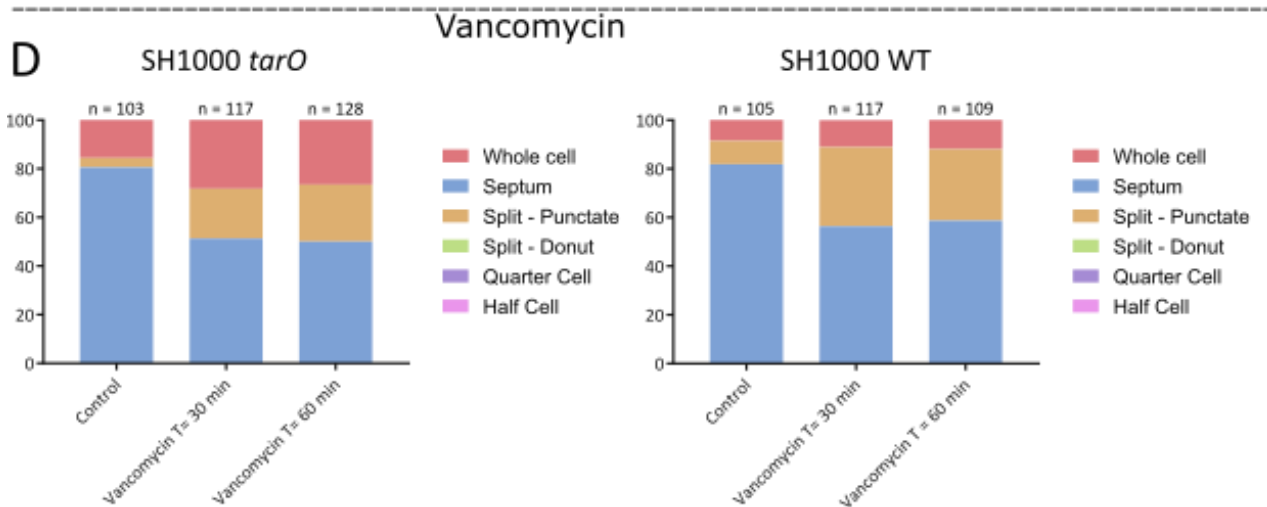
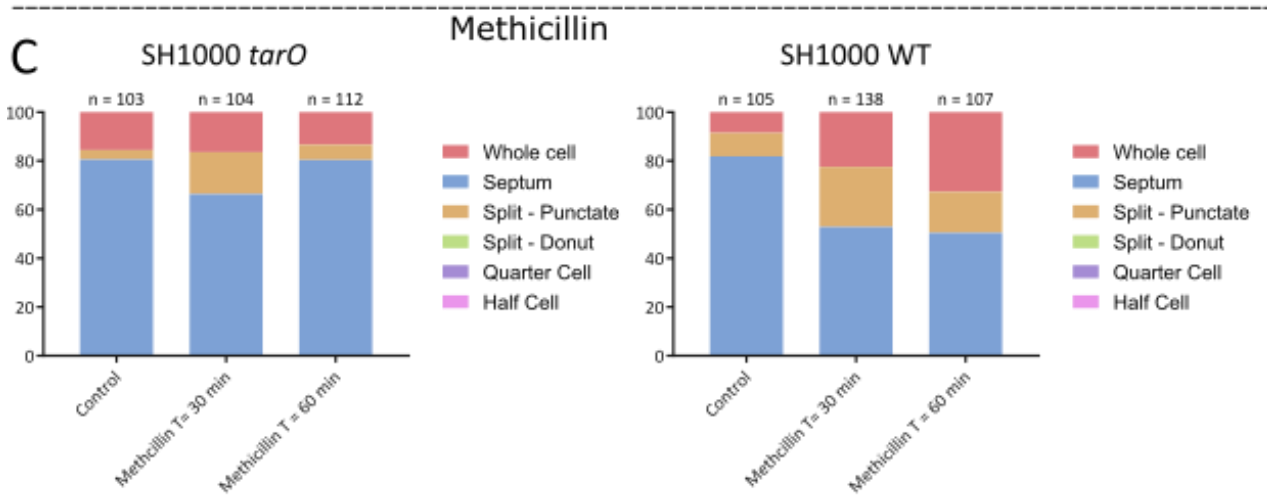
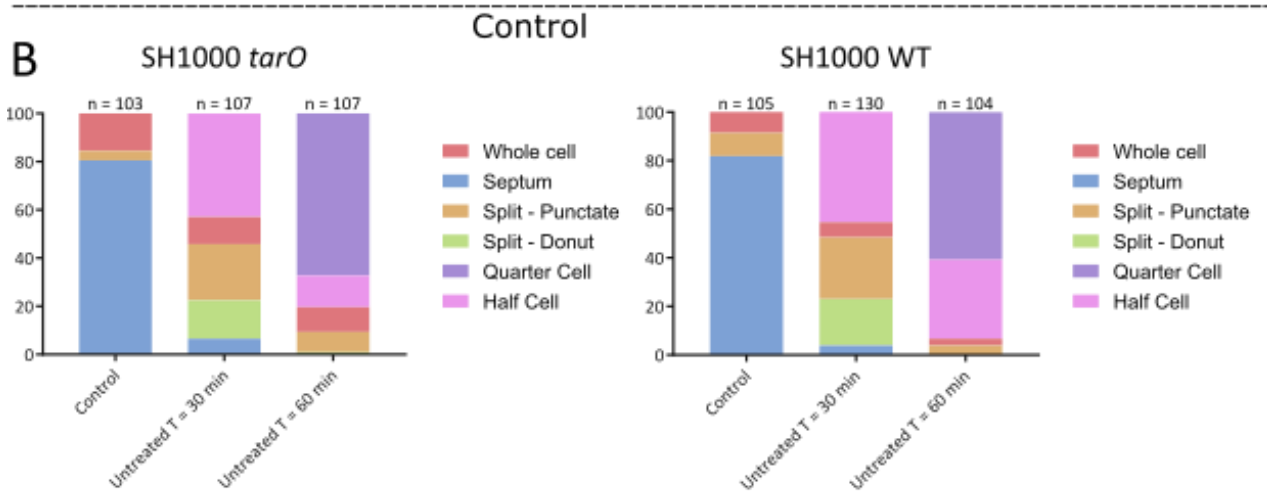
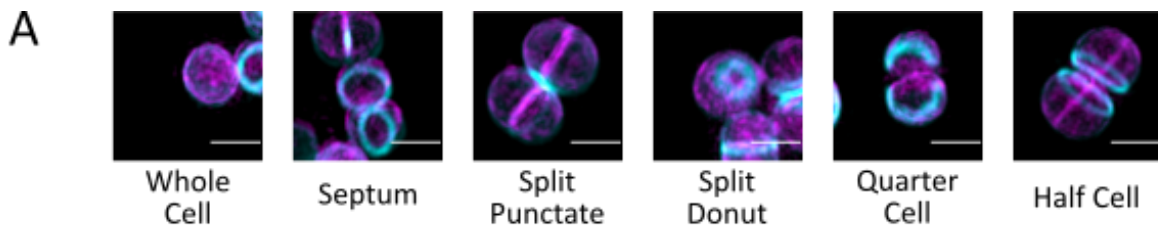


**Figure 5.16. Quantification of fate of newly synthesised material over 60 minutes.** Cells were grown in the presence of ADA for 5 minutes before being washed and resuspended in media without ADA or treated with 40 µg/mL methicillin or 40 µg/mL vancomycin. Cells were fixed 0, 30 & 60 minutes after resuspension. The incorporated ADA was clicked with Atto 488 and the cells were labelled with WGA 594. (A) Representative cells of each observed morphology. Maximum projection composite images are presented where cyan is ADA Clicked with Atto 488 and magenta is WGA 594. Scale bars 1 µm. (B) Quantification of fate of newly synthesised material over time in *S. aureus* SH1000 *tarO*. Wild-type data presented for comparison. (C) Quantification of fate of newly synthesised material over time in *S. aureus* SH1000 *tarO* after treatment with 10 x MIC methicillin. Wild-type data presented for comparison. (D) Quantification of fate of newly synthesised material over time in *S. aureus* SH1000 *tarO* after treatment with 10 x MIC vancomycin. Wild-type data presented for comparison.

### 5.3. Discussion

#### 5.3.1. The role of glucosaminidases in cell wall killing of *S. aureus*

The individual inactivation of each glucosaminidase encoding gene did not lead to significant changes in killing by vancomycin or methicillin. This indicates that none of the putative glucosaminidases in *S. aureus* SH1000 are single handedly responsible for the killing of *S. aureus* SH1000 by methicillin or vancomycin. When triple glucosaminidase mutants were tested, no significant decrease in killing was observed either. This suggests that as a class of hydrolases, glucosaminidases are not solely responsible for death after treatment with 10 x MIC methicillin or 10 x MIC vancomycin.

Cell volume increases significantly in all the single glucosaminidase mutants after treatment with 10 x MIC methicillin (Figure 5.5). However, the cell volume increases by a smaller factor in all the single glucosaminidase mutants than in the wild-type. The smallest increase in cell size was observed in *S. aureus* SH1000 *sagB*, with a size increase, after 60 minutes of methicillin treatment, of 1.4 x compared to 2.5 x in the wild-type (Figure 5.17). This suggests all the glucosaminidases function in the observed increase in cell size after treatment with methicillin but that SagB has the leading role. This is supported by previous research, which shows that glucosaminidases, in particular SagB, are responsible for cell growth (Wheeler et al., 2015). The same applies to the triple glucosaminidase mutants. *S. aureus* SH1000 *atl sagA scaH*, the strain still containing the *sagB* gene, shows a bigger increase in cell size than the three triple mutants lacking SagB. All of the other strains also show a slight decrease in the amount of cell size increase observed after methicillin treatment compared to the wild-type. This supports the idea that SagB plays the biggest role out of all four putative glucosaminidases in the increase in cell size observed after treatment of *S. aureus* SH1000 with 10 x MIC methicillin. Atl, ScaH and SagA also have a role but are responsible for a smaller part of the observed increase in cell size after treatment with methicillin.

After 60 minutes of treatment with vancomycin all the triple glucosaminidase mutants had increased in size less than the wild-type. All of the mutants increased in size by the same factor, suggesting that all four glucosaminidases play an equal role in the cell expansion observed after 60 minutes of vancomycin treatment.

These results indicate that cell size increase is not the main reason for cell death. However, cell wall hydrolysis may still play a major role in cell death. Other hydrolases, although not involved in swelling of the cell, may be involved in weakening the cell wall, eventually leading to mechanical failure. Although no decrease in killing by methicillin or vancomycin is observed in the single or triple glucosaminidase mutants, hydrolases could still have a function in beta-lactam killing. There are 19 known hydrolases in *S. aureus* giving the organisms a large amount of redundancy (Frankel et al., 2011; Pourmand et al., 2006; Ramadurai & Jayaswal, 1997; Stapleton et al., 2007; Wheeler, 2012; Wheeler et al., 2015).

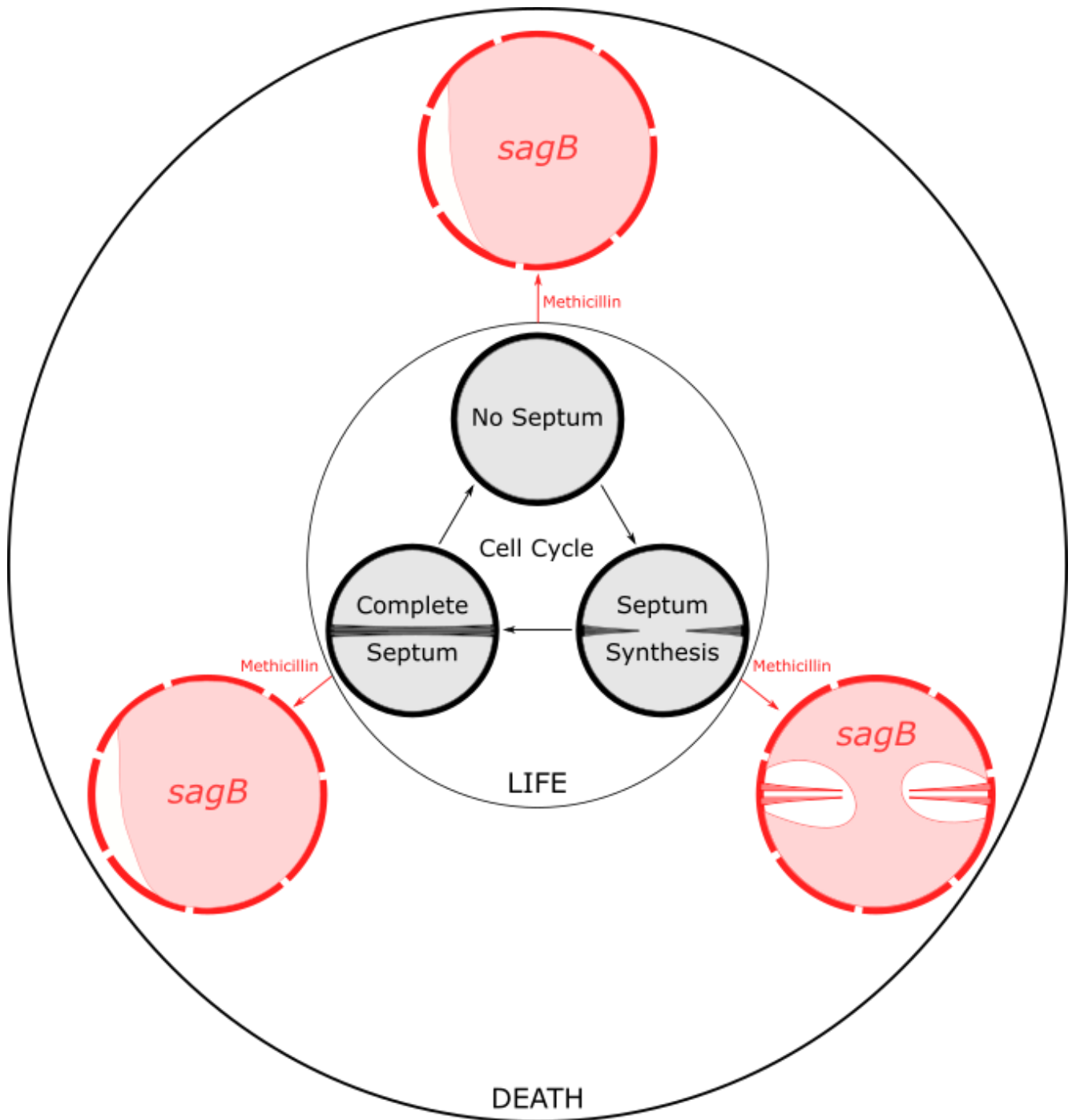


**Figure 5.17. Model of methicillin induced killing of *S. aureus* SH1000 *sagB*.** The “life” circle represents the three main morphologies differentiating different stages of the life cycle. The “death” circle represents morphological changes that occur after methicillin treatment and are thought to be involved in cell death. After treatment with 10 x MIC methicillin *S. aureus* SH1000 *sagB* cells increase in volume by a factor of 1.4. This increase is represented to scale in the diagram. Irrelevant of the stage of the cell cycle, many cells will have the cell membrane pulled away from the cell wall and their cell wall will be hydrolysed by the remaining hydrolases. Any complete or incomplete septum present are hydrolysed into their two component halves. If

the septum was complete, this produces two daughter cells. If the septum was incomplete, an incomplete split septum is observed after treatment with likely concomitant death.

### 5.3.2. The role of wall teichoic acid in the cell wall antibiotic killing of *S. aureus*

The MIC of vancomycin and methicillin are the same for *S. aureus* SH1000 and *S. aureus* SH1000 *tarO*, so any observed differences in killing cannot be attributed to a change in MIC.

The absence of wall teichoic acids leads to increased sensitivity of *S. aureus* to methicillin with 99.9% killing after 4 hours of treatment, compared to 90% killing in the wild-type (Figure 5.11). *S. aureus* SH1000 *tarO* also died faster after treatment with vancomycin, although the increase in killing rate between the mutant and the wild-type is less after vancomycin treatment than after methicillin treatment. Previous research has shown that modification or absence of WTAs can lead to increased sensitivity to autolysis. Two different mechanisms have been proposed to be involved: change in localisation of Atl and a decrease in peptidoglycan crosslinking (Atilano et al., 2010; Schlag et al., 2010). The difference in killing between *S. aureus* SH1000 and *S. aureus* SH1000 *tarO* after treatment with methicillin or vancomycin could be explained by increased sensitivity to cell wall hydrolysis.

Treatment of *S. aureus* SH1000 *tarO* with both methicillin and vancomycin gave a rate of killing the same as after treatment with just vancomycin. This suggests that vancomycin could be inhibiting the process that is leading to the accelerated killing of *S. aureus* SH1000 *tarO* by methicillin. As discussed above we know that two different processes could be leading to increased sensitivity to hydrolysis and therefore quicker killing. Previous studies have shown that vancomycin binds directly to Atl, inhibiting its activity (Eirich et al., 2011). Inhibition of Atl by vancomycin would help explain why treatment of *S. aureus* SH1000 *tarO* with both vancomycin and methicillin shows a slower rate of killing than methicillin on its own. If reduced crosslinking, mislocalisation of Atl and increased sensitivity to Atl are responsible for increase methicillin killing of *S. aureus* SH1000 *tarO*, inhibition of Atl by vancomycin would reduce the amount of killing.

The increased killing still observed after vancomycin or vancomycin and methicillin treatment of *S. aureus* SH1000 *tarO* compared to *S. aureus* SH1000 could be explained by increased sensitivity to other hydrolases in the cell due to the lack of WTA. Previous research shows that a lack of D-alanylation of WTA or absence of WTA have an effect on the activity of vancomycin and other antimicrobial peptides (Brown et al., 2012; Farha et al., 2013).

In EM images of methicillin-treated *S. aureus* SH1000 over 20% of cells showed an “incomplete split septum” morphology (Figure 3.6). These are incomplete septa that have been hydrolysed into their two component halves after methicillin treatment. It is possible that this hydrolysis was carried out by Atl, which is known to be one of the hydrolases involved in splitting of the mature septum during cell division (Foster, 1995). Only 2% of the cells in the wild-type sample show a complete septum or an incomplete septum that hasn't been split after 60 minutes of methicillin treatment. This is also likely due to the action of Atl and other cell division

hydrolases in the absence of peptidoglycan synthesis. In the EM images of *S. aureus* SH1000 *tarO* 16% of cells have a complete septum and 22% of the cells have an incomplete septum, which is not split (Figure 5.14). In *S. aureus* SH1000 only 1% of the cells have a complete septa after 60 minutes of methicillin treatment (Figure 3.6). This suggests there is significantly less hydrolysis of the septal plate after methicillin treatment in *S. aureus* SH1000 *tarO* compared to *S. aureus* SH1000. This supports the hypothesis that Atl is mislocalised in the absence of WTA and is therefore no longer splitting the septal plate correctly. In vancomycin the morphologies have not changed in the mutant compared to the wild-type. This is because Atl will be inhibited by direct binding of vancomycin irrelevant of whether WTA are present or not.

In the EM images of *S. aureus* SH1000 *tarO* the membrane pulled away from the cell wall in 65% of the cells after treatment with methicillin for 60 minutes compared to 17.4% of the cells in *S. aureus* SH1000. This suggests that this space is not filled with WTA as was hypothesised in chapter 3. Other teichoic acids, such as LTAs could be occupying this space, or it could simply be liquid filled space between the wall in the cell membrane after loss of turgor through leaking of the cytoplasm. The significant increase in the number of cells exhibiting this morphology after 60 minutes of treatment with methicillin in the cells lacking WTA compared to the wild-type is likely due to the increased rate of killing. *S. aureus* SH1000 *tarO* cells imaged after 60 minutes of methicillin treatment are likely to be further along in the killing process than *S. aureus* SH1000. Figure 5.18 summarises the above data in a model of antibiotic killing of *S. aureus* SH1000 *tarO*.

The fate of newly incorporated peptidoglycan was investigated in untreated, vancomycin-treated and methicillin-treated populations of *S. aureus* SH1000 *tarO* (Figure 5.16). To allow for easy comparison the equivalent *S. aureus* SH1000 data was included again in this chapter, it is first presented in Chapters 3 & 4.

In the untreated *S. aureus* SH1000 *tarO* sample, we see progression through the cell cycle with the appearance of the same patterns of ADA as were seen in the wild-type. The patterns are present at slightly different proportions, which is likely due to the slower growth rate of *S. aureus* SH1000 *tarO* compared to *S. aureus* SH1000 and possible changes to hydrolase activity.

After 60 minutes of methicillin treatment there is very little change in the observed patterns of ADA distribution across the cell compared to the control (before treatment). Approximately 80% of the cells still have the incorporated ADA at their septum, with the remaining cells either having just divided (split-punctate) or showing no distinct foci of ADA localisation (whole cell). After 60 minutes of treatment with 10 x MIC of methicillin *S. aureus* SH1000 showed an increase in the number of cells exhibiting a split punctate and whole cell pattern of ADA, suggesting that hydrolases were still allowing for cell division and hydrolysis of the incorporated material into a less distinct pattern. The absence of these changes in *S. aureus* SH1000 *tarO* corroborates the idea that wall teichoic acids play a role in the action of methicillin on *S. aureus*.

Treatment of *S. aureus* SH1000 *tarO* with 10 x MIC vancomycin led to results very similar to those seen after treatment of *S. aureus* SH1000 with vancomycin. In all the antibiotic treated samples we saw a halt in progression through the cell cycle, supporting what was observed in *S. aureus* SH1000. The difference between methicillin and vancomycin is likely due to the differences described earlier in this discussion. If mislocalisation of Atl through lack of WTA is the main reason for changes in the action of methicillin *S. aureus* SH1000 *tarO* vs. *S. aureus* SH1000, then the inhibition of Atl by vancomycin explains why the mutant and the wild-type behave in similar ways after treatment with vancomycin (Figure 5.18).

All of the above results suggest that there are two sets of hydrolases involved in killing – those that hydrolyse the entire cell wall and those that act on the septal plate, mainly Atl. After methicillin treatment, the action of both of these sets of hydrolases leads to killing. After treatment with vancomycin, the action of hydrolases active across the cell wall but not the hydrolases active at the septum leads to cell death.

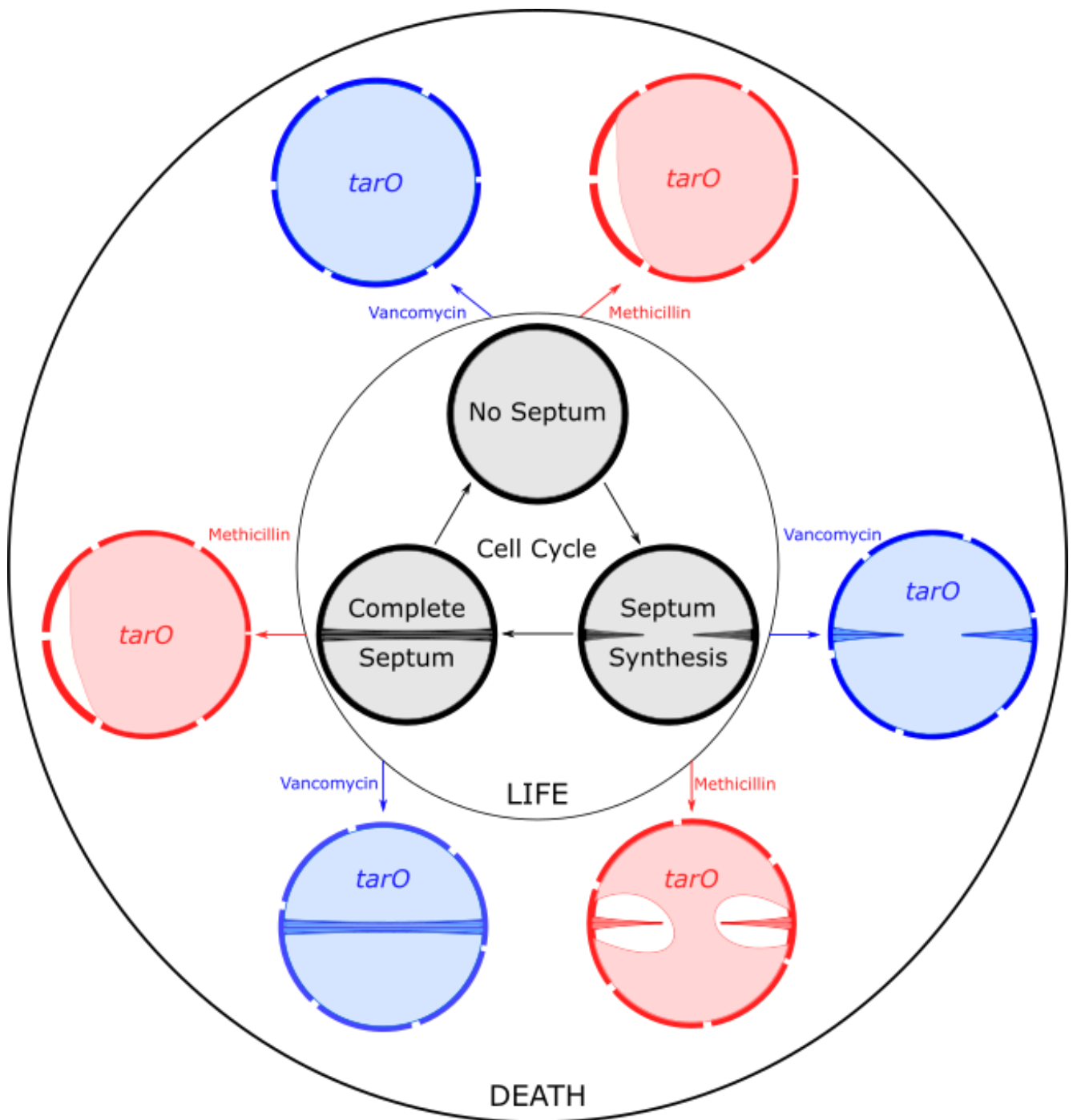


**Figure 5.18. Model of vancomycin and methicillin induced killing of *S. aureus* SH1000 *tarO*.** The “life” circle represents the three main morphologies differentiating different stages of the life cycle. The “death” circle represents morphological changes that occur after methicillin or vancomycin treatment and are thought to be involved in cell death. Cell volume of *S. aureus* SH1000 *tarO* was not quantified after antibiotic treatment, circle sizes are therefore not representative. After methicillin treatment, but not vancomycin treatment, the membrane appeared to have pulled away from the cell wall. In *S. aureus* SH1000 *tarO*, the complete and incomplete septa do not appear to have been hydrolysed into their two component halves. Treatment with vancomycin and methicillin simultaneously leads to the same effects as vancomycin treatment on its own.



## Chapter 6

### General Discussion

This project was set within a wider body of research that encompasses a broad range of specialist technologies and fields. These coalesce to give a deeper understanding of the action of cell wall antibiotics. Thus, to come to overall conclusions, it is important to contextualise the presented research.

#### 6.1. Associated data

The data presented in this section provides a brief overview of work carried out by other PhD students. Their data contributes to the model of cell wall antibiotic killing presented later in this discussion.

##### 6.1.1. The impact of cell wall antibiotics on peptidoglycan architecture

The work presented here was carried out by Laia Pasquina, PhD student, University of Sheffield.

Recent high resolution AFM has shed light on the structure of the *S. aureus* cell wall (Pasquina-Lemonche et al., n.d.; Turner et al., 2010). The ring and knobby structures on the outside of the cell and the smooth interior of the cell wall were described. The presented data suggests that hydrolases play a role in the action of cell wall antibiotics. AFM is therefore an interesting tool to investigate potential changes to cell wall architecture after treatment.

AFM was used after treatment of *S. aureus* with 40 µg/mL (10 x MIC) methicillin or vancomycin. Samples were grown and treated with methicillin or vancomycin using the same protocol as for the other imaging experiments presented in this thesis. Samples were collected at different times before and after antibiotic addition and boiled. Cells were then broken by FastPrep, and the sacculi were stripped of all teichoic acids using hydrofluoric acid (HF). To remove all proteins from the sacculi, SDS, DTT and pronase were used. The sacculi were then imaged in air and in liquid using AFM.

Cell wall thickness was measured in control samples and after 60 minutes of antibiotic treatment. This data was acquired by imaging in air. A significant decrease in cell wall thickness was observed after treatment with vancomycin or methicillin (Figure 6.1). This thinning could be explained by the lack of peptidoglycan incorporation coupled with continued autolysis activity. The existing cell wall material gets thinner as it is hydrolysed and the cells increase in size after antibiotic treatment without additional synthesis. The thinning is more pronounced after methicillin treatment, which could explain the fact that cells have increased in size more after 60 minutes of methicillin treatment (2.5 x) than after 60 minutes of vancomycin treatment (1.7 x).

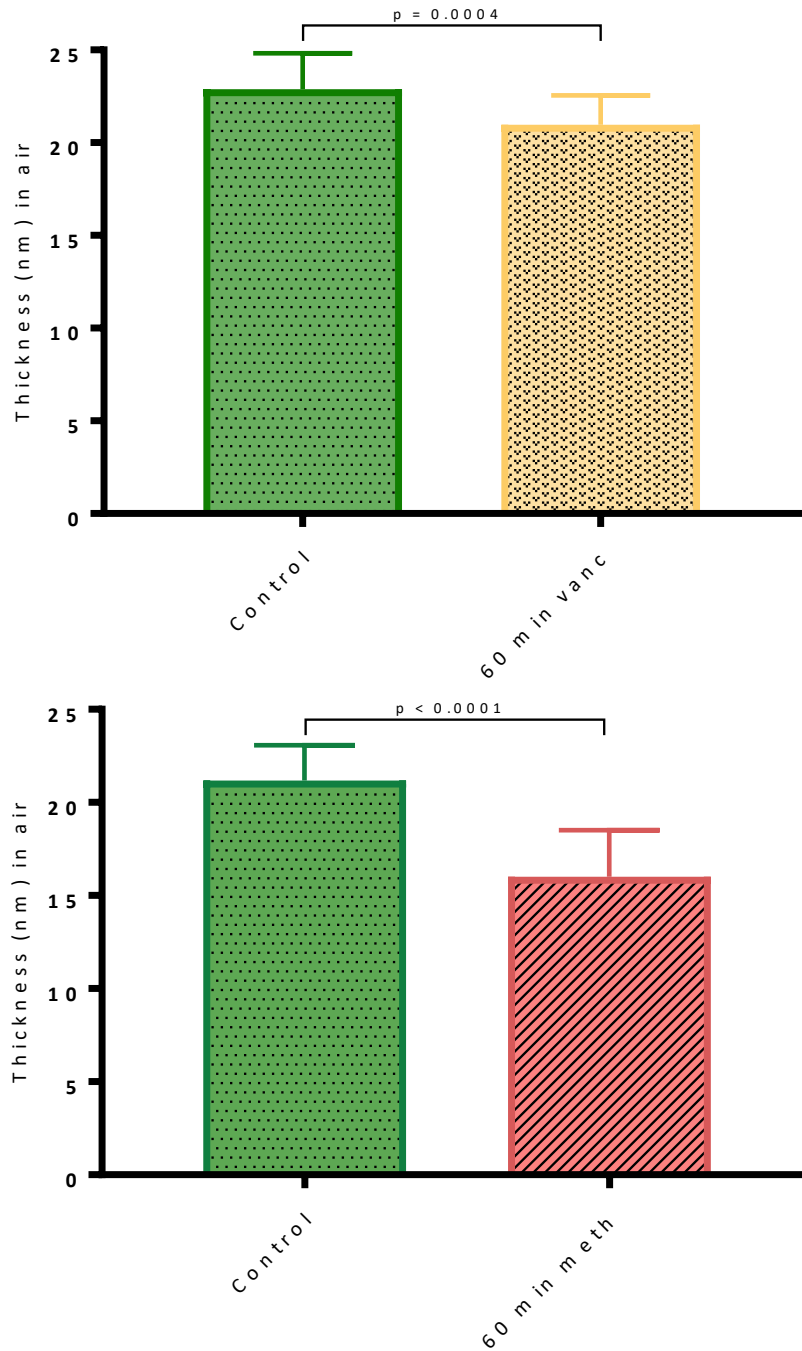


**Figure 6.1. Changes to cell wall thickness after treatment with methicillin (meth) or vancomycin (vanc).** Mean and standard deviation are plotted. P-values were calculated by unpaired t-test. N = 28. Data acquired and analysed by Laia Pasquina.

The inside of the sacculi were imaged in liquid and the number of pores/ $\mu\text{m}^2$  was quantified. A pore in the sacculi was counted as such if it crossed the entire depth of the peptidoglycan cell wall. A significant increase in the number of holes on the inside of sacculi was observed after 60 minutes of methicillin or vancomycin treatment (Figure 6.2). This suggests peptidoglycan hydrolase activity on the inside of the cell surface. Cell death may be due to holes developing such that cell membrane integrity can no longer be maintained leading to cytoplasmic leakage.

#### 6.1.2. Role of WalkR in cell wall antibiotic killing of *S. aureus*

The data in this section was acquired by Lingyuan Kong, PhD Student, Xiamen University.

The WalkR two-component signalling system is essential in *S. aureus*. A conditional mutant with an IPTG-inducible *walkR* operon was used for this study. WalkR regulates nine putative cell wall hydrolases in *S. aureus* (Dubrac et al., 2007). In the presence of IPTG, the strain grows in the same way as the wild-type *S. aureus* SH1000. In the absence of IPTG, the mutant dies due to the absence of normal levels of peptidoglycan hydrolysis (Delaune et al., 2011).

In the absence of IPTG, the strain lacking WalkR died faster than the wild-type strain treated with methicillin or vancomycin. Treatment with methicillin or vancomycin significantly decreased the amount of death observed 3 hours after removal of IPTG in *S. aureus* SH1000 *walkR* (Figure 6.3 & Figure 6.4). This rescue could be explained by the inhibition of peptidoglycan synthesis by the antibiotics, correcting the imbalance between peptidoglycan synthesis and hydrolysis in the absence of the WalkR system. This supports the idea that treatment with methicillin or vancomycin changes the balance between peptidoglycan synthesis and hydrolysis (Table 6.1).

## 6.2. Beta-lactams vs. vancomycin: similarities and differences

$^{14}\text{C}$ -GlcNAc incorporation reaches baseline levels after 5 minutes of treatment with vancomycin, compared to significant amounts of residual incorporation after an hour of treatment with methicillin (Figure 3.11 & Figure 4.8). The decrease in incorporation of FDAA is similar within the first 30 minutes after treatment with both antibiotics (Figure 3.9 & Figure 4.6). This suggests both antibiotics may have a different effect on transglycosylation but a similar impact on transpeptidase activity.  $\beta$ -lactams bind PBPs, but Mgt, SgtA, FtsW & RodA have been shown to have transglycosylase activity (Emami et al., 2017; Reed et al., 2011; Taguchi et al., 2019). These are not currently known to be inhibited by beta-lactams and may therefore still be active and explain the residual  $^{14}\text{C}$ -GlcNAc incorporation. Vancomycin binds both the peptidoglycan precursors and product, and therefore is likely to hinder any transglycosylase activity as soon as it has bound the D-Ala-D-Ala terminus of the peptide side chain. The problem with this hypothesis is that FDAAs would still be incorporated

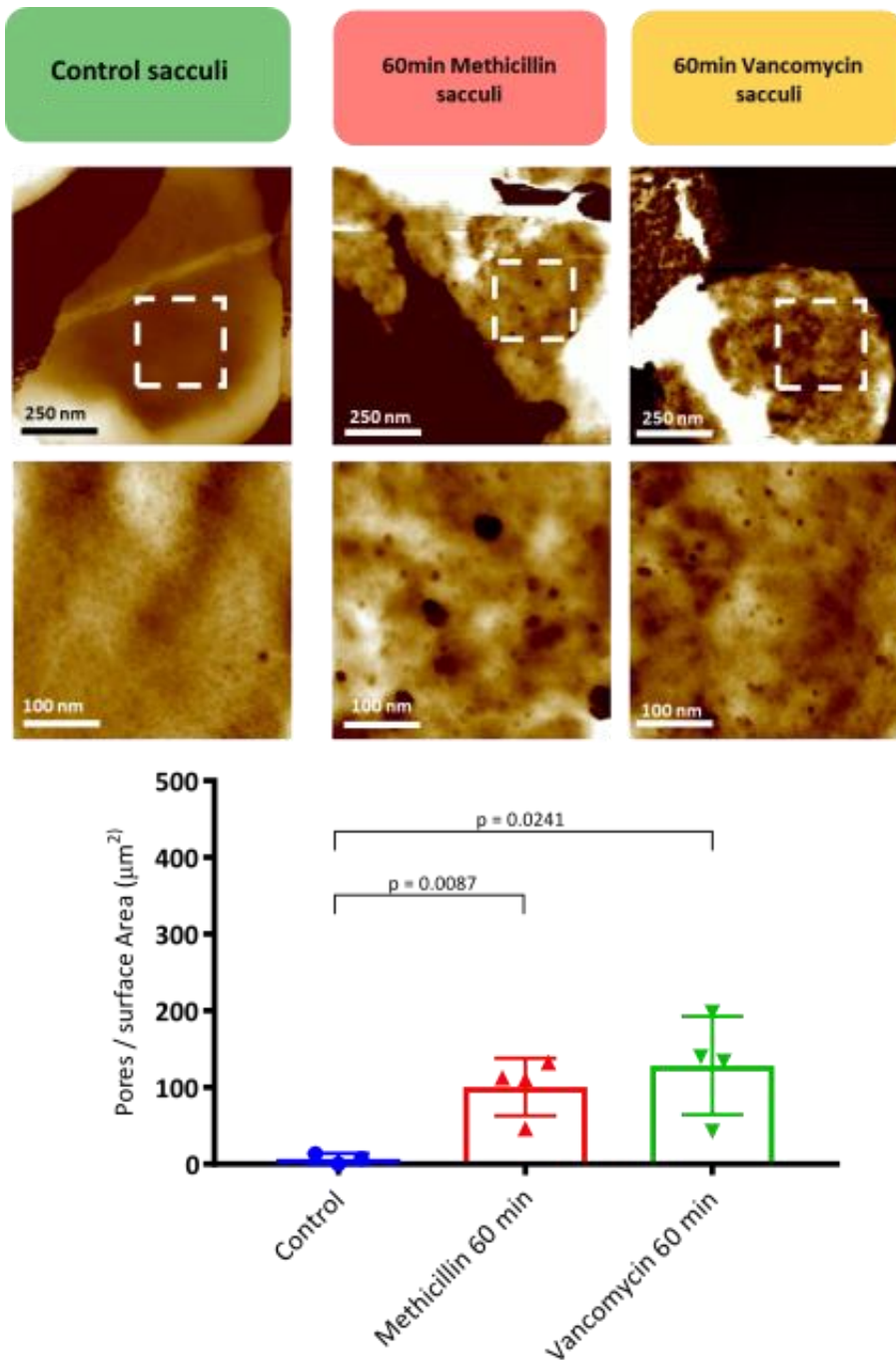


**Figure 6.2. Effect of methicillin and vancomycin on the number of pores present on the inside surface of sacculi.** AFM images of the inside of sacculi. The number of pores/µm<sup>2</sup> was quantified for 4 sections of sacculi per sample. Mean, standard deviation and individual sample values are plotted. P-values were calculated by unpaired t-test. Data acquired and analysed by Laia Pasquina.

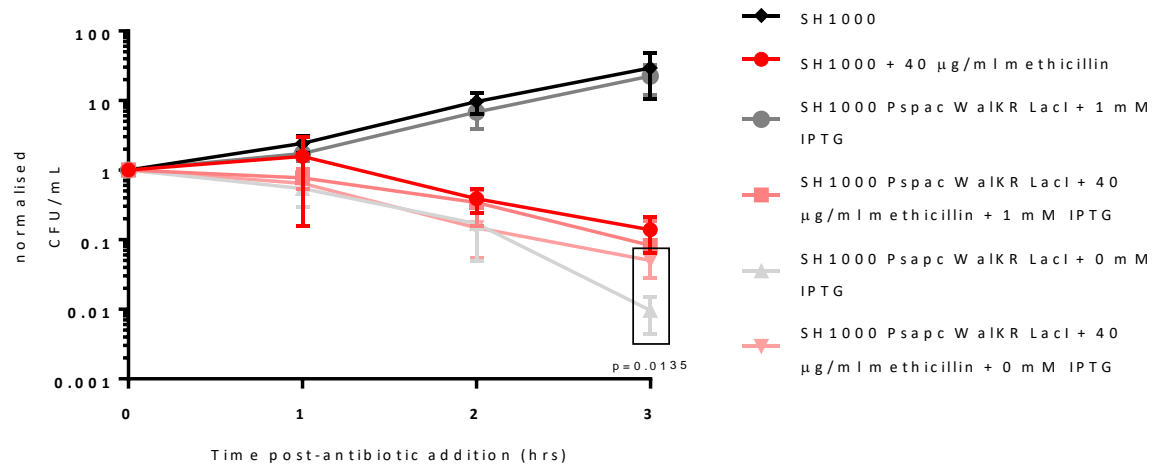


**Figure 6.3. Effect of methicillin treatment on *S. aureus* SH1000 *walkR* viability in the presence and absence of IPTG.** The initial data point was set to 1 to normalise the data. The experiment was done in triplicate. Mean and standard deviation are plotted. P-value calculated by unpaired t-test comparing the two 0mM IPTG samples. Data was acquired and analysed by Lingyuan Kong.

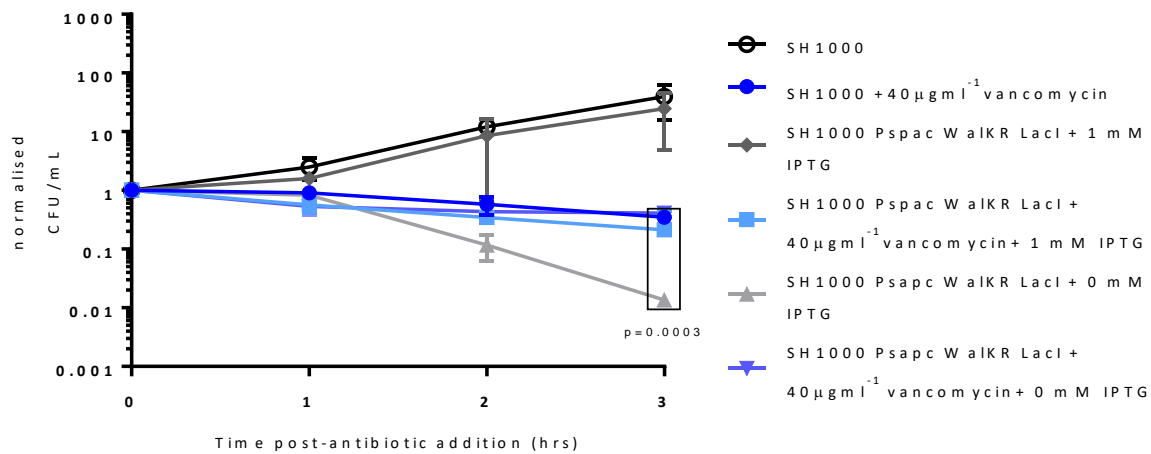


**Figure 6.4. Effect of vancomycin on *S. aureus* SH1000 *walkR* viability in the presence of absence of IPTG.** The initial data point for each sample was set to 1 to normalise the data. The experiment was done in triplicate. Mean and standard deviation are plotted. The p-value was calculated by unpaired t-test comparing the two 0mM IPTG samples. Data acquired and analysed by Lingyuan Kong.

	Synthesis	Hydrolysis	Life/Death
<i>S. aureus</i> SH1000	+	+	LIFE
<i>S. aureus</i> SH1000 + cell wall antibiotics	-	+	DEATH
<i>S. aureus</i> SH1000 <i>walkR</i> (no IPTG)	+	-	DEATH
<i>S. aureus</i> SH1000 <i>walkR</i> (no IPTG) + cell wall antibiotics	-	-	Stasis

Table 6.1. Synthesis and hydrolysis requirements for *S. aureus* survival.

if glycan chains were being synthesised but not crosslinked, as they are present on lipid II. Only residual  $^{14}\text{C}$ -GlcNAc and no residual FDAA incorporation are observed after 30 minutes of methicillin treatment. Another possibility is that vancomycin inhibits a different cellular process that requires GlcNAc and is not inhibited by methicillin treatment. GlcNAc is utilised in the first step of WTA synthesis and vancomycin has been shown to inhibit WTA synthesis in *S. aureus* (Singh et al., 2017).  $^{14}\text{C}$ -GlcNAc incorporation studies in a mutant lacking WTA (*S. aureus* SH1000 *tarO*) would show whether WTA synthesis is responsible for the observed residual incorporation after methicillin treatment.

After treatment with methicillin an amorphous exoplasmic material appears in between the peptidoglycan and the lipid bilayer in some cells (Figure 3.5). No such material is observed after treatment with vancomycin (Figure 4.4). This difference in the EM morphologies, also explains the difference between the NHS ester labelled images. After treatment with methicillin, cells with deformed septa are observed in the SIM images of NHS ester labelled *S. aureus* SH1000 (Figure 3.3). This is likely due to the NHS ester binding to and labelling the amorphous exoplasmic material or being “trapped” in between the cell membrane and cell wall, if this is simply empty space due to the cell membrane pulling away from the cell wall. After vancomycin treatment, such deformations are not observed in the SIM images of NHS ester labelled cells, which agrees with the differences observed by EM (Figure 4.2). As the nature of the amorphous exoplasmic material has not yet been identified, we cannot draw conclusions from this observation, but it may simply be a space created by plasmolysis due to loss of turgor.

Quantification of cell morphologies after EM treatment revealed a difference in morphologies after 60 minutes of vancomycin or methicillin treatment. After 60 minutes of methicillin treatment only 1% of cells had a complete septum compared to 17% of the cells 60 minutes after vancomycin treatment (Figure 3.6). This difference suggests that cells with complete septa are still splitting into two daughter cells after methicillin but not vancomycin treatment. Atl is known to be amongst the main hydrolases involved in cell division and is known to be inhibited by vancomycin (Eirich et al., 2011). Inhibition of Atl after vancomycin but not methicillin is a possible explanation for the observed differences. This could also explain the difference in kill curve shape (Figure 3.1 & Figure 4.1). After  $\beta$ -lactam treatment there is a small increase in CFU/mL, which is not observed after vancomycin treatment. The increase is potentially due to cells with complete septa dividing into two daughter cells.

The investigation into the fate of newly incorporated peptidoglycan after antibiotic treatment revealed that progression through the cell cycle was halted after both vancomycin and methicillin treatment (3.2.4.2 & 4.2.4).

Cells increased in volume by a factor of 2.5 after 60 minutes of methicillin treatment and only a factor of 1.7 after 60 minutes of vancomycin treatment (3.2.2.1 & 4.2.2). The inhibition of Atl by vancomycin may also be

involved in this observed difference between the two drugs. Although Atl is active at the septum, it also carries out hydrolysis across the whole cell wall (Foster, 1995). This could also be due to inhibition of WTA synthesis after vancomycin treatment, leading to irregularities in WTA content in the cell wall after vancomycin treatment (Singh et al., 2017). There is also the intriguing possibility of unidentified interactions between vancomycin and other cell wall hydrolases.

### 6.3. Model of beta-lactam and vancomycin killing of *S. aureus*

We propose that  $\beta$ -lactam and vancomycin killing of *S. aureus* is achieved through similar mechanisms, with some important differences (Figure 6.5). Although different cell wall antibiotic classes affect the same cellular processes, our results have shown that there are differences in the run up to cell death after treatment with the two different drug classes.

After  $\beta$ -lactam treatment, hydrolases that act across the cell wall and those at the septum are digesting the cell wall. The action of these hydrolases coupled with the lack of peptidoglycan synthesis leads to weakening of the cell wall and presumptive cell division with unfinished septa. Both are proposed to lead to cell death. The appearance of holes, of increasing number and size, in the cell wall is thought to eventually lead to an inability of the membrane to maintain turgor and cytoplasmic leakage with concomitant cell death.

After vancomycin treatment evidence suggests that Atl action is inhibited. This inhibition is likely due to binding of vancomycin to the peptidoglycan and direct binding to and inhibition of Atl. The smaller number of hydrolases acting on the cell wall, after treatment with vancomycin compared to methicillin, explains the smaller increase in cell size observed. After vancomycin treatment the eventual formation of pores in the cell wall leads to cell death through cytoplasmic leakage.

This model suggests that cell wall antibiotics kill through a simple imbalance between peptidoglycan synthesis and hydrolysis (Table 6.1). This model is also supported by the fact that cell wall antibiotics are not active against stationary phase cells and that hydrolase activity has been shown to be reduced during stationary phase (Lioliou et al., 2016). The exact manifestation of the imbalance between synthesis and hydrolysis is altered after treatment with different cell wall antibiotics (Figure 6.5).

This model is further supported by evidence that increased hydrolase activity leads to increased sensitivity to  $\beta$ -lactams (Rice et al., 2003). In the case of vancomycin, VISA strains have been shown to have decreased autolysis activity, decreasing the number of hydrolases at work and slowing down the killing process (Cameron et al., 2016).

#### 6.3.1. Comparison to previous models

Giesbrecht proposed that after treatment with penicillin (a  $\beta$ -lactam) cells completed their current division

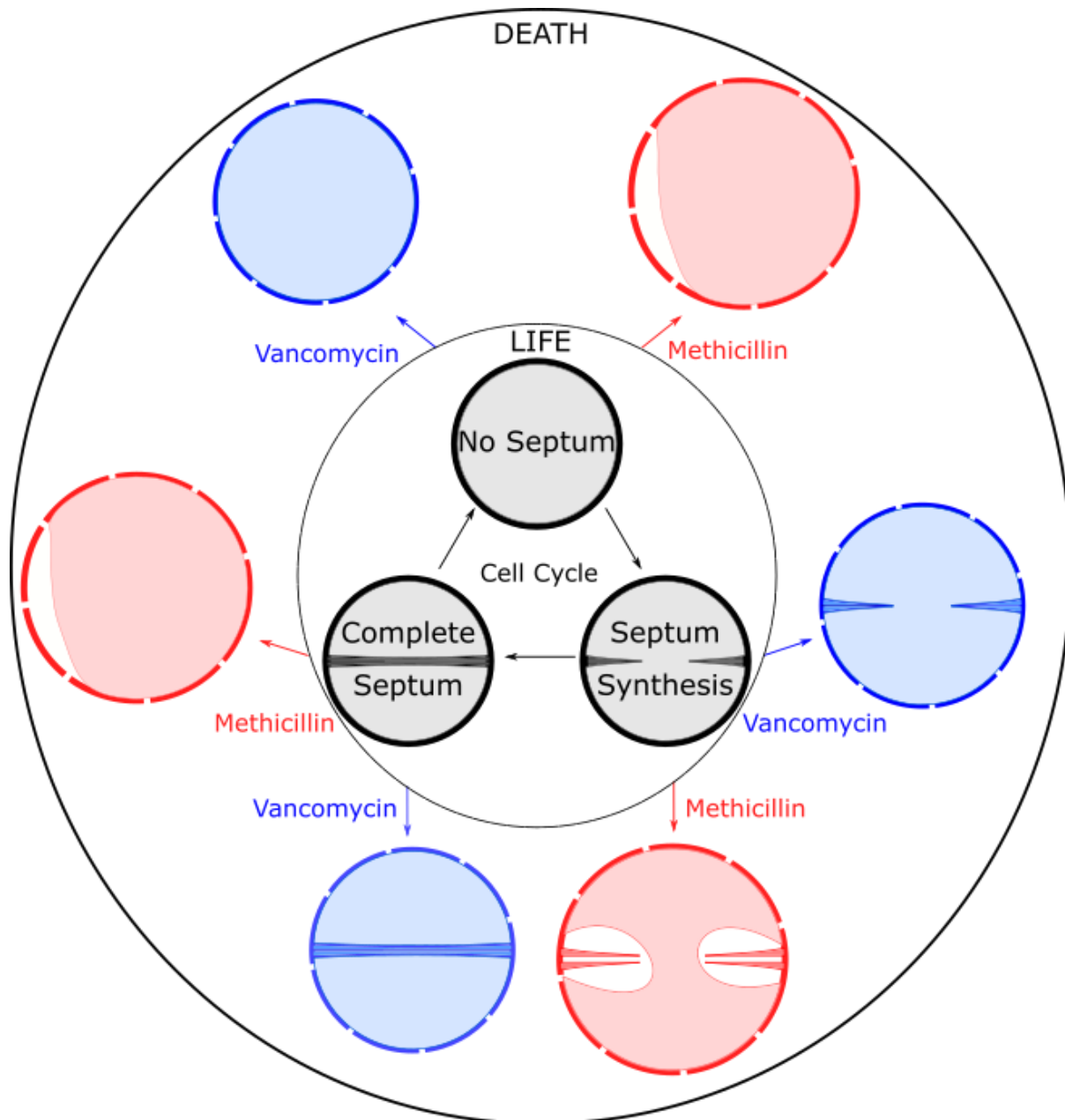


**Figure 6.5. Model of the effect of methicillin and vancomycin treatment on *S. aureus* SH1000.** The “life” circle represents the three main morphologies cells transition through as they go through the cell cycle. The “death” circle represents the changes to cell morphology observed after treatment with methicillin (red) or vancomycin (blue), depending on which stage of the cell cycle the cell was in upon addition of the antibiotic. Increases in cell size after treatment are represented to scale. Independent of the cell cycle and antibiotic, cells increased in size after treatment and holes appeared in the cell wall. No matter the stage of the cell cycle at the time of treatment, cell size increased more after methicillin than vancomycin treatment and the cell membrane separated from the cell wall after methicillin treatment only. If a cell had an incomplete septum, the incomplete septum was hydrolysed into its two component parts with ensuing death after methicillin

treatment but not vancomycin treatment. If cells had a complete septum upon methicillin addition, cell hydrolases split the cell into two daughter cells.

cycle and died attempting to complete the second division cycle after antibiotic treatment (Giesbrecht et al., 1998). His EM images also showed bulging areas in the septal region, but these were interpreted as peptidoglycan incorporated after treatment. Our images show that the septal plate is in fact still displaying a thin pointed morphology. The problem with this model is that it considers that peptidoglycan synthesis is still taking place. However, our data suggests that peptidoglycan synthesis is significantly inhibited within 15 minutes of antibiotic addition (3.2.3 & 4.2.3). Giesbrecht was right to suggest that incorrect initiation of cell division could lead to cell death after  $\beta$ -lactam treatment. Cells with complete septa also finish their current division cycle by dividing into two daughter cells, whereas vancomycin treatment prevents any progression through the cell cycle.

The futile cycle of peptidoglycan synthesis and hydrolysis shown by Thomas Bernhardt in *E. coli* is the most recently published comprehensive model of  $\beta$ -lactam killing (Cho et al., 2014). This model requires peptidoglycan synthesis as well as hydrolysis to be taking place. The data presented in this thesis shows that no incorporation of peptidoglycan precursors is taking place after *S. aureus* treatment with methicillin or vancomycin. The difference between the observed effects in *E. coli* and *S. aureus* is likely due to the absence of the Rod system in *S. aureus*, which is thought to be responsible for the futile cycle observed after mecillinam treatment of *E. coli*.

The original models around  $\beta$ -lactam killing align best with the results presented in this thesis. These were based on the hypothesis that peptidoglycan crosslinking would be inhibited but that glycan chains were still assembled, creating a loose cell wall being hydrolysed and leading to cytoplasm leakage (Alexander Tomasz, 1979). Although the details of the model proposed here differ, the overall concept of a weakened cell wall leading to localised failure is the same.

#### 6.4. Future directions

Further experiments are required to elucidate the role of hydrolases in cell wall antibiotic killing of *S. aureus*. Studies in strains lacking different combinations of hydrolases will be required to find which hydrolases play the biggest role in killing after peptidoglycan synthesis is inhibited. The large redundancy in peptidoglycan hydrolases will make this work difficult, as well as the likely essentiality of different groups of hydrolases. Hydrolases can be categorised in three different ways, according to activity (bond specificity), regulation or localisation. Inhibiting hydrolases according to either of these different groups may allow for new insight into their role.

The presented research brings to the forefront our limited understanding of hydrolase activity and control in *S. aureus*. There are 19 putative hydrolases in *S. aureus*, many of which have never been studied. WalkR is thought to positively regulate the transcription of 10 putative hydrolases. The putative hydrolases that are

most upregulated by WalkR have not been studied. Transcription of some of these is upregulated up to 15-fold by the WalkR system (Dubrac et al., 2007). Although an increase in RNA does not necessarily translate to an increase in protein, it would still be of interest to investigate these genes further. An initial investigation might involve measuring changes to protein levels to determine whether these mirror the reported changes in RNA. Deletion or inactivation of the genes encoding individual putative hydrolases and study of the ensuing strains would give us insight into their functions and the role they play in the cell wall metabolism. Further study of hydrolase regulation would also be of interest.

To better understand the differences between vancomycin and  $\beta$ -lactams further investigation into the interlinked role of WTA and hydrolases is necessary. Studies in a double *atl tarO* mutant would confirm whether the difference in vancomycin and methicillin killing of *S. aureus* SH1000 *tarO* is indeed due to the action of Atl. If Atl is responsible for the difference between methicillin and vancomycin killing of *S. aureus* SH1000 *tarO*, its absence would lead to both antibiotics having the same killing dynamics.

Previous research has shown that inhibition of WTA synthesis sensitises MRSA to  $\beta$ -lactam treatment (Lee et al., 2016). A number of compounds exist that inhibit wall teichoic acid synthesis, one of these is tunicamycin. No published data has investigated treatment of MSSA infections with WTA synthesis inhibitors. Researching possible synergistic interactions between cell wall antibiotics and WTA synthesis inhibitors could lead to interesting translational studies.

Further research is required to understand how this model of cell wall antibiotic treatment can be generalised to a range of different organisms, particularly gram-negative, which were not studied here.

Overall my work has established a simple, coarse grain model for the action of the most important set of clinically relevant antibiotics. This gives a framework to elucidate the complex molecular interactions that control microbial life and death.



## References

- Anderson, J. S., Matsushashi, M., Haskin, M. A., & Strominger, J. L. (1965). Lipid-phosphoacetylmuramyl-pentapeptide and lipid-phosphodisaccharide-pentapeptide: presumed membrane transport intermediates in cell wall synthesis. *Proceedings of the National Academy of Sciences of the United States of America*, *53*(4), 881–889. Retrieved from <http://www.ncbi.nlm.nih.gov/pubmed/14324547>
- Aoki, H., & Okuhara, M. (1980). Natural beta-lactam antibiotics. *Annual Review of Microbiology*, *34*(1), 159–181. <https://doi.org/10.1146/annurev.mi.34.100180.001111>
- Araki, Y., Nakatani, T., Hayashi, H., & Ito, E. (1971). Occurrence of non-N-substituted glucosamine residues in lysozyme-resistant peptidoglycan from *Bacillus cereus* cell walls. *Biochemical and Biophysical Research Communications*, *42*(4), 691–697. [https://doi.org/10.1016/0006-291X\(71\)90543-2](https://doi.org/10.1016/0006-291X(71)90543-2)
- Atilano, M. L., Pereira, P. M., Yates, J., Reed, P., Veiga, H., Pinho, M. G., & Filipe, S. R. (2010). Teichoic acids are temporal and spatial regulators of peptidoglycan cross-linking in *Staphylococcus aureus*. *Proceedings of the National Academy of Sciences of the United States of America*, *107*(44), 18991–18996. <https://doi.org/10.1073/pnas.1004304107>
- Bailey, R. G., Turner, R. D., Mullin, N., Clarke, N., Foster, S. J., & Hobbs, J. K. (2014). The interplay between cell wall mechanical properties and the cell cycle in *Staphylococcus aureus*. *Biophysical Journal*, *107*(11), 2538–2545. <https://doi.org/10.1016/j.bpj.2014.10.036>
- Balaban, N. Q., Merrin, J., Chait, R., Kowalik, L., & Leibler, S. (2004). Bacterial persistence as a phenotypic switch. *Science (New York, N.Y.)*, *305*(5690), 1622–1625. <https://doi.org/10.1126/science.1099390>
- Banzhaf, M., van den Berg van Saparoea, B., Terrak, M., Fraipont, C., Egan, A., Philippe, J., ... Vollmer, W. (2012). Cooperativity of peptidoglycan synthases active in bacterial cell elongation. *Molecular Microbiology*, *85*(1), 179–194. <https://doi.org/10.1111/j.1365-2958.2012.08103.x>
- Barna, J. C. J., & Williams, D. H. (1984). The structure and mode of action of glycopeptide antibiotics of the vancomycin group. *Annual Review of Microbiology*, *38*(1), 339–357. <https://doi.org/10.1146/annurev.mi.38.100184.002011>
- Bateman, A., & Rawlings, N. D. (2003). The CHAP domain: a large family of amidases including GSP amidase and peptidoglycan hydrolases. *Trends in Biochemical Sciences*, *28*(5), 234–237. [https://doi.org/10.1016/S0968-0004\(03\)00061-6](https://doi.org/10.1016/S0968-0004(03)00061-6)
- Beeby, M., Gumbart, J. C., Roux, B., & Jensen, G. J. (2013). Architecture and assembly of the Gram-positive cell wall. *Molecular Microbiology*, *88*(4), 664–672. <https://doi.org/10.1111/mmi.12203>
- Bensen, D. C., Rodriguez, S., Nix, J., Cunningham, M. L., & Tari, L. W. (2012). Structure of MurA (UDP-N-acetylglucosamine enolpyruvyl transferase) from *Vibrio fischeri* in complex with substrate UDP-N-acetylglucosamine and the drug fosfomycin. *Acta Crystallographica. Section F, Structural Biology and Crystallization Communications*, *68*(Pt 4), 382–385. <https://doi.org/10.1107/S1744309112006720>
- Bera, A., Biswas, R., Herbert, S., Kulauzovic, E., Weidenmaier, C., Peschel, A., & Götz, F. (2007). Influence of wall teichoic acid on lysozyme resistance in *Staphylococcus aureus*. *Journal of Bacteriology*, *189*(1), 280–283. <https://doi.org/10.1128/JB.01221-06>
- Bernhardt, T. G., & De Boer, P. A. J. (2005). SlmA, a nucleoid-associated, FtsZ binding protein required for blocking septal ring assembly over chromosomes in *E. coli*. *Molecular Cell*, *18*(5), 555–564. <https://doi.org/10.1016/j.molcel.2005.04.012>
- Bisicchia, P., Noone, D., Lioliou, E., Howell, A., Quigley, S., Jensen, T., ... Devine, K. M. (2007). The essential YycFG two-component system controls cell wall metabolism in *Bacillus subtilis*. *Molecular Microbiology*,

65(1), 180–200. <https://doi.org/10.1111/j.1365-2958.2007.05782.x>

- Biswas, R., Martinez, R. E., Göhring, N., Schlag, M., Josten, M., Xia, G., ... Peschel, A. (2012). Proton-binding capacity of *staphylococcus aureus* wall teichoic acid and its role in controlling autolysin activity. *PLoS ONE*, 7(7). <https://doi.org/10.1371/journal.pone.0041415>
- Biswas, R., Voggu, L., Simon, U. K., Hentschel, P., Thumm, G., & Gaetz, F. (2006). Activity of the major staphylococcal autolysin Atl. *FEMS Microbiology Letters*, 259(2), 260–268. <https://doi.org/10.1111/j.1574-6968.2006.00281.x>
- Boneca, I. G., Huang, Z.-H., Gage, D. A., & Tomasz, A. (2000). Characterization of *Staphylococcus aureus* cell wall glycan strands, evidence for a new beta-N-acetylglucosaminidase activity. *Journal of Biological Chemistry*, 275(14), 9910–9918. <https://doi.org/10.1074/jbc.275.14.9910>
- Bottomley, A. L. (2011). *Identification and characterisation of the cell division machinery in Staphylococcus aureus*.
- Boucher, H. W., & Corey, G. R. (2008). Epidemiology of methicillin-resistant *Staphylococcus aureus*. *Clinical Infectious Diseases : An Official Publication of the Infectious Diseases Society of America*, 46 Suppl 5(Suppl 5), S344-9. <https://doi.org/10.1086/533590>
- Bouhss, A., Crouvoisier, M., Blanot, D., & Mengin-Lecreux, D. (2004). Purification and characterization of the bacterial MraY translocase catalyzing the first membrane step of peptidoglycan biosynthesis. *Journal of Biological Chemistry*, 279(29), 29974–29980. <https://doi.org/10.1074/jbc.M314165200>
- Bouhss, A., Mengin-Lecreux, D., Blanot, D., Van Heijenoort, J., & Parquet, C. (1997). Invariant amino acids in the Mur peptide synthetases of bacterial peptidoglycan synthesis and their modification by site-directed mutagenesis in the UDP-MurNac:L-alanine ligase from *Escherichia coli*. *Biochemistry*, 36(39), 11556–11563. <https://doi.org/10.1021/bi970797f>
- Bouhss, A., Trunkfield, A. E., Bugg, T. D. H., & Mengin-Lecreux, D. (2008). The biosynthesis of peptidoglycan lipid-linked intermediates. *FEMS Microbiology Reviews*, 32(2), 208–233. <https://doi.org/10.1111/j.1574-6976.2007.00089.x>
- Bramkamp, M., Emmins, R., Weston, L., Donovan, C., Daniel, R. A., & Errington, J. (2008). A novel component of the division-site selection system of *Bacillus subtilis* and a new mode of action for the division inhibitor MinCD. *Molecular Microbiology*, 70(6), 1556–1569. <https://doi.org/10.1111/j.1365-2958.2008.06501.x>
- Brauner, A., Fridman, O., Gefen, O., & Balaban, N. Q. (2016). Distinguishing between resistance, tolerance and persistence to antibiotic treatment. *Nature Reviews Microbiology*, 14(5), 320–330. <https://doi.org/10.1038/nrmicro.2016.34>
- Brown, S., Xia, G., Luhachack, L. G., Campbell, J., Meredith, T. C., Chen, C., ... Walker, S. (2012). Methicillin resistance in *Staphylococcus aureus* requires glycosylated wall teichoic acids. *Proceedings of the National Academy of Sciences of the United States of America*, 109(46), 18909–18914. <https://doi.org/10.1073/pnas.1209126109>
- Brown, S., Zhang, Y.-H., & Walker, S. (2008). A revised pathway proposed for *Staphylococcus aureus* wall teichoic acid biosynthesis based on in vitro reconstitution of the intracellular steps. *Chemistry & Biology*, 15(1), 12–21. <https://doi.org/10.1016/j.chembiol.2007.11.011>
- Bugg, T. D. H., Braddick, D., Dowson, C. G., & Roper, D. I. (2011). Bacterial cell wall assembly: still an attractive antibacterial target. *Trends in Biotechnology*, 29(4), 167–173. <https://doi.org/10.1016/J.TIBTECH.2010.12.006>
- Cameron, D. R., Jiang, J.-H., Kostoulias, X., Foxwell, D. J., & Peleg, A. Y. (2016). Vancomycin susceptibility in methicillin-resistant *Staphylococcus aureus* is mediated by YycH activation of the WalRK essential two-

component regulatory system. *Scientific Reports*, 6. <https://doi.org/10.1038/srep30823>

- Canepari, P., Varaldo, P. E., Fontana, R., & Satta, G. (1985). Different staphylococcal species contain various numbers of penicillin-binding proteins ranging from four (*Staphylococcus aureus*) to only one (*Staphylococcus hyicus*). *Journal of Bacteriology*, 163(2), 796–798. Retrieved from <http://jb.asm.org/content/163/2/796>
- Cassini, A., Högberg, L. D., Plachouras, D., Quattrocchi, A., Hoxha, A., Simonsen, G. S., ... Hopkins, S. (2019). Attributable deaths and disability-adjusted life-years caused by infections with antibiotic-resistant bacteria in the EU and the European Economic Area in 2015: a population-level modelling analysis. *The Lancet. Infectious Diseases*, 19(1), 56–66. [https://doi.org/10.1016/S1473-3099\(18\)30605-4](https://doi.org/10.1016/S1473-3099(18)30605-4)
- Cava, F., de Pedro, M. A., Lam, H., Davis, B. M., & Waldor, M. K. (2011). Distinct pathways for modification of the bacterial cell wall by non-canonical D-amino acids. *The EMBO Journal*, 30(16), 3442–3453. <https://doi.org/10.1038/emboj.2011.246>
- Chambers, H. F. (1997, October). Methicillin resistance in staphylococci: Molecular and biochemical basis and clinical implications. *Clinical Microbiology Reviews*. <https://doi.org/10.1128/cmr.10.4.781>
- Cho, H., Uehara, T., & Bernhardt, T. G. (2014). Beta-lactam antibiotics induce a lethal malfunctioning of the bacterial cell wall synthesis machinery. *Cell*, 159(6), 1300–1311. <https://doi.org/10.1016/j.cell.2014.11.017>
- Cho, H., Wivagg, C. N., Kapoor, M., Barry, Z., Rohs, P. D. A., Suh, H., ... Bernhardt, T. G. (2016). Bacterial cell wall biogenesis is mediated by SEDS and PBP polymerase families functioning semi-autonomously. *Nature Microbiology*, 1(10), 16172. <https://doi.org/10.1038/nmicrobiol.2016.172>
- Chung, H. S., Yao, Z., Goehring, N. W., Kishony, R., Beckwith, J., & Kahne, D. (2009). Rapid beta-lactam-induced lysis requires successful assembly of the cell division machinery. *Proceedings of the National Academy of Sciences of the United States of America*, 106(51), 21872–21877. <https://doi.org/10.1073/pnas.0911674106>
- Cleverley, R. M., Barrett, J. R., Baslé, A., Bui, N. K., Hewitt, L., Solovyova, A., ... Lewis, R. J. (2014). Structure and function of a spectrin-like regulator of bacterial cytokinesis. *Nature Communications*, 5(1), 5421. <https://doi.org/10.1038/ncomms6421>
- Courvalin, P. (2006). Vancomycin resistance in gram-positive cocci. *Clinical Infectious Diseases*, 42(Supplement 1), S25–S34. <https://doi.org/10.1086/491711>
- Cuquemelle, E., Soulis, F., Villers, D., Roche-Campo, F., Ara Somohano, C., Fartoukh, M., ... A/H1N1 REVA-SRLF Study Group. (2011). Can procalcitonin help identify associated bacterial infection in patients with severe influenza pneumonia? A multicentre study. *Intensive Care Medicine*, 37(5), 796–800. <https://doi.org/10.1007/s00134-011-2189-1>
- Daniel, R. A., & Errington, J. (2003). Control of cell morphogenesis in bacteria: Two distinct ways to make a rod-shaped cell. *Cell*, 113(6), 767–776. [https://doi.org/10.1016/S0092-8674\(03\)00421-5](https://doi.org/10.1016/S0092-8674(03)00421-5)
- De Pedro, M. A., Quintela, J. C., Höltje, J. V., & Schwarz, H. (1997). Murein segregation in *Escherichia coli*. *Journal of Bacteriology*, 179(9), 2823–2834. <https://doi.org/10.1128/jb.179.9.2823-2834.1997>
- Delaune, A., Poupel, O., Mallet, A., Coic, Y.-M., Msadek, T., & Dubrac, S. (2011). Peptidoglycan crosslinking relaxation plays an important role in *Staphylococcus aureus* WalkR-dependent cell viability. *PLoS One*, 6(2), e17054. <https://doi.org/10.1371/journal.pone.0017054>
- Dengler, V., McCallum, N., Kiefer, P., Christen, P., Patrignani, A., Vorholt, J. A., ... Senn, M. M. (2013). Mutation in the C-di-AMP cyclase *dacA* affects fitness and resistance of methicillin resistant *Staphylococcus aureus*. *PLoS One*, 8(8), e73512. <https://doi.org/10.1371/journal.pone.0073512>

- Dmitriev, B. A., Ehlers, S., & Rietschel, E. T. (1999). Layered murein revisited: A fundamentally new concept of bacterial cell wall structure, biogenesis and function. *Medical Microbiology and Immunology*, *187*(3), 173–181. <https://doi.org/10.1007/s004300050090>
- Dmitriev, B. A., Toukach, F. V., Holst, O., Rietschel, E. T., & Ehlers, S. (2004). Tertiary structure of *Staphylococcus aureus* cell wall murein. *Journal of Bacteriology*, *186*(21), 7141–7148. <https://doi.org/10.1128/JB.186.21.7141-7148.2004>
- Dmitriev, B. A., Toukach, F. V., Schaper, K. J., Holst, O., Rietschel, E. T., & Ehlers, S. (2003). Tertiary structure of bacterial murein: The scaffold model. *Journal of Bacteriology*, *185*(11), 3458–3468. <https://doi.org/10.1128/JB.185.11.3458-3468.2003>
- Domínguez-Escobar, J., Chastanet, A., Crevenna, A. H., Fromion, V., Wedlich-Söldner, R., & Carballido-López, R. (2011). Processive movement of MreB-associated cell wall biosynthetic complexes in bacteria. *Science*, *333*(6039), 225–228. <https://doi.org/10.1126/science.1203466>
- Donachie, W. D., & Begg, K. J. (1989). Cell length, nucleoid separation, and cell division of rod-shaped and spherical cells of *Escherichia coli*. *Journal of Bacteriology*, *171*(9), 4633–4639. <https://doi.org/10.1128/jb.171.9.4633-4639.1989>
- Dubrac, S., Boneca, I. G., Poupel, O., & Msadek, T. (2007). New insights into the Walk/WalR (YycG/YycF) essential signal transduction pathway reveal a major role in controlling cell wall metabolism and biofilm formation in *Staphylococcus aureus*. *Journal of Bacteriology*, *189*(22), 8257–8269. <https://doi.org/10.1128/JB.00645-07>
- Dubrac, S., & Msadek, T. (2004). Identification of genes controlled by the essential YycG/YycF two-component system of *Staphylococcus aureus*. *Journal of Bacteriology*, *186*(4), 1175–1181. <https://doi.org/10.1128/JB.186.4.1175-1181.2004>
- Durand-Heredia, J. M., Yu, H. H., De Carlo, S., Lesser, C. F., & Janakiraman, A. (2011). Identification and characterization of ZapC, a stabilizer of the FtsZ ring in *Escherichia coli*. *Journal of Bacteriology*, *193*(6), 1405–1413. <https://doi.org/10.1128/JB.01258-10>
- ECDC. (2017). *Surveillance of antimicrobial resistance in Europe. Annual report of EARS - NET 2017*. Retrieved from <https://ecdc.europa.eu/en/publications-data/surveillance-antimicrobial-resistance-europe-2017>
- Eirich, J., Orth, R., & Sieber, S. A. (2011). Unraveling the protein targets of vancomycin in living *S. aureus* and *E. faecalis* cells. *Journal of the American Chemical Society*, *133*(31), 12144–12153. <https://doi.org/10.1021/ja2039979>
- Emami, K., Guyet, A., Kawai, Y., Devi, J., Wu, L. J., Allenby, N., ... Errington, J. (2017). RodA as the missing glycosyltransferase in *Bacillus subtilis* and antibiotic discovery for the peptidoglycan polymerase pathway. *Nature Microbiology*, *2*(3), 16253. <https://doi.org/10.1038/nmicrobiol.2016.253>
- Eveland, S. S., Pompliano, D. L., & Anderson, M. S. (1997). Conditionally lethal *Escherichia coli* murein mutants contain point defects that map to regions conserved among murein and folyl poly- $\gamma$ - glutamate ligases: Identification of a ligase superfamily. *Biochemistry*, *36*(20), 6223–6229. <https://doi.org/10.1021/bi9701078>
- Farha, M. A., Leung, A., Sewell, E. W., D’Elia, M. A., Allison, S. E., Ejim, L., ... Brown, E. D. (2013). Inhibition of WTA synthesis blocks the cooperative action of pbps and sensitizes MRSA to  $\beta$ -lactams. *ACS Chemical Biology*, *8*(1), 226–233. <https://doi.org/10.1021/cb300413m>
- Faron, M. L., Ledebøer, N. A., & Buchan, B. W. (2016, October 1). Resistance mechanisms, epidemiology, and approaches to screening for vancomycin-resistant Enterococcus in the health care setting. *Journal of Clinical Microbiology*. American Society for Microbiology. <https://doi.org/10.1128/JCM.00211-16>

- Foster, S. J. (1995). Molecular characterization and functional analysis of the major autolysin of *Staphylococcus aureus* 8325/4. *Journal of Bacteriology*, 177(19), 5723–5725. <https://doi.org/10.1128/jb.177.19.5723-5725.1995>
- Frankel, M. B., Hendrickx, A. P. A., Missiakas, D. M., & Schneewind, O. (2011). LytN, a murein hydrolase in the cross-wall compartment of *Staphylococcus aureus*, is involved in proper bacterial growth and envelope assembly. *Journal of Biological Chemistry*, 286(37), 32593–32605. <https://doi.org/10.1074/jbc.M111.258863>
- Frankel, M. B., & Schneewind, O. (2012). Determinants of murein hydrolase targeting to cross-wall of *Staphylococcus aureus* peptidoglycan. *Journal of Biological Chemistry*, 287(13), 10460–10471. <https://doi.org/10.1074/jbc.M111.336404>
- Fuchs Cleveland, E., & Gilvarg, C. (1976). Oligomeric intermediate in peptidoglycan biosynthesis in *Bacillus megaterium*. *Proceedings of the National Academy of Sciences of the United States of America*, 73(11), 4200–4204. <https://doi.org/10.1073/pnas.73.11.4200>
- Fuchs, S., Pané-Farré, J., Kohler, C., Hecker, M., & Engelmann, S. (2007). Anaerobic gene expression in *Staphylococcus aureus*. *Journal of Bacteriology*, 189(11), 4275–4289. <https://doi.org/10.1128/JB.00081-07>
- Fuda, C., Suvorov, M., Vakulenko, S. B., & Mobashery, S. (2004). The basis for resistance to  $\beta$ -lactam antibiotics by penicillin-binding protein 2a of methicillin-resistant *Staphylococcus aureus*. *Journal of Biological Chemistry*, 279(39), 40802–40806. <https://doi.org/10.1074/jbc.M403589200>
- Galli, E., & Gerdes, K. (2010). Spatial resolution of two bacterial cell division proteins: ZapA recruits ZapB to the inner face of the Z-ring. *Molecular Microbiology*, 76(6), 1514–1526. <https://doi.org/10.1111/j.1365-2958.2010.07183.x>
- Gan, L., Chen, S., & Jensen, G. J. (2008). Molecular organization of Gram-negative peptidoglycan. *Proceedings of the National Academy of Sciences of the United States of America*, 105(48), 18953. <https://doi.org/10.1073/PNAS.0808035105>
- Gardete, S., & Tomasz, A. (2014). Mechanisms of vancomycin resistance in *Staphylococcus aureus*. *Journal of Clinical Investigation*. <https://doi.org/10.1172/JCI68834>
- Germain, E., Castro-Roa, D., Zenkin, N., & Gerdes, K. (2013). Molecular mechanism of bacterial persistence by HipA. *Molecular Cell*, 52(2), 248–254. <https://doi.org/10.1016/j.molcel.2013.08.045>
- Giesbrecht, P., Kersten, T., Maidhof, H., Kruger, D., Blumel, P., Grob, H., & Wecke, J. (1994). A novel, “hidden” penicillin-induced death of staphylococci at high drug concentration, occurring earlier than murosomes-mediated killing processes. *Archives of Microbiology*, 161(5), 370–383. Retrieved from <http://www.ncbi.nlm.nih.gov/pubmed/8042899>
- Giesbrecht, P., Kersten, T., Maidhof, H., & Wecke, J. (1997). Two alternative mechanisms of cell separation in staphylococci: one lytic and one mechanical. *Archives of Microbiology*, 167(4), 239–250. Retrieved from <http://www.ncbi.nlm.nih.gov/pubmed/9075623>
- Giesbrecht, Peter, Kersten, T., Maidhof, H., & Wecke, J. (1998). Staphylococcal cell wall: morphogenesis and fatal variations in the presence of penicillin. *Microbiology and Molecular Biology Reviews*, 62(4), 1371–1414. Retrieved from <http://www.ncbi.nlm.nih.gov/pmc/articles/PMC98950/>
- Gillet, Y., Vanhems, P., Lina, G., Bes, M., Vandenesch, F., Floret, D., & Etienne, J. (2007). Factors Predicting Mortality in Necrotizing Community-Acquired Pneumonia Caused by *Staphylococcus aureus* Containing Panton-Valentine Leukocidin. *Clinical Infectious Diseases*, 45(3), 315–321. <https://doi.org/10.1086/519263>

- Goodell, E. W., Lopez, R., & Tomasz, A. (1976). Suppression of lytic effect of beta lactams on *Escherichia coli* and other bacteria. *Proceedings of the National Academy of Sciences of the United States of America*, 73(9), 3293–3297. Retrieved from <http://www.ncbi.nlm.nih.gov/pmc/articles/PMC431014/>
- Groicher, K. H., Firek, B. A., Fujimoto, D. F., & Bayles, K. W. (2000). The *Staphylococcus aureus* IrgAB operon modulates murein hydrolase activity and penicillin tolerance. *Journal of Bacteriology*, 182(7), 1794–1801. <https://doi.org/10.1128/JB.182.7.1794-1801.2000>
- Gustafsson, M. G. L. (2005). Nonlinear structured-illumination microscopy: Wide-field fluorescence imaging with theoretically unlimited resolution. *Proceedings of the National Academy of Sciences of the United States of America*, 102(37), 13081–13086. <https://doi.org/10.1073/pnas.0406877102>
- Hamoen, L. W., Meile, J.-C., de Jong, W., Noirot, P., & Errington, J. (2006). SepF, a novel FtsZ-interacting protein required for a late step in cell division. *Molecular Microbiology*, 59(3), 989–999. <https://doi.org/10.1111/j.1365-2958.2005.04987.x>
- Hartman, B. J., & Tomasz, A. (1984). Low-affinity penicillin-binding protein associated with beta-lactam resistance in *Staphylococcus aureus*. *Journal of Bacteriology*, 158(2), 513–516. Retrieved from <http://www.ncbi.nlm.nih.gov/pubmed/6563036>
- Hayhurst, E. J., Kailas, L., Hobbs, J. K., & Foster, S. J. (2008). Cell wall peptidoglycan architecture in *Bacillus subtilis*. *Proceedings of the National Academy of Sciences*, 105(38), 14603–14608. <https://doi.org/10.1073/pnas.0804138105>
- Heilmann, C., Hartleib, J., Hussain, M. S., & Peters, G. (2005). The multifunctional *Staphylococcus aureus* autolysin Aaa mediates adherence to immobilized fibrinogen and fibronectin. *Infection and Immunity*, 73(8), 4793–4802. <https://doi.org/10.1128/IAI.73.8.4793-4802.2005>
- Heintzmann, R., Jovin, T. M., & Cremer, C. (2002). Saturated patterned excitation microscopy—a concept for optical resolution improvement. *Journal of the Optical Society of America A*, 19(8), 1599. <https://doi.org/10.1364/JOSAA.19.001599>
- Höltje, J. V., & Heidrich, C. (2001). Enzymology of elongation and constriction of the murein sacculus of *Escherichia coli*. *Biochimie*, 83(1), 103–108. Retrieved from <http://www.ncbi.nlm.nih.gov/pubmed/11254982>
- Horsburgh, M. J., Aish, J. L., White, I. J., Shaw, L., Lithgow, J. K., & Foster, S. J. (2002). SigmaB modulates virulence determinant expression and stress resistance: characterization of a functional *rsbU* strain derived from *Staphylococcus aureus* 8325-4. *Journal of Bacteriology*, 184(19), 5457–5467. <https://doi.org/10.1128/JB.184.19.5457-5467.2002>
- Howden, B. P., Davies, J. K., Johnson, P. D. R., Stinear, T. P., & Grayson, M. L. (2010, January). Reduced vancomycin susceptibility in *Staphylococcus aureus*, including vancomycin-intermediate and heterogeneous vancomycin-intermediate strains: Resistance mechanisms, laboratory detection, and clinical implications. *Clinical Microbiology Reviews*. <https://doi.org/10.1128/CMR.00042-09>
- Hu, Z., & Lutkenhaus, J. (1999). Topological regulation of cell division in *Escherichia coli* involves rapid pole to pole oscillation of the division inhibitor MinC under the control of MinD and MinE. *Molecular Microbiology*, 34(1), 82–90. <https://doi.org/10.1046/j.1365-2958.1999.01575.x>
- Huang, B., Babcock, H., & Zhuang, X. (2010). Breaking the diffraction barrier: super-resolution imaging of cells. *Cell*, 143(7), 1047–1058. <https://doi.org/10.1016/j.cell.2010.12.002>
- Inoue, A., Murata, Y., Takahashi, H., Tsuji, N., Fujisaki, S., & Kato, J. I. (2008). Involvement of an essential gene, *mviN*, in murein synthesis in *Escherichia coli*. *Journal of Bacteriology*, 190(21), 7298–7301. <https://doi.org/10.1128/JB.00551-08>

- Jia, Z., O'Mara, M. L., Zuegg, J., Cooper, M. A., & Mark, A. E. (2013). Vancomycin: ligand recognition, dimerization and super-complex formation. *FEBS Journal*, *280*(5), 1294–1307. <https://doi.org/10.1111/febs.12121>
- Kahne, D., Leimkuhler, C., Lu, W., & Walsh, C. (2005). Glycopeptide and lipoglycopeptide antibiotics. *Chemical Reviews*, *105*(2), 425–448. <https://doi.org/10.1021/cr030103a>
- Kajimura, J., Fujiwara, T., Yamada, S., Suzawa, Y., Nishida, T., Oyamada, Y., ... Sugai, M. (2005). Identification and molecular characterization of an N-acetylmuramyl-L-alanine amidase Sle1 involved in cell separation of *Staphylococcus aureus*. *Molecular Microbiology*, *58*(4), 1087–1101. <https://doi.org/10.1111/j.1365-2958.2005.04881.x>
- Kaspy, I., Rotem, E., Weiss, N., Ronin, I., Balaban, N. Q., & Glaser, G. (2013). HipA-mediated antibiotic persistence via phosphorylation of the glutamyl-tRNA-synthetase. *Nature Communications*, *4*, 3001. <https://doi.org/10.1038/ncomms4001>
- Keren, I., Wu, Y., Inocencio, J., Mulcahy, L. R., & Lewis, K. (2013). Killing by bactericidal antibiotics does not depend on reactive oxygen species. *Science*, *339*(6124), 1213–1216. <https://doi.org/10.1126/science.1232688>
- Kluytmans, J. (1997). Nasal carriage of *Staphylococcus aureus*: epidemiology, underlying mechanisms, and associated risks. *Clinical Microbiology ...*, *10*(3), 505–520. Retrieved from <http://cmr.asm.org/content/10/3/505.short>
- Koch, A L. (1998). Orientation of the peptidoglycan chains in the sacculus of *Escherichia coli*. *Research in Microbiology*. [https://doi.org/10.1016/S0923-2508\(99\)80016-3](https://doi.org/10.1016/S0923-2508(99)80016-3)
- Koch, Arthur L. (1998). The three-for-one model for Gram-negative wall growth: a problem and a possible solution. *FEMS Microbiology Letters*, *162*(1), 127–134. <https://doi.org/10.1111/j.1574-6968.1998.tb12989.x>
- Koch, H. U., Haas, R., & Fischer, W. (1984). The role of lipoteichoic acid biosynthesis in membrane lipid metabolism of growing *Staphylococcus aureus*. *European Journal of Biochemistry*, *138*(2), 357–363. <https://doi.org/10.1111/j.1432-1033.1984.tb07923.x>
- Kohanski, M. A., Dwyer, D. J., Hayete, B., Lawrence, C. A., & Collins, J. J. (2007). A common mechanism of cellular death induced by bactericidal antibiotics. *Cell*, *130*(5), 797–810. <https://doi.org/10.1016/j.cell.2007.06.049>
- Komatsuzawa, H., Sugai, M., Nakashima, S., Yamada, S., Matsumoto, A., Oshida, T., & Suginaka, H. (1997). Subcellular localization of the major autolysin, Atl and its processed proteins in *Staphylococcus aureus*. *Microbiology and Immunology*, *41*(6), 469–479. <https://doi.org/10.1111/j.1348-0421.1997.tb01880.x>
- Kuru, E., Hughes, H. V., Brown, P. J., Hall, E., Tekkam, S., Cava, F., ... VanNieuwenhze, M. S. (2012). *In situ* probing of newly synthesized peptidoglycan in live bacteria with fluorescent D-amino acids. *Angewandte Chemie (International Ed. in English)*, *51*(50), 12519–12523. <https://doi.org/10.1002/anie.201206749>
- Kuru, E., Tekkam, S., Hall, E., Brun, Y. V., & Van Nieuwenhze, M. S. (2015). Synthesis of fluorescent D-amino acids and their use for probing peptidoglycan synthesis and bacterial growth *in situ*. *Nature Protocols*, *10*(1), 33–52. <https://doi.org/10.1038/nprot.2014.197>
- Lambert, M. P., & Neuhaus, F. C. (1972). Mechanism of D-cycloserine action: alanine racemase from *Escherichia coli* W. *Journal of Bacteriology*, *110*(3), 978. Retrieved from <https://www.ncbi.nlm.nih.gov/pmc/articles/PMC247518/>
- Leaver, M., & Errington, J. (2005). Roles for MreC and MreD proteins in helical growth of the cylindrical cell wall in *Bacillus subtilis*. *Molecular Microbiology*, *57*(5), 1196–1209. <https://doi.org/10.1111/j.1365->

2958.2005.04736.x

- Lee, S. H., Wang, H., Labroli, M., Koseoglu, S., Zuck, P., Mayhood, T., ... Roemer, T. (2016). TarO-specific inhibitors of wall teichoic acid biosynthesis restore  $\beta$ -lactam efficacy against methicillin-resistant staphylococci. *Science Translational Medicine*, 8(329), 329ra32. <https://doi.org/10.1126/scitranslmed.aad7364>
- Leimkuhler, C., Chen, L., Barrett, D., Panzone, G., Sun, B., Falcone, B., ... Kahne, D. (2005). Differential inhibition of *Staphylococcus aureus* PBP2 by glycopeptide antibiotics. *Journal of the American Chemical Society*, 127(10), 3250–3251. <https://doi.org/10.1021/ja043849e>
- Lenarcic, R., Halbedel, S., Visser, L., Shaw, M., Wu, L. J., Errington, J., ... Hamoen, L. W. (2009). Localisation of DivIVA by targeting to negatively curved membranes. *The EMBO Journal*, 28(15), 2272–2282. <https://doi.org/10.1038/emboj.2009.129>
- Levin, P. A., Kurtser, I. G., & Grossman, A. D. (1999). Identification and characterization of a negative regulator of FtsZ ring formation in *Bacillus subtilis*. *Proceedings of the National Academy of Sciences of the United States of America*, 96(17), 9642–9647. <https://doi.org/10.1073/pnas.96.17.9642>
- Levine, D. P. (2006). Vancomycin: a history. *Clinical Infectious Diseases*, 42(Supplement\_1), S5–S12. <https://doi.org/10.1086/491709>
- Liang, H., DeMeester, K. E., Hou, C.-W., Parent, M. A., Caplan, J. L., & Grimes, C. L. (2017). Metabolic labelling of the carbohydrate core in bacterial peptidoglycan and its applications. *Nature Communications*, 8, 15015. <https://doi.org/10.1038/ncomms15015>
- Liechti, G. W., Kuru, E., Hall, E., Kalinda, A., Brun, Y. V., Vannieuwenhze, M., & Maurelli, A. T. (2014). A new metabolic cell-wall labelling method reveals peptidoglycan in *Chlamydia trachomatis*. *Nature*, 506(7489), 507–510. <https://doi.org/10.1038/nature12892>
- Lim, D., & Strynadka, N. C. J. (2002). Structural basis for the  $\beta$ -lactam resistance of PBP2a from methicillin-resistant *Staphylococcus aureus*. *Nature Structural Biology*, 9(11), 870–876. <https://doi.org/10.1038/nsb858>
- Lioliou, E., Fechter, P., Caldelari, I., Jester, B. C., Dubrac, S., Helfer, A.-C., ... Geissmann, T. (2016). Various checkpoints prevent the synthesis of *Staphylococcus aureus* peptidoglycan hydrolase LytM in the stationary growth phase. *RNA Biology*, 13(4), 427–440. <https://doi.org/10.1080/15476286.2016.1153209>
- Liu, Y., & Imlay, J. A. (2013). Cell death from antibiotics without the involvement of reactive oxygen species. *Science*, 339(6124), 1210–1213. <https://doi.org/10.1126/science.1232751>
- Loose, M., & Mitchison, T. J. (2014). The bacterial cell division proteins FtsA and FtsZ self-organize into dynamic cytoskeletal patterns. *Nature Cell Biology*, 16(1), 38–46. <https://doi.org/10.1038/ncb2885>
- Lovering, A. L., Safadi, S. S., & Strynadka, N. C. J. (2012). Structural perspective of peptidoglycan biosynthesis and assembly. *Annual Review of Biochemistry*, 81(1), 451–478. <https://doi.org/10.1146/annurev-biochem-061809-112742>
- Lowy, F. D. (1998, August 20). Medical progress: *Staphylococcus aureus* infections. *New England Journal of Medicine*. <https://doi.org/10.1056/NEJM199808203390806>
- Lund, V. A. (2016). *Peptidoglycan dynamics in Staphylococcus aureus using super-resolution microscopy*. University of Sheffield.
- Lund, V. A., Wacnik, K., Turner, R. D., Cotterell, B. E., Walther, C. G., Fenn, S. J., ... Foster, S. J. (2018). Molecular coordination of *Staphylococcus aureus* cell division. *eLife*, 7. <https://doi.org/10.7554/eLife.32057>
- Macheboeuf, P., Contreras-Martel, C., Job, V., Dideberg, O., & Dessen, A. (2006). Penicillin Binding Proteins:

- key players in bacterial cell cycle and drug resistance processes. *FEMS Microbiology Reviews*, 30(5), 673–691. <https://doi.org/10.1111/j.1574-6976.2006.00024.x>
- Maki, H., Miura, K., & Yamano, Y. (2001). Katanosin B and plusbacin A3, inhibitors of peptidoglycan synthesis in methicillin-resistant *Staphylococcus aureus*. *Antimicrobial Agents and Chemotherapy*, 45(6), 1823–1827. <https://doi.org/10.1128/AAC.45.6.1823-1827.2001>
- Margolin, W. (2000). Themes and variations in prokaryotic cell division. *FEMS Microbiology Reviews*, 24(4), 531–548. <https://doi.org/10.1111/j.1574-6976.2000.tb00554.x>
- Matias, V. R. F., & Beveridge, T. J. (2005). Cryo-electron microscopy reveals native polymeric cell wall structure in *Bacillus subtilis* 168 and the existence of a periplasmic space. *Molecular Microbiology*, 56(1), 240–251. <https://doi.org/10.1111/j.1365-2958.2005.04535.x>
- Matias, V. R. F., & Beveridge, T. J. (2006). Native cell wall organization shown by cryo-electron microscopy confirms the existence of a periplasmic space in *Staphylococcus aureus*. *Journal of Bacteriology*, 188(3), 1011–1021. <https://doi.org/10.1128/JB.188.3.1011-1021.2006>
- Memmi, G., Filipe, S. R., Pinho, M. G., Fu, Z., & Cheung, A. (2008). *Staphylococcus aureus* PBP4 is essential for  $\beta$ -lactam resistance in community-acquired methicillin-resistant strains. *Antimicrobial Agents and Chemotherapy*, 52(11), 3955–3966. <https://doi.org/10.1128/AAC.00049-08>
- Merad, T., Archibald, A. R., Hancock, I. C., Harwood, C. R., & Hobot, J. A. (1989). Cell wall assembly in *Bacillus subtilis*: visualization of old and new wall material by electron microscopic examination of samples stained selectively for teichoic acid and teichuronic acid. *Microbiology*, 135(6), 1777–1777. <https://doi.org/10.1099/00221287-135-6-1777>
- Merchante, R., Pooley, H. M., & Karamata, D. (1995). A periplasm in *Bacillus subtilis*. *Journal of Bacteriology*, 177(21), 6176–6183. <https://doi.org/10.1128/jb.177.21.6176-6183.1995>
- Migocki, M. D., Freeman, M. K., Wake, R. G., & Harry, E. J. (2002). The Min system is not required for precise placement of the midcell Z ring in *Bacillus subtilis*. *EMBO Reports*, 3(12), 1163–1167. <https://doi.org/10.1093/embo-reports/kvf233>
- Mohammadi, T., van Dam, V., Sijbrandi, R., Vernet, T., Zapun, A., Bouhss, A., ... Breukink, E. (2011). Identification of FtsW as a transporter of lipid-linked cell wall precursors across the membrane. *The EMBO Journal*, 30(8), 1425–1432. <https://doi.org/10.1038/emboj.2011.61>
- Monteiro, J. M., Fernandes, P. B., Vaz, F., Pereira, A. R., Tavares, A. C., Ferreira, M. T., ... Pinho, M. G. (2015). Cell shape dynamics during the staphylococcal cell cycle. *Nature Communications*, 6, 8055. <https://doi.org/10.1038/ncomms9055>
- Mwangi, M. M., Kim, C., Chung, M., Tsai, J., Vijayadamodar, G., Benitez, M., ... Tomasz, A. (2013). Whole-genome sequencing reveals a link between  $\beta$ -lactam resistance and synthetases of the alarmone (p)ppGpp in *Staphylococcus aureus*. *Microbial Drug Resistance (Larchmont, N.Y.)*, 19(3), 153–159. <https://doi.org/10.1089/mdr.2013.0053>
- Neidhardt, F. C., Ingraham, J. L., & Schaechter, M. (1990). *Physiology of the bacterial cell: a molecular approach*. Sunderland, Mass.: Sinauer Associates.
- Neuhaus, F. C., & Baddiley, J. (2003). A continuum of anionic charge: structures and functions of D-alanyl-teichoic acids in gram-positive bacteria. *Microbiology and Molecular Biology Reviews*, 67(4), 686–723. <https://doi.org/10.1128/mubr.67.4.686-723.2003>
- Neuhaus, F. C., & Lynch, J. L. (1964). The enzymatic synthesis of d-alanyl-d-alanine. III. On the inhibition of d-Alanyl-d-alanine synthetase by the antibiotic d-cycloserine. *Biochemistry*, 3(4), 471–480. <https://doi.org/10.1021/bi00892a001>

- Ng, W. L., Kazmierczak, K. M., & Winkler, M. E. (2004). Defective cell wall synthesis in *Streptococcus pneumoniae* R6 depleted for the essential PcsB putative murein hydrolase or the VicR (YycF) response regulator. *Molecular Microbiology*, 53(4), 1161–1175. <https://doi.org/10.1111/j.1365-2958.2004.04196.x>
- Nikolaidis, I., Favini-Stabile, S., & Dessen, A. (2014). Resistance to antibiotics targeted to the bacterial cell wall. *Protein Science : A Publication of the Protein Society*, 23(3), 243. <https://doi.org/10.1002/PRO.2414>
- Ohnishi, R., Ishikawa, S., & Sekiguchi, J. (1999). Peptidoglycan hydrolase LytF plays a role in cell separation with Cwlf during vegetative growth of *Bacillus subtilis*. *Journal of Bacteriology*, 181(10), 3178–3184. Retrieved from <http://www.ncbi.nlm.nih.gov/pubmed/10322020>
- Oshida, T., Takano, M., Sugai, M., Suginaka, H., & Matsushita, T. (1998). Expression analysis of the autolysin gene (*atl*) of *Staphylococcus aureus*. *Microbiology and Immunology*, 42(9), 655–659. <https://doi.org/10.1111/j.1348-0421.1998.tb02336.x>
- Panchal, V. V. (2018). *The molecular basis of high-level methicillin resistance in Staphylococcus aureus*.
- Pasquina-Lemonche, L., Burns, J., Turner, R. D., Kumar, S., Tank, R., Mullin, N., ... Hobbs, J. K. (n.d.). The molecular architecture of the gram positive bacterial cell wall.
- Pasztor, L., Ziebandt, A.-K., Nega, M., Schlag, M., Haase, S., Franz-Wachtel, M., ... Götz, F. (2010). Staphylococcal major autolysin (Atl) is involved in excretion of cytoplasmic proteins. *The Journal of Biological Chemistry*, 285(47), 36794–36803. <https://doi.org/10.1074/jbc.M110.167312>
- Percy, M. G., & Gründling, A. (2014). Lipoteichoic acid synthesis and function in gram-positive bacteria. *Annual Review of Microbiology*, 68(1), 81–100. <https://doi.org/10.1146/annurev-micro-091213-112949>
- Pereira, S. F. F., Henriques, A. O., Pinho, M. G., de Lencastre, H., & Tomasz, A. (2009). Evidence for a dual role of PBP1 in the cell division and cell separation of *Staphylococcus aureus*. *Molecular Microbiology*, 72(4), 895–904. <https://doi.org/10.1111/j.1365-2958.2009.06687.x>
- Perkins, H. R. (1969). Specificity of combination between mucopeptide precursors and vancomycin or ristocetin. *The Biochemical Journal*, 111(2), 195–205. <https://doi.org/10.1042/BJ1110195>
- Pichoff, S., & Lutkenhaus, J. (2002). Unique and overlapping roles for ZipA and FtsA in septal ring assembly in *Escherichia coli*. *The EMBO Journal*, 21(4), 685–693. <https://doi.org/10.1093/emboj/21.4.685>
- Pinho, M G, de Lencastre, H., & Tomasz, A. (2000). Cloning, characterization, and inactivation of the gene *pbpC*, encoding penicillin-binding protein 3 of *Staphylococcus aureus*. *Journal of Bacteriology*, 182(4), 1074–1079. <https://doi.org/10.1128/jb.182.4.1074-1079.2000>
- Pinho, M G, & Errington, J. (2003). Dispersed mode of *Staphylococcus aureus* cell wall synthesis in the absence of the division machinery. *Molecular Microbiology*, 50(3), 871–881. <https://doi.org/10.1046/j.1365-2958.2003.03719.x>
- Pinho, Mariana G., De Lencastre, H., & Tomasz, A. (2001). An acquired and a native penicillin-binding protein cooperate in building the cell wall of drug-resistant staphylococci. *Proceedings of the National Academy of Sciences of the United States of America*, 98(19), 10886–10891. <https://doi.org/10.1073/pnas.191260798>
- Pourmand, M. R., Clarke, S. R., Schuman, R. F., Mond, J. J., & Foster, S. J. (2006). Identification of antigenic components of *Staphylococcus epidermidis* expressed during human infection. *Infection and Immunity*, 74(8), 4644–4654. <https://doi.org/10.1128/IAI.00521-06>
- Pratt, R. F. (2008). Substrate specificity of bacterial DD-peptidases (penicillin-binding proteins). *Cellular and Molecular Life Sciences*, 65(14), 2138–2155. <https://doi.org/10.1007/s00018-008-7591-7>
- Ramadurai, L., & Jayaswal, R. K. (1997). Molecular cloning, sequencing, and expression of *lytM*, a unique

autolytic gene of *Staphylococcus aureus*. *Journal of Bacteriology*, 179(11), 3625–3631. Retrieved from <http://www.ncbi.nlm.nih.gov/pubmed/9171409>

- Raskin, D. M., & De Boer, P. A. J. (1997). The MinE ring: An FtsZ-independent cell structure required for selection of the correct division site in *E. coli*. *Cell*, 91(5), 685–694. [https://doi.org/10.1016/S0092-8674\(00\)80455-9](https://doi.org/10.1016/S0092-8674(00)80455-9)
- Reed, P., Atilano, M. L., Alves, R., Hoiczky, E., Sher, X., Reichmann, N. T., ... Pinho, M. G. (2015). *Staphylococcus aureus* survives with a minimal peptidoglycan synthesis machine but sacrifices virulence and antibiotic resistance. *PLoS Pathogens*, 11(5), e1004891. <https://doi.org/10.1371/journal.ppat.1004891>
- Reed, P., Veiga, H., Jorge, A. M., Terrak, M., & Pinho, M. G. (2011). Monofunctional transglycosylases are not essential for *Staphylococcus aureus* cell wall synthesis? *Journal of Bacteriology*, 193(10), 2549–2556. <https://doi.org/10.1128/JB.01474-10>
- Reichmann, N. T., Tavares, A. C., Saraiva, B. M., Jouselin, A., Reed, P., Pereira, A. R., ... Pinho, M. G. (2019). SEDS–bPBP pairs direct lateral and septal peptidoglycan synthesis in *Staphylococcus aureus*. *Nature Microbiology*, 1. <https://doi.org/10.1038/s41564-019-0437-2>
- Reynolds, P. E. (1961). Studies on the mode of action of vancomycin. *Biochimica et Biophysica Acta*, 52(2), 403–405. [https://doi.org/10.1016/0006-3002\(61\)90698-9](https://doi.org/10.1016/0006-3002(61)90698-9)
- Reynolds, P. E. (1989). Structure, biochemistry and mechanism of action of glycopeptide antibiotics. *European Journal of Clinical Microbiology & Infectious Diseases: Official Publication of the European Society of Clinical Microbiology*, 8(11), 943–950. Retrieved from <http://files/816/art%3A10.1007%2FBF01967563.pdf>
- Rice, K. C., Firek, B. A., Nelson, J. B., Yang, S.-J., Patton, T. G., & Bayles, K. W. (2003). The *Staphylococcus aureus* cidAB operon: evaluation of its role in regulation of murein hydrolase activity and penicillin tolerance. *Journal of Bacteriology*, 185(8), 2635–2643. <https://doi.org/10.1128/jb.185.8.2635-2643.2003>
- Ruiz, N. (2008). Bioinformatics identification of MurJ (MviN) as the peptidoglycan lipid II flippase in *Escherichia coli*. *Proceedings of the National Academy of Sciences of the United States of America*, 105(40), 15553–15557. <https://doi.org/10.1073/pnas.0808352105>
- Ruiz, N. (2015). Lipid flippases for bacterial peptidoglycan biosynthesis. *Lipid Insights*, 2015(8), 21–31. <https://doi.org/10.4137/Lpi.s31783>
- Sabath, L. D. (1982). Mechanisms of resistance to beta-lactam antibiotics in strains of *Staphylococcus aureus*. *Annals of Internal Medicine*, 97(3), 339–344. <https://doi.org/10.7326/0003-4819-97-3-339>
- Sargent, M. G. (1975). Control of cell length in *Bacillus subtilis*. *Journal of Bacteriology*, 123(1), 7–19. Retrieved from <http://www.ncbi.nlm.nih.gov/pubmed/806582>
- Sarkar, P., Yarlagadda, V., Ghosh, C., & Haldar, J. (2017). A review on cell wall synthesis inhibitors with an emphasis on glycopeptide antibiotics. *MedChemComm*, 8(3), 516–533. <https://doi.org/10.1039/c6md00585c>
- Sauvage, E., Kerff, F., Terrak, M., Ayala, J. A., & Charlier, P. (2008). The penicillin-binding proteins: structure and role in peptidoglycan biosynthesis. *FEMS Microbiology Reviews*, 32(2), 234–258. <https://doi.org/10.1111/j.1574-6976.2008.00105.x>
- Scheffers, D.-J., & Pinho, M. G. (2005). Bacterial cell wall synthesis: new insights from localization studies. *Microbiology and Molecular Biology Reviews*, 69(4), 585–607. <https://doi.org/10.1128/MMBR.69.4.585-607.2005>
- Scheffers, D. J., & Driessen, A. J. M. (2001). The polymerization mechanism of the bacterial cell division protein FtsZ. *FEBS Letters*, 506(1), 6–10. [https://doi.org/10.1016/S0014-5793\(01\)02855-1](https://doi.org/10.1016/S0014-5793(01)02855-1)

- Schlag, M., Biswas, R., Krismer, B., Kohler, T., Zoll, S., Yu, W., ... Götz, F. (2010). Role of staphylococcal wall teichoic acid in targeting the major autolysin Atl. *Molecular Microbiology*, *75*(4), 864–873. <https://doi.org/10.1111/j.1365-2958.2009.07007.x>
- Schleifer, K. H., & Kandler, O. (1972). Peptidoglycan types of bacterial cell walls and their taxonomic implications. *Bacteriological Reviews*, *36*(4), 407–477. Retrieved from <http://www.ncbi.nlm.nih.gov/pubmed/4568761>
- Sham, L.-T., Butler, E. K., Lebar, M. D., Kahne, D., Bernhardt, T. G., & Ruiz, N. (2014). Bacterial cell wall. MurJ is the flippase of lipid-linked precursors for peptidoglycan biogenesis. *Science (New York, N.Y.)*, *345*(6193), 220–222. <https://doi.org/10.1126/science.1254522>
- Sharpe, M. E., & Errington, J. (1998). A fixed distance for separation of newly replicated copies of *oriC* in *Bacillus subtilis*: implications for co-ordination of chromosome segregation and cell division. *Molecular Microbiology*, *28*(5), 981–990. Retrieved from <http://www.ncbi.nlm.nih.gov/pubmed/9663684>
- Siegrist, M. S., Whiteside, S., Jewett, J. C., Aditham, A., Cava, F., & Bertozzi, C. R. (2013). (D)-Amino acid chemical reporters reveal peptidoglycan dynamics of an intracellular pathogen. *ACS Chemical Biology*, *8*(3), 500–505. <https://doi.org/10.1021/cb3004995>
- Silhavy, T. J., Kahne, D., & Walker, S. (2010). The bacterial cell envelope. *Cold Spring Harbor Perspectives in Biology*, *2*(5), a000414. <https://doi.org/10.1101/cshperspect.a000414>
- Singh, M., Chang, J., Coffman, L., & Kim, S. J. (2017). Hidden mode of action of glycopeptide antibiotics: inhibition of wall teichoic acid biosynthesis. *The Journal of Physical Chemistry B*, *121*(16), 3925–3932. <https://doi.org/10.1021/acs.jpccb.7b00324>
- Singh, S. K., SaiSree, L., Amrutha, R. N., & Reddy, M. (2012). Three redundant murein endopeptidases catalyse an essential cleavage step in peptidoglycan synthesis of *Escherichia coli* K12. *Molecular Microbiology*, *86*(5), 1036–1051. <https://doi.org/10.1111/mmi.12058>
- Snowden, M. A., & Perkins, H. R. (1990). Peptidoglycan cross-linking in *Staphylococcus aureus*. An apparent random polymerisation process. *European Journal of Biochemistry*, *191*(2), 373–377. <https://doi.org/10.1111/j.1432-1033.1990.tb19132.x>
- Stapleton, M. R., Horsburgh, M. J., Hayhurst, E. J., Wright, L., Jonsson, I. M., Tarkowski, A., ... Foster, S. J. (2007). Characterization of IsaA and SceD, two putative lytic transglycosylases of *Staphylococcus aureus*. *Journal of Bacteriology*, *189*(20), 7316–7325. <https://doi.org/10.1128/JB.00734-07>
- Stapleton, P. D., & Taylor, P. W. (2002). Methicillin resistance in *Staphylococcus aureus*: mechanisms and modulation. *Science Progress*, *85*(Pt 1), 57–72. Retrieved from <http://www.ncbi.nlm.nih.gov/pubmed/11969119>
- Steele, V. R., Bottomley, A. L., Garcia-Lara, J., Kasturiarachchi, J., & Foster, S. J. (2011). Multiple essential roles for EzrA in cell division of *Staphylococcus aureus*. *Molecular Microbiology*, *80*(2), 542–555. <https://doi.org/10.1111/j.1365-2958.2011.07591.x>
- Strauss, M. P., Liew, A. T. F., Turnbull, L., Whitchurch, C. B., Monahan, L. G., & Harry, E. J. (2012). 3D-SIM super resolution microscopy reveals a bead-like arrangement for FtsZ and the division machinery: implications for triggering cytokinesis. *PLoS Biology*, *10*(9), e1001389. <https://doi.org/10.1371/journal.pbio.1001389>
- Sugai, M., Fujiwara, T., Komatsuzawa, H., & Hidekazu, S. (1998). Identification and molecular characterization of a gene homologous to *epr* (endopeptidase resistance gene) in *Staphylococcus aureus*. *Gene*, *224*(1–2), 67–75. [https://doi.org/10.1016/S0378-1119\(98\)00508-3](https://doi.org/10.1016/S0378-1119(98)00508-3)
- Szwedziak, P., Wang, Q., Bharat, T. A. M., Tsim, M., & Löwe, J. (2014). Architecture of the ring formed by the tubulin homologue FtsZ in bacterial cell division. *eLife*, *3*, e04601. <https://doi.org/10.7554/eLife.04601>

- Taguchi, A., Welsh, M. A., Marmont, L. S., Lee, W., Sjodt, M., Kruse, A. C., ... Walker, S. (2019). FtsW is a peptidoglycan polymerase that is functional only in complex with its cognate penicillin-binding protein. *Nature Microbiology*, 4(4), 587–594. <https://doi.org/10.1038/s41564-018-0345-x>
- Tipper, D. J., & Strominger, J. L. (1965). Mechanism of action of penicillins: a proposal based on their structural similarity to acyl-D-alanyl-D-alanine. *Proceedings of the National Academy of Sciences of the United States of America*, 54(4), 1133–1141. Retrieved from <http://www.ncbi.nlm.nih.gov/pubmed/5219821>
- Tomasz, A. (1979). The mechanism of the irreversible antimicrobial effects of penicillins: How the beta-lactam antibiotics kill and lyse bacteria. *Annual Review of Microbiology*, 33(1), 113–137. <https://doi.org/10.1146/annurev.mi.33.100179.000553>
- Tomasz, Alexander. (1979). From penicillin-binding proteins to the lysis and death of bacteria: A 1979 view. *Reviews of Infectious Diseases*, 1(3), 434–467. <https://doi.org/10.1093/clinids/1.3.434>
- Tomasz, Alexander, Albino, A., & Zanati, E. (1970). Multiple antibiotic resistance in a bacterium with suppressed autolytic system. *Nature*, 227(5254), 138–140. <https://doi.org/10.1038/227138a0>
- Tong, S. Y. C., Davis, J. S., Eichenberger, E., Holland, T. L., & Fowler, V. G. (2015). Staphylococcus aureus Infections: Epidemiology, Pathophysiology, Clinical Manifestations, and Management. *Clinical Microbiology Reviews*, 28(3), 603–661. <https://doi.org/10.1128/CMR.00134-14>
- Touhami, A., Jericho, M. H., & Beveridge, T. J. (2004). Atomic force microscopy of cell growth and division in *Staphylococcus aureus*. *Journal of Bacteriology*, 186(11), 3286–3295. <https://doi.org/10.1128/JB.186.11.3286-3295.2004>
- Trueba, F. J. (1982). On the precision and accuracy achieved by *Escherichia coli* cells at fission about their middle. *Archives of Microbiology*, 131(1), 55–59. Retrieved from <http://www.ncbi.nlm.nih.gov/pubmed/7039546>
- Tuomanen, E., Durack, D. T., & Tomasz, A. (1986). Antibiotic tolerance among clinical isolates of bacteria. *Antimicrobial Agents and Chemotherapy*, 30(4), 521–527. Retrieved from <http://www.ncbi.nlm.nih.gov/pmc/articles/PMC176473/>
- Turner, R. D., Hurd, A. F., Cadby, A., Hobbs, J. K., & Foster, S. J. (2013). Cell wall elongation mode in Gram-negative bacteria is determined by peptidoglycan architecture. *Nature Communications*, 4, 1496. <https://doi.org/10.1038/ncomms2503>
- Turner, R. D., Mesnage, S., Hobbs, J. K., & Foster, S. J. (2018). Molecular imaging of glycan chains couples cell-wall polysaccharide architecture to bacterial cell morphology. *Nature Communications*, 9(1), 1263. <https://doi.org/10.1038/s41467-018-03551-y>
- Turner, R. D., Ratcliffe, E. C., Wheeler, R., Golestanian, R., Hobbs, J. K., & Foster, S. J. (2010). Peptidoglycan architecture can specify division planes in *Staphylococcus aureus*. *Nature Communications*, 1, 26. <https://doi.org/10.1038/ncomms1025>
- Turner, R. D., Vollmer, W., & Foster, S. J. (2014). Different walls for rods and balls: the diversity of peptidoglycan. *Molecular Microbiology*, 91(5), 862–874. <https://doi.org/10.1111/mmi.12513>
- Typas, A., Banzhaf, M., Gross, C. A., & Vollmer, W. (2012). From the regulation of peptidoglycan synthesis to bacterial growth and morphology. *Nature Reviews Microbiology*, 10(2), 123–136. <https://doi.org/10.1038/nrmicro2677>
- Tzagoloff, H., & Novick, R. (1977). Geometry of cell division in *Staphylococcus aureus*. *Journal of Bacteriology*, 129(1), 343–350. Retrieved from <http://www.ncbi.nlm.nih.gov/pubmed/830642>
- Umeda, A., Ueki, Y., & Amako, K. (1987). Structure of the *Staphylococcus aureus* cell wall determined by the freeze-substitution method. *Journal of Bacteriology*, 169(6), 2482–2487.

<https://doi.org/10.1128/jb.169.6.2482-2487.1987>

- van Dam, V., Olrichs, N., & Breukink, E. (2009). Specific labeling of peptidoglycan precursors as a tool for bacterial cell wall studies. *ChemBiochem: A European Journal of Chemical Biology*, 10(4), 617–624. <https://doi.org/10.1002/cbic.200800678>
- van Heijenoort, Y., Gómez, M., Derrien, M., Ayala, J., & van Heijenoort, J. (1992). Membrane intermediates in the peptidoglycan metabolism of *Escherichia coli*: possible roles of PBP 1b and PBP 3. *Journal of Bacteriology*, 174(11), 3549–3557. <https://doi.org/10.1128/jb.174.11.3549-3557.1992>
- Varma, A., de Pedro, M. A., & Young, K. D. (2007). FtsZ directs a second mode of peptidoglycan synthesis in *Escherichia coli*. *Journal of Bacteriology*, 189(15), 5692–5704. <https://doi.org/10.1128/JB.00455-07>
- Veiga, H., Jorge, A. M., & Pinho, M. G. (2011). Absence of nucleoid occlusion effector Noc impairs formation of orthogonal FtsZ rings during *Staphylococcus aureus* cell division. *Molecular Microbiology*, 80(5), 1366–1380. <https://doi.org/10.1111/j.1365-2958.2011.07651.x>
- Verwer, R. W. H., & Nanninga, N. (1976). Electron microscopy of isolated cell walls of *Bacillus subtilis* var. niger. *Archives of Microbiology*, 109(1–2), 195–197. <https://doi.org/10.1007/BF00425135>
- Vijaranakul, U., Nadakavukaren, M. J., de Jonge, B. L., Wilkinson, B. J., & Jayaswal, R. K. (1995). Increased cell size and shortened peptidoglycan interpeptide bridge of NaCl-stressed *Staphylococcus aureus* and their reversal by glycine betaine. *Journal of Bacteriology*, 177(17), 5116–5121. <https://doi.org/10.1128/jb.177.17.5116-5121.1995>
- Vollmer, W. (2008). Structural variation in the glycan strands of bacterial peptidoglycan. *FEMS Microbiology Reviews*, 32(2), 287–306. <https://doi.org/10.1111/j.1574-6976.2007.00088.x>
- Vollmer, W., Blanot, D., & de Pedro, M. A. (2008). Peptidoglycan structure and architecture. *FEMS Microbiology Reviews*, 32(2), 149–167. <https://doi.org/10.1111/j.1574-6976.2007.00094.x>
- Vollmer, W., & Höltje, J.-V. (2004). The architecture of the murein (peptidoglycan) in gram-negative bacteria: vertical scaffold or horizontal layer(s)? *Journal of Bacteriology*, 186(18), 5978–5987. <https://doi.org/10.1128/JB.186.18.5978-5987.2004>
- Vollmer, W., Joris, B., Charlier, P., & Foster, S. (2008). Bacterial peptidoglycan (murein) hydrolases. *FEMS Microbiology Reviews*, 32(2), 259–286. <https://doi.org/10.1111/j.1574-6976.2007.00099.x>
- Vollmer, W., & Seligman, S. J. (2010). Architecture of peptidoglycan: more data and more models. *Trends in Microbiology*, 18(2), 59–66. <https://doi.org/10.1016/j.tim.2009.12.004>
- Wacnik, K. (2016). *Dissecting cell division in the human pathogen Staphylococcus aureus*.
- Wang, X., & Zhao, X. (2009). Contribution of oxidative damage to antimicrobial lethality. *Antimicrobial Agents and Chemotherapy*, 53(4), 1395–1402. <https://doi.org/10.1128/AAC.01087-08>
- Ward, J. B., & Perkins, H. R. (1973). The direction of glycan synthesis in a bacterial peptidoglycan. *The Biochemical Journal*, 135(4), 721–728. <https://doi.org/10.1042/bj1350721>
- Watanakunakorn, C. (1984). Mode of action and in-vitro activity of vancomycin. *Journal of Antimicrobial Chemotherapy*, 14(suppl D), 7–18. [https://doi.org/10.1093/jac/14.suppl\\_D.7](https://doi.org/10.1093/jac/14.suppl_D.7)
- Weart, R. B., Lee, A. H., Chien, A.-C., Haeusser, D. P., Hill, N. S., & Levin, P. A. (2007). A metabolic sensor governing cell size in bacteria. *Cell*, 130(2), 335–347. <https://doi.org/10.1016/j.cell.2007.05.043>
- Wheeler, R. (2012). *Peptidoglycan architecture and dynamics of Gram-positive bacteria*.
- Wheeler, R., Mesnage, S., Boneca, I. G., Hobbs, J. K., & Foster, S. J. (2011). Super-resolution microscopy reveals cell wall dynamics and peptidoglycan architecture in ovococcal bacteria. *Molecular Microbiology*, 82(5),

1096–1109. <https://doi.org/10.1111/j.1365-2958.2011.07871.x>

- Wheeler, R., Turner, R. D., Bailey, R. G., Salamaga, B., Mesnage, S., Mohamad, S. A. S., ... Foster, S. J. (2015). Bacterial cell enlargement requires control of cell wall stiffness mediated by peptidoglycan hydrolases. *MBio*, *6*(4), e00660. <https://doi.org/10.1128/mBio.00660-15>
- Wise, E. M., Park, J. T., & Park, J. T. (1965). Penicillin: its basic site of action as an inhibitor of a peptide cross-linking reaction in cell wall mucopeptide synthesis. *Proceedings of the National Academy of Sciences of the United States of America*, *54*(1), 75–81. <https://doi.org/10.1073/pnas.54.1.75>
- Wu, L. J., & Errington, J. (2012). Nucleoid occlusion and bacterial cell division. *Nature Reviews Microbiology*, *10*(1), 8–12. <https://doi.org/10.1038/nrmicro2671>
- Wyke, A. W., Ward, J. B., Hayes, M. V., & Curtis, N. A. C. (1981). A Role in vivo for Penicillin-Binding Protein-4 of *Staphylococcus aureus*. *European Journal of Biochemistry*, *119*(2), 389–393. <https://doi.org/10.1111/j.1432-1033.1981.tb05620.x>
- Xia, G., Kohler, T., & Peschel, A. (2010). The wall teichoic acid and lipoteichoic acid polymers of *Staphylococcus aureus*. *International Journal of Medical Microbiology*, *300*(2–3), 148–154. <https://doi.org/10.1016/J.IJMM.2009.10.001>
- Yamada, S., Sugai, M., Komatsuzawa, H., Nakashima, S., Oshida, T., Matsumoto, A., & Suginaka, H. (1996). An autolysin ring associated with cell separation of *Staphylococcus aureus*. *Journal of Bacteriology*, *178*(6), 1565–1571. <https://doi.org/10.1128/jb.178.6.1565-1571.1996>
- Yao, X., Jericho, M., Pink, D., & Beveridge, T. (1999). Thickness and elasticity of gram-negative murein sacculi measured by atomic force microscopy. *Journal of Bacteriology*, *181*(22), 6865–6875. Retrieved from <http://www.ncbi.nlm.nih.gov/pubmed/10559150>
- Zapun, A., Contreras-Martel, C., & Vernet, T. (2008). Penicillin-binding proteins and beta-lactam resistance. *FEMS Microbiology Reviews*, *32*(2), 361–385. <https://doi.org/10.1111/j.1574-6976.2007.00095.x>
- Zapun, A., Vernet, T., & Pinho, M. G. (2008). The different shapes of cocci. *FEMS Microbiology Reviews*, *32*(2), 345–360. <https://doi.org/10.1111/j.1574-6976.2007.00098.x>
- Zhao, X., Hong, Y., & Drlica, K. (2015). Moving forward with reactive oxygen species involvement in antimicrobial lethality. *Journal of Antimicrobial Chemotherapy*, *70*(3), 639–642. <https://doi.org/10.1093/jac/dku463>
- Zhou, X., Halladin, D. K., Rojas, E. R., Koslover, E. F., Lee, T. K., Huang, K. C., & Theriot, J. A. (2015). Mechanical crack propagation drives millisecond daughter cell separation in *Staphylococcus aureus*. *Science*, *348*(6234), 574–578. <https://doi.org/10.1126/science.aaa1511>